AN INVERSE SOURCE LOCATION ALGORITHM FOR RADIATION PORTAL MONITOR APPLICATIONS

A Dissertation

by

KAREN ANN MILLER

Submitted to the Office of Graduate Studies of
Texas A&M University
in partial fulfillment of the requirements for the degree of

DOCTOR OF PHILOSOPHY

May 2010

Major Subject: Nuclear Engineering

AN INVERSE SOURCE LOCATION ALGORITHM FOR RADIATION PORTAL MONITOR APPLICATIONS

A Dissertation

by

KAREN ANN MILLER

Submitted to the Office of Graduate Studies of
Texas A&M University
in partial fulfillment of the requirements for the degree of

DOCTOR OF PHILOSOPHY

Approved by:

Chair of Committee,	William Charlton
Committee Members,	Marvin Adams
	Guergana Petrova
	Pavel Tsvetkov
Head of Department,	Raymond Juzaitis

May 2010

Major Subject: Nuclear Engineering

ABSTRACT

An Inverse Source Location Algorithm for Radiation Portal Monitor Applications.

(May 2010)

Karen Ann Miller, B.S., Texas A&M University

Chair of Advisory Committee: Dr. William Charlton

Radiation portal monitors are being deployed at border crossings throughout the world to prevent the smuggling of nuclear and radiological materials; however, a tension exists between security and the free-flow of commerce. Delays at ports-of-entry have major economic implications, so it is imperative to minimize portal monitor screening time. We have developed an algorithm to locate a radioactive source using a distributed array of detectors, specifically for use at border crossings.

To locate the source, we formulated an optimization problem where the objective function describes the least-squares difference between the actual and predicted detector measurements. The predicted measurements are calculated by solving the 3-D deterministic neutron transport equation given an estimated source position. The source position is updated using the steepest descent method, where the gradient of the objective function with respect to the source position is calculated using adjoint transport calculations. If the objective function is smaller than a predetermined convergence criterion, then the source position has been identified.

To test the algorithm, we first verified that the 3-D forward transport solver was working correctly by comparing to the code PARTISN (Parallel Time-Dependent S_N). Then, we developed a baseline scenario to represent a typical border crossing. Test cases were run for various source positions within each vehicle and convergence criteria, which showed that the algorithm performed well in situations where we have perfect knowledge of parameters such as the material properties of the vehicles. We also ran a sensitivity analysis to determine how uncertainty in various parameters—the optical thickness of the vehicles, the fill level in the gas tank, the physical size of the vehicles, and the detector efficiencies—affects the results. We found that algorithm is most sensitive to the optical thickness of the vehicles. Finally, we tested the simplifying assumption of one energy group by using measurements obtained from MCNPX (Monte Carlo N-Particle Extended). These results showed that the one-energy-group assumption will not be sufficient if the code is deployed in a real-world scenario. While this work describes the application of the algorithm to a land border crossing, it has potential for use in a wide array of nuclear security problems.

DEDICATION

To Mom and Dad

ACKNOWLEDGEMENTS

I would first like to thank my committee chair, Dr. William Charlton, for his guidance, mentoring, and encouragement throughout my college career. He helped mold me from a clueless undergraduate into, quite possibly, a young professional. Thanks go to Dr. Marvin Adams for introducing me to neutron transport theory and inspiring me with his incredible work ethic. I would also like to thank Dr. Pavel Tsvetkov and Dr. Guergana Petrova for their helpful comments and feedback on this work.

Thanks also go to the entire faculty and staff of the Nuclear Engineering Department for making my time at Texas A&M University a rewarding experience. In addition to my formal education, my colleagues at Los Alamos National Laboratory taught me how to turn my classroom knowledge into solutions for real problems. I also want to extend my gratitude to the U.S. Department of Homeland Security Science and Technology Directorate for funding the bulk of this research.

Thanks to Kristen Epresi, Ashley Cockerham, and Laura Strban for their friendship over the years. Special thanks to my boyfriend, Tim Kelton, whose patience and love is unmatched. Little did he know when we met that I would still be a student almost seven years later. Finally, I would like to thank my family: my sister, Jessica, and, of course, my parents, Dennis and Sue. Without their unconditional support, none of this work would be possible.

This research was performed under an appointment to a dissertation award program sponsored by the Department of Homeland Security (DHS), administered by the Oak Ridge Institute for Science and Education (ORISE) through an interagency agreement by the U.S. Department of Energy (DOE) and DHS. ORISE is managed by Oak Ridge Associated Universities (ORAU) under DOE contract number DE-AC05-06OR23100. All opinions expressed in this paper are the author's and do not necessarily reflect the policies and views of DHS, DOE, or ORAU/ORISE.

TABLE OF CONTENTS

Page

ABSTRACT iii

DEDICATION v

ACKNOWLEDGEMENTS vi

TABLE OF CONTENTS viii

LIST OF FIGURES x

LIST OF TABLES xv

CHAPTER

I INTRODUCTION 1

I.A. Description of the Problem 1
I.B. Illicit Trafficking of Nuclear and Radiological Materials 4
I.C. Radiation Portal Monitors 7
I.D. Inverse Problem Theory 8
I.E. Overview of Chapters 11

II OPTIMIZATION PROBLEM 14

II.A. Least-Squares Approximation 14
II.B. Gradient-Based Minimization Schemes 17
II.C. Problem Setup 18
II.D. Penalty Terms 25

III SOLUTION METHOD 27

III.A. Overview 27
III.B. Angular Discretization 28
III.C. Spatial Discretization 29
III.D. Solving the Forward Problem 32
III.E. Solving the Inverse Problem 35
III.F. Initial Guess 38

CHAPTER Page

III.G. Penalty Term 40
III.H. Convergence Criteria 41
III.I. The Full Algorithm 42

IV FORWARD CODE RESULTS 45

IV.A. Introduction 45
IV.B. Test Problem 1 46
IV.C. Test Problem 2 48
IV.D. Test Problem 3 51
IV.E. Test Problem 4 53
IV.F. Test Problem 5 55
IV.G. Summary of Forward Model Verification 57

V INVERSE CODE RESULTS 58

V.A. Model Parameters 58
V.B. Baseline Test Case 65
V.C. Sensitivity Analysis 81
V.C.1. Optical Thickness 82
V.C.2. Gas Tank Fill Level 85
V.C.3. Physical Size 87
V.C.4. Detector Efficiency 89
V.C.5. Summary of Results 92
V.D. Assessment of the One-Energy-Group Assumption 102

VI CONCLUSIONS AND RECOMMENDATIONS 105

VI.A. Summary of Results 105
VI.B. Recommendations for Future Work 107

REFERENCES 110

APPENDIX A: INVERSE CODE PLOTS 114

APPENDIX B: SAMPLE PARTISN INPUT DECK 151

APPENDIX C: SAMPLE MCNPX INPUT DECK 153

APPENDIX D: INVERSE CODE 175

VITA 194

LIST OF FIGURES

FIGURE		Page
1	Land border crossing with several lanes and a portal monitor in each lane	2
2	Detail view of a portal monitor	3
3	79.5 g HEU seized in Georgia	5
4	Flowcharts for forward and inverse problems	9
5	Least-squares approximation for fitting a line to a set of measured data points	16
6	(a) Ill-posed line-fitting problem and (b) use of *a priori* information	26
7	Example grid for Taylor series expansion	30
8	Triangulation concept	39
9	Flowchart showing the full source location algorithm	43
10	Forward test problem geometry and origin	46
11	Scalar flux surface plots for forward test problem 1 showing (a) PARTISN and (b) forward code results	47
12	1-D scalar flux plot for forward test problem 1	48
13	Scalar flux surface plots for forward test problem 2 showing (a) PARTISN and (b) forward code results	49
14	1-D scalar flux plot for forward test problem 2	50
15	1-D scalar flux plot for forward test problem 2 on a semi-log plot	50
16	1-D scalar flux plot for forward test problem 3	52
17	1-D scalar flux plot for forward test problem 3 on a semi-log plot	52

FIGURE Page

18 1-D scalar flux plot for forward test problem 4 54

19 1-D scalar flux plot for forward test problem 4 showing PARTISN results using both DSA and no acceleration 54

20 1-D scalar flux plot for forward test problem 5 56

21 1-D scalar flux plot for forward test problem 5 showing PARTISN results using both DSA and no acceleration 56

22 3-D rendering of the MCNPX baseline scenario 59

23 MCNPX model of a vehicle (side view) 59

24 MCNPX model of a radiation portal monitor (top and side views) 61

25 Execution time for homogeneous problems as a function of the number of cells 63

26 Execution time for the baseline scenario as a function of the number of cells 65

27 Vehicle numbering scheme 66

28 Source position and convergence tolerance baseline test for vehicle (1,1) 70

29 Source position and convergence tolerance baseline test for vehicle (2,1) 71

30 Source position and convergence tolerance baseline test for vehicle (3,1) 72

31 Source position and convergence tolerance baseline test for vehicle (1,2) 73

32 Source position and convergence tolerance baseline test for vehicle (2,2) 74

33 Source position and convergence tolerance baseline test for vehicle (3,2) 75

FIGURE Page

34 Source position and convergence tolerance baseline test for vehicle (1,3) 76

35 Source position and convergence tolerance baseline test for vehicle (2,3) 77

36 Source position and convergence tolerance baseline test for vehicle (3,3) 78

37 Summary of source position and convergence baseline tests 80

38 Three distributions of perturbed vehicles for the sensitivity analysis 83

39 Summary of optical thickness sensitivity analysis results showing the average distance between the true and predicted source as a function of the ratio of optical thicknesses in the perturbed case to the baseline case 84

40 Summary of gas tank fill level sensitivity analysis results showing the average distance between the true and predicted source as a function of the ratio of gas tank fill levels in the perturbed case to the baseline case 86

41 Summary of physical size sensitivity analysis results showing the average distance between the true and predicted source as a function of the change in physical size of the vehicles 89

42 Summary of detector efficiency sensitivity analysis results showing the average distance between the true and predicted source as a function of the change in detector efficiency 91

43 Summary of results for vehicle (1,1) 93

44 Summary of results for vehicle (2,1) 94

45 Summary of results for vehicle (3,1) 95

46 Summary of results for vehicle (1,2) 96

47 Summary of results for vehicle (2,2) 97

48 Summary of results for vehicle (3,2) 98

FIGURE Page

49 Summary of results for vehicle (1,3)..... 99

50 Summary of results for vehicle (2,3)..... 100

51 Summary of results for vehicle (3,3)..... 101

A.1 Optical thickness sensitivity analysis results for vehicle (1,1)..... 115

A.2 Optical thickness sensitivity analysis results for vehicle (2,1)..... 116

A.3 Optical thickness sensitivity analysis results for vehicle (3,1)..... 117

A.4 Optical thickness sensitivity analysis results for vehicle (1,2)..... 118

A.5 Optical thickness sensitivity analysis results for vehicle (2,2)..... 119

A.6 Optical thickness sensitivity analysis results for vehicle (3,2)..... 120

A.7 Optical thickness sensitivity analysis results for vehicle (1,3)..... 121

A.8 Optical thickness sensitivity analysis results for vehicle (2,3)..... 122

A.9 Optical thickness sensitivity analysis results for vehicle (3,3)..... 123

A.10 Gas tank fill level sensitivity analysis results for vehicle (1,1)..... 124

A.11 Gas tank fill level sensitivity analysis results for vehicle (2,1)..... 125

A.12 Gas tank fill level sensitivity analysis results for vehicle (3,1)..... 126

A.13 Gas tank fill level sensitivity analysis results for vehicle (1,2)..... 127

A.14 Gas tank fill level sensitivity analysis results for vehicle (2,2)..... 128

A.15 Gas tank fill level sensitivity analysis results for vehicle (3,2)..... 129

A.16 Gas tank fill level sensitivity analysis results for vehicle (1,3)..... 130

A.17 Gas tank fill level sensitivity analysis results for vehicle (2,3)..... 131

A.18 Gas tank fill level sensitivity analysis results for vehicle (3,3)..... 132

FIGURE Page

A.19 Physical size sensitivity analysis results for vehicle (1,1) 133

A.20 Physical size sensitivity analysis results for vehicle (2,1) 134

A.21 Physical size sensitivity analysis results for vehicle (3,1) 135

A.22 Physical size sensitivity analysis results for vehicle (1,2) 136

A.23 Physical size sensitivity analysis results for vehicle (2,2) 137

A.24 Physical size sensitivity analysis results for vehicle (3,2) 138

A.25 Physical size sensitivity analysis results for vehicle (1,3) 139

A.26 Physical size sensitivity analysis results for vehicle (2,3) 140

A.27 Physical size sensitivity analysis results for vehicle (3,3) 141

A.28 Detector efficiency sensitivity analysis results for vehicle (1,1)..... 142

A.29 Detector efficiency sensitivity analysis results for vehicle (2,1)..... 143

A.30 Detector efficiency sensitivity analysis results for vehicle (3,1)..... 144

A.31 Detector efficiency sensitivity analysis results for vehicle (1,2)..... 145

A.32 Detector efficiency sensitivity analysis results for vehicle (2,2)..... 146

A.33 Detector efficiency sensitivity analysis results for vehicle (3,2)..... 147

A.34 Detector efficiency sensitivity analysis results for vehicle (1,3)..... 148

A.35 Detector efficiency sensitivity analysis results for vehicle (2,3)..... 149

A.36 Detector efficiency sensitivity analysis results for vehicle (3,3)..... 150

LIST OF TABLES

TABLE		Page
1	Forward Test Problem 1 Material Properties	47
2	Forward Test Problem 3 Material Properties	51
3	Forward Test Problem 4 Material Properties	53
4	Forward Test Problem 5 Material Properties	55
5	Vehicle Materials and Macroscopic Cross Sections	60
6	Portal Monitor Materials and Macroscopic Cross Sections	62
7	Execution Times for Homogeneous Problems	63
8	Execution Times for the Baseline Scenario	64
9	Baseline Scenario Test Results of Varying Source Positions within each Vehicle	67
10	Comparison of Continuous-Energy and One-Group Test Case Results	103

CHAPTER I

INTRODUCTION

I.A. Description of the Problem

Radiation portal monitors are being deployed at border crossings throughout the world to prevent the smuggling of nuclear and radiological materials; however, a tension exists between security and the free flow of commerce. Today's companies rely on the efficient operation of global supply chains to stock their just-in-time inventories. Delays at ports-of-entry can have major economic implications, so it is imperative to minimize portal monitor screening time.[1]

Typically at land border crossings, there are several lanes of traffic, each equipped with a portal monitor. A typical setup is shown in Fig. 1 and Fig. 2. A vehicle containing a radioactive source can set off detectors in multiple lanes. Moreover, the vehicle does not have to be inside the portal monitor stall to set it off. If this happens, border agents must stop traffic and search for the source using handheld detectors. The screening process can be time-consuming and inefficient. This process could possibly be enhanced by using the portal monitor signals as a guide to where the source might be located throughout the lanes of traffic.

This dissertation follows the style of *Nuclear Science and Engineering*.

There has been at least one previous effort on the related problem of determining the lane in which a moving vehicle containing a radioactive source is located.[2] The method studied requires a detailed characterization of detector responses caused by a source in different locations prior to being implemented in a real traffic scenario. To calibrate the system, a grid is created within the field of the detectors. Measurements are taken of the detector responses from a source located at each grid point. These measurements are normalized and populate a table of detector responses based on different source positions. When a vehicle sets off the detectors, the detector responses are compared to the tabulated response functions in order to determine which simulation most closely matches the actual data, thus indicating the lane of the vehicle. One of the limiting factors of this method is that it relies solely on $1/r^2$ attenuation. Asymmetrical shielding in the field of view of the detectors due to other vehicles on the road can perturb the detector response and cause the source location algorithm to fail. No follow-up work was done on this project.

Fig. 1. Land border crossing with several lanes and a portal monitor in each lane.

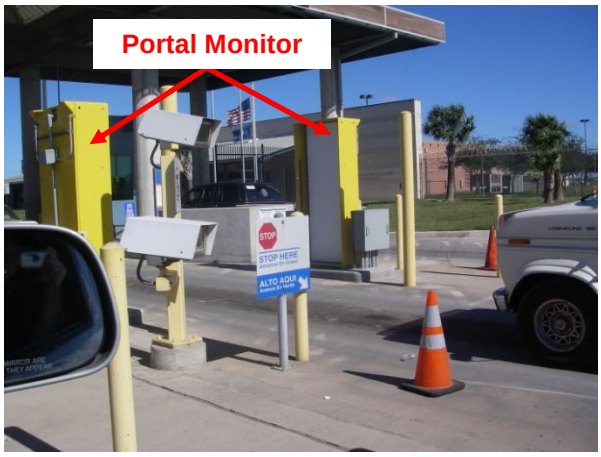

Fig. 2. Detail view of a portal monitor.

In this dissertation, we introduce, analyze, and numerically test a new approach to locating a radioactive source using a distributed array of detectors based on an inverse transport approach adapted from the general algorithm published by Norton.[3] The algorithm developed here is specifically for neutron transport, but it can be used for gamma rays, as well. Unlike the previous research, this method takes into account attenuation through vehicles near the source. The primary application is for use with portal monitors at land border crossings, but the method may be useful in other nuclear security applications as well as in medical imaging.

In the algorithm developed here, forward and adjoint deterministic transport calculations are used in an iterative solver to minimize an objective function. The objective function contains a weighted least-squares error functional describing the difference between calculated and measured detector responses. It is minimized using the least-squares method. An important step in the algorithm is calculating the gradients of the objective

function with respect to the unknown parameters. These gradients are called the Fréchet derivatives. Calculation of the Fréchet derivatives involves solving the adjoint transport equation for the system, where the objective function is the adjoint source. The algorithm uses a type of penalty term to account for *a priori* information about the problem.[4]

Adjoint functions have been used to calculate gradients in inverse problems in fields such as optical tomography, the geosciences, and heat conduction; however, there have been few instances of applications to the neutron transport equation. In outlining the general algorithm, Norton gave the examples of reconstructing unknown cross sections and scattering functions. Later, the method was used to determine interface locations and unknown materials in multilayer shields.[5,6] The work described in this dissertation applies the method to an inverse source problem, which has not been explored previously.

I.B. Illicit Trafficking of Nuclear and Radiological Materials

Illicit nuclear trafficking is defined as "the unauthorized acquisition, provision, possession, use, transfer, or disposal of nuclear or other radiological materials, whether intentional or unintentional and with or without crossing international borders."[7] It has become a growing concern due to several high-profile cases involving weapons-grade materials. The largest reported seizure occurred in 1993. An individual was arrested in

St. Petersburg, Russia in possession of nearly three kilograms of highly-enriched uranium, which he had stolen from a nuclear facility.[8] In February 2006, 79.5 g of 89%-enriched uranium, shown in Fig. 3, was confiscated during a sting in the South Ossetia region of Georgia.[9]

Fig. 3. 79.5 g HEU seized in Georgia.

There are a number of open-source databases and reports that contain information on incidents of illicit trafficking, including the International Atomic Energy Agency's Illicit Trafficking Database (ITDB), which was established in 1995. As of December 31, 2006, the ITDB contained 1,080 confirmed incidents. Several hundred other incidents reported in various open sources are tracked by the ITDB but not included in the statistics.[10]

The United States has two main initiatives aimed at deploying radiation portal monitors to detect illicit trafficking of nuclear materials. The National Nuclear Security

Administration's Second Line of Defense (SLD) program works with foreign partners to install radiation detection equipment at key transit points. SLD has two thrust areas: (1) the Core Program, which installs detection equipment at border crossings, strategic feeder seaports, and airports and (2) the Megaports Program, which installs detection equipment for screening maritime cargo at major international seaports.[11] The Department of Homeland Security's Customs and Border Protection agency is installing portal monitors domestically at land border crossings, seaports, rails crossings, international airports, and international mail and express consignment courier facilities.[12]

The same forces of globalization and interconnectivity that brought sushi to Arkansas and information technology to India have given small organizations the resources to build big weapons. The easiest way to stop rouge nations and terrorist organizations from acquiring nuclear weapons is to prevent the spread of nuclear materials. Using radiation portal monitors at border crossings can help detect and deter illicit nuclear trafficking, but the systems need to be optimized to reduce their impact on the throughput of vehicles. The implications of not acting to prevent illicit nuclear trafficking are serious threats to international peace and security, which is why it is important to develop portal monitors that work effectively and efficiently.

I.C. Radiation Portal Monitors

Radiation portal monitors are large-scale, field-deployable radiation detectors. Originally, the systems were developed for the exits of nuclear facilities and to prevent the inadvertent disposal of radioactive scrap metal. Today, portal monitors are also used at ports-of-entry to detect the illicit trafficking of nuclear and radiological materials.

Radiation portal monitors are capable of detecting both neutron and gamma radiation. Most portal monitors use ^{3}He tubes for neutron detection and a plastic scintillator such as polyvinyl toluene (PVT) for gamma detection. Because neutrons are neutral in charge, they do not interact directly with electrons in matter. Neutron detection relies on indirect measurements—by measuring charged particles released in neutron interactions. Helium-3 detectors utilize the following reaction:

$$^{3}He + n \rightarrow {}^{3}H + {}^{1}H + 765 \text{ keV}. \quad (1)$$

Helium-3 interacts with a neutron to produce one hydrogen atom and one tritium atom along with 756 keV of energy.

PVT is a type of organic scintillator. When a photon enters a PVT detector, it may deposit part of its kinetic energy, leaving atoms in an excited state. The excess energy is emitted as photons. The scintillating material is optically coupled to a photocathode. When the emitted photons impinge on the photocathode, electrons are emitted through

the photoelectric effect. The electrons are accelerated through a photomultiplier tube (PMT) onto an anode, where they create an electrical output signal.[13]

The portal monitors used at border crossings are configured in two pillars that are placed on either side of a roadway, partially shielded by a lead case as shown in Fig. 1 and Fig. 2. The detectors can be arranged and scaled for maximum efficiency. The software in typical systems is programmable and can integrate data from an array of detectors as well as cameras.[14]

I.D. Inverse Problem Theory

Inverse problems are often encountered in the applied sciences. Examples include fitting a curve to a set of measurements, evaluating geophysical data to determine the structure of the earth, and analyzing a computed tomography (CT) scan to diagnose medical conditions. Similarly, using portal monitor data to determine the location of a radioactive source is an inverse problem.

Inverse theory is the set of mathematical techniques used to make inferences about the physical world using measurements and observations. Within any physical system there are model parameters, which completely describe the system, and observable parameters, which are the things that can be measured. In a forward problem, the model parameters (e.g., geometry and material composition) are known. They are used in a

mathematical model to estimate observable parameters (e.g., a detector response). Inverse problems, on the other hand, work in the reverse direction. Observable parameters are used in a mathematical model to estimate model parameters.[15] This concept is illustrated in Fig. 4.

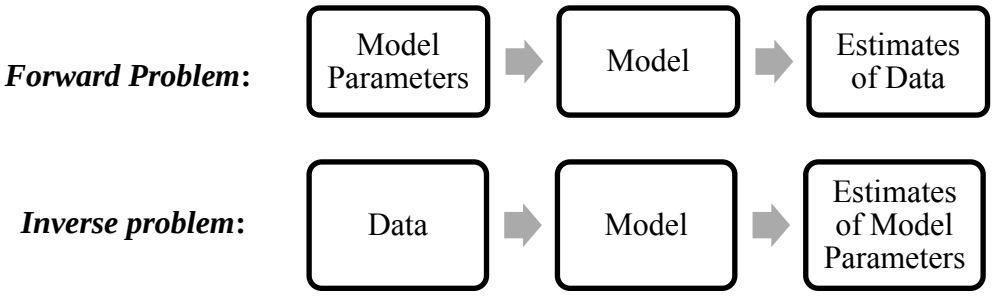

Fig. 4. Flowcharts for forward and inverse problems.

In the 1970s, Siewert, McCormick, and Sanchez began investigating inverse transport problems to determine scattering coefficients.[16,17,18,19,20] Most of their work concentrated on finding explicit expressions for the quantities of interest in terms of experimental data.

In the 1980s, Larsen, Sanchez and McCormick began using adjoint functions to solve inverse transport problems indirectly with iterative methods. Sanchez and McCormick used the adjoint of the transport operator in deriving a set of linear equations that could be solved for the isotropic scattering operator in a homogeneous slab.[21] Larsen showed that the adjoint angular flux is a measureable quantity on the surface of an object and

derived relationships using the adjoint angular fluxes to obtain information about the scattering function. He did this for multigroup, anisotropically-scattering problems as well as multidimensional problems.[22,23]

In 1997, Norton proposed a new solution method for solving inverse transport problems.[3] Although adjoint functions had been used previously in solving inverse transport problems, Norton used the adjoint flux in a novel way. The problem of determining some unknown material property was formulated as an optimization problem. The adjoint flux was used to calculate the Fréchet derivative of a global error functional, also referred to as the objective function, which related measured and calculated values and then used that derivative to minimize the error functional. The same idea had been implemented in solving inverse heat conduction problems.[24]

A similar method was developed in the field of optical tomography. Hielscher and Klose worked on a model-based iterative image reconstruction scheme for medical imaging problems.[25,26] They used a technique called adjoint differentiation to calculate the gradient of the objective function. In this technique, the chain rule is continually applied to the objective function to decompose it into a series of differentiable function steps. The disadvantage of adjoint differentiation is that it requires a large amount of computer storage.

Most recently, the 2006 American Nuclear Society Winter Meeting included a session on inverse methods for radiation transport problems. In this session, two papers called attention to the field of inverse source problems. Klose discussed the importance of inverse source problems in molecular imaging, where optical probes report on targeted molecular processes inside biological tissue.[27] Sanchez and McCormick noted that the growth of passive screening processes for radioactivity since September 11, 2001 has opened the door to research in inverse source problems.[28] Thoreson *et al.* also recognized the importance of inverse problems in homeland security applications.[29]

I.E. Overview of Chapters

In this chapter, we described the problem and explained the implications of the research. The consequences of not acting to prevent illicit nuclear trafficking were explained along with the detection mechanism of radiation portal monitors. Finally, we introduced general inverse theory and described previous efforts in inverse transport problems.

Chapter II describes optimization problems, specifically the least-squares approximation that we used to develop the source location algorithm. Gradient-based minimization schemes are discussed, and the Fréchet derivative with respect to the source location and strength is derived.

In Chapter III, the theory behind the solution mechanisms is explained. For the forward model, this includes the angular and spatial discretization and the source iteration method. For the inverse model, this is the steepest descent algorithm. Additionally, Chapter III explains how the initial guess for the source position is chosen, how penalty terms are used to decrease computational time, and how the convergence criterion was chosen. The chapter concludes by tying together the entire source location algorithm.

The results of forward model test problems are given in Chapter IV. The accuracy of the 3-D deterministic transport solver was determined by a comparison with a code called PARTISN. Based on the results of an array of 3-D problems with varying model parameters, it was determined that the forward solver was functioning as expected.

The results of the inverse model test problems are given in Chapter V. The chapter starts with a description of the model parameters such as mesh size, vehicle geometry, and cross sections as well as an assessment of the simplifying assumptions used such as one-group cross sections. We developed a baseline test case on which to compare all of the inverse test cases. The baseline scenario represents a typical configuration of vehicles and portal monitors with typical cross sections. It demonstrates the code's ability to locate the source position given perfect model parameters. We also conducted a sensitivity analysis to determine what factors (e.g., optical thickness of the vehicles or detection efficiency of the portal monitors) have the biggest affect on the solution.

We finish our discussion in Chapter VI with a summary of the results as well as general conclusions and recommendations.

CHAPTER II

OPTIMIZATION PROBLEM

II.A. Least-Squares Approximation

Unconstrained optimization problems have the form

$$\text{minimize } f(s), \tag{2}$$

where $f(s) : \mathbb{R}^n \to \mathbb{R}$ is an objective function.[30] The objective function is a measure of length, or the norm, of an *n*-dimensional vector. If that norm is the L_2 norm, then it is a special class of optimization problems called a least-squares problem. The L_2 norm is denoted by $\|\cdot\|_2$ and computed by[31]

$$\|\vec{r}\|_2^2 = r_1^2 + r_2^2 + \cdots + r_n^2 \ . \tag{3}$$

A least-squares problem can be recognized by verifying the objective function is a quadratic function. Consider the least-squares problem

$$\text{minimize } f(s) = \|As - b\|_2^2 \tag{4}$$

where A is a known matrix, s is an unknown vector, and b is a known vector. Expanding $f(s)$ gives the quadratic form

$$f(s) = s^T A^T As - 2b^T As + b^T b. \tag{5}$$

If A is a symmetric positive-definite matrix, then the gradient of $f(s)$ with respect to s is

$$\nabla f(s) = As - b. \tag{6}$$

By setting the gradient equal to zero, it can be seen that $f(s)$ is minimized by the solution to the system of equations $As = b$.

To illustrate the concept of a least-squares problem, take the example of fitting a line to a set of measurements. Recall that in an inverse problem, model parameters are recovered using measured data. When data is predicted based on estimated model parameters, there will be error between the predicted data and the measured data. Consider m_n, $n = 1 \ldots N$ measurements and the predictions of those measurements p_n. Using the least-squares approximation, a best-fit line is found with

$$\text{minimize } \|P - M\|_2^2 = \sum_{n=1}^{N} (p_n - m_n)^2. \tag{7}$$

Fig. 5 illustrates the line fitting problem. The error for each measurement is the difference between the data point and the predicted line. The line that minimizes the global error is the best fit.

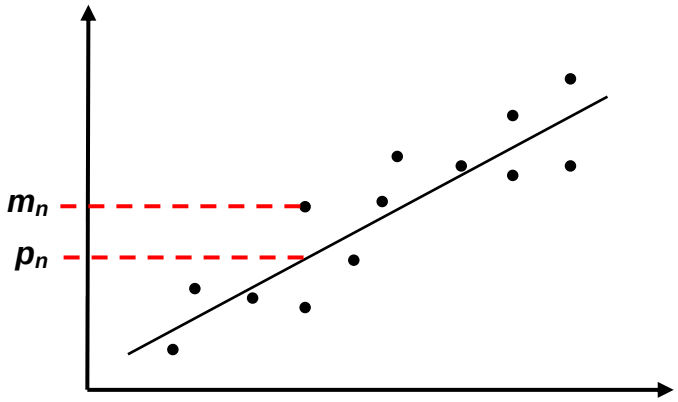

Fig. 5. Least-squares approximation for fitting a line to a set of measured data points.

The least-squares method has a number of statistical interpretations, and there are variations on the standard form of the equations to facilitate practical applications. One of those variations is the weighted least-squares approximation, where the objective function is weighted by a parameter such as the uncertainty in each measurement. This technique is used, for example, in recovering an unknown vector s when the measurements have been corrupted by Gaussian noise. The weighted least-squares problem has the form

$$\text{minimize } f(s) = \|W(As - b)\|_2^2 \tag{8}$$

where W is the weighting matrix.

II.B. Gradient-Based Minimization Schemes

At this point, it is necessary to know how the objective function is minimized. There are several different methods that can be used. One of those is Newton's method. While Newton's method works well for some problems, it requires the inversion of an ill-conditioned Jacobian matrix at each step in nonlinear problems. The method is not well-suited for large-scale inverse problems.[32] The Levenberg-Marquardt method can be used for solving least-squares problems. It also requires inverting an ill-conditioned Jacobian matrix, but convergence is not as dependent on the initial guess for the solution as it is in Newton's method. For this work, we use a gradient method called the steepest descent method.

The general form of gradient descent schemes represent the first order Taylor approximation of $f(s+\alpha)$ about s:

$$f(s+\alpha) = f(s) + \alpha f'(s). \tag{9}$$

Gradient methods have the form

$$s^{(\ell+1)} = s^{(\ell)} - \alpha^{(\ell)} \nabla f\left(s^{(\ell)}\right). \tag{10}$$

They are iterative methods, and the superscript ℓ denotes the iteration number. The unknown vector s is updated by adding a step size α times the negative of the gradient of $f(s)$. The step size is a parameter that specifies how far to go in the direction of the

gradient. There are various ways to calculate the step size such as a line search method or by using parameters derived at each iteration.

The matrix A is symmetric, positive-definite. This means that the quadratic function $f(s)$ is shaped like a paraboloid bowl. The gradient, by definition, points in the direction of greatest increase. The minus sign in Eq. 10 means that the search direction is the negative of the gradient, making it the direction of greatest decrease. Thus, to minimize the least-squares formulation for the portal monitor problem, we need the gradient of the quadratic function. The process is iterative, where the gradient can be recalculated at each iteration, and continues heading in that direction until the bottom of the paraboloid bowl is reached.

II.C. Problem Setup

The problem of locating a radioactive source at a border crossing using multiple portal monitor measurements is similar to a line-fitting problem. In this case, the goal is to recover the source position that produces the predicted measurements that best fit the actual measurements.

The equation we use to predict the measurements is the forward transport equation, or simply the transport equation. The transport equation describes the expected distribution

of free neutrons in a phase-space volume.[33] It is a balance equation that quantifies the change rate of neutrons as the production rate minus the loss rate. It can be written as

$$\frac{1}{v(E)}\frac{\partial\psi(\vec{r},E,\vec{\Omega},\mathrm{t})}{\partial t}+\vec{\Omega}\cdot\vec{\nabla}\psi(\vec{r},E,\vec{\Omega},\mathrm{t})+\sigma_t(\vec{r},E,t)\psi(\vec{r},E,\vec{\Omega},\mathrm{t})$$
$$=\int_{4\pi}d\Omega'\int_{0}^{\infty}dE'\sigma_s(\vec{r},E'\to E,\Omega'\to\Omega,\mathrm{t})\psi(\vec{r},E',\vec{\Omega}',\mathrm{t}) \qquad (11)$$
$$+Q(\vec{r},E,\vec{\Omega},\mathrm{t})$$

where the scalar flux is given by

$$\phi(\vec{\mathrm{r}})=\int_{4\pi}d\,\Omega\,\psi(\vec{r},\vec{\Omega}). \qquad (12)$$

The first term on the left-hand side of the equation represents the change rate of neutrons. The next two terms describe the net out-leakage rate and loss rate due to collisions, respectively. The first term on the right-hand side of the equation is the gain rate of neutrons due to scattering into the phase space. Finally, the last term represents an extraneous source. It is also called the inhomogeneous source. Other sources can be included in the transport equation (e.g., fission or delayed neutrons), but we consider only an inhomogenous source Q for the border monitoring application.

For the purposes of this dissertation, we use the steady-state, mono-energetic version of the transport equation. We also assume that scattering is isotropic. Thus, the equation can be simplified to

$$\vec{\Omega} \cdot \vec{\nabla}\psi(\vec{r},\vec{\Omega}) + \sigma_t(\vec{r})\psi(\vec{r},\vec{\Omega}) - \frac{\sigma_s(\vec{r})}{4\pi}\int_{4\pi} d\Omega'\psi(\vec{r},\vec{\Omega}') = Q(\vec{r},\vec{\Omega}). \tag{13}$$

For brevity, this can be written

$$H\psi = Q. \tag{14}$$

Recall that the weighted least-squares problem has the form

$$\text{minimize } f(s) = \|W(As-b)\|_2^2. \tag{15}$$

The response function of detector n is

$$\sigma_{d,n} = R_n\delta(\vec{r}-\vec{r}_n). \tag{16}$$

Letting M_n represent the measurements for $n = 1, \ldots, N$ detectors and ψ represent the calculated angular flux, the least-squares formulation for this problem is

$$\begin{aligned} \text{minimize } f(Q) &= \frac{1}{2}\left\|\frac{\sigma_d\psi(\vec{r},\vec{\Omega};\mathrm{Q}) - M}{M}\right\|_2^2 \\ &= \frac{1}{2}\int_{\Delta V} dV \int_{4\pi} d\Omega \sum_{n=1}^{N}\left(\frac{\sigma_{d,n}\psi - M_n}{M_n}\right)^2. \end{aligned} \tag{17}$$

The equation can be further simplified by combining the angular flux and detector response function into one variable to represent the estimated measurement $M_{est}(Q)$.

$$\begin{aligned}\text{minimize } f(Q) &= \frac{1}{2}\left\|\frac{M_{est}(\mathrm{Q}) - M}{M}\right\|_2^2 \\ &= \frac{1}{2}\int_{\Delta V} dV \int_{4\pi} d\Omega \sum_{n=1}^{N}\left(\frac{M_{est,n}(\mathrm{Q}) - M_n}{M_n}\right)^2.\end{aligned} \tag{18}$$

In this case and referring to Eq. 15, the known matrix A is merely the identity matrix, the unknown vector s is $M_{est}(\mathrm{Q})$, the known vector b is the actual measurements M, and the weighting function W is $1/2M$ to give a relative difference between the measurements.

To minimize Eq. 18 with a gradient method, it is necessary to take the derivative with respect to the quantities of interest. Here, we restrict the volume integral to the cell containing the source. Omitting several intermediate steps (derived similarly by Norton), taking the derivative with respect to x gives

$$\nabla_x f = \int_{\Delta V_s} dV_s \int_{4\pi} d\Omega \sum_{n=1}^{N} \frac{\partial \psi}{\partial x}\left(\frac{M_{est,n}(Q) - M_n}{M_n}\right). \tag{19}$$

Because we do not have an expression for the derivative of the angular flux with respect to x, we would like to replace it with something we can calculate. To do this, we need the adjoint neutron transport equation given by[34]

$$-\vec{\Omega}\cdot\vec{\nabla}\psi^{\dagger}(\vec{r},\vec{\Omega})+\sigma_t(\vec{r})\psi^{\dagger}(\vec{r},\vec{\Omega})-\frac{\sigma_s(\vec{r})}{4\pi}\int_{4\pi}d\Omega'\psi^{\dagger}(\vec{r},\vec{\Omega}')=Q^{\dagger}(\vec{r},\vec{\Omega}),\qquad(20)$$

which can be written concisely as

$$H^{\dagger}\psi^{\dagger}=Q^{\dagger}.\qquad(21)$$

The adjoint source is defined as the difference between the actual and predicted detector response. It is given by

$$Q^{\dagger}(Q)=\sum_{n=1}^{N}\left(\frac{M_{est,n}(Q)-M_n}{M_n}\right).\qquad(22)$$

Recognizing the adjoint source in Eq. 19, it can be rewritten as

$$\begin{aligned}\nabla_x f&=\int_{\Delta V_s}dV_s\int_{4\pi}d\Omega\frac{\partial\psi}{\partial x}Q^{\dagger}\\&=\int_{\Delta V_s}dV_s\int_{4\pi}d\Omega\frac{\partial\psi}{\partial x}H^{\dagger}\psi^{\dagger}.\end{aligned}\qquad(23)$$

Assuming vacuum boundary conditions, the duality principle reads[35]

$$\int_{V}dV\int_{4\pi}d\Omega\psi H^{\dagger}\psi^{\dagger}=\int_{V}dV\int_{4\pi}d\Omega\psi^{\dagger}H\psi.\qquad(24)$$

Using the duality principle, Eq. 23 can be transformed:

$$\nabla_x f = \int_{\Delta V_s} dV_s \int_{4\pi} d\Omega \frac{\partial \psi}{\partial x} H^\dagger \psi^\dagger = \int_{\Delta V_s} dV_s \int_{4\pi} d\Omega \psi^\dagger H \frac{\partial \psi}{\partial x}. \quad (25)$$

If the model parameters such as cross sections or the source position are perturbed, then there will be a change in the flux. Using the chain rule, the change in the transport equation is

$$\delta(H\psi = Q)$$

$$\delta H\psi + H\delta\psi = \delta Q, \text{ or}$$

$$H\delta\psi = \delta Q - \delta H\psi. \quad (26)$$

Using this expression to replace the derivative term in Eq. 25 gives

$$\nabla_x f = \int_{\Delta V_s} dV_s \int_{4\pi} d\Omega \psi^\dagger \left(\frac{\partial Q}{\partial x} - \frac{\partial H}{\partial x}\psi\right). \quad (27)$$

For the source location problem, the cross sections of the system are assumed to be known, so the transport operator H is a constant. Thus, the equation can be further simplified to

$$\nabla_x f = \int_{\Delta V_s} dV_s \int_{4\pi} d\Omega \psi^\dagger \frac{\partial Q}{\partial x}. \quad (28)$$

The source is modeled as a point source with strength q. In three-dimensions, this can be written as

$$\nabla_x f = \int_{\Delta x_s} dx_s \int_{\Delta y_s} dy_s \int_{\Delta z_s} dz_s \int_{4\pi} d\Omega \psi^{\dagger}\left(x, y, z, \vec{\Omega}\right) \frac{\partial}{\partial x} [q\delta(x - x_s)\delta(y - y_s)\delta(z - z_s)] \tag{29}$$

where (x_s, y_s, z_s) is the source position. Evaluating the integrals gives

$$\nabla_x f = \int_{\Delta x_s} dx_s \int_{\Delta y_s} dy_s \int_{\Delta z_s} dz_s \phi^{\dagger}(x, y, z) \frac{\partial}{\partial x} [q\delta(x - x_s)\delta(y - y_s)\delta(z - z_s)]$$

$$= q \int_{\Delta x_s} dx_s \int_{\Delta y_s} dy_s \int_{\Delta z_s} dz_s \phi^{\dagger}(x, y, z)\delta(y - y_s)\delta(z - z_s) \frac{\partial}{\partial x} [\delta(x - x_s)]$$

$$= q \int_{\Delta x_s} dx_s \phi^{\dagger}(x, y_s, z_s) \frac{\partial}{\partial x} [\delta(x - x_s)]. \tag{30}$$

To evaluate the integral involving the derivative of a delta function, integrate by parts using the following relationship:

$$\int_{x_s - \varepsilon}^{x_s + \varepsilon} dx_s \frac{d}{dx} [\delta(x - x_s)] f(x) = -\left.\frac{df(x)}{dx}\right|_{x = x_s}. \tag{31}$$

Thus, the gradient of the least-squares functional with respect to x is

$$\nabla_x f = -q \left.\frac{\partial \phi^{\dagger}(x, y_s, z_s)}{\partial x}\right|_{x = x_s}. \tag{32}$$

The gradient of the functional with respect to the y-position, z-position, and source strength q are derived using the same steps. The resultant equations are

$$\nabla_y f = -q \left. \frac{\partial \phi^\dagger(x_s, y, z_s)}{\partial y} \right|_{y=y_s}, \tag{33}$$

$$\nabla_z f = -q \left. \frac{\partial \phi^\dagger(x_s, y_s, z)}{\partial z} \right|_{z=z_s}, \tag{34}$$

and

$$\nabla_q f = \phi^\dagger(x_s, y_s, z_s). \tag{35}$$

These equations are used in a gradient method to minimize the least-squares functional and identify the source location.

II.D. Penalty Terms

It is well known that inverse problems are ill-posed, meaning they are sensitive to small perturbations in input data resulting from experimental uncertainty or a lack of data.[36] In other words, there are too many degrees of freedom and there may not be a unique solution. If *a priori* information about the problem can be quantified into a solution method, it can be very useful in constraining the solution. For example, consider the problem of fitting a line to a set of measurements. If there was only one data point as shown in Fig. 6(a), the problem would be ill-posed; however, if *a priori* it was known that the line passed through the origin, then a line could be fit as seen in Fig. 6(b).

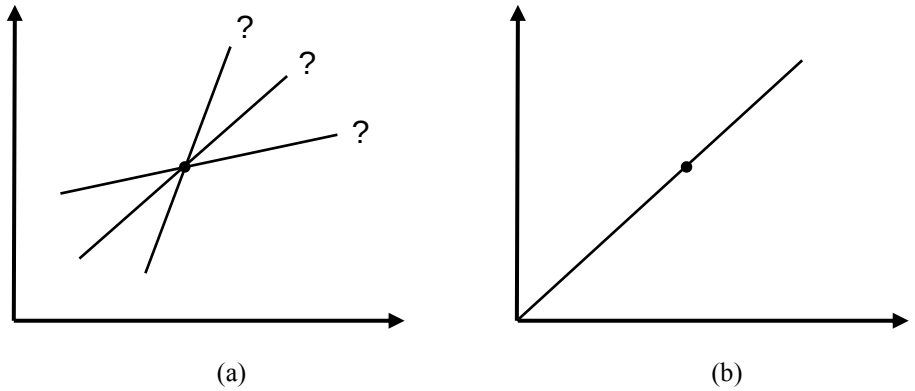

Fig. 6. (a) Ill-posed line-fitting problem and (b) use of *a priori* information.

Using penalty terms is a way to provide supplemental constraints on the solution space. Penalty terms are often incorporated into the solution mechanism as an additional term in the objective function. Chapter III explains how we use a penalty term to constrain the solution for the border application problem.

CHAPTER III

SOLUTION METHOD

III.A. Overview

The first step in the objective function minimization scheme is to understand the problem setup. For this problem, it is assumed that the geometry and material properties are known. The actual detector measurements are also known. The unknowns are the source location and source strength. To obtain the estimated detector measurements, we will choose a guess for the source information and solve for the scalar flux in the detectors. This guess will be updated via the steepest descent method until the objective function is minimized to a value below the convergence tolerance.

To minimize the objective function, we must be able to solve the neutron transport equation. This is the forward problem. One approach is to solve using a Monte Carlo method. This class of methods tracks particle histories through a medium by simulating the random nature of interactions.[37] While Monte Carlo methods are useful for many applications, the source location problem is not one of them. One of the objectives of this research is to locate the source quickly, and Monte Carlo solution methods are too time intensive. Another approach is to solve the transport equation using a deterministic method. To do this, the continuous information contained in the exact solution is replaced by discrete values, and the calculus problem is transformed into an algebra

problem. The flux is solved for at a number of finite locations called grid points. As the number of grip points gets large, the numerical solution is expected to approach the exact solution. Deterministic problems can generally be solved quickly, making them more suitable for the border security application.

The solution to the neutron transport equation is used to calculate estimated detector responses. The estimated detector responses are then used to solve the inverse problem. To find the source location that minimizes the difference between the estimated and actual detector response, we could test the source location at each grid point, but in a system with tens of thousands of cells, this method quickly becomes infeasible due to the time constraints. Instead, we make an initial guess of the source location and let the gradient of the objective function point us in the right direction.

III.B. Angular Discretization

Recall the steady-state, mono-energetic neutron transport equation with isotropic scattering:

$$\vec{\Omega} \cdot \vec{\nabla}\psi(\vec{r},\vec{\Omega}) + \sigma_t(\vec{r})\psi(\vec{r},\vec{\Omega}) - \frac{\sigma_s(\vec{r})}{4\pi}\int_{4\pi} d\Omega'\psi(\vec{r},\vec{\Omega}') = Q(\vec{r},\vec{\Omega}). \qquad (36)$$

The scalar flux is calculated by integrating the angular flux over 4π. To do this numerically, the angular variable is broken up into a number of discrete directions as shown by

$$\phi(\vec{r}) = \int_{4\pi} d\Omega\psi(\vec{r},\vec{\Omega}) \cong \sum_{m=1}^{M} w_m\psi(\vec{r},\Omega_{\mathrm{m}}). \tag{37}$$

The integral over the direction variable is replaced by a quadrature sum with quadrature weights w_m. This is called the discrete ordinates (S_N) method. Letting $\psi(\vec{r},\Omega_{\mathrm{m}}) = \psi_m(\vec{r})$,

$$\vec{\Omega}\cdot\vec{\nabla}\psi_m(\vec{r}) + \sigma_t(\vec{r})\psi_m(\vec{r}) - \frac{\sigma_s(\vec{r})}{4\pi}\sum_{m=1}^{M} w_m\psi_m(\vec{r}) = Q_m(\vec{r}), \tag{38}$$
$$m = 1 \ldots M.$$

The S_N method transforms the integro-differential transport equation into a set of M differential equations.

The quadrature set is chosen based on the application. For this research, we used the level symmetric quadrature set.[38] The angle vector $\vec{\Omega}$ is defined by (μ,η,ξ) coordinates. The quadrature is completely symmetric, meaning that the (μ,η,ξ) coordinates are invariant under all 90^{o} rotations.[39]

III.C. Spatial Discretization

The M differential equations derived by discretizing the angular variable also need to be discretized spatially. This involves superimposing a Cartesian mesh onto the system and

rewriting the equations to be consistent with the mesh. The following shows the equations written out in longhand:

$$\mu\frac{\partial\psi_m(x,y,z)}{\partial x}+\eta\frac{\partial\psi_m(x,y,z)}{\partial y}+\xi\frac{\partial\psi_m(x,y,z)}{\partial z}+\sigma_t(x,y,z)\psi_m(x,y,z)$$
$$-\frac{\sigma_s(x,y,z)}{4\pi}\sum_{m=1}^{M}w_m\psi_m(x,y,z)=Q_m(x,y,z),\qquad m=1\ldots M. \tag{39}$$

The discretized equations are derived by making approximations to the derivative terms using Taylor series expansions. Consider the grid shown in Fig. 7 for cell i with edges $i-\frac{1}{2}$ and $i+\frac{1}{2}$ and width Δx.

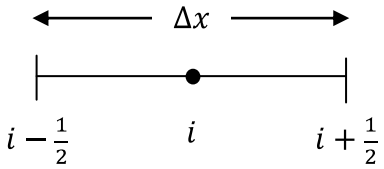

Fig. 7. Example grid for Taylor series expansion.

The Taylor series expansions of a function about i evaluated at $i+\frac{1}{2}$ and $i-\frac{1}{2}$ are given by[40]

$$f_{i+\frac{1}{2}}=f_i+f_i'\left(\frac{\Delta x}{2}\right)+\frac{1}{2}f_i''\left(\frac{\Delta x}{2}\right)^2+\frac{1}{6}f_i'''\left(\frac{\Delta x}{2}\right)^3+\cdots \tag{40}$$

$$f_{i-\frac{1}{2}}=f_i+f_i'\left(-\frac{\Delta x}{2}\right)+\frac{1}{2}f_i''\left(-\frac{\Delta x}{2}\right)^2+\frac{1}{6}f_i'''\left(-\frac{\Delta x}{2}\right)^3+\cdots \tag{41}$$

Subtracting the two equations, solving for f_i' , and truncating the Taylor series gives

$$f_i' = \frac{f_{i+\frac{1}{2}} - f_{i-\frac{1}{2}}}{\Delta x} + \sigma(\Delta x^2). \tag{42}$$

This is the centered-difference approximation of the derivative of f at i. The truncation error is second order and depends on the step size Δx. As the step size decreases, the truncation error decreases with Δx^2.

Substituting the centered-difference approximation into the transport equation produces a set of finite difference equations. For the three-dimensional case, the mesh is divided into (i, j, k) coordinates with cell widths of Δx, Δy, and Δz. The cross sections are assumed to be piecewise constant, changing values at cell edges only. The angular fluxes that are incoming and outgoing from a cell are defined as follows for μ and similarly for η and ξ:

$$\begin{aligned} \psi_{i_{inc}} &= \psi_{i-\frac{1}{2}}, \qquad \mu > 0 \\ \psi_{i_{inc}} &= \psi_{i+\frac{1}{2}}, \qquad \mu < 0 \\ \psi_{i_{out}} &= \psi_{i+\frac{1}{2}}, \qquad \mu > 0 \\ \psi_{i_{out}} &= \psi_{i-\frac{1}{2}}, \qquad \mu < 0. \end{aligned} \tag{43}$$

The fully discretized transport equation is given by

$$\mu \frac{\psi_{i_{out},j,k,m} - \psi_{i_{inc},j,k,m}}{\Delta x} + \eta \frac{\psi_{i,j_{out},k,m} - \psi_{i,j_{inc},k,m}}{\Delta y}$$

$$+ \xi \frac{\psi_{i,j,k_{out},m} - \psi_{i,j,k_{inc},m}}{\Delta z} + \sigma_{t,i,j,k}\psi_{i,j,k,m} \tag{44}$$

$$- \frac{\sigma_{s,i,j,k}}{4\pi} \sum_{m=1}^{M} w_m \psi_{i,j,k,m} = Q_{i,j,k,m}, \qquad m = 1 \dots M.$$

By discretizing the angular and spatial variables, the calculus problem is transformed into an algebra problem that can be solved using numerical methods.

III.D. Solving the Forward Problem

The discrete transport equation can be solved iteratively using source iteration.[41] Recall the operator notation for the transport equation from Chapter II:

$$H\psi = Q. \tag{45}$$

The transport operator H can be broken into its loss component L (streaming and collision) and its scattering component S:

$$H = L - S. \tag{46}$$

Source iteration has the following iteration scheme:

$$L\psi^{(\ell+1)} = S\psi^{(\ell)} + Q, \qquad \ell \geq 1 \tag{47}$$

where ℓ denotes the iteration number. Source iteration works by introducing the "old" estimate of the scalar flux on the right-hand side of the equation at each iteration. The "new" value for the angular flux is used to update the scalar flux with the relationship

$$\phi(\vec{r}) = \int_{4\pi} d\Omega \psi(\vec{r}, \vec{\Omega}). \tag{48}$$

The process is repeated until the difference between successive fluxes is less than the convergence criteria.

To solve the forward problem, we must make another approximation to the discretized transport equation. Eq. 44 contains both cell-centered angular fluxes and edge values of angular flux. The incoming fluxes are known from the boundary conditions, which in this application, are vacuum boundary conditions. We will solve for the cell-centered angular flux, so an auxiliary relationship is used to eliminate the outgoing flux. The most commonly used auxiliary relationship is the diamond difference approximation, but it can lead to negative flux values. To guarantee no negative fluxes, a method such as the step difference approximation can be used. The step difference approximation for the i component, is given by

$$\psi_{i_{out}} = \psi_i. \tag{49}$$

Substituting the step difference approximation into Eq. 44 gives the following:

$$\mu\frac{\psi_{i,j,k,m}-\psi_{i_{inc},j,k,m}}{\Delta x}+\eta\frac{\psi_{i,j,k,m}-\psi_{i,j_{inc},k,m}}{\Delta y}+\xi\frac{\psi_{i,j,k,m}-\psi_{i,j,k_{inc},m}}{\Delta z}$$

$$+\sigma_{t,i,j,k}\psi_{i,j,k,m}-\frac{\sigma_{s,i,j,k}}{4\pi}\sum_{m=1}^{M}w_m\psi_{i,j,k,m}=Q_{i,j,k,m}, \qquad (50)$$

$$m=1\ldots M.$$

Two additional simplifications are made to this equation. First, the angular flux in the scattering term can be replaced by the scalar flux. Second, the source for this application is assumed to be isotropic. The angularly-dependent source $Q_{i,j,k,m}$ can be replaced by the isotropic source $q_{i,j,k}$ to yield

$$\mu\frac{\psi_{i,j,k,m}-\psi_{i_{inc},j,k,m}}{\Delta x}+\eta\frac{\psi_{i,j,k,m}-\psi_{i,j_{inc},k,m}}{\Delta y}+\xi\frac{\psi_{i,j,k,m}-\psi_{i,j,k_{inc},m}}{\Delta z}$$

$$+\sigma_{t,i,j,k}\psi_{i,j,k,m}-\frac{\sigma_{s,i,j,k}}{4\pi}\phi_{i,j,k}=q_{i,j,k}, \qquad m=1\ldots M. \qquad (51)$$

Rearranging to solve for $\psi_{i,j,k,m}$ gives the following:

$$\psi_{i,j,k,m}=\frac{\frac{\mu}{\Delta x}\psi_{i_{inc},j,k,m}+\frac{\eta}{\Delta y}\psi_{i,j_{inc},k,m}+\frac{\xi}{\Delta z}\psi_{i,j,k_{inc},m}+\frac{\sigma_{s,i,j,k}}{4\pi}\phi_{i,j,k}+q_{i,j,k}}{\sigma_{t,i,j,k}+\frac{\mu}{\Delta x}+\frac{\eta}{\Delta y}+\frac{\xi}{\Delta z}}, \qquad (52)$$

$$m=1\ldots M.$$

In this form, everything on the right-hand side is known and the cell-centered angular flux can be solved for directly. We know the "old" scalar flux from the previous

iteration. Also, all incoming angular fluxes are known from the vacuum boundary conditions.

III.E. Solving the Inverse Problem

The forward model predicts a set of measurements for a given source position. In the inverse model, an objective function is defined that describes the difference between the actual and predicted measurements. Least-squares methods are based on the premise that the residual at the solution is small. Recall from Chapter II that a weighted least-squares optimization problem has the form

$$\text{minimize } f(s) = \|W(As - b)\|_2^2. \tag{53}$$

In this case, the optimization problem is

$$\text{minimize } f(Q) = \frac{1}{2}\left\|\frac{M_{est}(\mathrm{Q}) - M}{M}\right\|_2^2. \tag{54}$$

In this form, the coefficient matrix A is equal to the identity matrix; however, it is not a trivial problem. It is a nonlinear problem because the estimated measurements are a function of the source position, which is also the unknown parameter. The residual is defined as the value of $f(Q)$.

For the arbitrary detector, we assume that the measurements are proportional to the scalar flux in the detector. While we do have an expression for the Fréchet derivative of the objective function with respect to the source strength q, we devised an alternative to solving for the source strength. Because we are comparing the measurements of an array of detectors, the response pattern should be the same regardless of the source strength. To exploit this, we normalize the actual and predicted measurements before comparing them. This eliminates the need to know the source strength.

The general minimization algorithm is given by the following:

Given a starting point $x \in dom(f)$
Repeat
1. Determine a descent direction $\nabla f(x)$
2. Line search
3. Update $x : x + \alpha \nabla f(x)$

Until the stopping criteria is met

To minimize the objective function, the first step is to take the gradient with respect to the unknown parameter. Then, perform a line minimization in the negative direction of the gradient. Once the new minimum along the line is found, a new gradient at that position is calculated. This is repeated until the convergence criteria are met. The remainder of this section will discuss the specifics of the algorithm.

The adjoint flux is calculated using the same mesh and source iteration solver as the forward transport problem. The difference is that instead of the driving term being the

actual radioactive source, it is the residual of the objective function evaluated at each detector position:

$$Q^{\dagger}(Q) = \sum_{n=1}^{N} \left(\frac{M_{est,n}(Q) - M_n}{M_n} \right). \tag{55}$$

The gradient terms were derived in Chapter II and given by Eq. 32-34. The source strength is not used, so it is set equal to one ($q = 1$) in the derivative terms. The gradient is calculated by taking finite differences of the adjoint flux.

Because the unknown parameter is the source position and the spatial dimension is broken up into discrete values, the unit step size is naturally suited to be the cell width. For the line search, the residual is calculated for each cell in the direction of steepest descent. The cell with the minimum residual value is used as the estimated source position to calculate the next gradient. The minimization is a function of three unknown variables: x-, y-, and z-direction. The line searches alternate between the three directions. Once the minimum x-value is calculated along a line, the new gradient is calculated at that point and a line search is performed in the y-direction. Similarly, the minimum y-value is found along that line before moving on to the z-direction.

III.F. Initial Guess

An ill-posed optimization problem is one that does not have a well-defined global minimum. This can be due to the existence of several local minima or to a global minimum surrounded by other possible solutions that result in almost identical residuals. The border application is an ill-posed problem and thus has a strong dependence on the initial guess for source position.

Heurisitic techniques are often employed to determine an initial guess. These are techniques that are based on experimentation or trial-and-error methods. One technique that was explored was to triangulate the position of the source given the actual measurements while assuming a vacuum. Fig. 8 illustrates the triangulation concept. While computationally efficient, this technique was however abandoned due to erroneous results for certain detector configurations.

Instead, a different heuristic approach was used to acquire an initial guess for the source position. The spatial mesh was divided such that one coarse region was used per vehicle. A forward transport problem was run for each region with the source located in the center of the region. The residuals calculated at each position were then ranked in ascending order. The position with the smallest residual was used as the initial guess. The minimization scheme was given a user-specified number of iterations to converge before jumping to the vehicle with the next smallest residual.

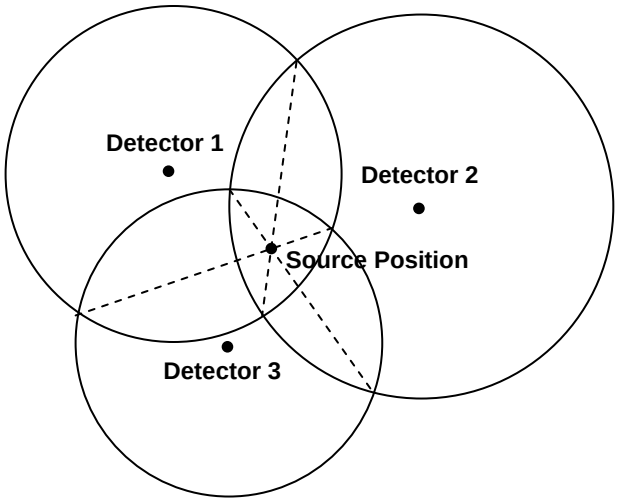

Fig. 8. Triangulation concept.

Furthermore, if the residual calculated in the initial guess algorithm is more than five times that of the smallest residual, then that region is eliminated as a feasible solution. This helps save computational time by not allowing the code to spend time in areas that are highly unlikely to be the source position. A scenario where this is a useful feature is when the modeling error is such that the residual at the actual source position is larger than the convergence tolerance. If no position falls below the tolerance after all of the plausible vehicles are investigated, then a "best guess" solution is returned. Of all the positions investigated, this is the one that produced the smallest residual.

The approach that was chosen represents a very accurate method of obtaining the initial guess but is less computationally efficient than the triangulation method. If the computational time associate with the method is too big in practice, there are several

intermediate approaches that could be used. Alternatives could include using a coarser grid for the initial guess than is used for the minimization or even using ray tracing through a homogeneous (or vacuum) space. These approaches represent a compromise between computational time and accuracy.

III.G. Penalty Term

Penalty terms quantify *a priori* information about the problem to provide supplemental constraints on the solution space. Often, they are incorporated into the solution mechanism as an additional term in the objective function. We used a variation on the typical penalty term to constrain the solution to only the cells contained within a vehicle as opposed to the air space or concrete floor. Instead of adding a term to the objective function, the penalty term was incorporated simply by adding a cross-section check during the line search. As the line minimization runs along a line, it will stop when it gets to a cell with the cross section of air or concrete. This constrains the line minimization to a vehicle, thus saving an enormous amount of computational effort. If the residual does not meet the convergence criteria inside a given vehicle after a preassigned number of iterations, then the solver jumps to the next most likely vehicle.

III.H. Convergence Criteria

The convergence criterion on the objective function signals when the steepest descent method should stop. The objective function is defined as the relative difference between the actual and estimated detector measurements, so the convergence criterion is the acceptable difference between the measured and simulated detector signals.

In the real-world application of the code, there will be modeling uncertainties associated with the geometric and material properties of the vehicles (i.e., the optical thickness of each vehicle, the amount of gasoline in the gas tank, the physical size of each vehicle, etc.) as well as the efficiency of the detectors and statistical error in the counts. In addition, there will be computational error based on the size of the spatial mesh. Minimizing the computational time is an important aspect of the real-world application of the code, so there must be a balance between the accuracy of the solution and the time it takes to converge. Given the potential for large uncertainties in modeling parameters, the convergence goal is simply to identifying the correct vehicle. Given perfect knowledge of the geometry and cross sections and with unlimited time, it is likely possible to identify the exact position of the source within the vehicle given very good measurement statistics.

The convergence criterion is the sum of two independent contributions. The first represents the maximum tolerance to reliably identify the correct vehicle given perfect

knowledge about the model parameters. This quantity is empirically derived using a series of test cases that approximate a real-world scenario. The second contribution to the convergence criterion is a value based on the assumed uncertainty in the model. The total represents the maximum-allowable percent difference in the actual and estimated measurements.

III.I. The Full Algorithm

Pulling together the forward and inverse models along with the initial guess, Fig. 9 shows a flowchart with the full source location algorithm. The source code for the full algorithm is given in Appendix D. The algorithm steps are the following:

1. The algorithm begins when a source is detected and the model parameters (i.e., material and geometry of the system) are determined.
2. Next, the computational system setup is performed. This includes steps such as reading the input files containing the model parameters and measurements, allocating arrays, and creating the mesh.
3. After that, the initial guess algorithm is run.
4. Once the initial guess is determined, the code moves onto the forward model. The initial guess for the source position is run through the forward transport solver to give the estimated detector measurements.
5. The estimated detector measurements are compared to the actual detector measurements using the least-squares objective function. If the relative

difference is less than the specified convergence tolerance, then the source location has been identified. If it is larger than the convergence tolerance, then the code moves onto the inverse model.

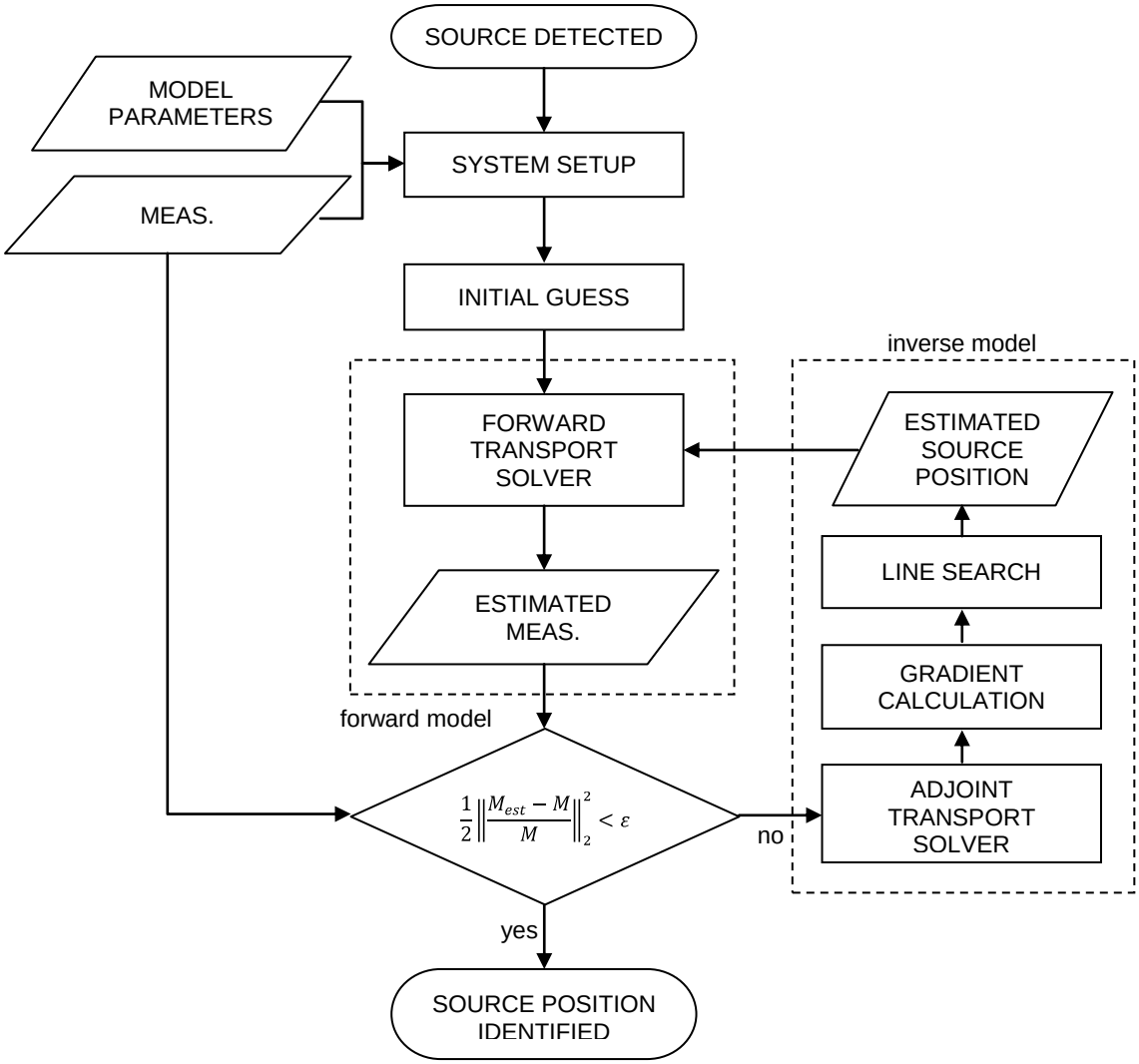

Fig. 9. Flowchart showing the full source location algorithm.

6. In the inverse model, the adjoint transport solver calculates the adjoint flux in the system. The value of the objective function at each detector location is the inhomogeneous source term.
7. The gradient of the objective function with respect to the quantity of interest—the x-, y-, and z-position of the source—is calculated using the adjoint flux.
8. Once the gradient is calculated, the code performs a line search in either the x-, y-, or z-direction. The line search identifies a new estimated source position.
9. The code now returns to the forward model. The new estimated source position is used in the forward model to produce a new set of estimated detector measurements.
10. This process is iterated until the convergence criteria are met.

There are also nuances within some of the steps. For instance, if the source position has not been identified after five x-y-z iterations, then the estimated source position jumps to the next most likely region identified in the initial guess algorithm. The same process is repeated until either the relative difference between estimated and actual measurements is less than the convergence tolerance or the system runs out of plausible solution regions. Throughout the iteration process between forward and inverse models, the source location that resulted in the absolute minimum residual is stored. If the code investigates all plausible solution regions with converging, then the estimated source position that produced the absolute minimum residual is identified as the most likely source position.

CHAPTER IV

FORWARD CODE RESULTS

IV.A. Introduction

To verify that the 3-D forward transport solver works correctly, a series of test problems were compared to problems run using PARTISN.[42] PARTISN is a deterministic S_N transport code developed at Los Alamos National Laboratory. It can solve the neutral-particle transport equation on a number of grid types, including a 3-D Cartesian grid. The spatial discretization used for the test problems was diamond difference with a fix-up to eliminate negative fluxes. The angular variable was discretized using a Gauss Legendre (P_8) quadrature.

Five cases were chosen to test the code under a variety of different conditions. The five test cases were:

1. A distributed source with average cross sections (i.e., in a medium with no strong absorbers or highly scattering materials),
2. A point source (i.e., a distributed source in only one cell) with average cross sections,
3. A point source in a highly scattering medium,
4. A point source in a strongly absorbing medium, and
5. A point source in a near vacuum.

For each of the test cases, the system was 18 cm×18 cm×18 cm with 15 cells per side. Although this is significantly smaller in scale than the portal monitor applications, the forward model tests are merely show that the forward code is functioning as expected. The source strength was 19.82 n/cm^3-sec. All cases had homogeneous cross sections and vacuum boundary conditions. The test cases were all 3-D, but the results shown are 1-D and 2-D slices through the geometry. Fig. 10 shows the geometry of the system with the origin at $(x, y, z) = (0,0,0)$. A sample PARTISN input deck is included in Appendix B.

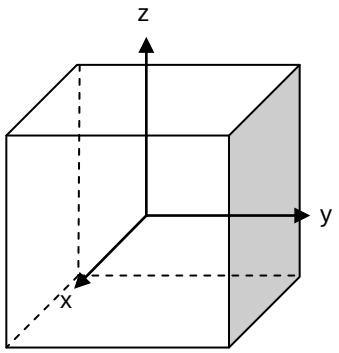

Fig. 10. Forward test problem geometry and origin.

IV.B. Test Problem 1

The first test problem was a distributed source problem with average cross sections. The cross sections and scattering ratio, c, used are given in Table 1.

Table 1. Forward Test Problem 1 Material Properties.

σ_s	0.085 cm^{-1}
σ_t	0.097 cm^{-1}
c	0.876

Fig. 11 shows plots of the scalar flux in the x- and y-directions outputted from both PARTISN and the forward model code for the mid-plane of the test problem in the z-direction. Fig. 12 shows a plot of the scalar flux in the x-direction along $y = 0$ and $z = 0$. Also shown in Fig. 12 is the analytical diffusion solution, which is hyperbolic cosine shaped. Generally good agreement is found between PARTISN and the forward model code. The peak flux differs by 4% with PARTISN slightly overestimating the peak flux and the forward model code slightly underestimating the peak flux. Differences in the results are from differences in the solution mechanism used by each code (i.e., quadrature set, spatial approximations, etc.).

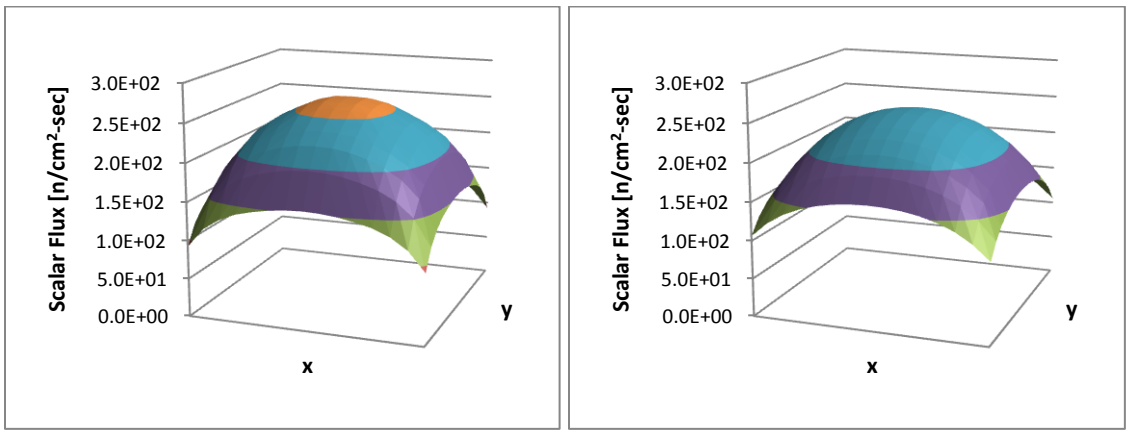

(a) (b)

Fig. 11. Scalar flux surface plots for forward test problem 1 showing (a) PARTISN and (b) forward code results.

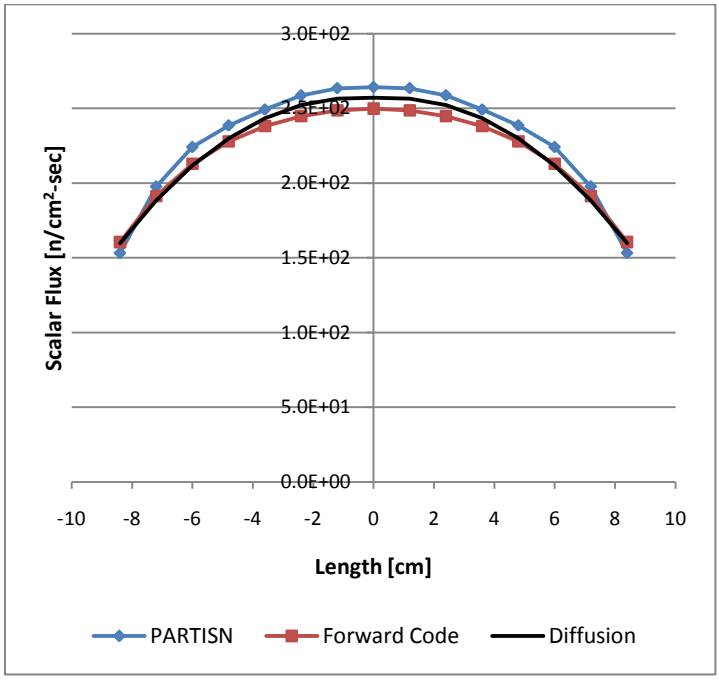

Fig. 12. 1-D scalar flux plot for forward test problem 1.

IV.C. Test Problem 2

Test problems 2-5 all contained a point source in the center of the cube rather than a distributed source, and they differed in the cross sections used. The results were normalized such that the peak scalar flux is equal to unity. The normalization better shows small differences in the flux shape. Recall that the forward code results and actual measurements were normalized in the inverse algorithm for comparison, which eliminates the need to solve for source strength.

Test problem 2 was very similar to test problem 1. The cross sections used as the same as those given in Table 1. Fig. 13 shows surface plots of the scalar flux through the $z = 0$ mid-plane for both PARTISN and the forward model code. Both plots show the flux at a maximum in the center where the point source is located with a sharp drop-off moving away from the center, which generally agrees with our intuition.

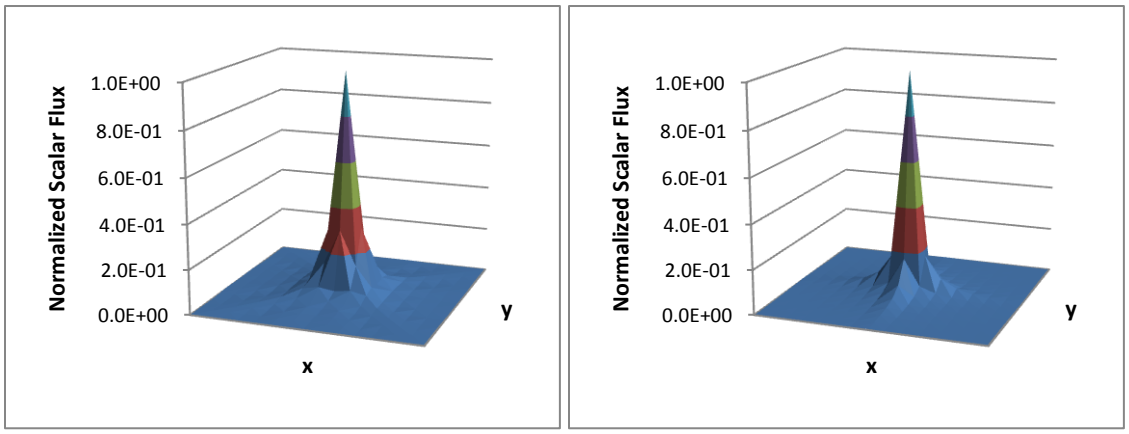

(a) (b)

Fig. 13. Scalar flux surface plots for forward test problem 2 showing (a) PARTISN and (b) forward code results.

Fig. 14 shows the scalar flux in the x-direction for $y = 0$ and $z = 0$. The PARTISN results are slightly higher than the forward model code just beyond the center peak, but the two codes generally agree well throughout the rest of the domain. Fig. 15 shows the same data on a semi-log plot.

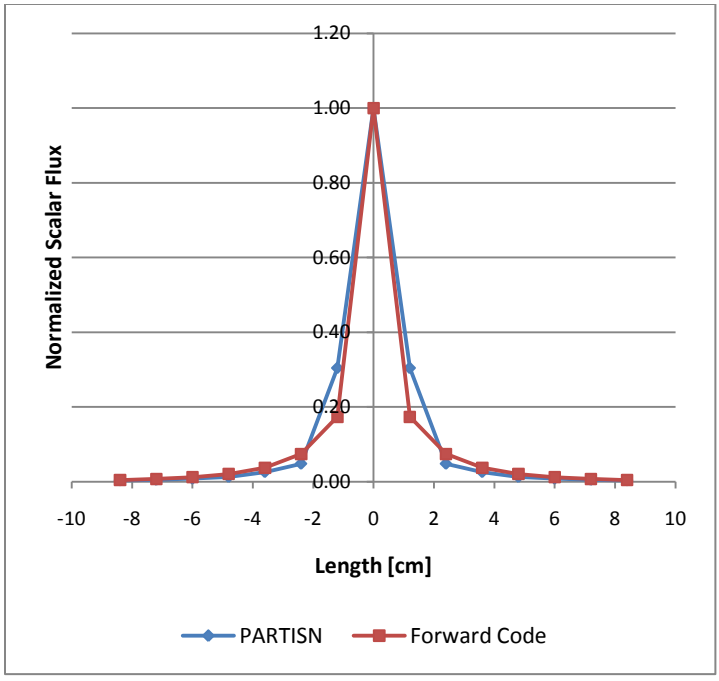

Fig. 14. 1-D scalar flux plot for forward test problem 2.

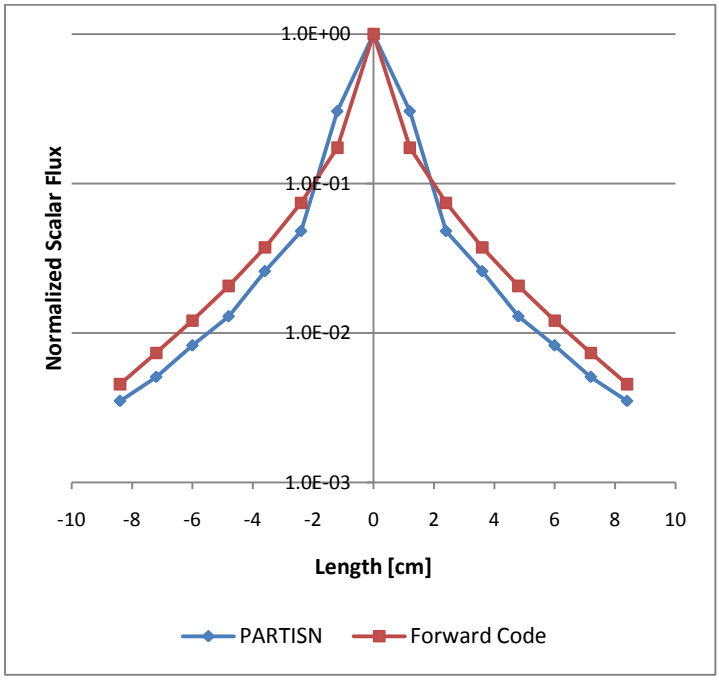

Fig. 15. 1-D scalar flux plot for forward test problem 2 on a semi-log plot.

IV.D. Test Problem 3

In the remaining forward test problems, the surface plots were omitted because of the similarity to Fig. 13. Test problem 3 was a point source within a highly scattering medium. The cross sections and scattering ratio used are given in Table 2. Here, the scattering ratio was increased from 0.876 for the case of average cross sections to 0.986 in this case. The total cross section was also increased by approximately an order of magnitude.

Table 2. Forward Test Problem 3 Material Properties.

σ_s	1.884 cm^{-1}
σ_t	1.910 cm^{-1}
c	0.986

Fig. 16 shows the scalar flux in the x-direction for $y = 0$ and $z = 0$. Again, the data is shown on a semi-log plot in Fig. 17. As in test problem 2, there is a distinctive peak in the center of the plot where the source is located. Also, the PARTISN results are higher near the peak but fit well with the forward code results away from the center of the plot. Finally, even with a significantly larger total cross section compared to test problem 2, we can see that the width of the peak is still larger in Fig. 16 than in Fig. 14 due to an increased scattering ratio.

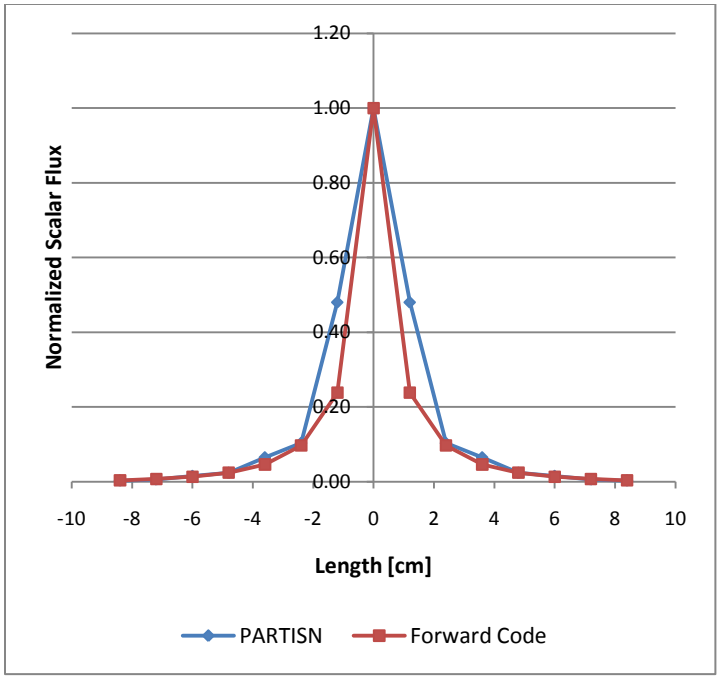

Fig. 16. 1-D scalar flux plot for forward test problem 3.

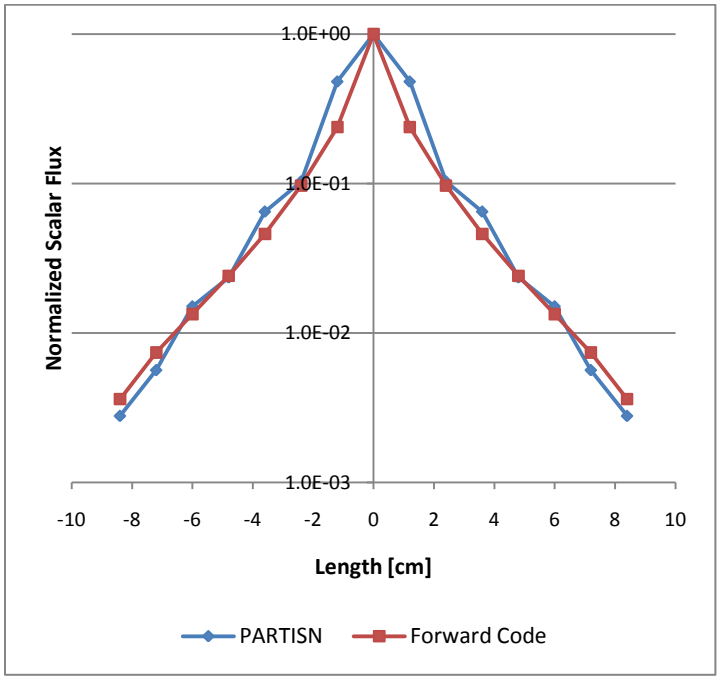

Fig. 17. 1-D scalar flux plot for forward test problem 3 on a semi-log plot.

IV.E. Test Problem 4

Forward test problem 4 was a point source in a strongly absorbing medium. The cross sections used are given in Table 3. In this case, the scattering ratio was 0.300.

Table 3. Forward Test Problem 4 Material Properties.

σ_s	0.666 cm^{-1}
σ_t	2.221 cm^{-1}
c	0.300

Fig. 18 shows the scalar flux in the x-direction for $y = 0$ and $z = 0$. As expected, the peak is narrower than in the other test cases due to a relatively high absorption cross section. With what is shown in Fig. 18, PARTISN and the forward code appear to have excellent agreement. However, this is only because the results are difficult to visualize on a linear scale. When viewed on a semi-log scale (as shown in Fig. 19), it is clear that the scalar flux calculated using PARTISN does not decrease exponentially with distance from the source as is expected for a strongly absorbing medium. This is because one of the default settings in PARTISN is to solve the transport equation using diffusion synthetic acceleration (DSA), which can degrade in performance for extreme cases of non-diffuse problems such as test problem 4. The problem was run a second time using PARTISN but with DSA turned off. The results are shown on a semi-log scale in Fig. 19. The non-accelerated PARTISN solution shown in green matches the exponential fall off of the forward code closely. The DSA solution is shown in blue.

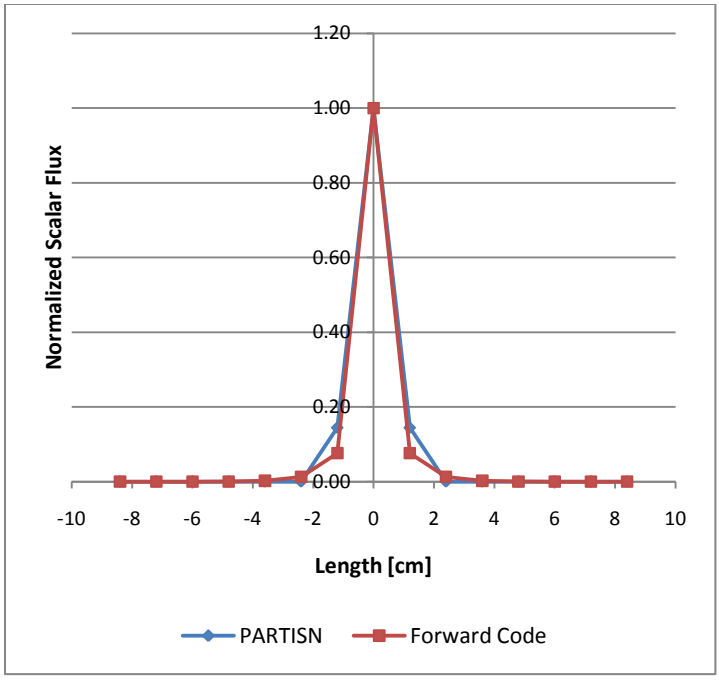

Fig. 18. 1-D scalar flux plot for forward test problem 4.

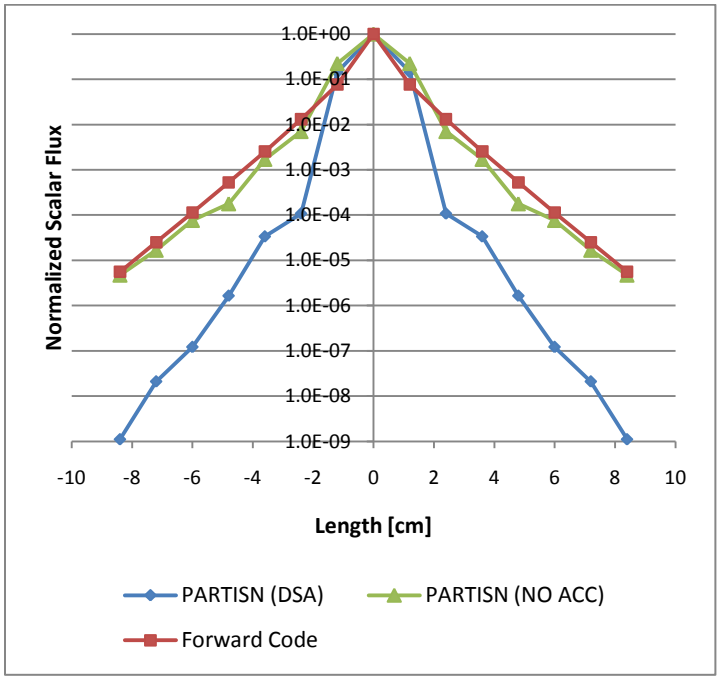

Fig. 19. 1-D scalar flux plot for forward test problem 4 showing PARTISN results using both DSA and no acceleration.

IV.F. Test Problem 5

The final forward test case is a point source in a near-vacuum medium. The cross sections are given in Table 4. In this case, the total cross section is three orders of magnitude small than in the average case (test problems 1 and 2).

Table 4. Forward Test Problem 5 Material Properties.

σ_s	7.50E-05 cm^{-1}
σ_t	8.57E-05 cm^{-1}
c	0.875

The results are shown in Fig. 20. As seen in the plot, there seems to be good agreement between the PARTISN and forward code results; however, examination of the results on a semi-log plot shows otherwise. Again, we ran the problem in PARTISN with DSA turned off, yielding the additional curve in Fig. 21. The PARTISN solution approaches zero faster than the forward code, but overall, the two codes match very well when PARTISN is run without acceleration.

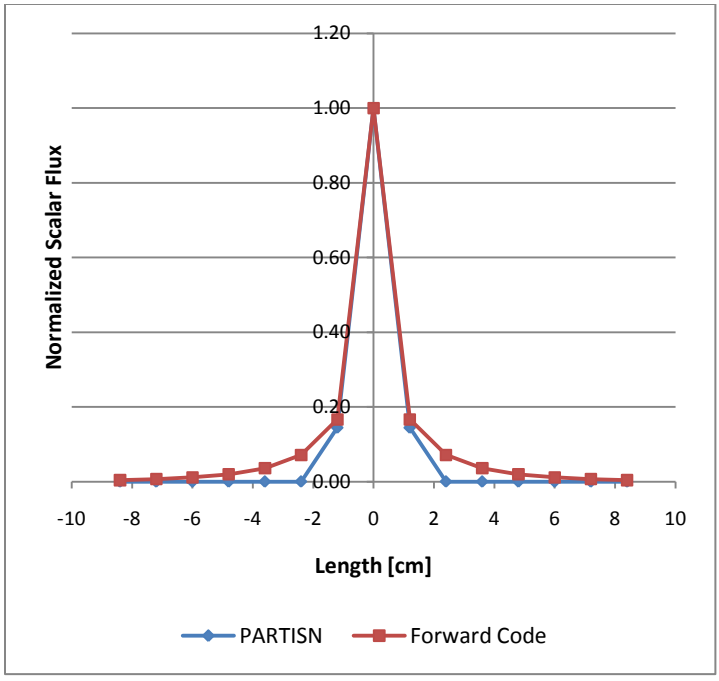

Fig. 20. 1-D scalar flux plot for forward test problem 5.

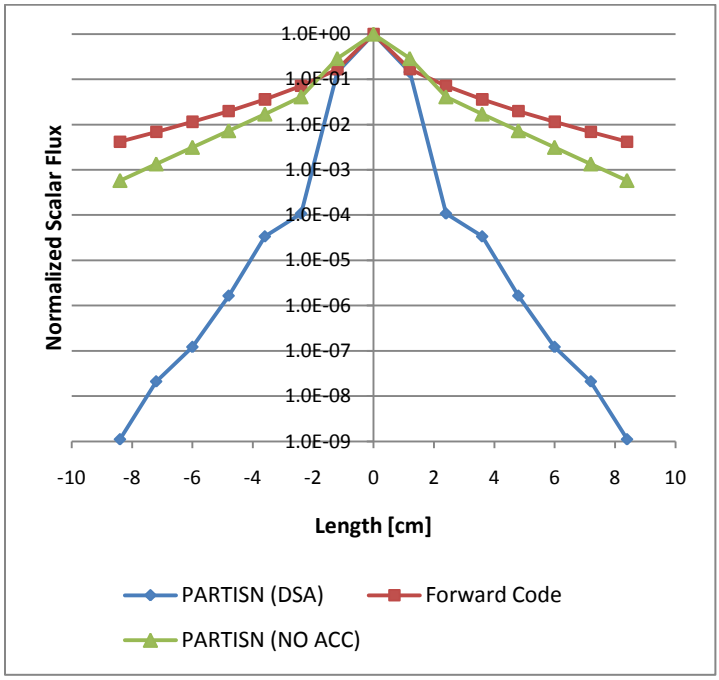

Fig. 21. 1-D scalar flux plot for forward test problem 5 showing PARTISN results using both DSA and no acceleration.

IV.G. Summary of Forward Model Verification

In this chapter, the 3-D forward transport code was verified using PARTISN as well as analytical results where appropriate. Five test problems were run using both codes. The problems were chosen to test the forward code under a wide variety of source and material property configurations.

In test problem 1, it was shown that the magnitude of the scalar flux calculation was reasonably close to the magnitude calculated with PARTISN and the homogeneous, distributed source problem was cosine-shaped, as expected. The forward code results for test problems 2-5 displayed good agreement with PARTISN for average, highly scattering, near vacuum, and especially strongly absorbing cross sections. Because of the overall concordance between the two codes, it can be concluded that the forward code is functioning correctly.

CHAPTER V

INVERSE CODE RESULTS

V.A. Model Parameters

The model setup for the inverse code included creating both the geometry and cross section sets for a border crossing. Instead of starting with a Cartesian mesh and assigning cross sections to each cell, the geometry was first modeled using MCNPX. MCNPX is a general Monte Carlo radiation transport code developed at Los Alamos National Laboratory.[43] To test the inverse code, a baseline model was created to approximate a typical border crossing. A sample MCNPX input deck is given in Appendix C. We tested the code on the baseline model and then made perturbations to the baseline model to analyze the sensitivity of the code to parameters with uncertainty such as the optical thickness of the vehicles and the detection efficiency of the portal monitors.

The baseline model consisted of three lanes of traffic, three vehicles deep, for a total of nine vehicles. Each lane has one portal monitor. A 3-D rendering of the MCNPX model is shown in Fig. 22. Each vehicle was divided into four compartments: the engine block, the passenger cabin, the windows, and the trunk. This is shown in Fig. 23. The gasoline tank in the vehicle was located at the bottom of the trunk. The vehicle shown has 16-gallons of gasoline and rubber tires. A list of materials is given in Table 5.

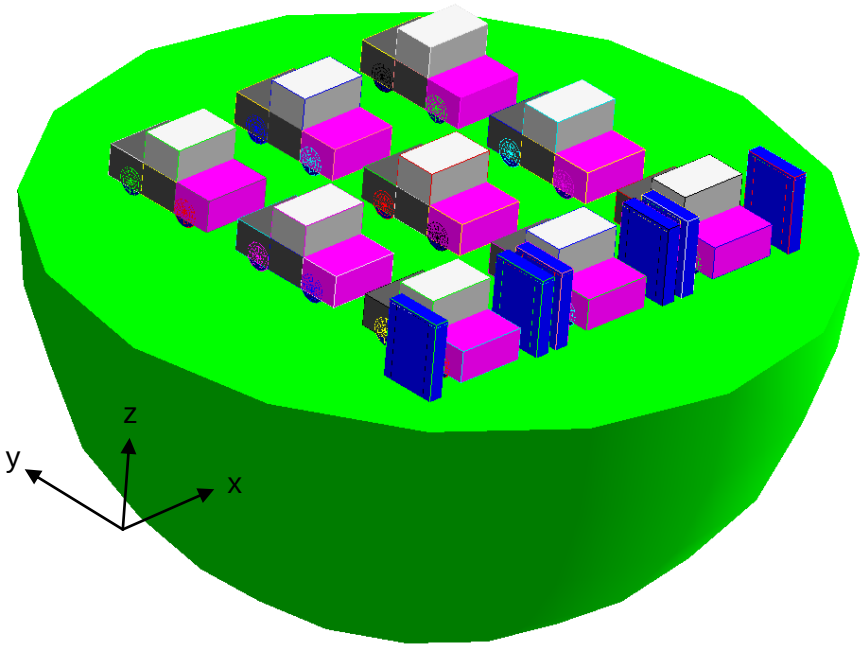

Fig. 22. 3-D rending of the MCNPX baseline scenario.

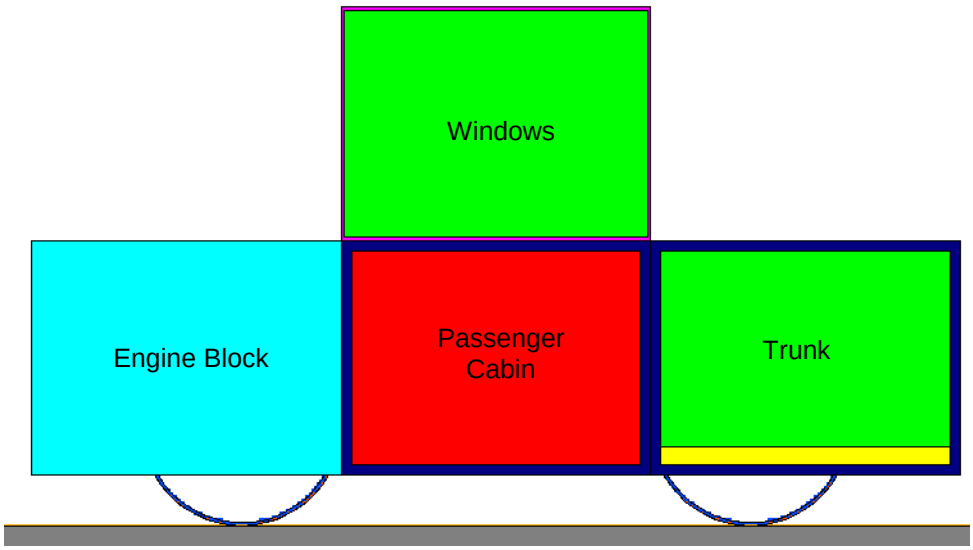

Fig. 23. MCNPX model of a vehicle (side view).

Table 5. Vehicle Materials and Macroscopic Cross Sections.

Material	**Density [g/cm^3]**	**Total Cross Section [cm^{-1}]**	**Scattering Cross Section [cm^{-1}]**
Stainless Steel	1.98E+00	3.024E-01	2.495E-01
Carbon Steel	7.84E+00	1.121E+00	2.521E-01
Polyurethane Foam	1.00E-02	1.340E-02	1.319E-02
Gasoline	7.00E-01	2.245E+00	2.239E+00
Glass	2.52E+00	2.924E-01	2.830E-01
Rubber	1.50E+00	2.518E+00	2.485E+00
Dry Air	1.20E-03	5.009E-04	4.350E-04

The portal monitors are based on the Yantar-1A systems. They contain ^{3}He tubes embedded in polyethylene for neutron counting and a plastic scintillator for gamma-ray counting. The entire system is enclosed in a thin aluminum case. The MCNPX model is displayed in Fig. 24, which shows the top and side views of a portal monitor. A list of materials is given in Table 6.

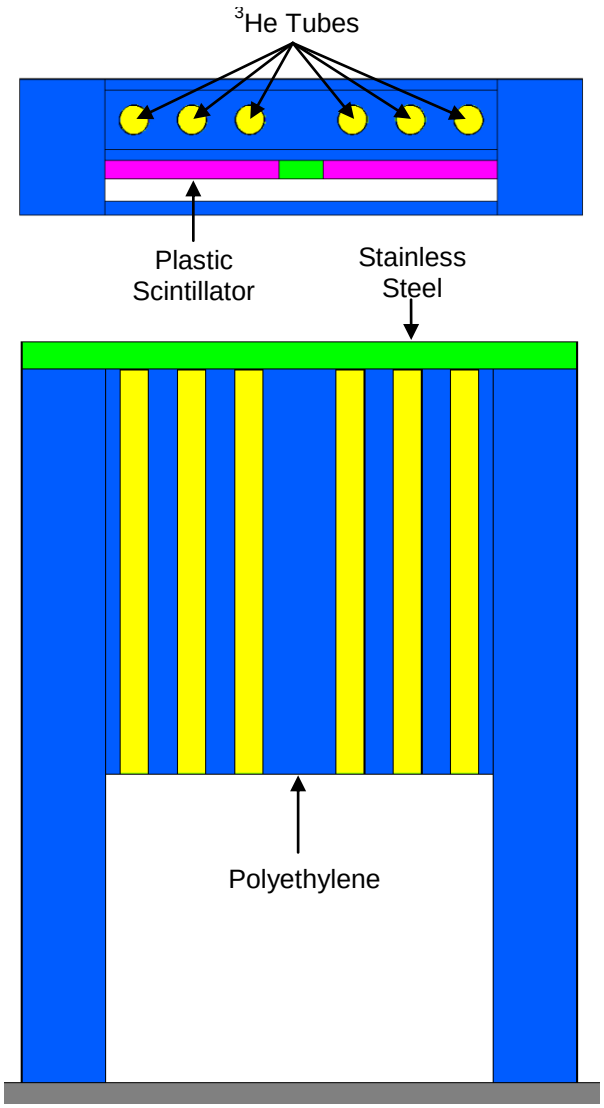

Fig. 24. MCNPX model of a radiation portal monitor (top and side views).

Table 5 and 6 also show the one-group cross sections used in the deterministic code. The one-group cross sections for each material were calculated using the Maxwellian averaged cross sections at 0.0235 eV from the *Table of Nuclides*.[44]

Table 6. Portal Monitor Materials and Macroscopic Cross Sections.

Material	**Density [g/cm^3]**	**Total Cross Section [cm^{-1}]**	**Scattering Cross Section [cm^{-1}]**
Helium-3	5.00E-04	4.735E-01	3.130E-04
Plastic Scintillator	1.03E+00	6.832E+00	6.731E+00
Polyethylene	9.60E-01	1.910E+00	1.884E+00
Stainless Steel	1.98E+00	3.024E-01	2.495E-01
Dry Air	1.20E-03	5.009E-04	4.350E-04

We used the MCNPX-generated geometries of the vehicles and portal monitors to create a mesh for the deterministic code. The cross sections were volume averaged to match the MCNPX model as closely as possible. One of the considerations when creating the mesh was the trade-off between the fineness of the mesh and computational time. A finer mesh gives more accurate results, but the code also takes more time to execute. To get an idea of the appropriate size mesh for the time constraints of the border crossing problem, several homogeneous problems were run. For each problem, a different sized grid was used. Table 7 shows the number of cells and the execution time for each problem. The execution time refers to the time for the transport solver to converge. The results are also plotted in Fig. 25. As seen on the plot, the execution time increases linearly with the number of cells.

Table 7. Execution Times for Homogeneous Problems.

Cells [x-dir]	Cells [y-dir]	Cells [z-dir]	Total Cells	Time [sec]
35	35	35	42,875	203.17
30	30	30	27,000	123.84
25	25	25	15,625	68.55
20	20	20	8,000	27.86
15	15	15	3,375	8.09
10	10	10	1,000	1.45

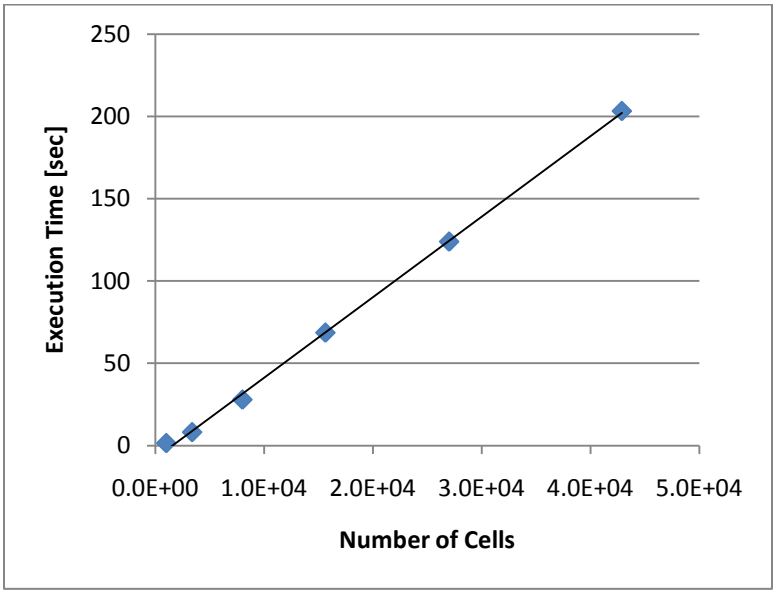

Fig. 25. Execution time for homogeneous problems as a function of the number of cells.

The time constraints of the border crossing problem require that the source position be identified in a matter of minutes. Because the transport solver must be run several times

before the source position is identified, the execution time needs to be on the order of seconds, not minutes. We want the execution time to be less than 30 seconds.

Using the results from the homogeneous problems as a guide to approximate execution times, we created four meshes for the baseline scenario with the number of cells ranging from approximately 4,000 cells to 50,000 cells. The execution times are given in Table 8 and plotted in Fig. 26. Again, the execution time increases linearly with the number of cells. These execution times are longer than the times in the heterogeneous cases discussed later. The 64×31×4-cell mesh was chosen for the baseline test cases because it represents an appropriate balance between accuracy and computational time.

Table 8. Execution Times for the Baseline Scenario.

Cells [x-dir]	**Cells [y-dir]**	**Cells [z-dir]**	**Total Cells**	**Time [sec]**
64	64	12	49,152	116.78
32	64	12	24,576	66.17
64	31	4	7,936	13.69
32	31	4	3,968	7.75

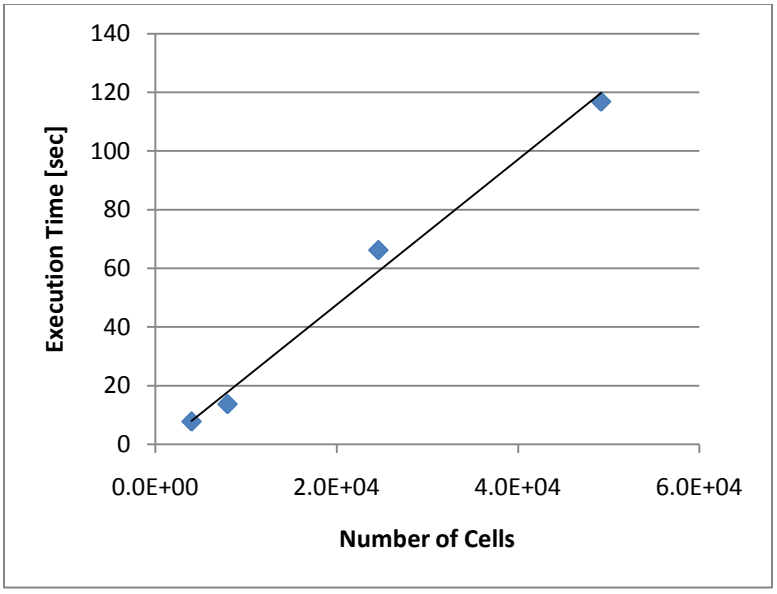

Fig. 26. Execution time for the baseline scenario as a function of the number of cells.

V.B. Baseline Test Case

The first test of the source locating algorithm was on the baseline scenario. This test shows how the code performs given perfect knowledge about the model parameters. The measurements were generated by running the forward code given the baseline cross sections and were taken as the scalar flux within the detectors. The forward-model-generated measurements were then used as input into the full source location code along with the baseline cross sections.

To aid in understanding the results, we developed a numbering scheme for the vehicles. An overhead view of the baseline geometry is shown in Fig. 27. The first number

indicates the lane and the second number indicates the row. The vehicles in the row closest to the portal monitors make up row one.

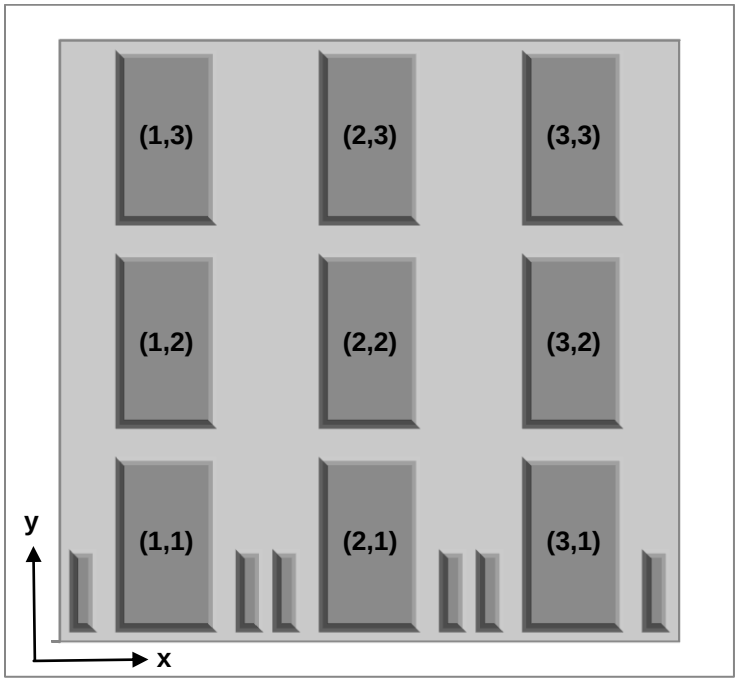

Fig. 27. Vehicle numbering scheme.

We focused on two factors in the baseline test: (1) the source position and (2) the convergence tolerance. With the first factor, we tested the code with the source located in each of the nine vehicles. Within each vehicle, five different locations were tested for a total of 45 different locations. The five locations tested were the center, left, and right side of the passenger compartment, the trunk, and the engine block. The results are given in Table 9. The column labeled “Distance from Source” gives the distance in centimeters between the actual source position and the source position predicted by the inverse model.

Table 9. Baseline Scenario Test Results of Varying Source Positions within each Vehicle.

Compartment	Vehicle	Correct Vehicle?	Distance from Source [cm]
Engine	(1,1)	Yes	141.51
	(2,1)	Yes	108.17
	(3,1)	Yes	108.17
	(1,2)	No	120.93
	(2,2)	Yes	30.00
	(3,2)	Yes	30.00
	(1,3)	Yes	33.54
	(2,3)	Yes	0.00
	(3,3)	Yes	68.74
Passenger Cabin Center	(1,1)	Yes	0.00
	(2,1)	Yes	0.00
	(3,1)	Yes	0.00
	(1,2)	Yes	30.00
	(2,2)	Yes	30.00
	(3,2)	Yes	30.00
	(1,3)	Yes	0.00
	(2,3)	Yes	60.00
	(3,3)	Yes	33.54
Passenger Cabin Right Side	(1,1)	Yes	0.00
	(2,1)	Yes	0.00
	(3,1)	Yes	0.00
	(1,2)	Yes	15.00
	(2,2)	Yes	0.00
	(3,2)	Yes	30.00
	(1,3)	Yes	30.00
	(2,3)	Yes	30.00
	(3,3)	Yes	42.43
Passenger Cabin Left Side	(1,1)	Yes	0.00
	(2,1)	Yes	0.00
	(3,1)	Yes	84.85
	(1,2)	Yes	68.74
	(2,2)	Yes	0.00
	(3,2)	Yes	30.00
	(1,3)	Yes	214.77
	(2,3)	Yes	30.00
	(3,3)	Yes	73.48
Trunk	(1,1)	Yes	0.00
	(2,1)	Yes	0.00
	(3,1)	Yes	0.00
	(1,2)	Yes	0.00
	(2,2)	No	189.74
	(3,2)	Yes	90.00
	(1,3)	Yes	68.74
	(2,3)	Yes	30.00
	(3,3)	Yes	30.00

In all but two cases, the code converged to the correct vehicle for a success rate of 96%. In the case of vehicle (1,2) with the source located in the engine compartment, the code predicted the source was located in vehicle (1,1). This is a reasonable error considering the engine compartment is located at the front of vehicle (1,2). In the case of the vehicle (2,2) with the source located in the trunk, again, the error is reasonable because the estimated source position was the vehicle directly behind (2,2).

The average distance from the expected to the actual source for this test was 41.83 cm. If the engine compartment, which is an unlikely place for a source to be located, is omitted from the results, the average distance drops to 31.03 cm. This test shows that the algorithm performs very well when the geometry, cross sections, and detector efficiencies are known with absolute certainty.

In the source position test, the total convergence tolerance for the objective function was set to 0.5, which represents the sum of the errors for all of the detectors. A tighter convergence would likely have resulted in a 100% success rate, but the computational time would also likely be prohibitively expensive.

In the next baseline test case, the convergence tolerance was perturbed to assess the effect on the code's ability to identify the correct vehicle. In this test, the same 45 source locations were run for tolerances ranging from 0.5 to 2.5 in increments of 0.5.

A graphical representation of the results is shown in Fig. 28 through Fig. 36. Each figure represents the results for one vehicle. In other words, Fig. 28 shows the estimated source locations when the actual source location was in vehicle (1,1). This includes test cases of all five locations within vehicle (1,1) for the entire range of tolerances (i.e., 25 test cases on each plot—five locations per vehicle including the center, left, and right side of the passenger cabin; the engine block; and the trunk for five different tolerance values).

In each figure, the upper plot is an overhead map of the three lanes of vehicles. It provides a clear view of where code estimated the source to be for a series of test cases on a single vehicle. The estimated locations are shaded. The lower plot is a rotated view of the three lanes of traffic. The vehicles and portal monitors appear as gray boxes. The frequency of each solution is superimposed on top of the vehicles. It shows how often a given location was the expected source location for the vehicle under consideration. The combination of these plots provides an overall picture of how the source location algorithm performs for a variety of locations within each vehicle and for different convergence tolerance values.

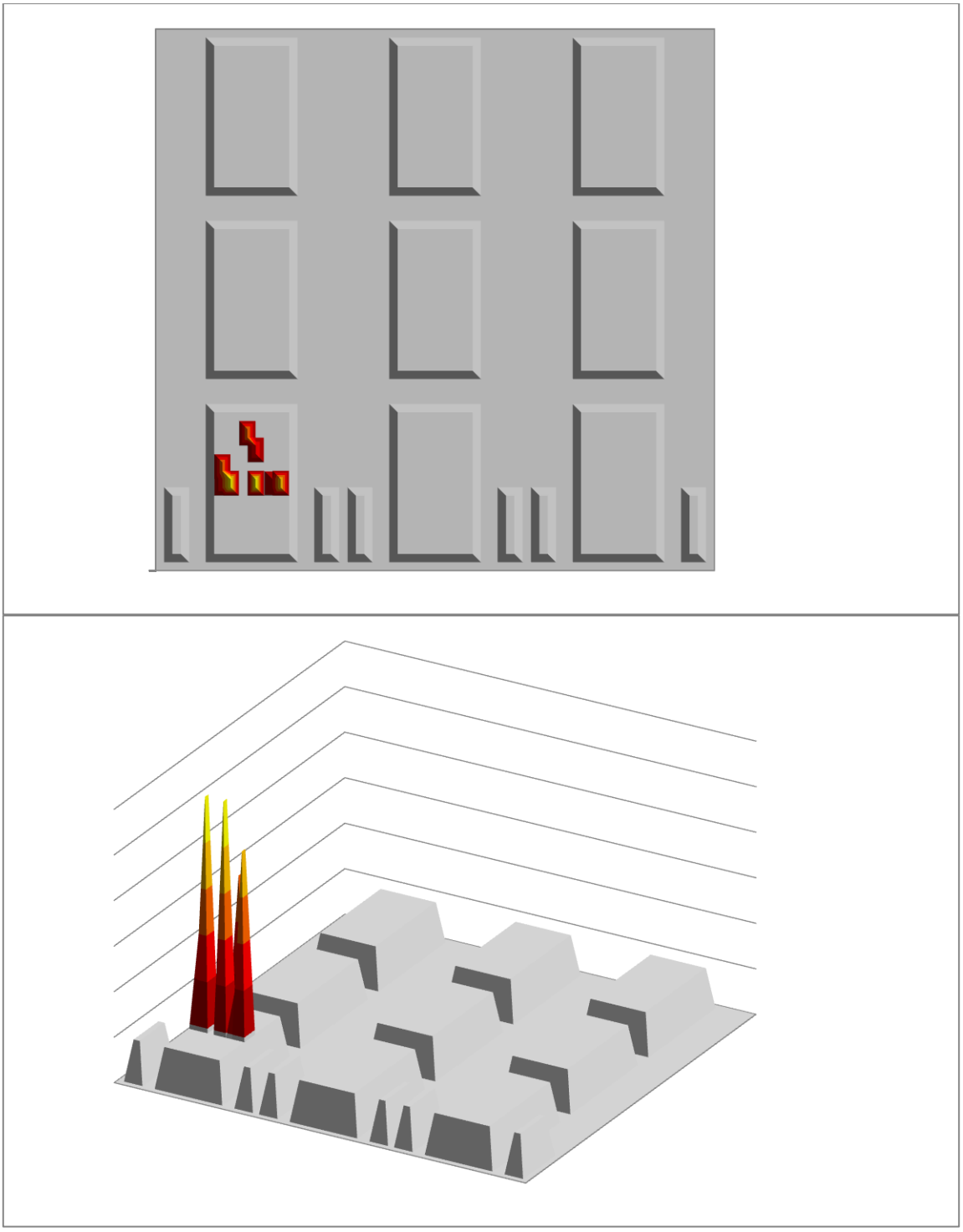

Fig. 28. Source position and convergence tolerance baseline test for vehicle (1,1).

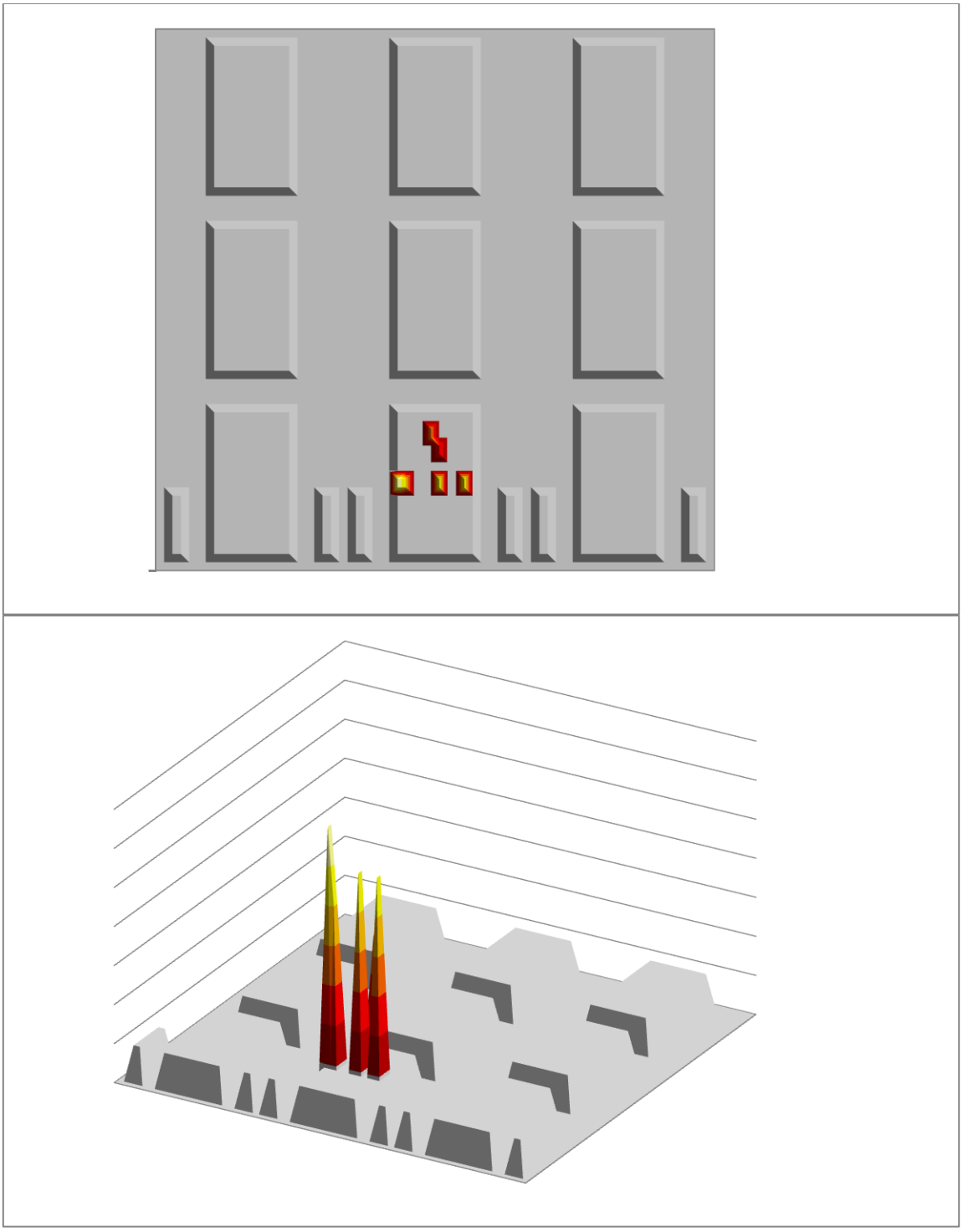

Fig. 29. Source position and convergence tolerance baseline test for vehicle (2,1).

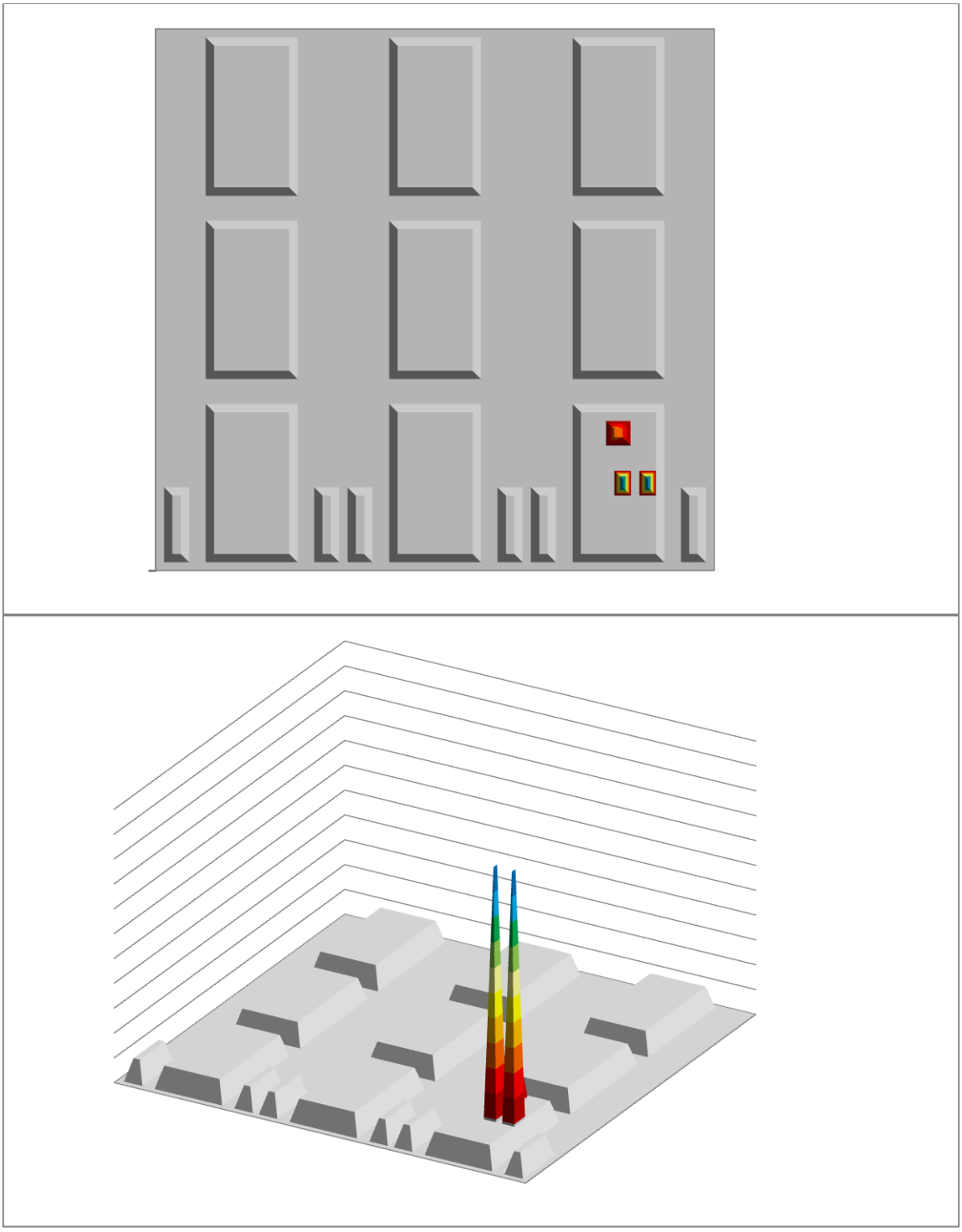

Fig. 30. Source position and convergence tolerance baseline test for vehicle (3,1).

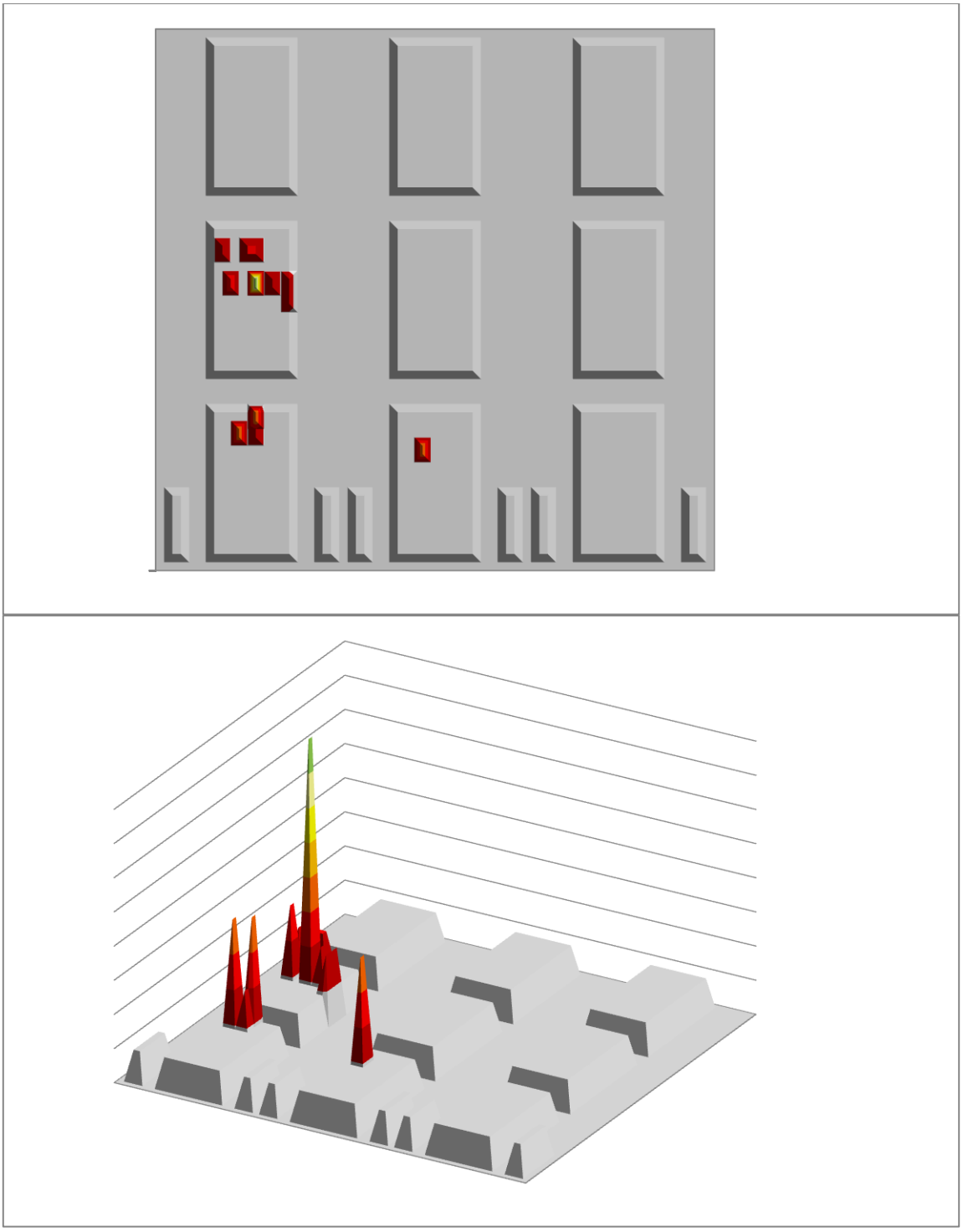

Fig. 31. Source position and convergence tolerance baseline test for vehicle (1,2).

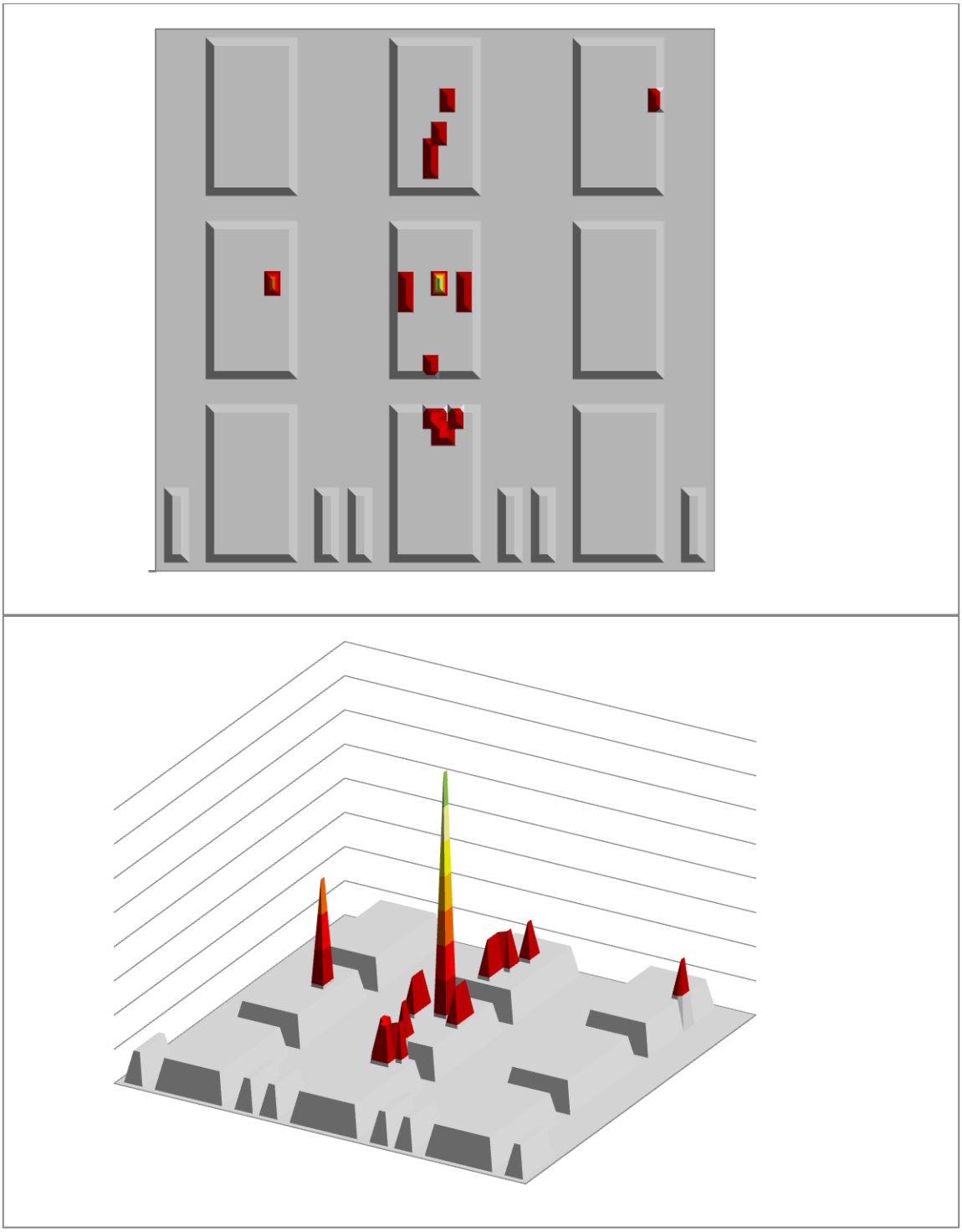

Fig. 32. Source position and convergence tolerance baseline test for vehicle (2,2).

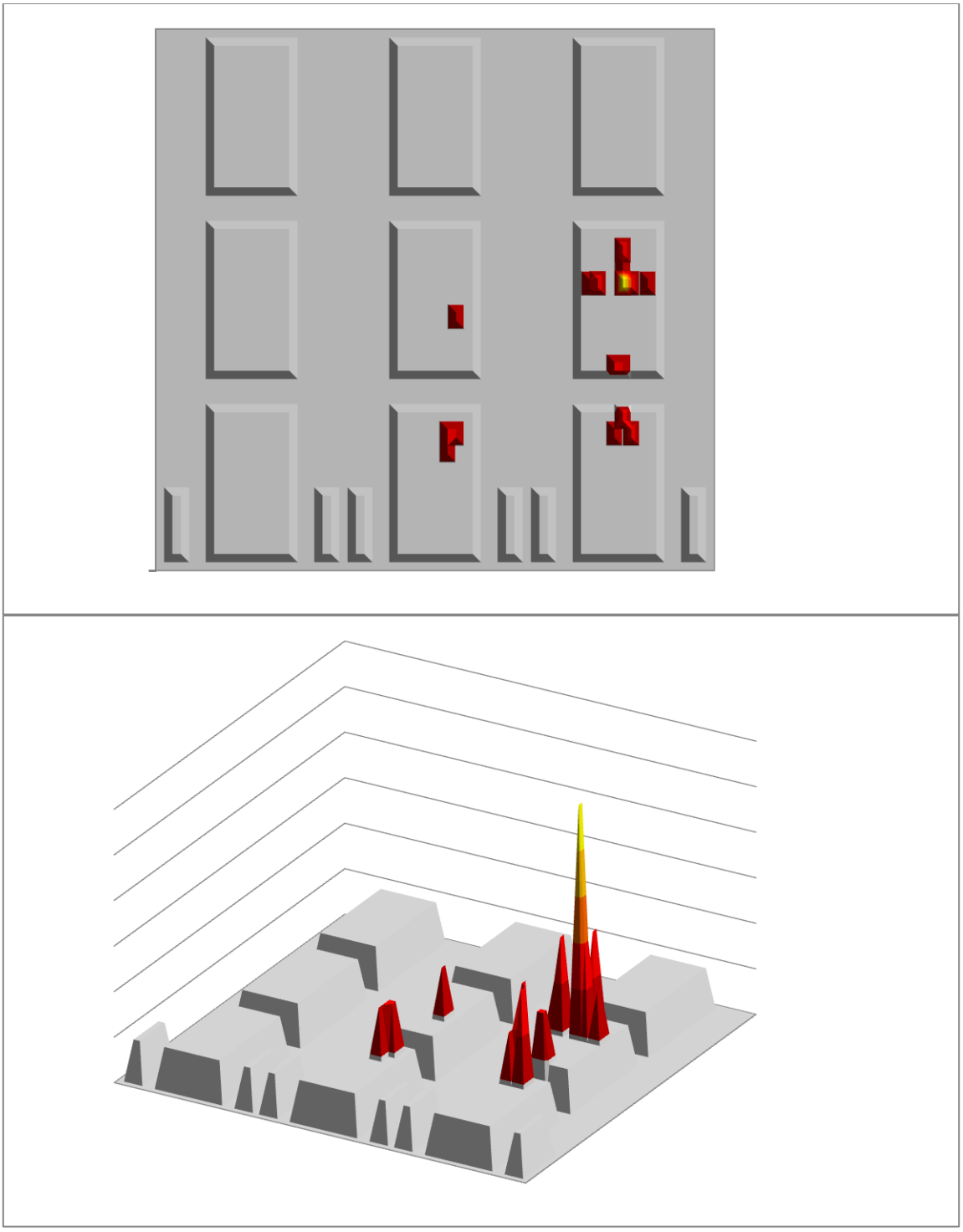

Fig. 33. Source position and convergence tolerance baseline test for vehicle (3,2).

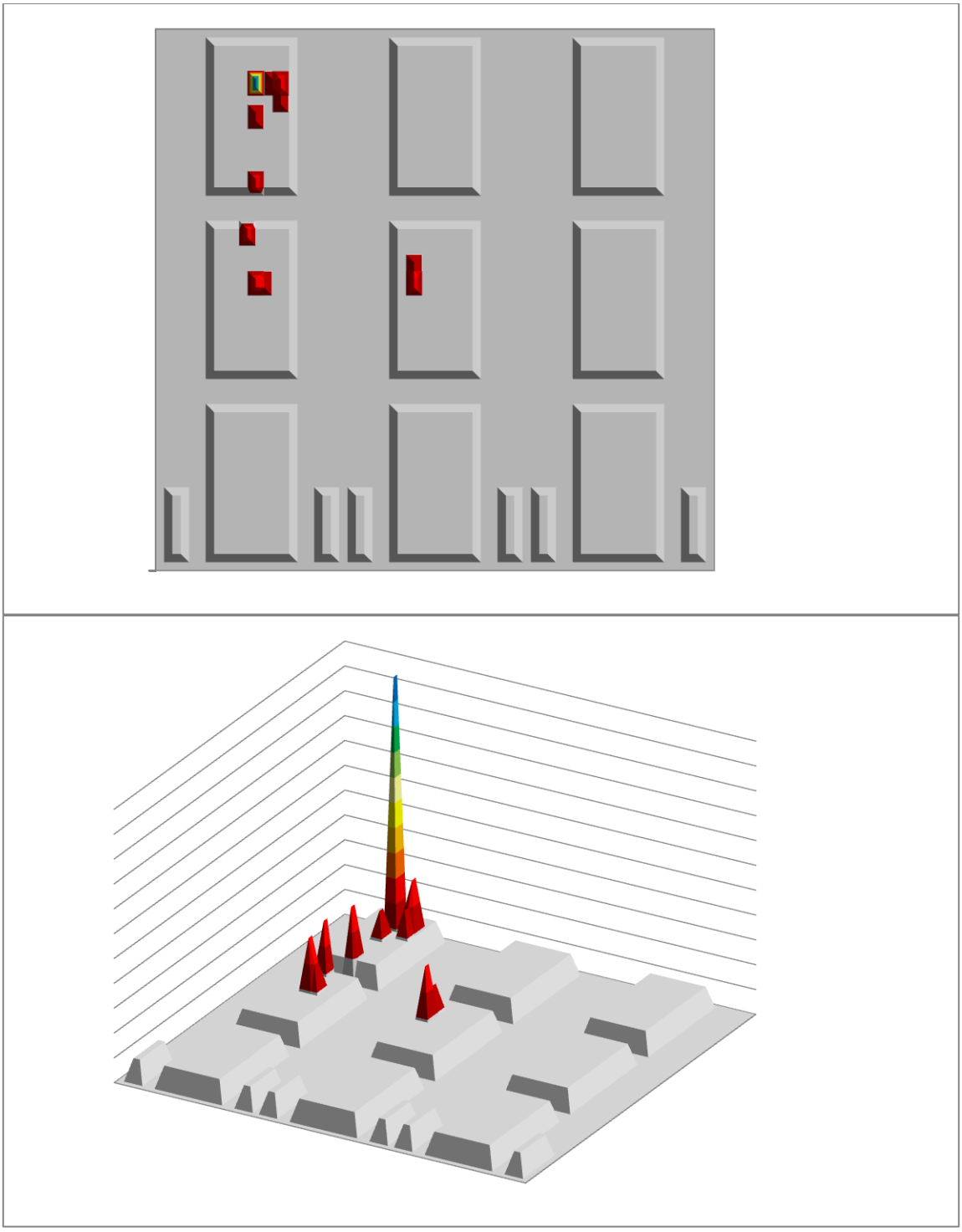

Fig. 34. Source position and convergence tolerance baseline test for vehicle (1,3).

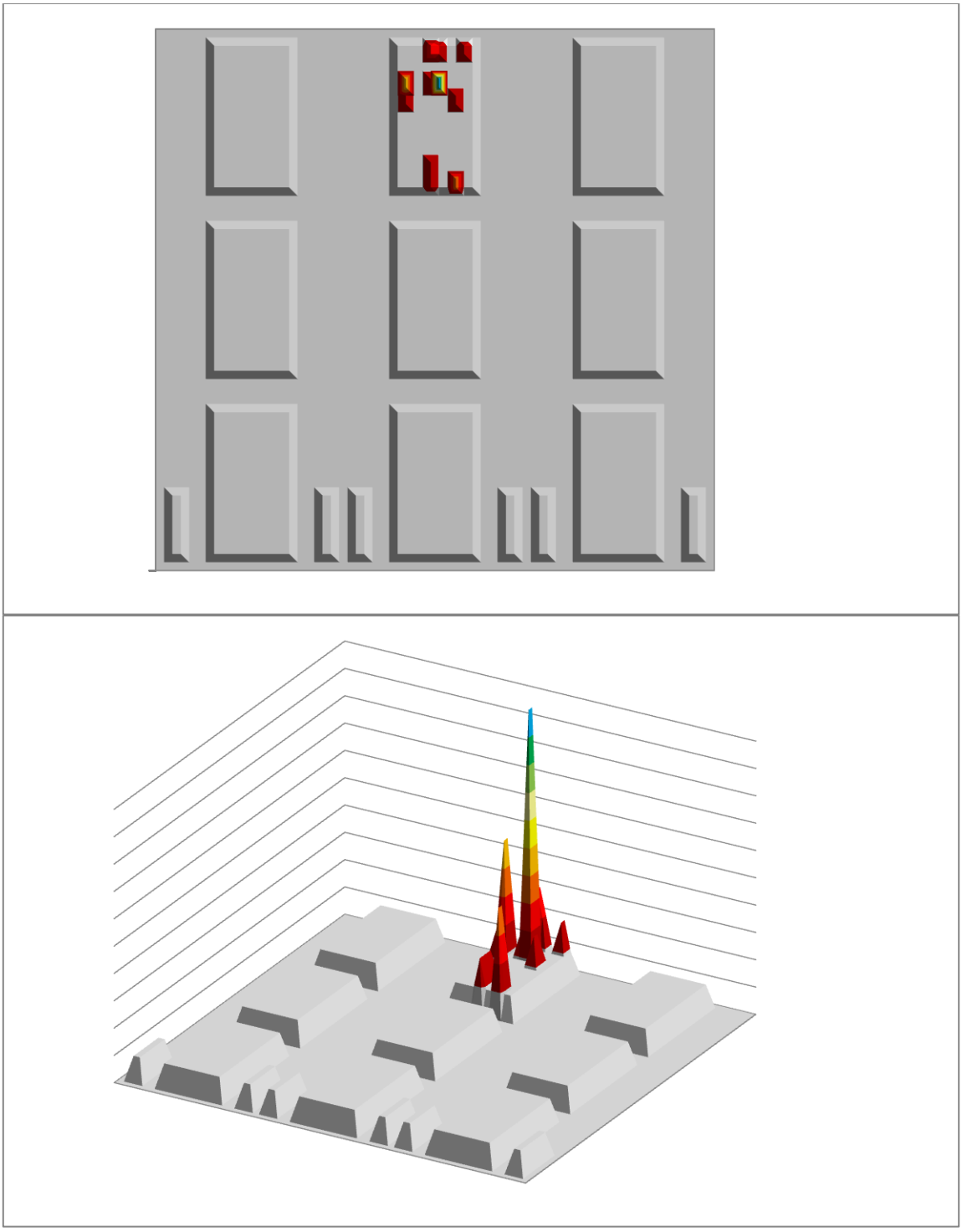

Fig. 35. Source position and convergence tolerance baseline test for vehicle (2,3).

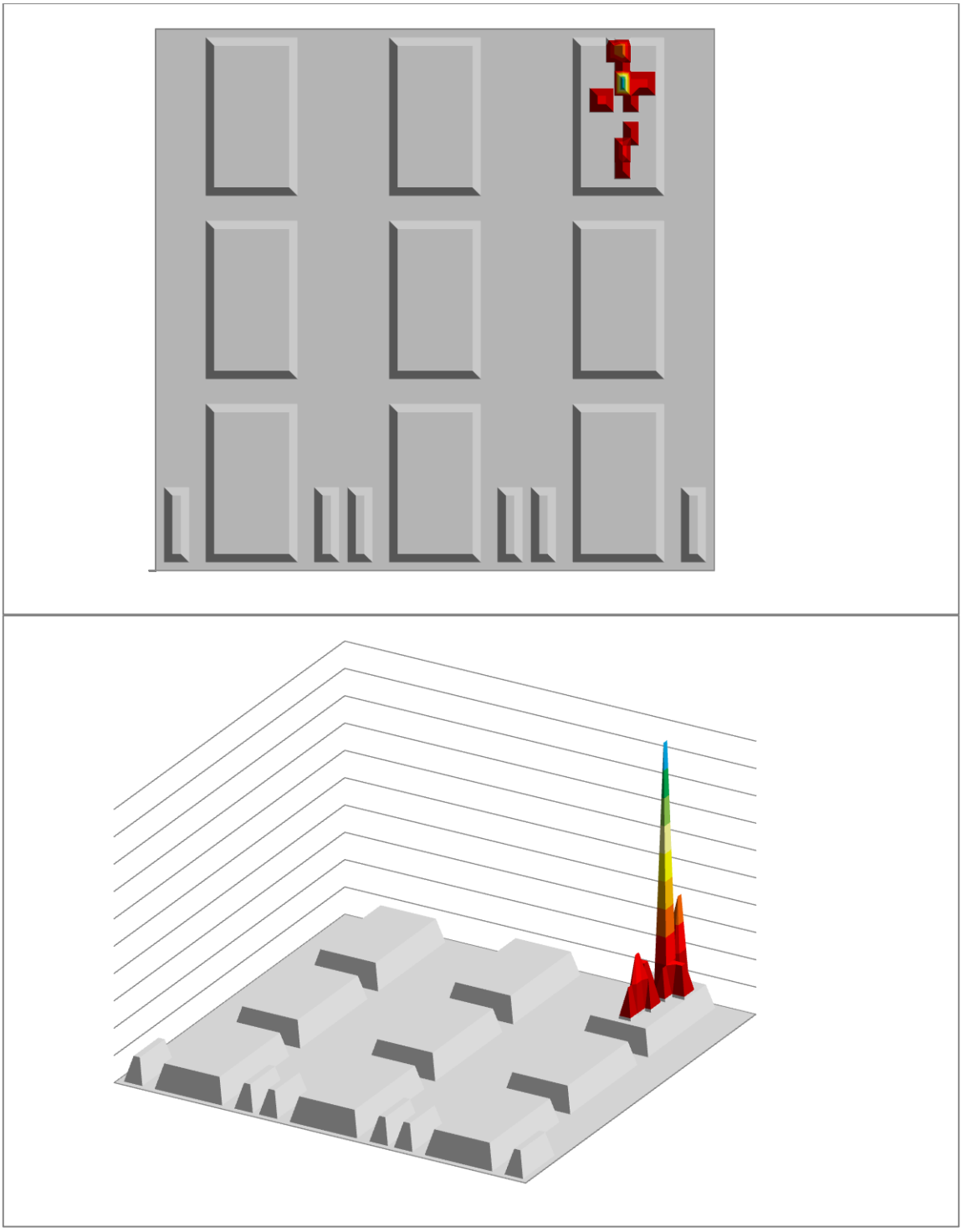

Fig. 36. Source position and convergence tolerance baseline test for vehicle (3,3).

The first feature to notice about the plots is that the results of the vehicles located in the first row, closest to the portal monitors, all converged to the correct vehicle. Based solely on the relative distances from the vehicles to the portal monitors, the first-row vehicles should be the easiest cases for the code to identify correctly as containing the source.

The code performed the worst when the source was located in a second-row vehicle. In principle, third-row vehicles should be the most difficult to identify correctly, but the fact that the system boundary is behind the third row in the baseline case contained the spread of solutions that was seen in the second-row vehicles. The spread was largest for vehicle (2,2), which had adjacent vehicles in all directions.

A final note on Fig. 28 through Fig. 36 concerns the lack of symmetry in the results. While it would be logical to think that, for instance, vehicles (1,1) and (3,1) should have results that mirror each other from symmetry, this is not the case. The reason has to do with the mesh used in the deterministic transport solver. The vehicles have an even number of cells in the x-direction, so when the source is said to be located on the centerline of the vehicle (engine, center of the passenger cabin, or the trunk), it is actually shifted slightly to one side or the other. The source locations at the left and right sides of the passenger cabin are similarly shifted. The result of this is an asymmetry in the results.

Fig. 37 shows the average distance from the predicted source position to the true source position versus convergence tolerance. The data in Fig. 37 shows the overall average distance as well as the distances broken down into the specific locations inside each vehicle (center, left, and right sides of the passenger cabin; engine; and trunk). In general, we see that the distance increases with increasing tolerance (especially above a tolerance of 1.0); however, the results vary drastically by starting location.

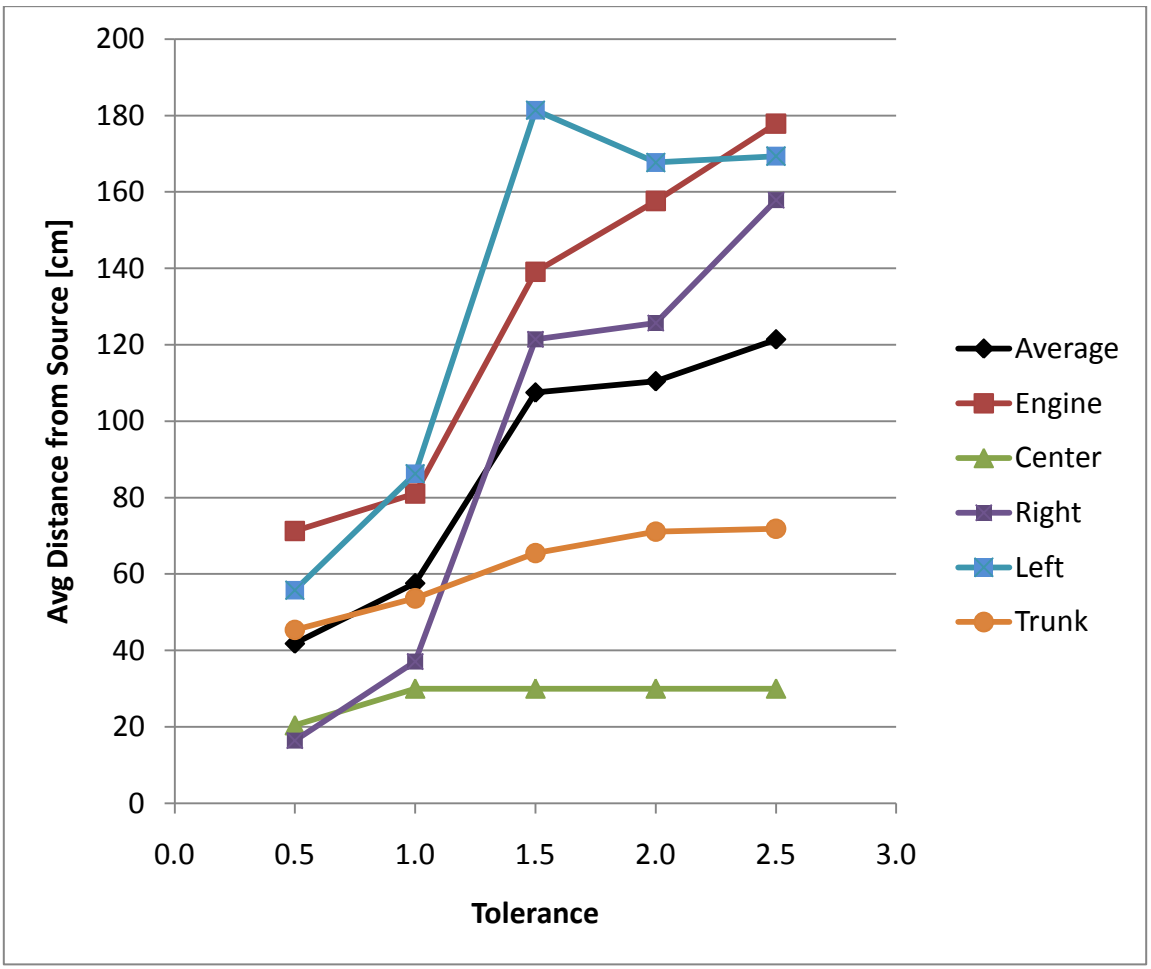

Fig. 37. Summary of source position and convergence tolerance baseline tests.

Fig. 37 generally shows that the results are well behaved, meaning there is no exponential functionality or other drastic increase, which would be cause for concern. Also, there is a clear distinction in the results for different locations within each vehicle. When the actual source location is in the center of the passenger cabin, the code performs very well, even when the convergence tolerance is increased. This is because the initial guess algorithm starts the forward model at the center of the most likely vehicle. When the actual source location is in the trunk, the code performs better than average, while the left, right, and engine locations perform worse than average for large tolerance values.

The plot also shows that the error remains relatively small for tolerances of 0.5 and 1.0, jumps up, and then saturates at a tolerance of about 1.5. Because of the jump in error between tolerances of 1.0 and 1.5, we can conclude that the total tolerance should not exceed 1.0 for optimal results.

V.C. Sensitivity Analysis

In the baseline test cases, we assumed perfect knowledge of the geometry, cross sections, and detector efficiencies; however, in a real-world application, there may, in fact, be large uncertainties in some or all of these parameters. A sensitivity analysis was performed to explore the effects of these uncertainties. This can provide a quantitative means of understanding which parameters are the most important. The parameters we

investigated are (1) the optical thickness of the vehicles, (2) the fill level in the gas tank, (3) the physical size of the vehicles, and (4) the detector efficiencies. In the following test cases, the code was tested with the actual source located in the center of the passenger cabin and in the trunk of each vehicle with different combinations of perturbed values.

V.C.1. Optical Thickness

In the optical thickness suite of tests, the total and scattering cross sections that make up the vehicles used to obtain the actual measurements were increased or decreased in order-of-magnitude steps from 0.001 to 1,000 times the baseline cross sections. In other words, the ratio of optical thicknesses in the perturbed cases to the baseline case ranged from 0.001 to 1,000. This large range is not inconsistent with a real scenario where, based on the values in Table 5, the total cross sections of common vehicle materials span four orders of magnitude. The cross sections of the air space and detectors were not perturbed.

We tested three different distributions of perturbed vehicles, shown by the blue shaded vehicles in Fig. 38. In the first distribution, all of the vehicles are perturbed. In the second and third distributions, the perturbed vehicles are in opposite checkerboard patterns. Plots of the results for each vehicle are given in Appendix A. Each figure shows the results for the actual source located in the center of the passenger cabin and

the trunk for all three distributions over the range of perturbed values (optical thicknesses) for a given vehicle.

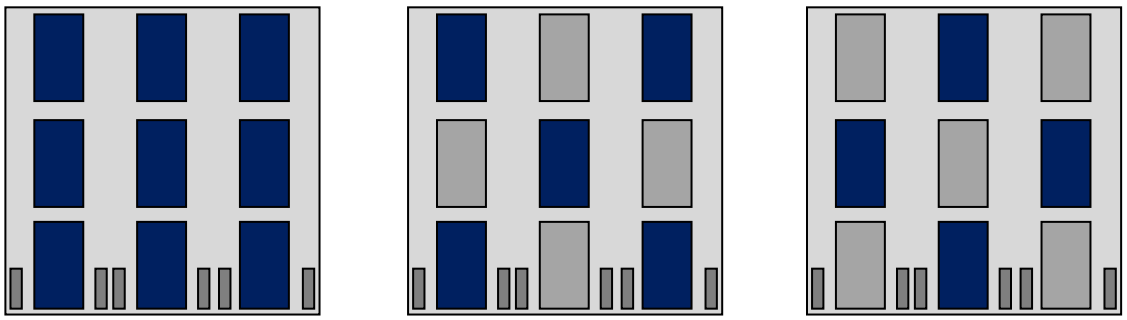

Fig. 38. Three distributions of perturbed vehicles for the sensitivity analysis.

In these sensitivity analysis test cases, the feature we are looking at on the frequency plots is the spread of the results. The more spread in the results, the more sensitive the code is to that particular parameter. In this case, the plots show that the code is very sensitive to the optical thickness of the vehicles. There is significant spread in the first- and third-row vehicles, and the results of the second-row vehicles are all over the map, especially vehicle (2,2).

Fig. 39 shows the average distance between the predicted source position and the true source position versus the ratio of optical thicknesses. The summary plot shows what happened to the error (i.e., the distance between the true and predicted source positions) as a function of the optical thickness of the vehicles. There are three curves on the plot showing the overall average error as well as the error broken down by whether the true source position was located in the passenger cabin or the trunk.

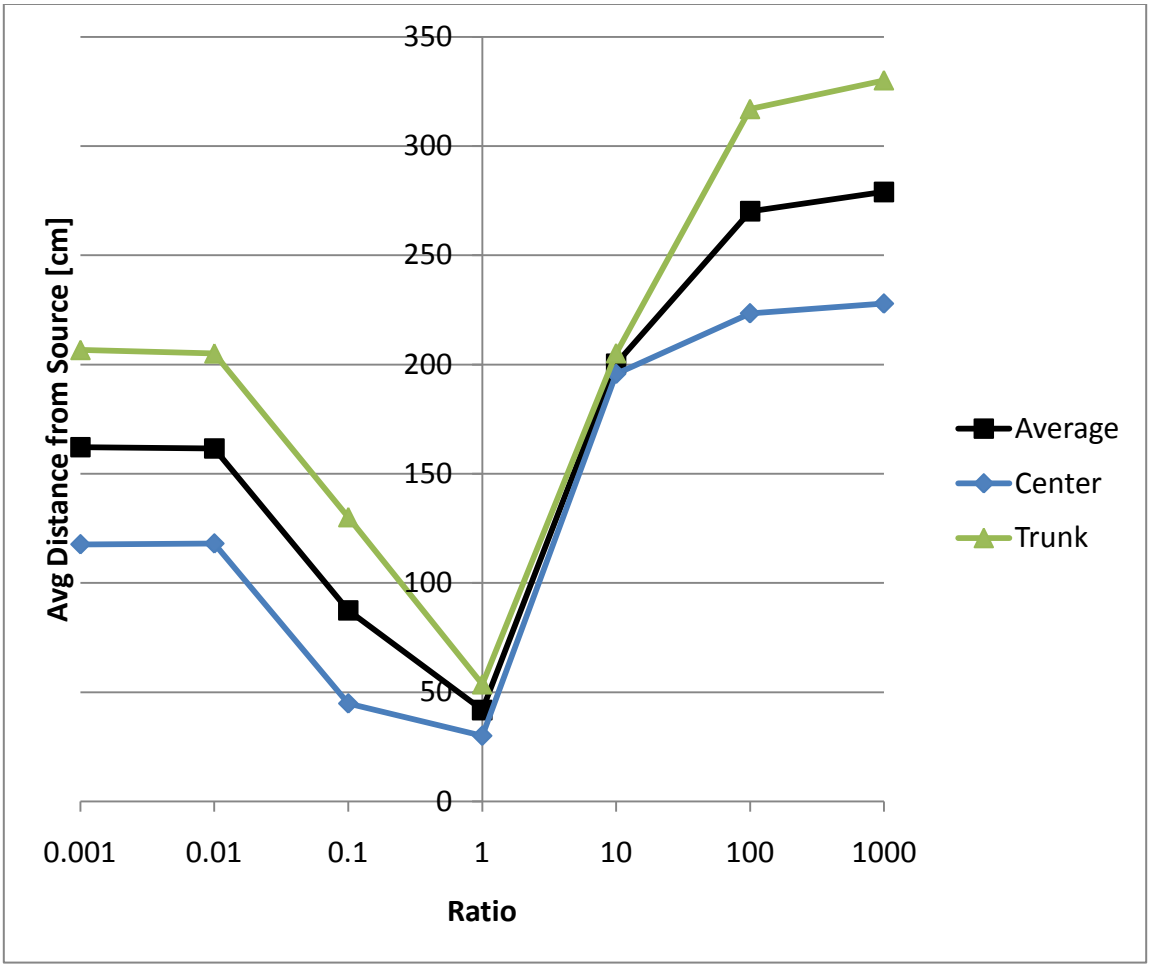

Fig. 39. Summary of optical thickness sensitivity analysis results showing the average distance between the true and predicted source as a function of the ratio of optical thickness in the perturbed case to the baseline case.

The results behave in a predictable manner, with the error increasing with the change in optical thickness. The error plateaus in both directions once the optical thickness reaches a two-order-of magnitude change. At those points, the vehicles essentially become invisible or totally opaque to the radiation and further increasing or decreasing the optical thickness ceases to affect the results.

V.C.2. Gas Tank Fill Level

The second parameter investigated in the sensitivity analysis was the fill level in the gas tank. Gasoline has a high scattering ratio for neutrons and thus has the potential to shift the results. The gas tank is located at the bottom of the trunk in the vehicle modeled. In the baseline case, the gas tank contains 16 gallons of gasoline. This test examines how the code performs over a range of fill levels—from an almost empty (0.16 gallons) gas tank to the entire trunk being filled with gasoline with two intermediate fill levels. As with the optical thickness test, three distributions of perturbed vehicles were used (Fig. 38) to obtain the actual measurements. The baseline cross sections were used in the inverse code to locate the source. Two source positions were tested for each vehicle: the center of the passenger cabin and the trunk. The results for each vehicle are given in Appendix A.

Recall that we are looking for the spread of the results in the sensitivity analysis. In this case of the gas tank fill level, the spread is very minimal. The first row vehicles were not affected at all by the change. There was some minor spread in the second- and third-row vehicles, with only the case of vehicle (2,2) being identified incorrectly.

The summary of the gas tank fill level results is given in Fig. 40. The figure shows the average distance between the true and predicted source position as a function of the ratio of perturbed gas tank fill level to the baseline fill level. There are three curves on the plot

showing the overall average error as well as the error broken down by whether the true position was in the passenger cabin or the trunk.

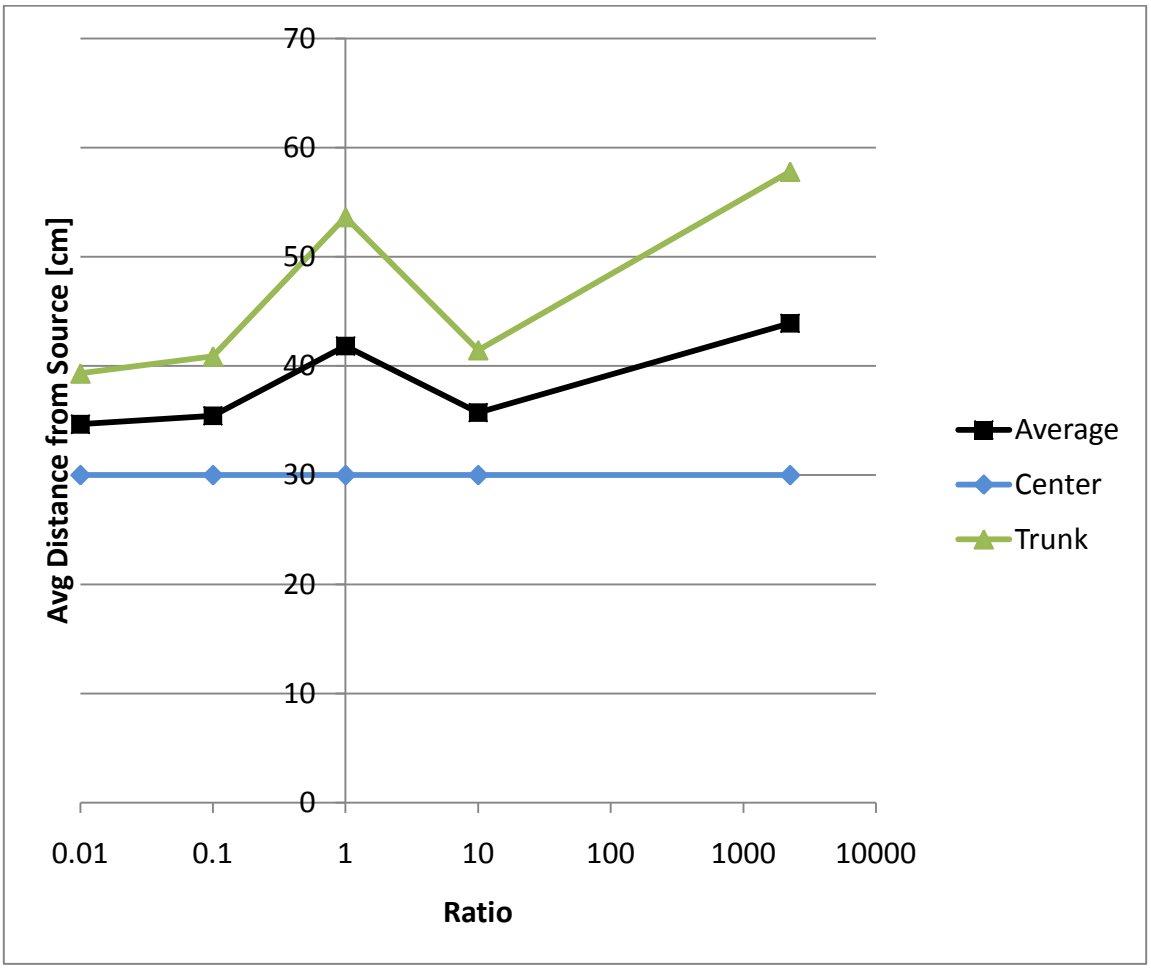

Fig. 40. Summary of gas tank fill level sensitivity analysis results showing the average distance between the true and predicted source as a function of the ratio of gas tank fill levels in the perturbed case to the baseline case.

As evident on the plot, when the source was located in the center of the passenger cabin, the results were not affected. This is a rational result considering the gas tank is located in the trunk of the vehicle. While there would certainly have been a change in the

amount of neutrons scattered from a source located in the passenger cabin by the change in the gas tank fill level, that change was not enough to change the expected source position.

The summary plot shows an unexpected result in that the average error decreases from the unperturbed value, except for the extreme case of the entire trunk being full of gasoline. However, if the magnitude of the change in error is compared to that of the optical thickness case, it seems the effect of the gas tank fill level is all in the noise. Over the range of values investigated for the optical thickness of the vehicles, the average error changed by over 200 cm and over 250 cm if only the trunk is considered. The change in error due to the gas tank fill level spans less than 20 cm. The relative effect of each of these parameters is not surprising considering the optical thickness is a wide-area change and the gas tank fill level is much more localized.

V.C.3. Physical Size

The third sensitivity parameter we examined was the physical size of the vehicles. For this test, the volume of the vehicles was perturbed by ±22%. The size was only changed in the x- and y- directions. The results for each vehicle are given in Appendix A.

As with the optical thickness and gas tank fill level tests, three distributions were tested with the source located in the center of the passenger cabin and the trunk of each vehicle.

The physical size of the vehicles affects the results by opening or closing streaming lanes for the neutrons from the source location to the portal monitors. The frequency maps show an intermediate level of spread in the results. The summary plot in Fig. 41 shows the average distance between the true and predicted source position as a function of the percent change in the physical size of the vehicles. There are three curves representing the overall error and the error associated with a true source position in either the passenger cabin or the trunk. The plot shows a range of approximately 30 cm in the error due to the change in volume of the vehicles, which is consistent with the frequency plots.

A final observation about the results of the physical size sensitivity analysis concerns the shape of the error shown in Fig. 41. The center and trunk curves have almost identical shapes, with the magnitude difference likely stemming from the initial guess algorithm. While a wider range of size differences are needed to say conclusively, this suggests that the physical size of the vehicles affects both source locations in the same way.

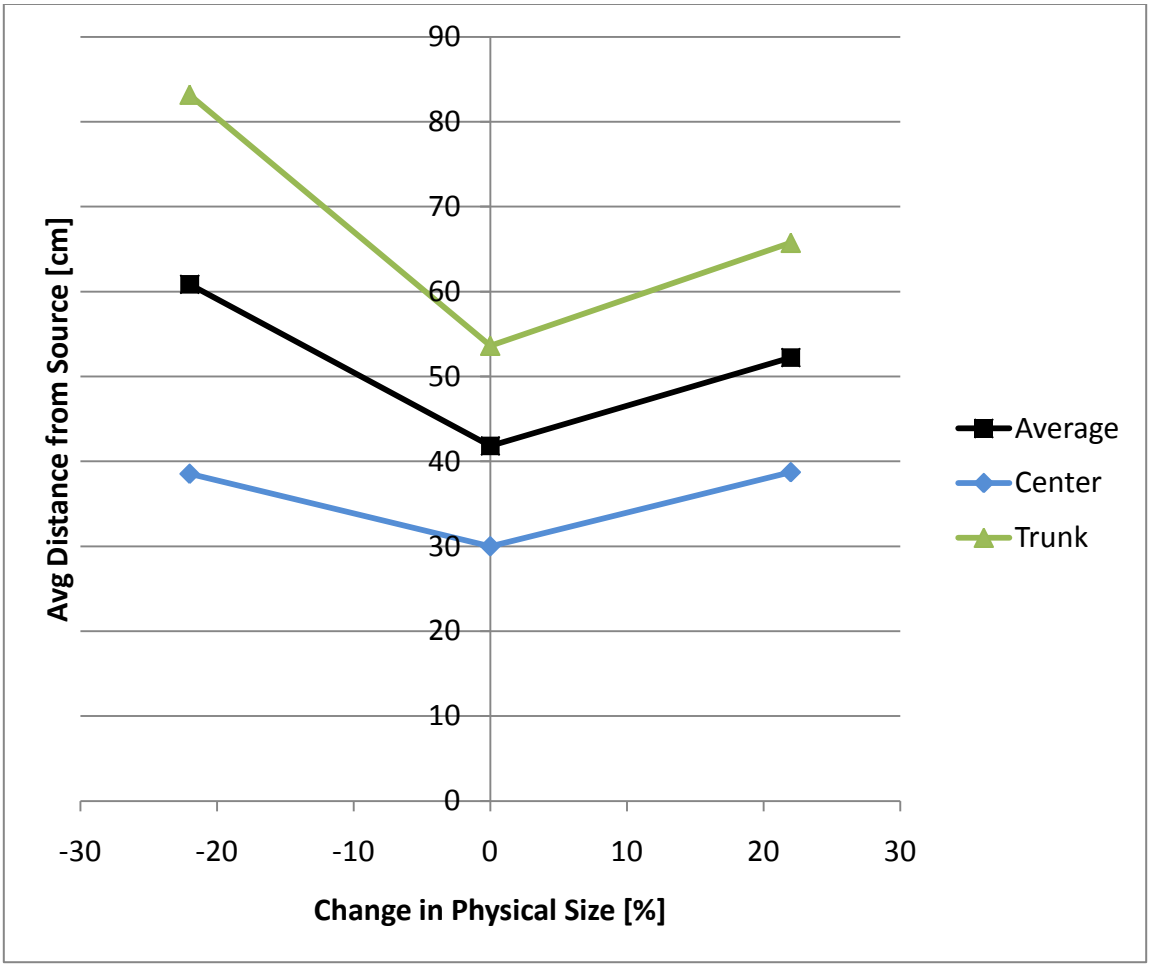

Fig. 41. Summary of physical size sensitivity analysis results showing the average distance between the true and predicted source as a function of the change in physical size of the vehicles.

V.C.4. Detector Efficiency

The final parameter studied in the sensitivity analysis was the detector efficiency. The previous cases have examined changes in the vehicles in three different distributions. For this case, the baseline cross sections were used, but three distributions of detector efficiencies were analyzed. In the first distribution, the portal monitors in lanes one and three (i.e., the outside lanes) were perturbed. In the second distribution, only the portal

monitor in lane two was perturbed, and in the third distribution, lanes one and two were perturbed. None of the test cases perturbed the portal monitors in all three lanes because the objective function only compares the relative difference in the measurements, which would not be affected if all of the measurements were perturbed by the same amount. The efficiency perturbations ranged from -50% to 50% in increments of 25%.

As in the previous sensitivity tests, the source positions in the center of the passenger cabin and in the trunk were tested for each vehicle for the three distributions of detector efficiencies. The results for each vehicle are given in Appendix A.

The results of the test cases showed a fairly wide spread of estimated source positions, suggesting that detector efficiency is one of the more dominant sensitivity parameters. While there was not as much spread as seen in the optical thickness case, it was a significant amount, especially in the second- and third-row vehicles. This test case has more singular outliers (as seen in vehicles (1,2) and (3,2)) than in the gas tank fill level and physical size tests. In those cases, there was more clustering between preferred locations within one or two vehicles.

Fig. 42 shows the summary plot. The average distance between the true and predicted source positions is plotted as a function of the change in detector efficiency. The three curves correspond to the overall error, the error resulting when the true source position is

in the passenger cabin of the vehicle, and the error resulting when the true source position is in the trunk.

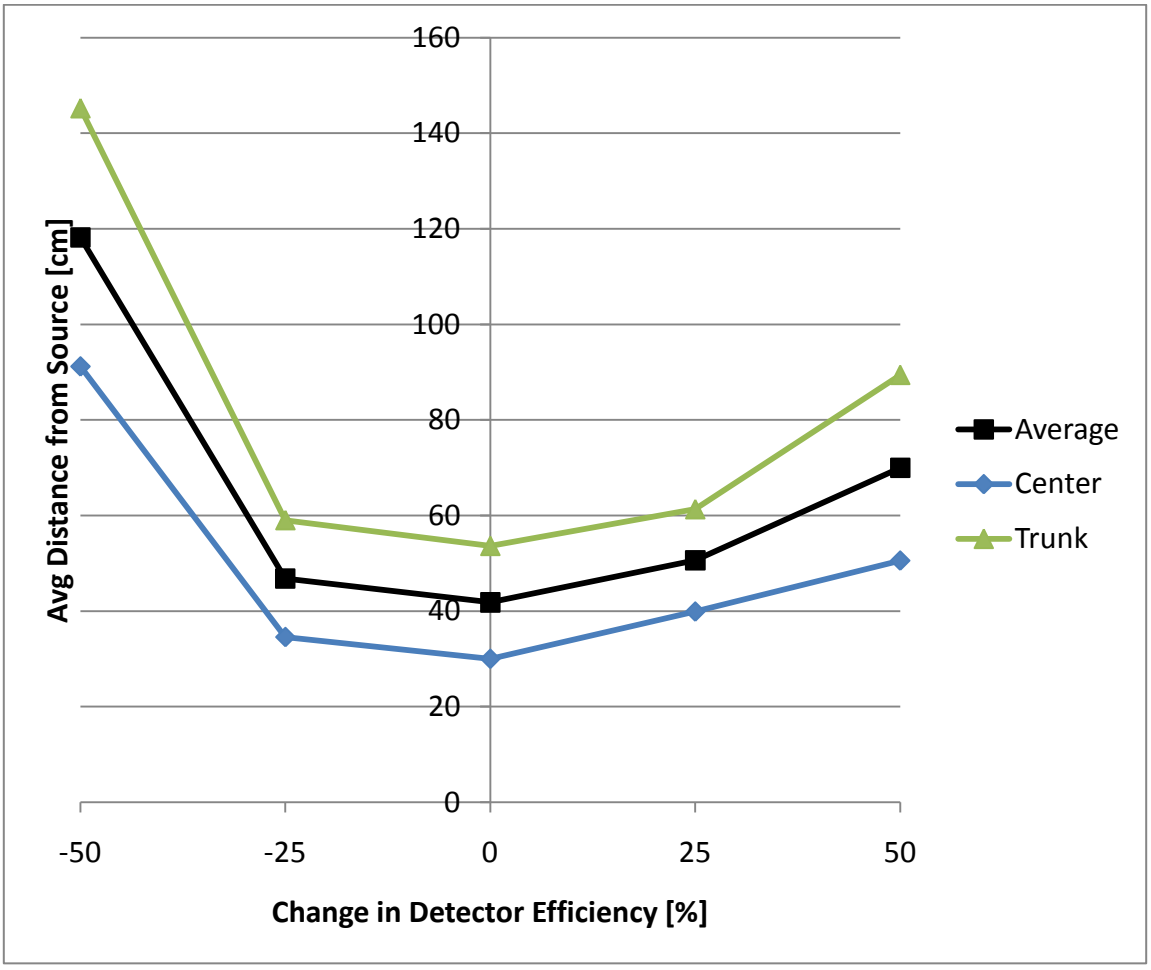

Fig. 42. Summary of detector efficiency sensitivity analysis results showing the average distance between the true and predicted source as a function of the change in detector efficiency.

The error increases as the change in efficiency grows. The average change spans slightly less than 80 cm, making the efficiency parameter second to only the optical thickness of the vehicles in the error it induces. As with the physical size case, the shape of the curves

for the center and trunk cases is nearly identical, meaning the detector efficiency affects both positions equally.

V.C.5. Summary of Results

A summary of the results for each vehicle is given in Fig. 43 through Fig. 51. Each figure shows the predicted source locations when the true source location is in a given vehicle. These plots combine the baseline test cases that looked at five different locations within each vehicle for a range of tolerance values as well as the test cases in the sensitivity analysis for the optical thickness of the vehicles, the gas tank fill level, the physical size of the vehicles, and the detector efficiencies. The upper plot in each figure shows an overhead map of the three lanes of traffic. The shaded areas represent the predicted source locations. The lower plot is a tilted view of the three lanes superimposed with the frequency with which each position was predicted.

Each of the plots contains 145 data points for a total of 1,305 test cases for all nine vehicles. Although there is spread in the results and the wrong vehicle was identified in some cases, the frequency plots show that, overwhelmingly, the correct vehicle was identified as possessing the source. There is always a chance that the code will chose the wrong vehicle as containing the source, but the overall success rate was 84.4%. Because the probablilty that an adversary will be caught is so high, this technology can serve as a deterent against smuggling as well as a means to detect it.

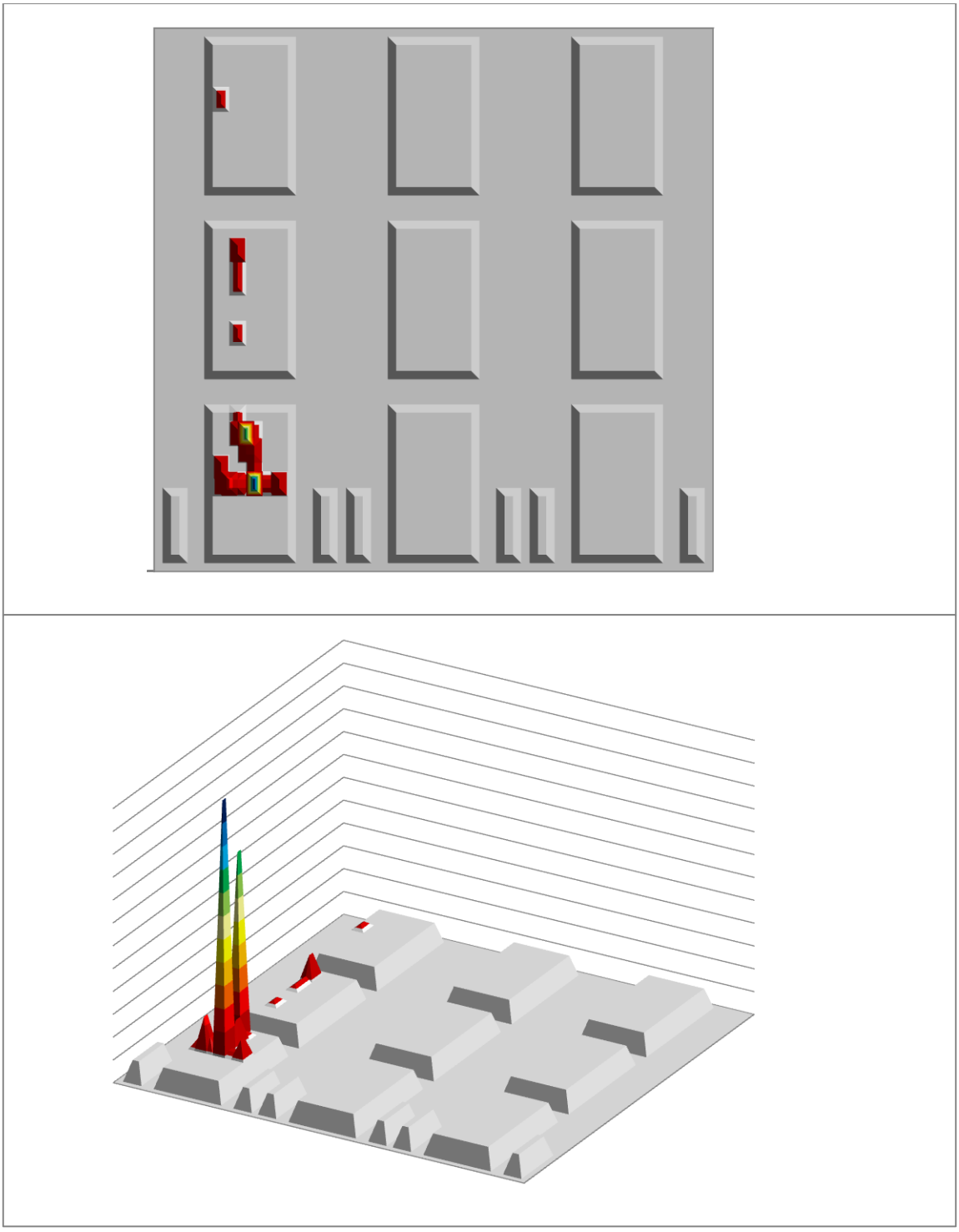

Fig. 43. Summary of results for vehicle (1,1).

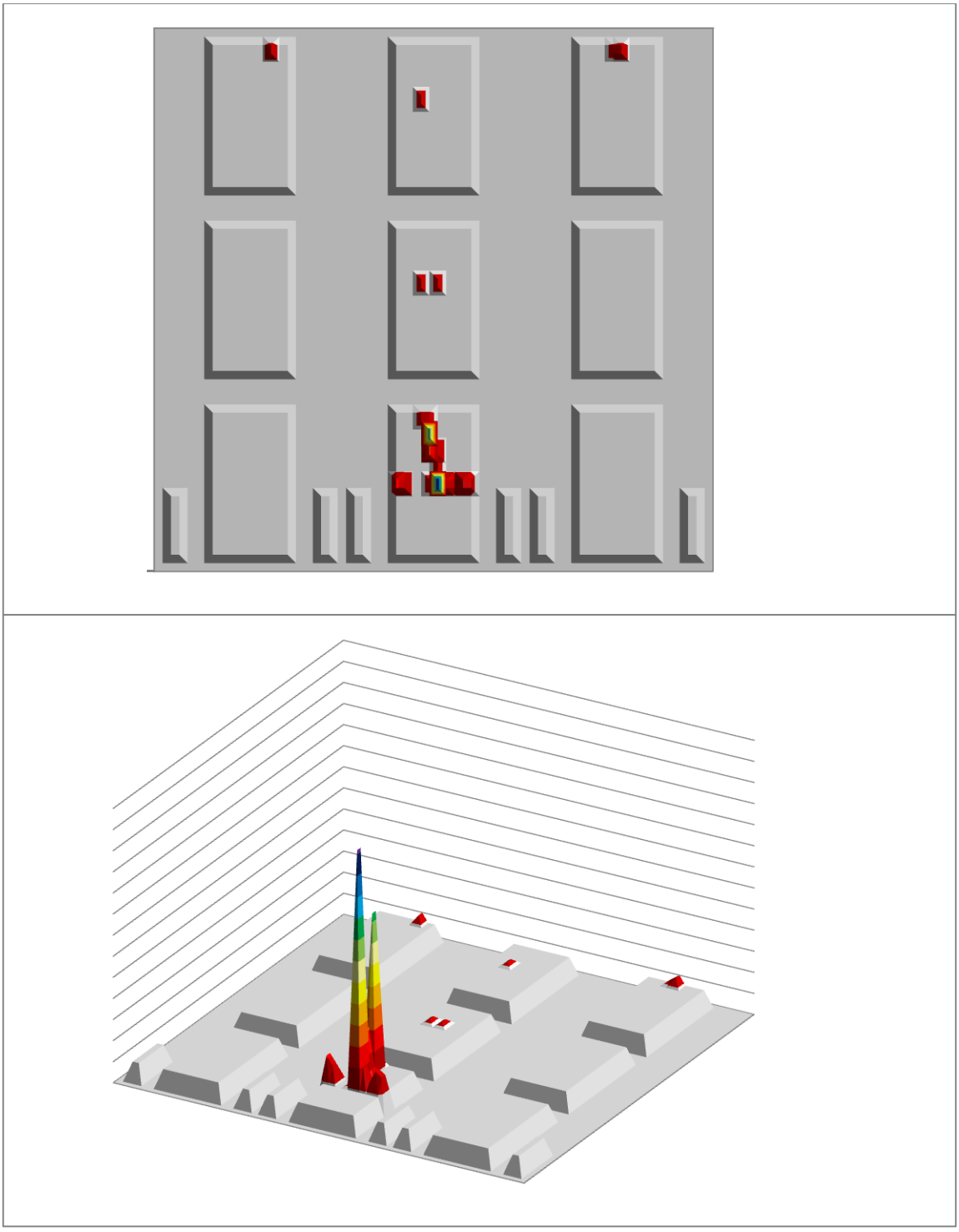

Fig. 44. Summary of results for vehicle (2,1).

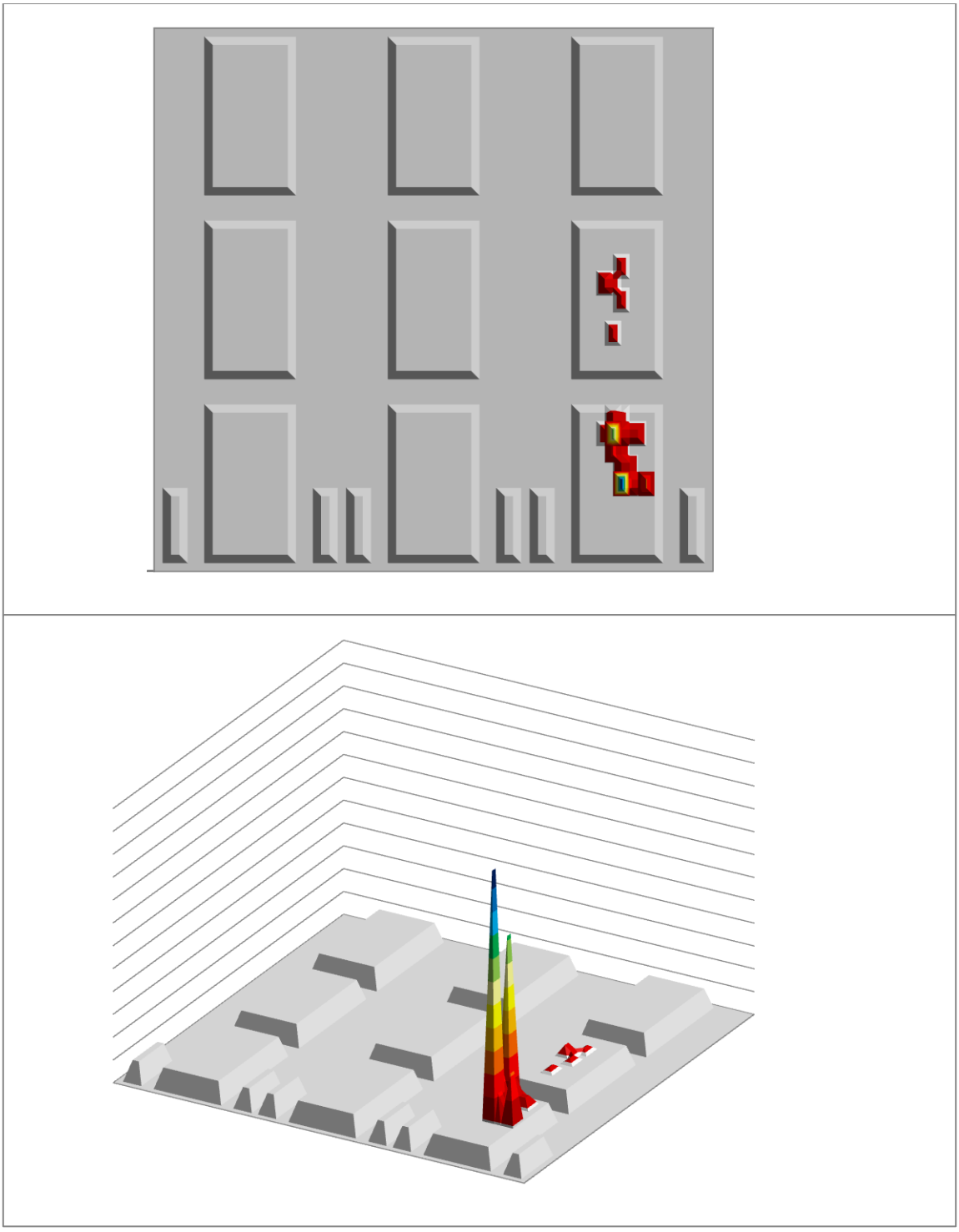

Fig. 45. Summary of results for vehicle (3,1).

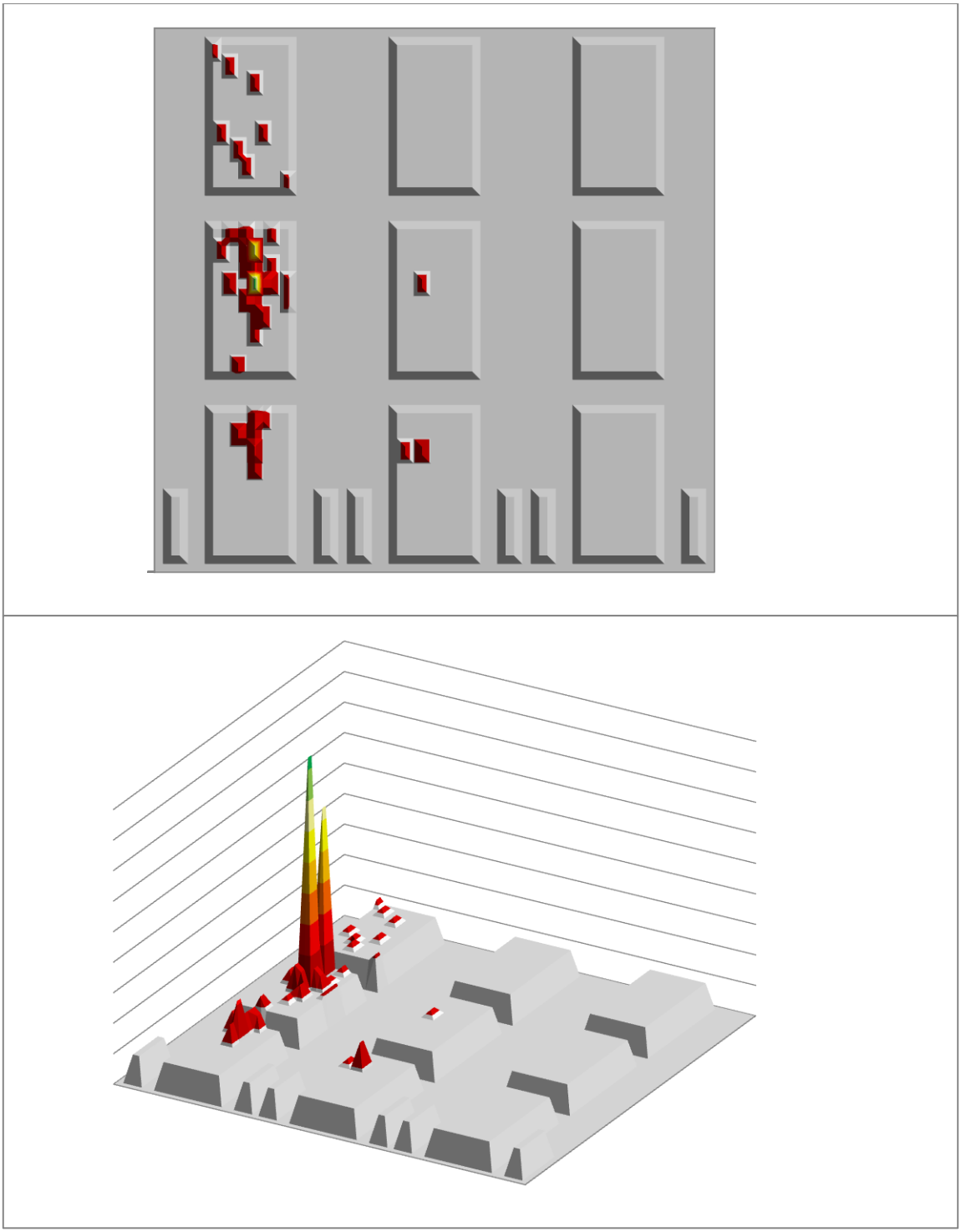

Fig. 46. Summary of results for vehicle (1,2).

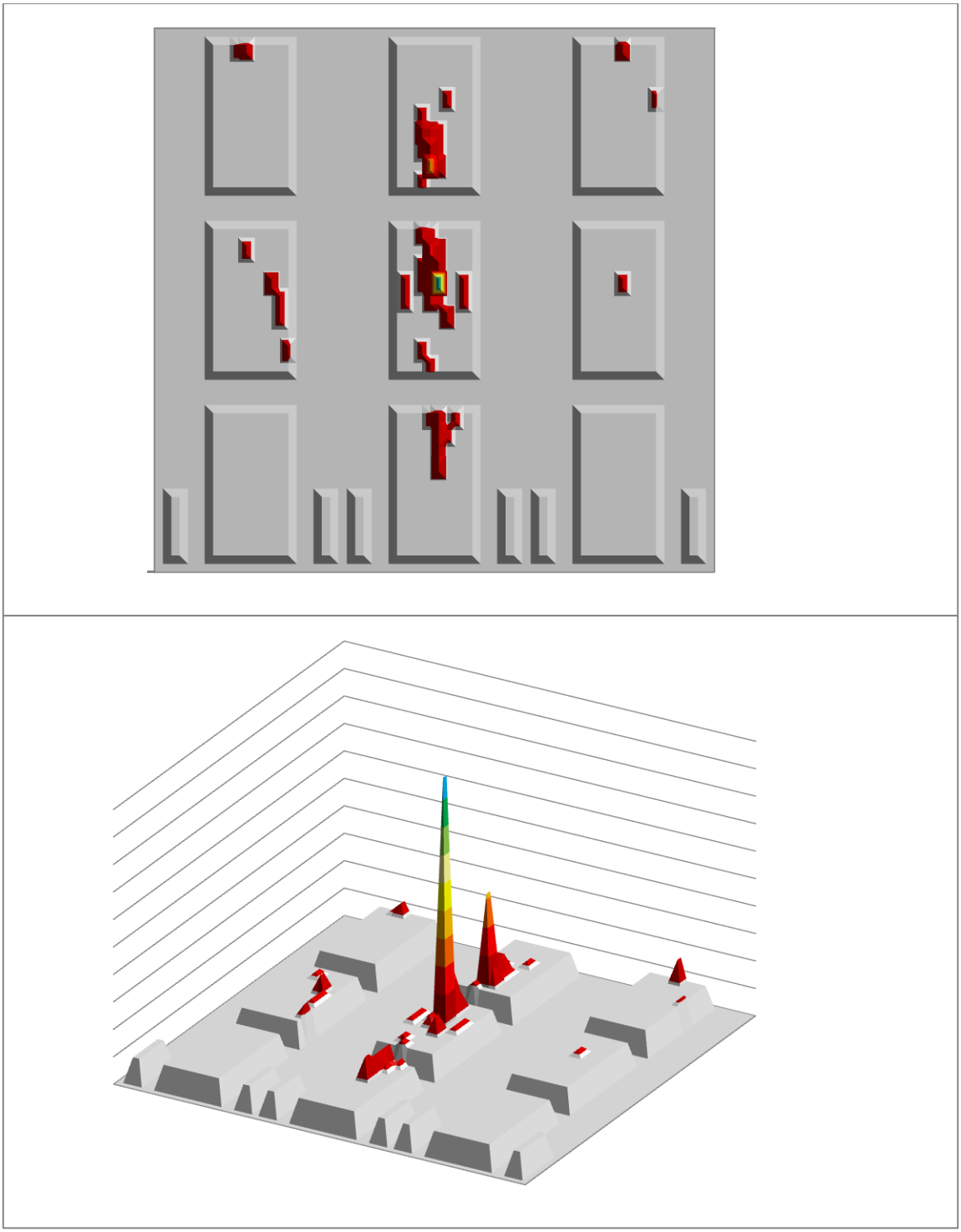

Fig. 47. Summary of results for vehicle (2,2).

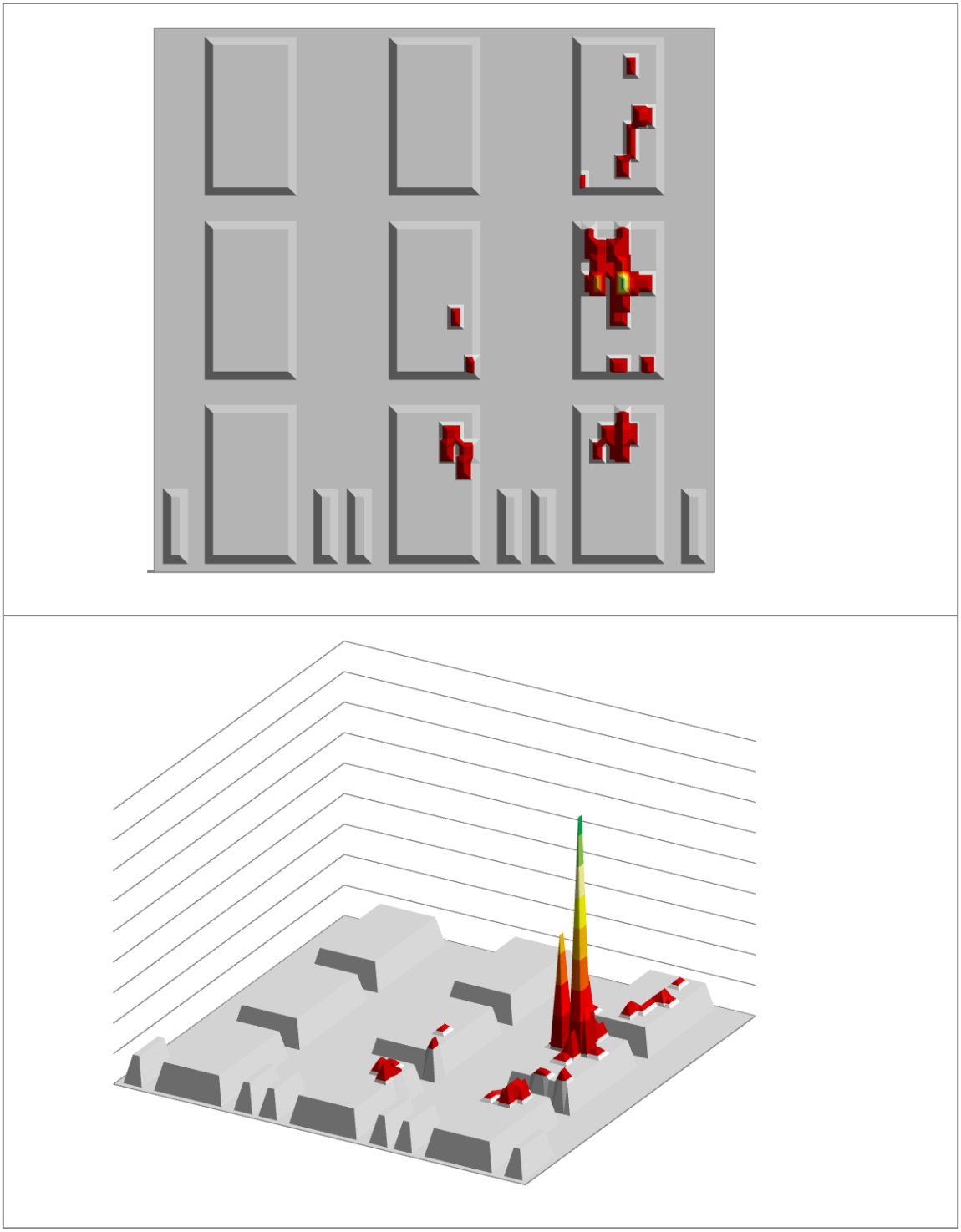

Fig. 48. Summary of results for vehicle (3,2).

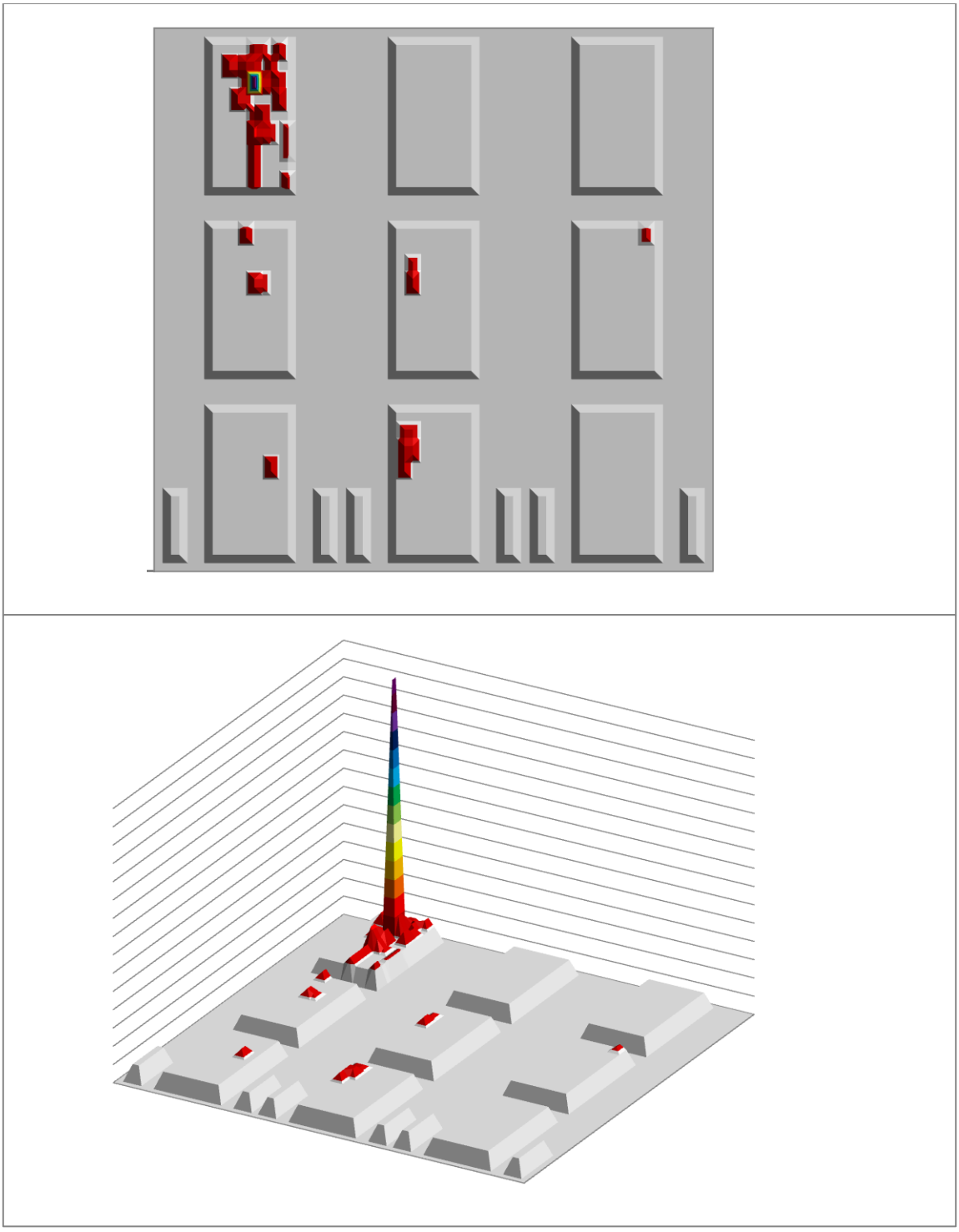

Fig. 49. Summary of results for vehicle (1,3).

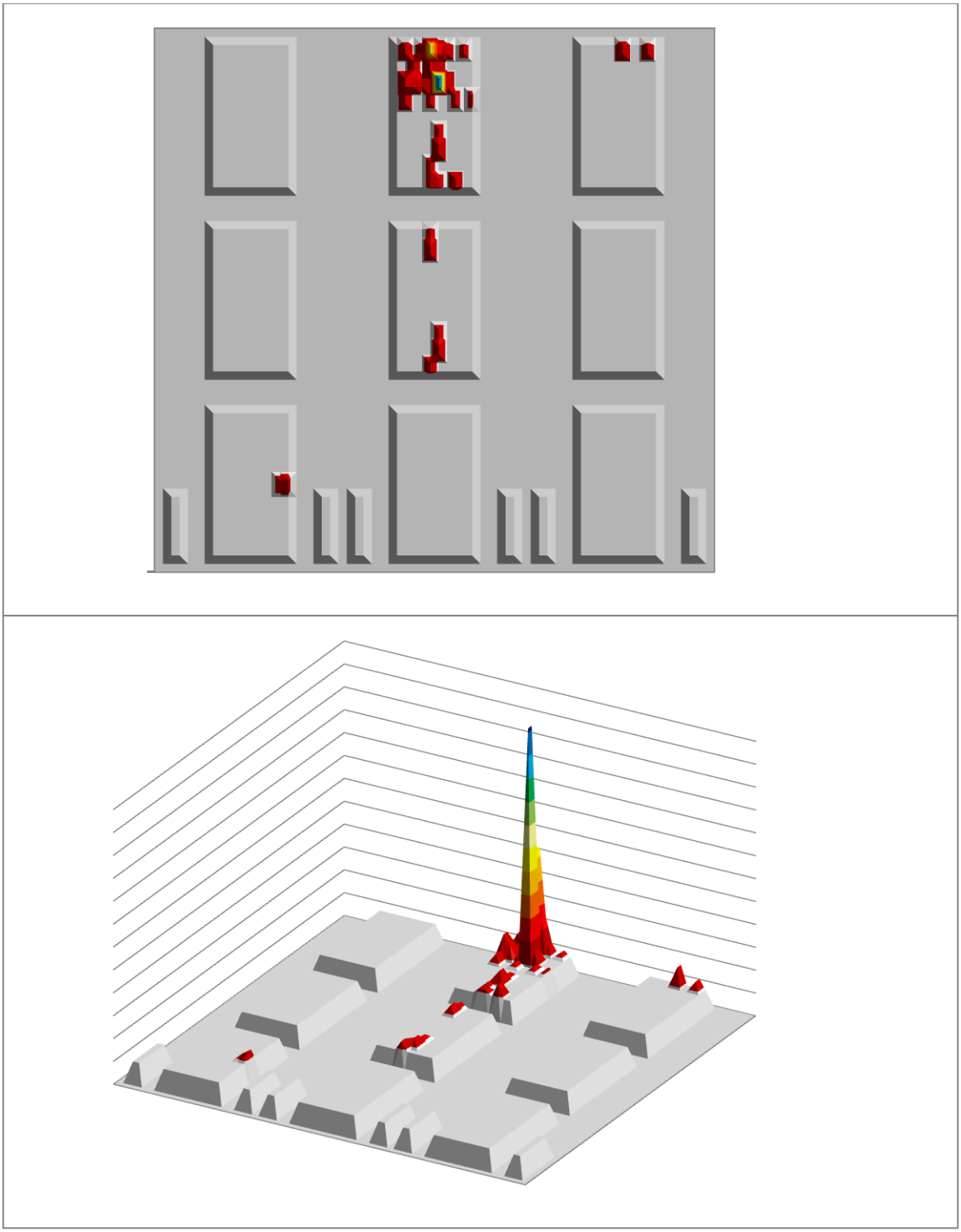

Fig. 50. Summary of results for vehicle (2,3).

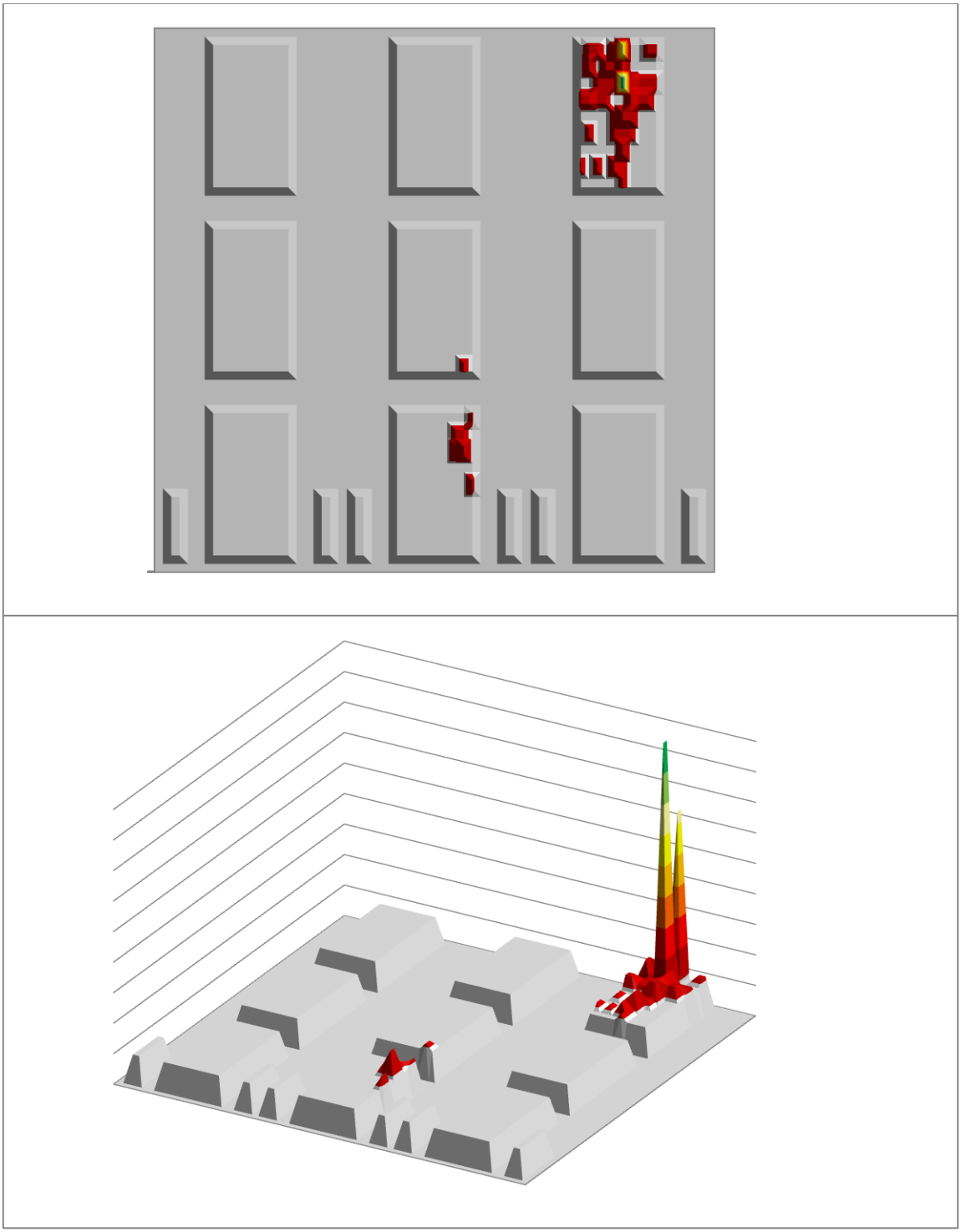

Fig. 51. Summary of results for vehicle (3,3).

V.D. Assessment of the One-Energy-Group Assumption

Recall from the problem setup in Chapter II that we used several simplifying assumptions in the transport equation including the assumption of only one energy group. The MCNPX baseline model shown in Fig. 22 was used to assess the validity of this assumption. MCNPX is a continuous-energy code, and the portal monitor measurements calculated by MCNPX are as close to experimental values as was possible for this project.

Measurements from the MCNPX baseline case were obtained by modeling a point source in the center of the passenger cabin of each vehicle. Two different energy spectra were modeled for each location: a ^{252}Cf spontaneous fission source and a 100 keV mono-energetic source. A total of nine simulations were run. There was one for the source located in each vehicle for two different neutron energy spectra. Reaction rate tallies (i.e, F4 tallies) for each portal monitor were used to calculate the detector signals. These measurements were then used as input in the inverse source location algorithm.

The results showed that the one-group assumption is probably inadequate for real-world applications. For the case of the ^{252}Cf source, the correct vehicle was only identified three out of nine times with an average error of 304.10 cm. Using the measurements from the mono-energetic source test, the correct vehicle was identified four out of nine times with an average error of 230.21 cm. A comparison to the code's performance

using measurements obtained from the forward model is given in Table 10. One thing to note is that the forward and inverse models are self consistent. The same grid spacing and cross sections were used to obtain the measurements as were used to solve the inverse problem.

Table 10. Comparison of Continuous-Energy and One-Group Test Case Results.

Measurement Origin	**Correct Vehicle ID'ed / Total Test Cases**	**Average Distance from Source [cm]**
MCNPX, ^{252}Cf Source	3 / 9	304.10
MCNPX, Mono-Energetic Source	4 / 9	230.21
Forward Model	9 / 9	30.00

The results in Table 10 were obtained from test cases using the same source locations and a total convergence tolerance of 1.0. The inverse source location code performed slightly better with the 100 keV mono-energetic source, but there is not enough data to say this conclusively. It is, however, clear from the inability of the code to reliably identify the correct vehicle and the large average error in the results that more energy groups should be added for any real-world application of the code. We have shown that one-group simulations work in identifying the correct vehicle in most cases. There is nothing special about the group we chose, so because the Law of Superposition applies, the algorithm should work for multiple groups. It is more a question of how long the code will take to run. Again, computational time and accuracy will need to be optimized, but an upgrade to two or three groups is unlikely to make a major difference in

computational time and is likely justified by increased accuracy. If the increase in computational time from running a multi-group transport solver is too large, it can also be balanced by running on a coarser grid.

CHAPTER VI

CONCLUSIONS AND RECOMMENDATIONS

VI.A. Summary of Results

In this work, we have demonstrated an algorithm to locate a radioactive source using a distributed array of detectors. The algorithm was specified for use with radiation portal monitors at land border crossings, where delays caused by radiation detectors can have major economic implications. In the algorithm, we derived a mathematical technique based on radiation transport theory to reconstruct information about the location of a source within a field of vehicles.

The algorithm uses forward and adjoint transport calculations in an optimization problem posed to minimize an objective function. The objective function describes the least-squares difference between the actual and estimated detector measurements and is minimized using the steepest-descent method. The gradient used in the steepest-descent method is calculated using the adjoint flux in the estimated source location. The algorithm iterates between the forward and inverse models until the source location is identified. The forward model consists entirely of a forward transport solver; whereas, the inverse model includes the adjoint transport solver, gradient calculation, and line search algorithm.

To verify that the forward solver performed as expected, a series of test problems were executed with a 3-D transport solver and compared to results for the same problems run using PARTISN. Five test cases were chosen to test the code under a variety of conditions: (1) a distributed source with average cross sections, (2) a point source with average cross sections, (3) a point source in a highly scattering medium, (4) a point source in a strongly absorbing medium, and (5) a point source in a near vacuum. The test problems showed that, with reasonable certainty, the forward transport code produced good results.

To test the inverse code, we first developed a baseline scenario to represent a typical land border crossing. The baseline scenario consisted of three lanes of traffic, three vehicles deep, with a radiation portal monitor in each lane. A series of tests were run to assess the performance of the code under different conditions. These included the following: the position of the source within a given vehicle, convergence tolerance, optical thickness of the vehicles, fill level in the gas tank, physical size of the vehicles, detector efficiency, and measurements obtained using MCNPX (a continuous-energy code).

Using the baseline cross sections and geometry, the code was tested with the source in five different locations within each vehicle (the center, left, and right side of the passenger cabin; the engine; and the trunk). The inverse code performed extremely well with a success rate for identifying the correct vehicle of 96%.

Because there is a need to balance the computational time with accuracy, the convergence tolerance was also assessed. It was found that the average error increases with increasing tolerance, and a tolerance value of 1.0 represents the optimal compromise between time and accuracy.

In the baseline case, we assumed perfect knowledge of the geometry and cross sections. To assess the effect of uncertainties in various parameters, we performed a sensitivity analysis. Our analysis revealed that, in order of most to least impact, the code is sensitive to the optical thickness of the vehicles, the detector efficiency, the physical size of the vehicles, and the fill level in the gas tank.

Finally, we assessed the validity of the one-energy-group assumption to a real-world scenario. To do this, we modeled the baseline scenario using MCNPX to obtain the portal monitor measurements. The code did not perform well with these measurements, suggesting the one-energy-group assumption will not be valid for a real-world border scenario.

VI.B. Recommendations for Future Work

Within the defined scope of this project, the algorithm performed very well; however, a few fundamental improvements can be made to the code in future work:

1. Upgrade the code from one-energy group to multi-energy groups. The MCNPX comparison made it clear that the code will need to include more than just one energy group before it is deployed in a real-world situation. As seen throughout this project, the computational time and the accuracy of the code need to be optimized. It is expected that the addition of one to two energy groups should be enough to improve the accuracy of the code without seriously affecting the computational time. If the computational time associated with the addition of more energy groups is too large, then it can be balanced by running the transport solver on a coarser grid.
2. Develop more accurate geometry and material properties for the system. For the purposes of this work, we considered a fairly rough 3-D approximation of a vehicle with Maxwellian-averaged cross sections. While this was sufficient for a proof-of-concept project, more accurate models should be developed for a real-world application.
3. Incorporate camera and image recognition technology into the algorithm. For this work, we assumed that the geometry and cross sections of the vehicles were known quantities. In practice, this will not be known *a priori*. Cameras are already deployed at border crossings, so once the portal monitors are alarmed, photographic images of the vehicles can be processed with image recognition software. This information can be used with pre-built cross section libraries to build the model parameters. This type of general image recognition technology currently exists in commercial, off-the-shelf form.

4. Incorporate the ability to handle multiple sources and distributed sources. For this code, we assumed that there was only one source present in the system, but it is possible that multiple sources may be present. We also assumed the source was a point source, but it is possible that a source could be distributed. These two assumptions constrain the solution, so removing them adds more degrees of freedom to the problem. In principle, the code can be expanded to handle multiple and/or distributed sources if deemed an important feature, although it will also increase the computational time and the likelihood of the code making an error.
5. Benchmark the code with real measurements. While computational modeling can provide good predictions of how the code will perform in a real-world scenario, there is no better test than real measurements. For this work, real measurements were time and resource prohibitive, but the algorithm should be tested with real vehicles, portal monitors, and sources before it is used in a real-world scenario.
6. Investigated the algorithm in additional contexts. We have only investigated the code for use at a land border crossing, but there is potential for the code to be used in any number of situations where there is a distributed array of detectors. Examples include international safeguards (e.g., for use in a large glovebox), emergency response scenarios, and covert intelligence gathering. The potential for the inverse source location algorithm to be used in these alternate applications should be explored in future work.

REFERENCES

1. G. GILBERT, *Neutralizing the Nuclear and Radiological Threat: Securing the Global Supply Chain*, written testimony, U.S. Senate, Permanent Subcommittee on Investigations, Committee on Homeland Security and Governmental Affairs (2006).

2. E. A. MCKIGNEY, R. GHOLKAR, and D. VEGA, "A Study of Lane Differentiation Using an Array of Detectors," LA-UR-04-4405, Los Alamos National Laboratory (2004).

3. S. J. NORTON, "A General Nonlinear Inverse Transport Algorithm Using Forward and Adjoint Flux Computations," *IEEE Trans. Nucl. Sci.*, **44**, 2, 153 (1997).

4. A. H. HIELSCHER and S. BARTEL, "Use of Penalty Terms in Gradient-Based Iterative Reconstructive Schemes for Optical Tomography," *Journ. Biomed. Optics*, **6**, 2, 183 (2001).

5. J. A. FAVORITE and R. SANCHEZ, "An Inverse Method for Radiation Transport," *Rad. Prot. Dosimetry*, **116**, 1–4, 482 (2005).

6. J. A. FAVORITE and K. C. BLEDSOE, "Identification of an Unknown Material in a Radiation Shield Using the Schwinger Inverse Method," *Nucl. Sci. Eng.*, **152**, 106 (2006).

7. G. I. BALATSKY, S. L. EATON, and W. R. SEVERE, "Illicit Trafficking of Nuclear and Radiological Materials," in *Nuclear Safeguards, Security, and Nonproliferation: Achieving Security with Technology and Policy*, pp. 415-431, J. E. DOYLE, Ed., Butterworth-Heinemann (2008).

8. International Atomic Energy Agency, *Illicit Trafficking and Other Unauthorized Activities Involving Nuclear and Radioactive Materials*, Fact Sheet, <http://www.iaea.org/NewsCenter/Features/RadSources/PDF/fact_figures2005.pdf> (2006).

9. M. BRONNER, *100 Grams (and Counting…): Notes from the Nuclear Underworld*, Managing the Atom Project, Harvard University, Cambridge, Mass. (2008).

10. International Atomic Energy Agency, *IAEA Information System on Incident of Illicit Trafficking and Other Unauthorized Activities Involving Nuclear and Radioactive Materials*, Fact Sheet, <http://www.iaea.org/NewsCenter/Features/RadSources/PDF/fact_figures2006.pdf> (2007).

11. National Nuclear Security Administration, *NNSA's Second Line of Defense Program*, <http://nnsa.energy.gov/news/992.htm> (2008).

12. Customs and Border Protection, *Radiation Portal Monitors Safeguard America from Nuclear Devices and Radiological Material*, <http://www.cbp.gov/xp/cgov/border_security/port_activities/cargo_exam/rad_portal1.xml>.

13. D. REILLY, N. ENSSLIN, H. SMITH, and S. KREINER, *Passive Nondestructive Assay of Nuclear Materials*, Office of Nuclear Regulatory Research, NUREG/CR-5550, LA-UR-90-732 (1991).

14. Canberra Industries, Inc., *RadSentry™ Security Portal for SNM and Other Radionuclides*, <http://www.canberra.com/pdf/Products/Systems_pdf/C30008-RadSentry-SS.pdf> (2007).

15. W. MENKE, *Geophysical Data Analysis: Discrete Inverse Theory*, Revised ed., Academic Press, San Diego, California (1989).

16. N. J. MCCORMICK and I. KUSCER, "On the Inverse Problem in Radiative Transfer," *Journ. Math. Phys.*, **15**, 7, 926 (1974).

17. C. E. SIEWERT, "On a Possible Experiment to Evaluate the Validity of the One-Speed or Constant Cross Section Model of the Neutron-Transport Equation," *Journ. Math. Phys.*, **19**, 7, 1587 (1978).

18. C. E. SIEWERT, "A New Approach to the Inverse Problem," *Journ. Math. Phys.*, **19**, 12, 2619 (1978).

19. N. J. MCCORMICK, "Transport Scattering Coefficients from Reflection and Transmission Measurements," *Journ. Math. Phys.*, **20**, 7, 1504 (1979).

20. N. J. MCCORMICK and R. SANCHEZ, "Inverse Problem Transport Calculations for Anisotropic Scattering Coefficients," *Journ. Math. Phys.*, **22**, 1, 199 (1981).

21. R. SANCHEZ and N. J. MCCORMICK, "General Solutions to Inverse Transport Problems," *Journ. Math. Phys.*, **22**, 4, 847 (1981).

22. E. W. LARSEN, "Solution of the Inverse Problem in Multigroup Transport Theory," *Journ. Math. Phys.*, **22**, 1, 158 (1981).

23. E. W. LARSEN, "Solution of Multidimensional Inverse Transport Problems," *Journ. Math. Phys.*, **25**, 1, 131 (1983).

24. Y. JARNY, M. N. OZISIK, and J. P. BARDON, "A General Optimization Method Using Adjoint Equation for Solving Multidimensional Inverse Heat Conduction," *Int. Journ. Heat Mass Transfer*, **34**, 11, 2911 (1991).

25. A. H. HIELSCHER, A. D. KLOSE, and K. M. HANSON, "Gradient-Based Iterative Image Recontruction Scheme for Time-Resolved Optical Tomography," *IEEE Trans. Med. Imag.*, **18**, 3 (1999).

26. A. D. KLOSE and A. H. HIELSCHER, "Optical Tomography Using the Time-Independent Equation of Radiative Transfer–Part 2: Inverse Model," *Journ. Quant. Spect. Rad. Trans.*, **72**, 715 (2002).

27. A. D. KLOSE, "The Inverse Source Problem in Optical Molecular Imaging," *Trans. Am. Nucl. Soc.*, **95**, 525 (2006).

28. R. SANCHEZ and N. J. MCCORMICK, "Inverse Source Problems in Linear Transport Theory," *Trans. Am. Nucl. Soc.*, **95**, 523 (2006).

29. G. THORESON, J. C. RAGUSA, and W. BANGERTH, "Some Advances on Inverse Particle Transport Problems with Applications to Homeland Security," *Trans. Am. Nucl. Soc.*, **95**, 534 (2006).

30. S. BOYD and L. VANDENBERGHE, *Convex Optimization*, Cambridge University Press, Cambridge (2004).

31. R. L. BURDEN and J. D. FAIRES, *Numerical Analysis*, 7th ed., Brooks/Cole, United States of America (2001).

32. A. TARANTOLA, *Inverse Problem Theory: Methods for Data Fitting and Model Parameter Estimation*, Elsevier Science Publishing Company Inc., The Netherlands (1987).

33. W. M. STACEY, *Nuclear Reactor Physics*, John Wiley & Sons, Inc., New York City (2001).

34. E. E. LEWIS and W. F. MILLER, *Computational Methods of Neutron Transport*, American Nuclear Society, Inc., United States of America (1993).

35. J. C. RAGUSA, "Application of Duality Principles to Solve Inverse Particle Transport Problem: A Framework," *Trans. Am. Nucl. Soc.*, **93**, 427 (2005).

36. A. N. TIKHONOV and V. Y. ARSENIN, *Solutions of Ill-Posed Problems*, V. H. Winston & Sons, Washington, D.C. (1977).

37. J. K. SHAW and R. E. FAW, *Radiation Shielding*, Prentice Hall PTR, United States of America (1996).

38. B. G. CARLSON, "Transport Theory: Discrete Ordinates Quadrature Over the Unit Sphere," LA-4554, Los Alamos National Laboratory (1970).

39. K. D. LATHROP and B. G. CARLSON, "Discrete Ordinates Angular Quadrature of the Neutron Transport Equation," LA-3186, Los Alamos National Laboratory (1965).

40. D. BLEECKER and G. CSORDAS, *Basic Partial Differential Equations*, International Press, Cambridge, Massachusetts (2003).

41. M. L. ADAMS, "Fast Iterative Methods for Discrete-Ordinates Particle Transport Calculations," *Progress in Nuclear Energy*, **40**, 1, 3 (2002).

42. R. E. ALCOUFFE, R. S. BAKER, J. A. DAHL, S. A. TURNER and R. WARD, "PARTISN: A Time-Dependent, Parallel Neutral Particle Transport Code System," LA-UR-05-3925, Los Alamos National Laboratory (2005).

43. "MCNPX User's Manual Version 2.6.0," Ed. D. B. Pelowitz, LA-CP-07-1473, Los Alamos National Laboratory (2008).

44. *Table of Nuclides*, Korea Atomic Energy Research Institute, <http://atom.kaeri.re.kr/ton> (2000).

APPENDIX A

INVERSE CODE PLOTS

Optical Thickness Results

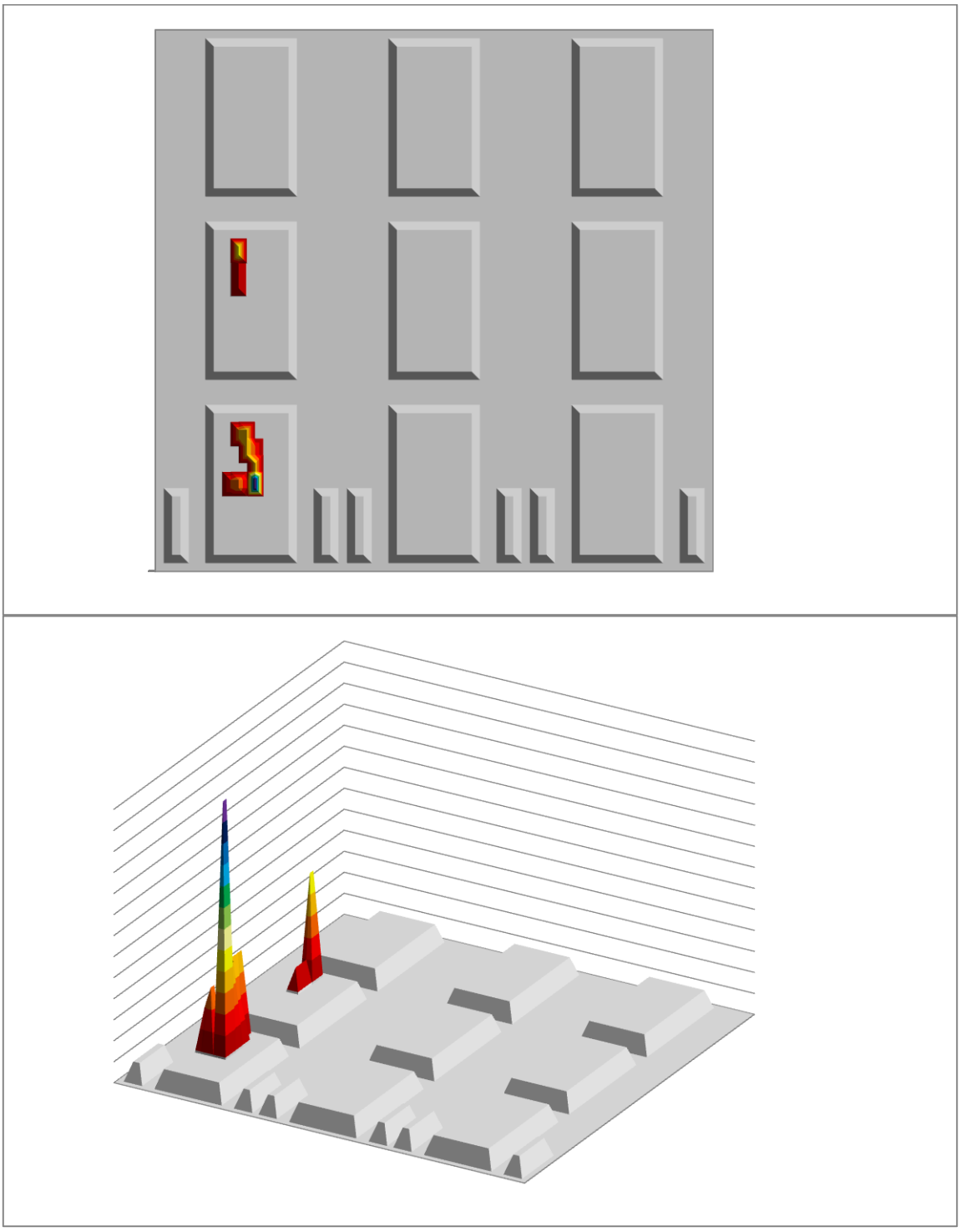

Fig. A.1. Optical thickness sensitivity analysis results for vehicle (1,1).

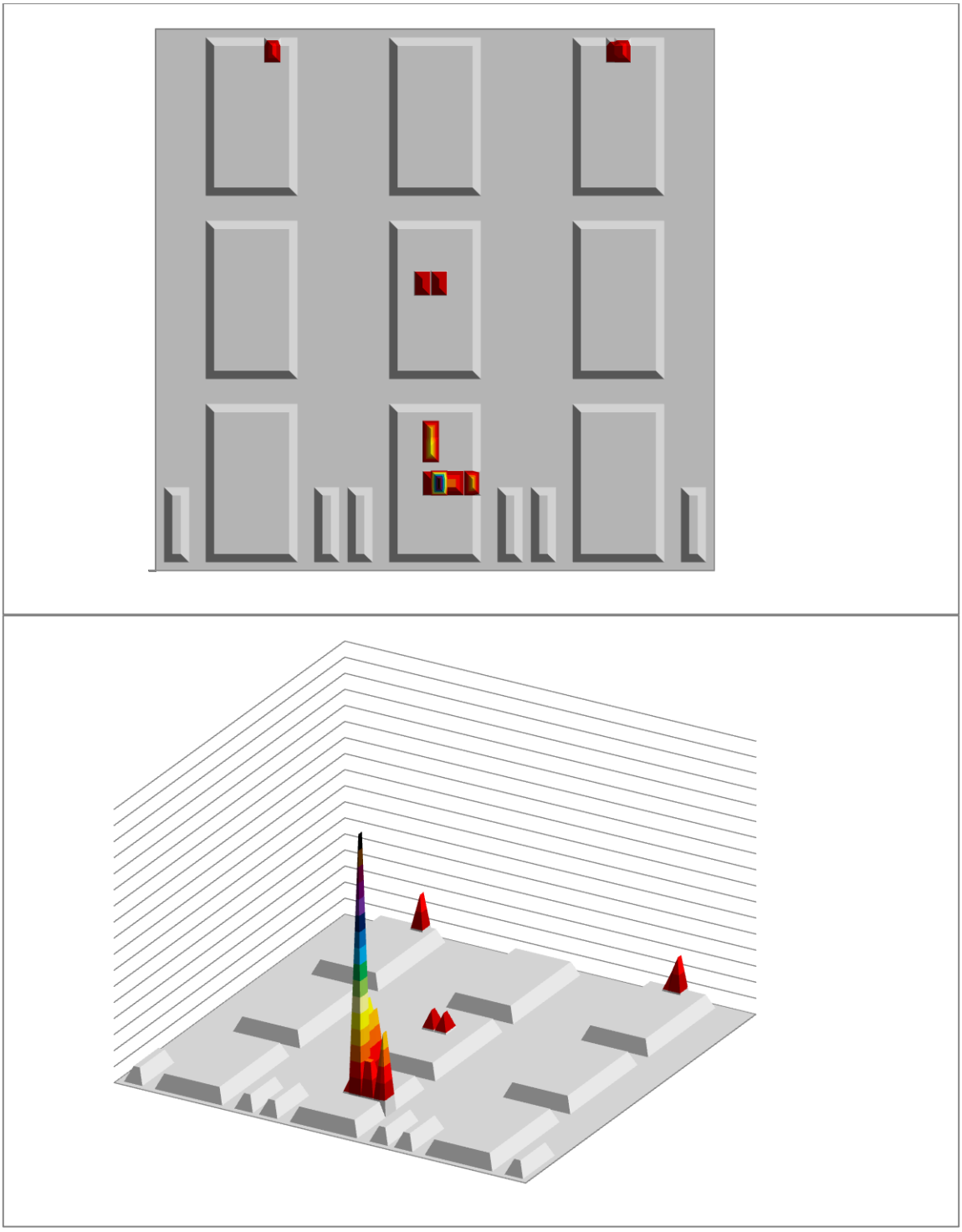

Fig. A.2. Optical thickness sensitivity analysis results for vehicle (2,1).

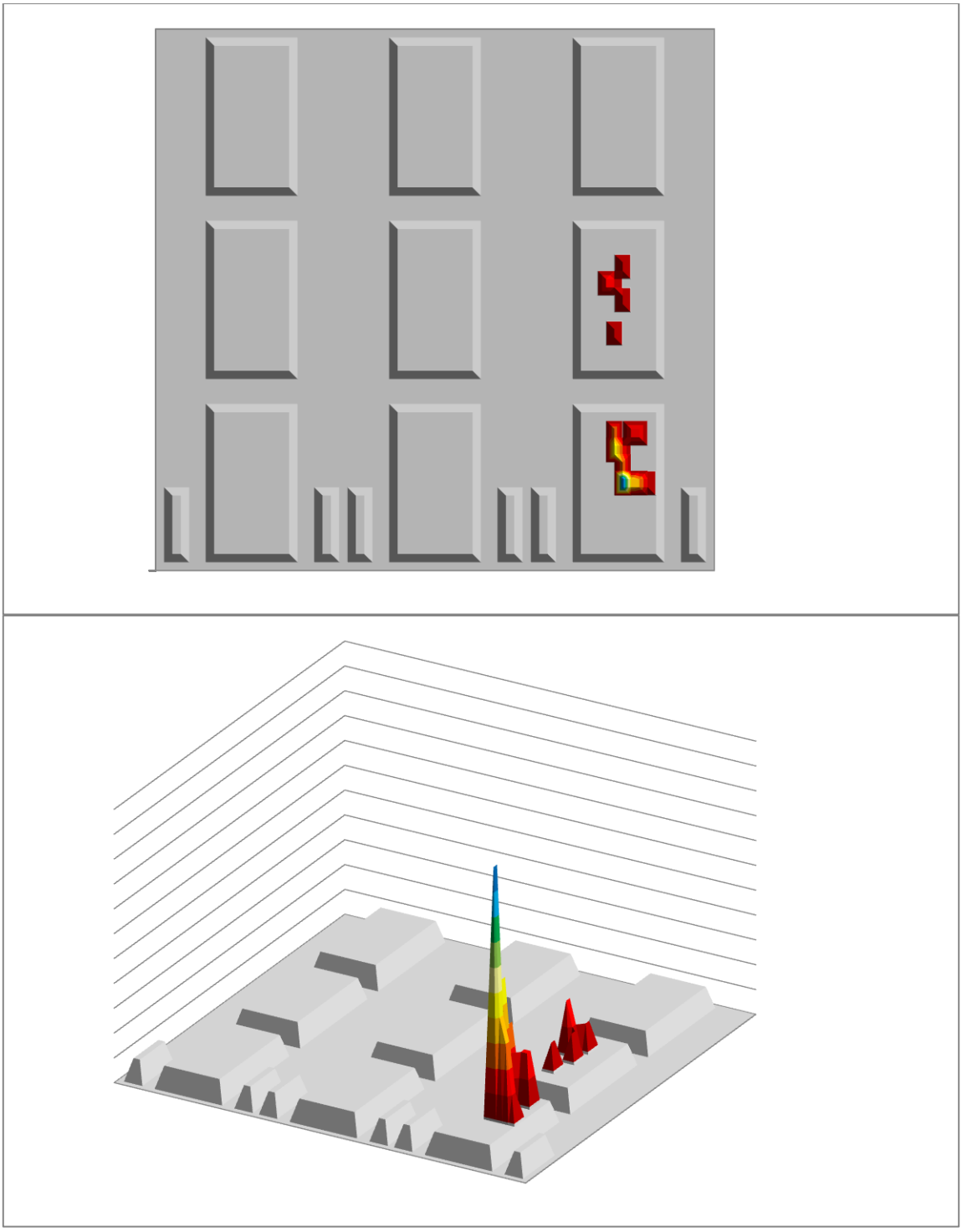

Fig. A.3. Optical thickness sensitivity analysis results for vehicle (3,1).

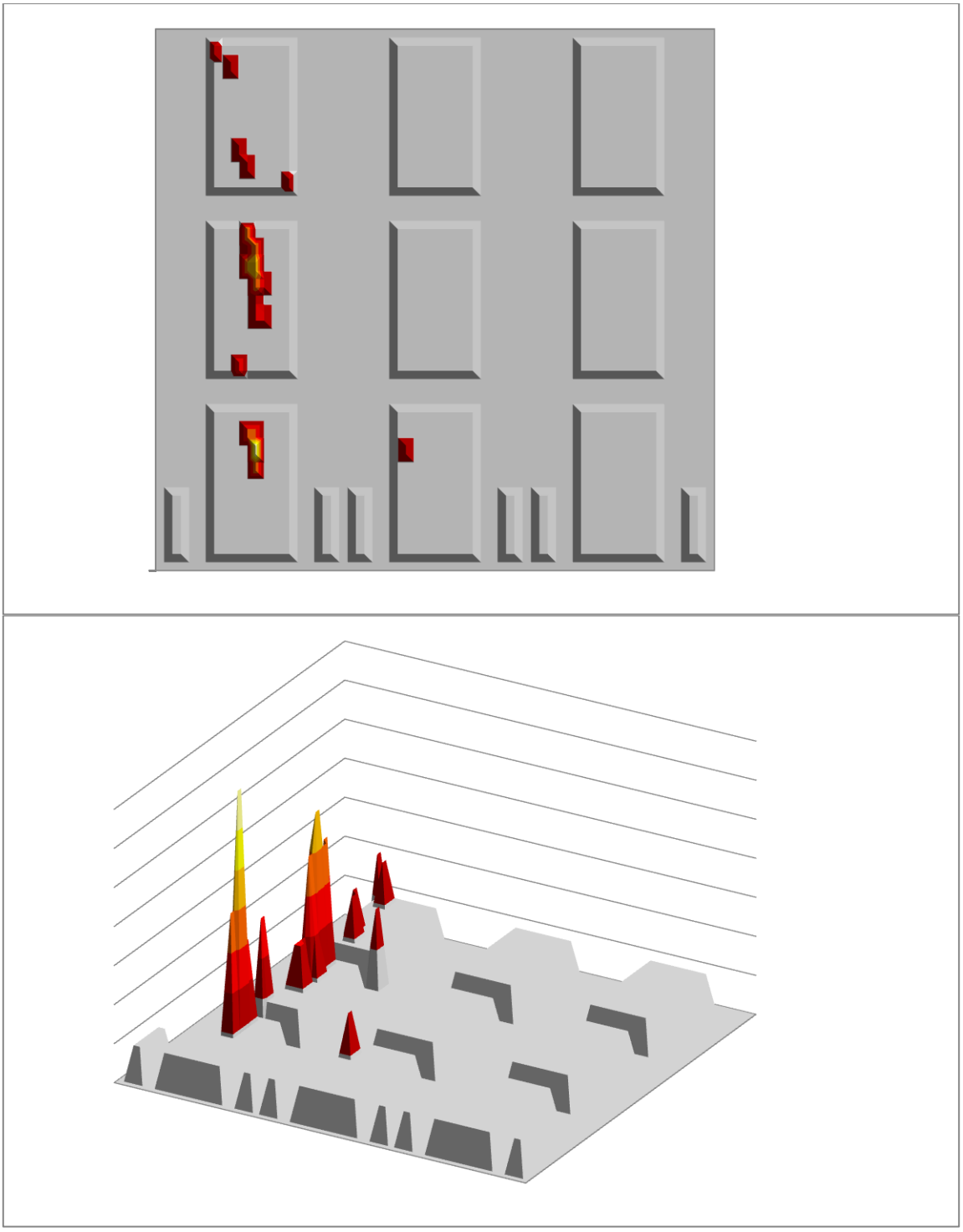

Fig. A.4. Optical thickness sensitivity analysis results for vehicle (1,2).

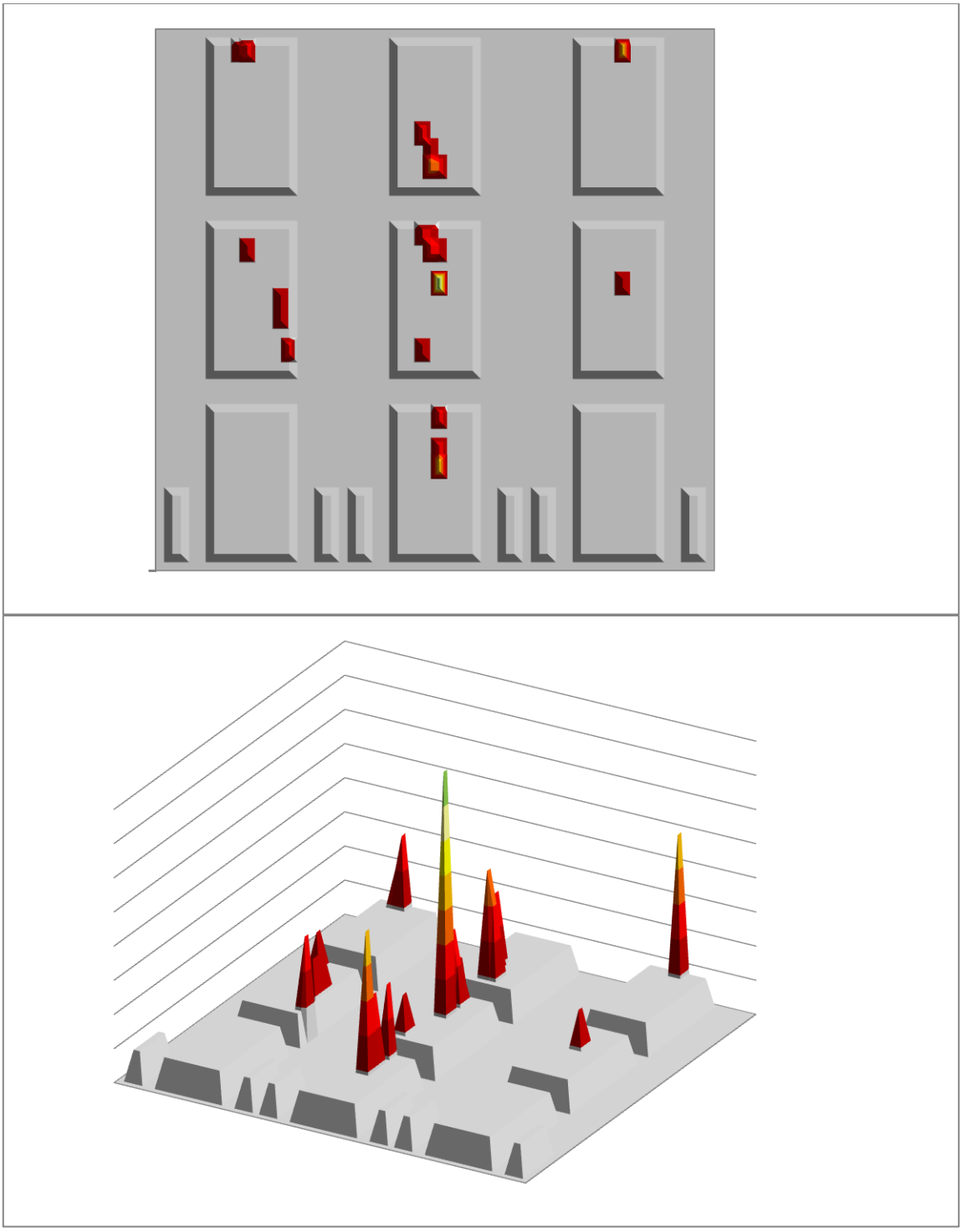

Fig. A.5. Optical thickness sensitivity analysis results for vehicle (2,2).

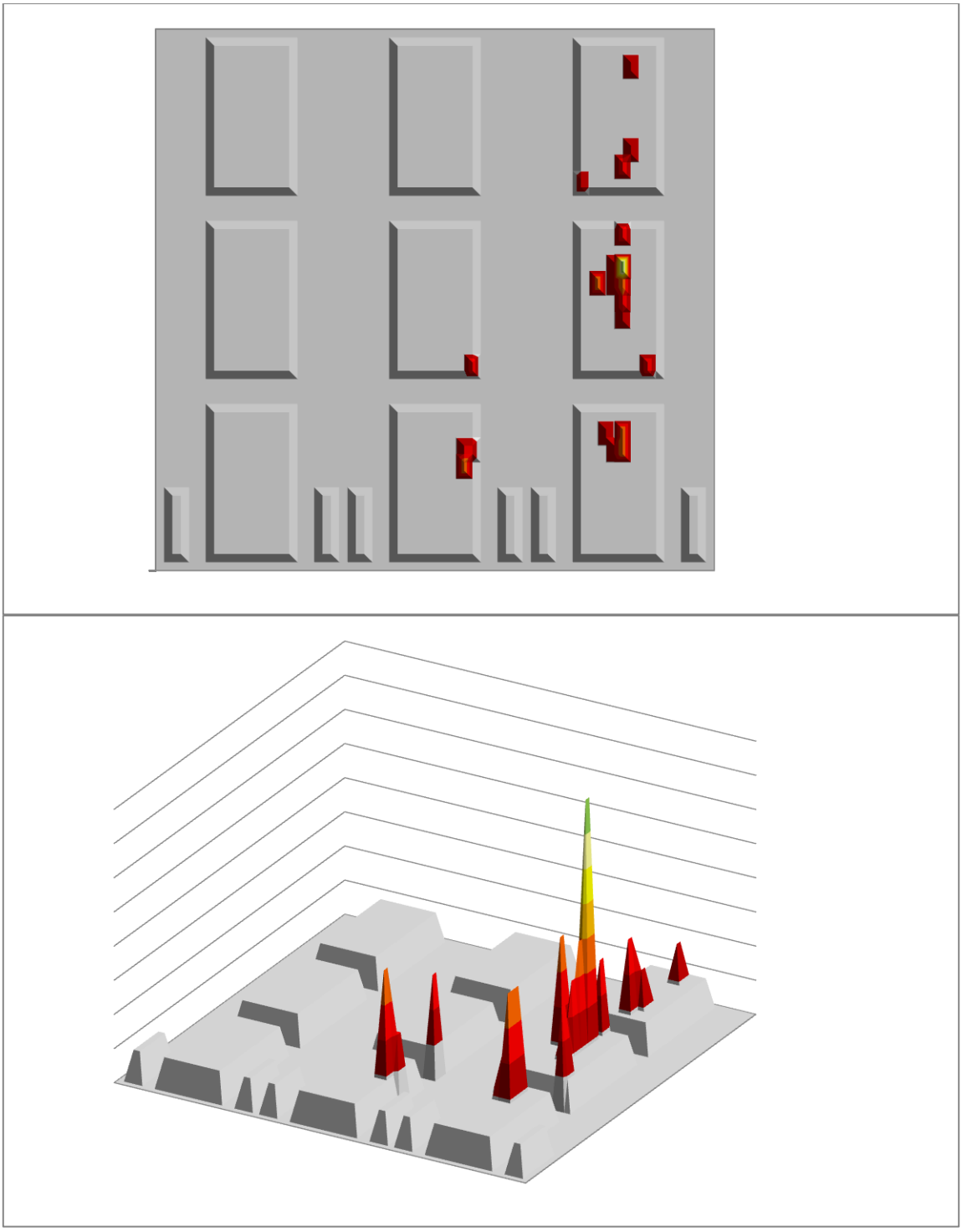

Fig. A.6. Optical thickness sensitivity analysis results for vehicle (3,2).

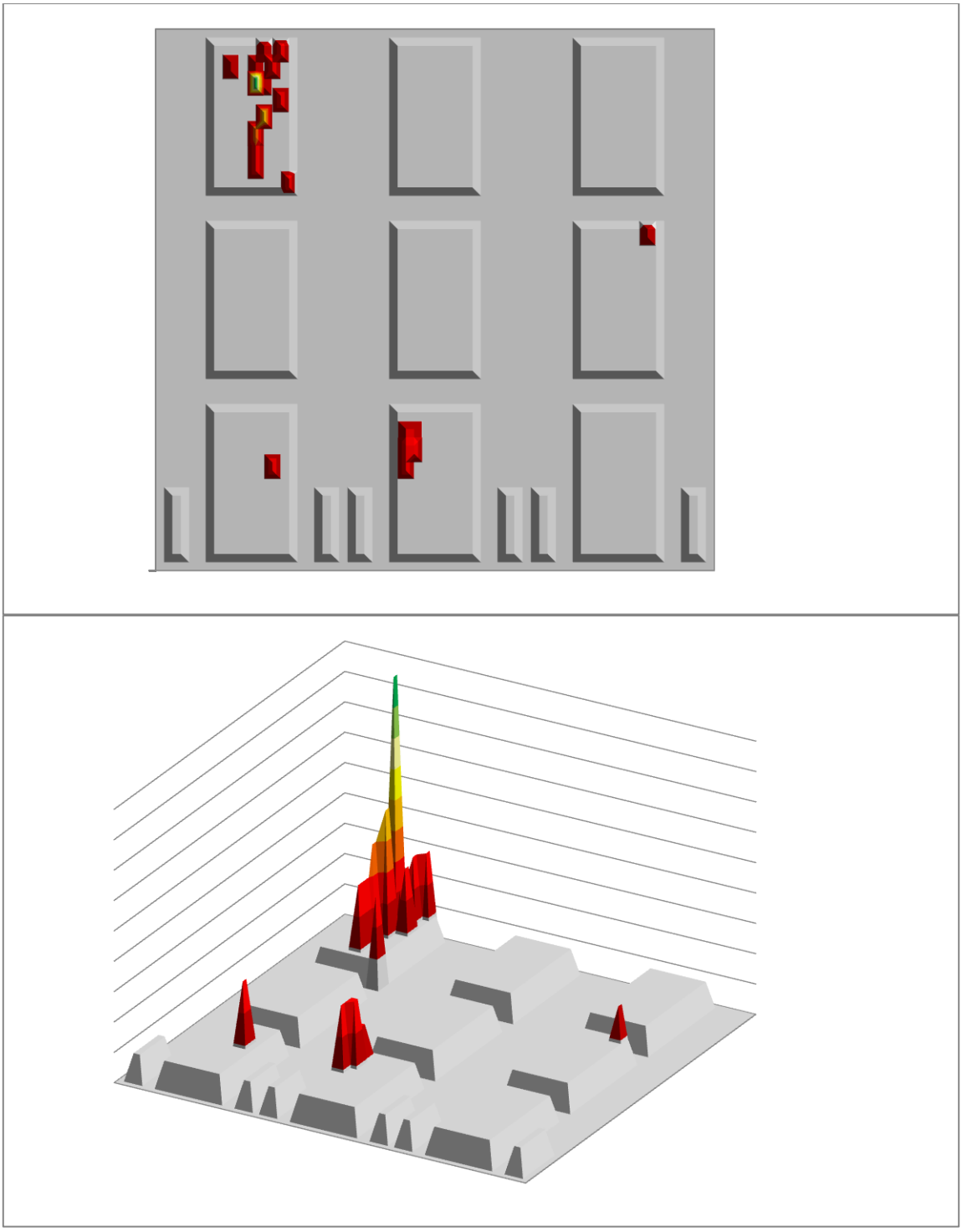

Fig. A.7. Optical thickness sensitivity analysis results for vehicle (1,3).

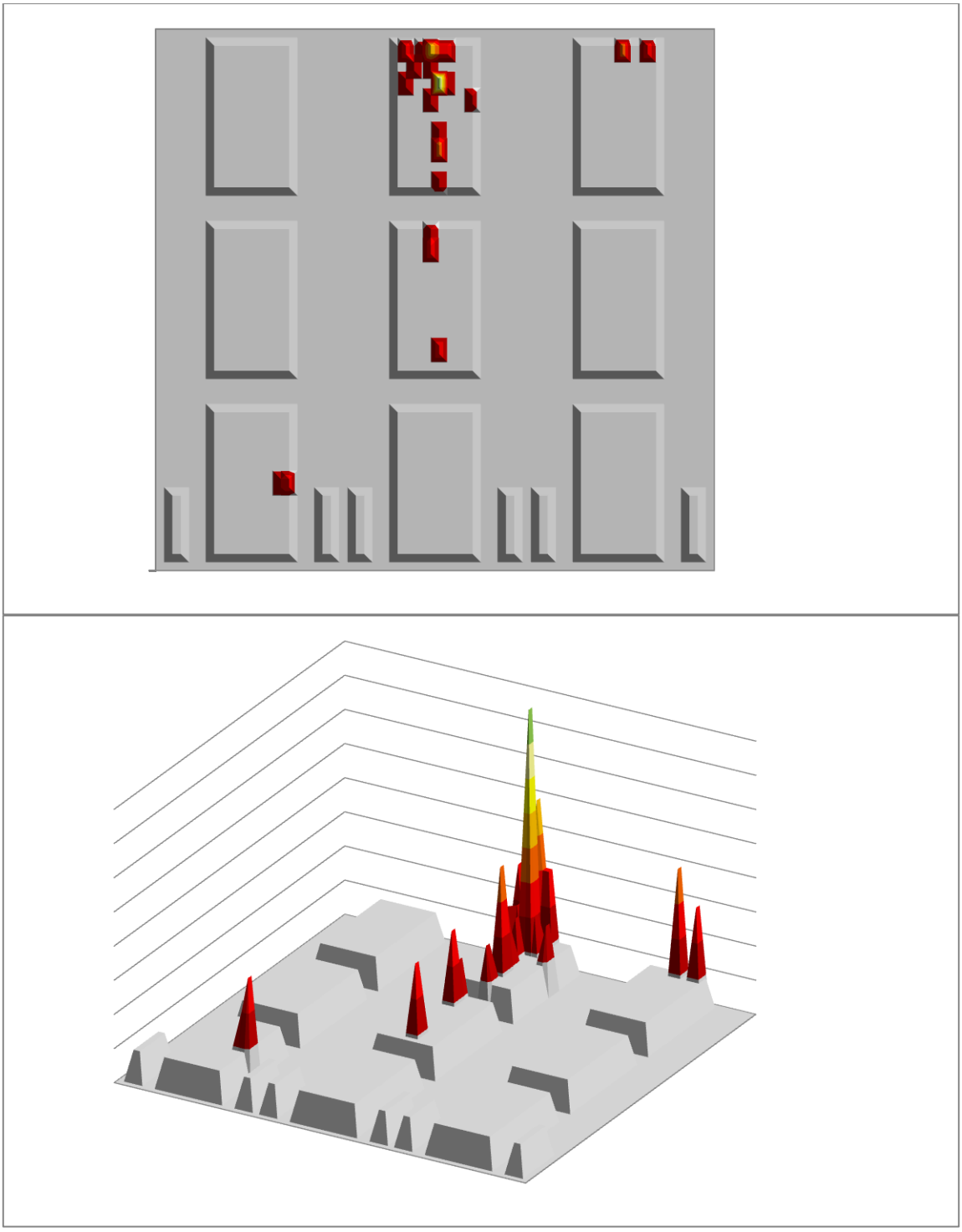

Fig. A.8. Optical thickness sensitivity analysis results for vehicle (2,3).

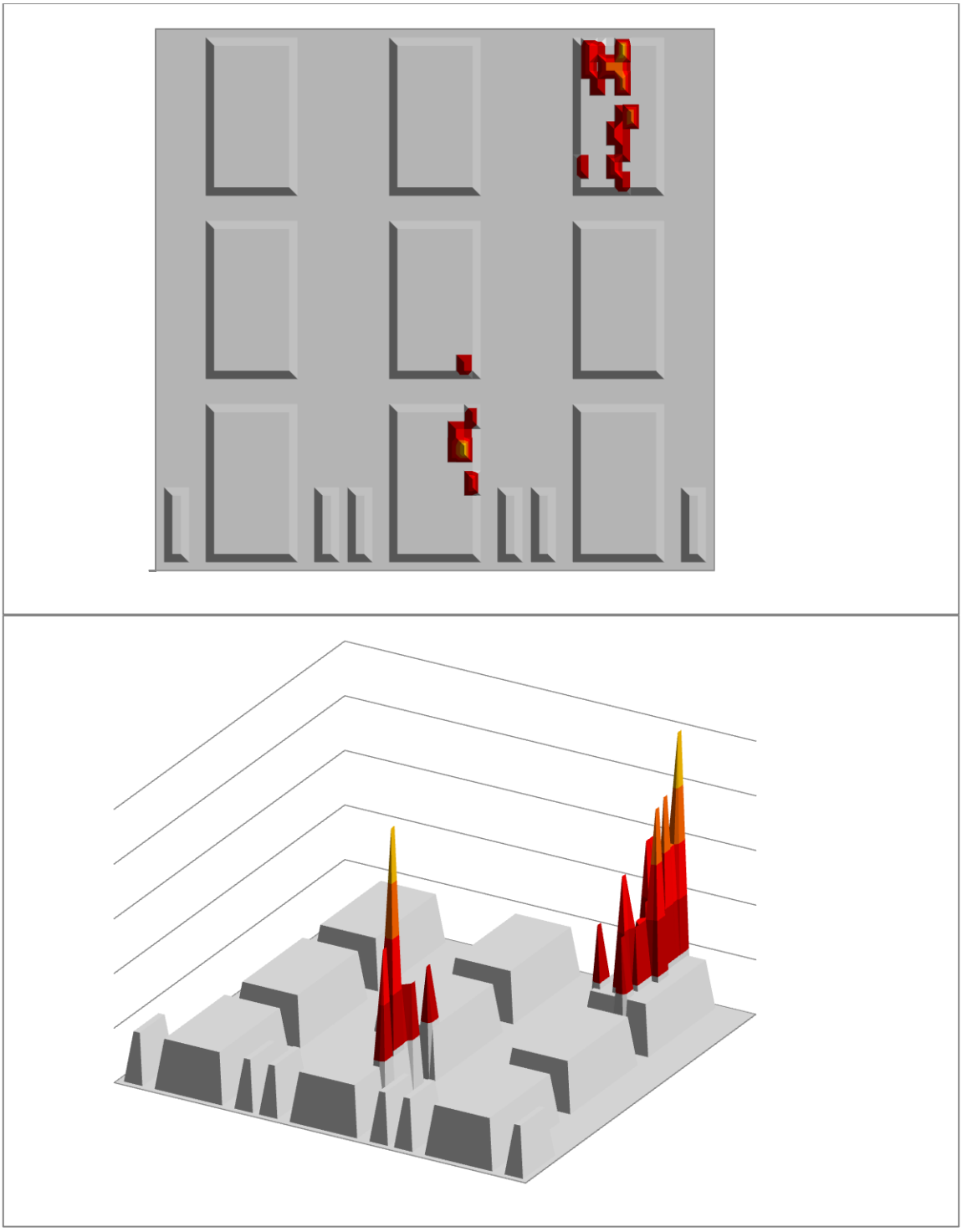

Fig. A.9. Optical thickness sensitivity analysis results for vehicle (3,3).

Gas Tank Fill Level Results

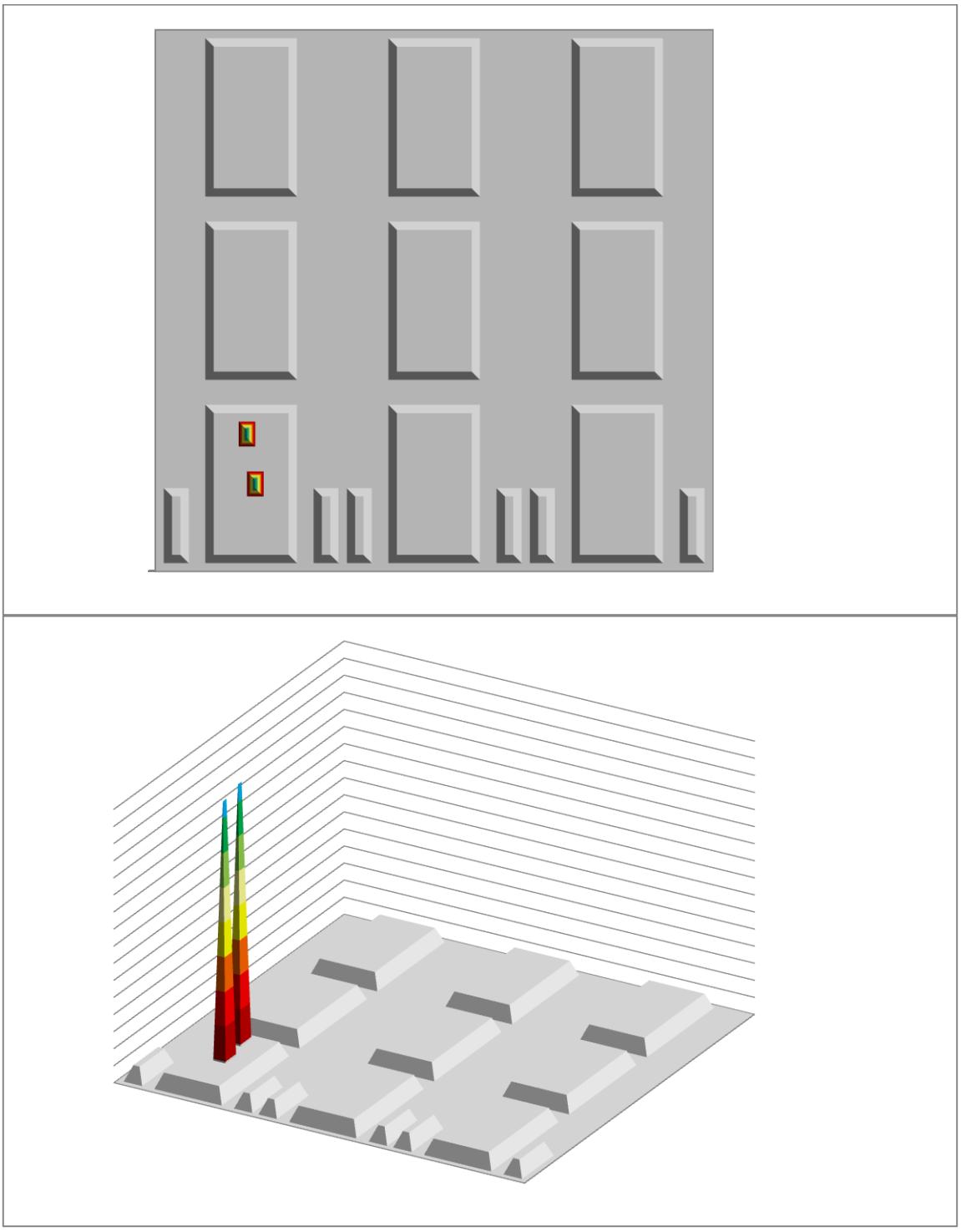

Fig. A.10. Gas tank fill level sensitivity analysis results for vehicle (1,1).

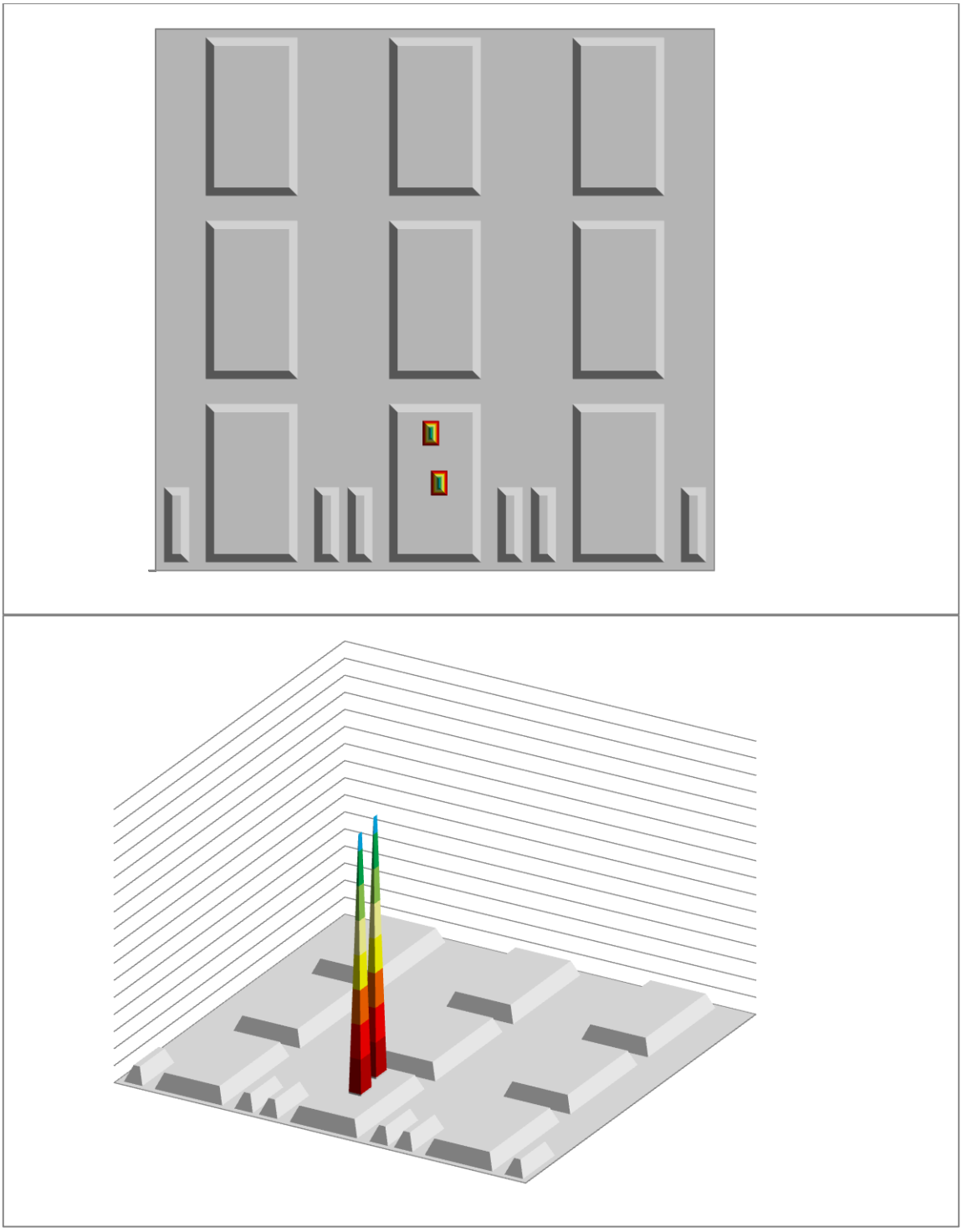

Fig. A.11. Gas tank fill level sensitivity analysis results for vehicle (2,1).

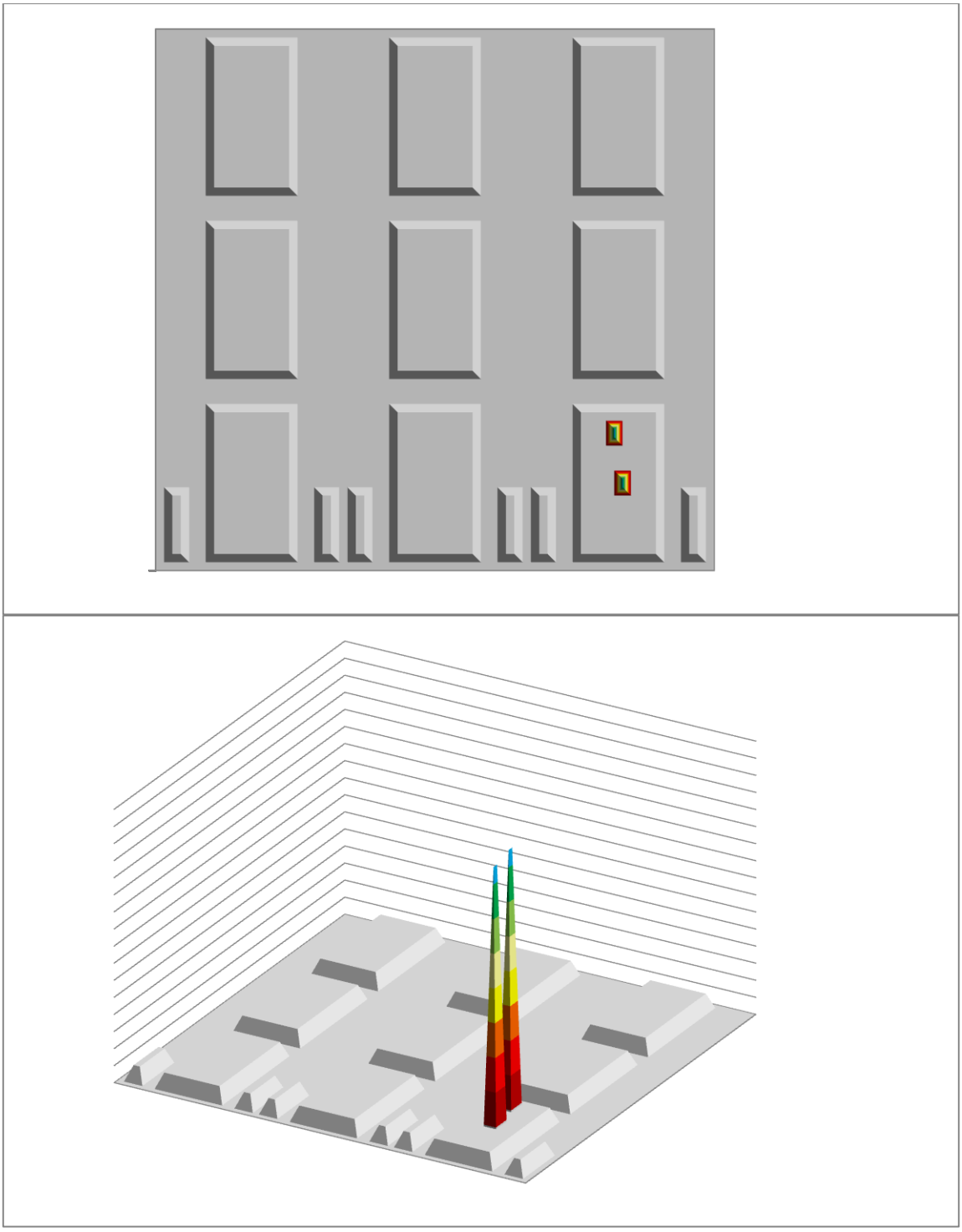

Fig. A.12. Gas tank fill level sensitivity analysis results for vehicle (3,1).

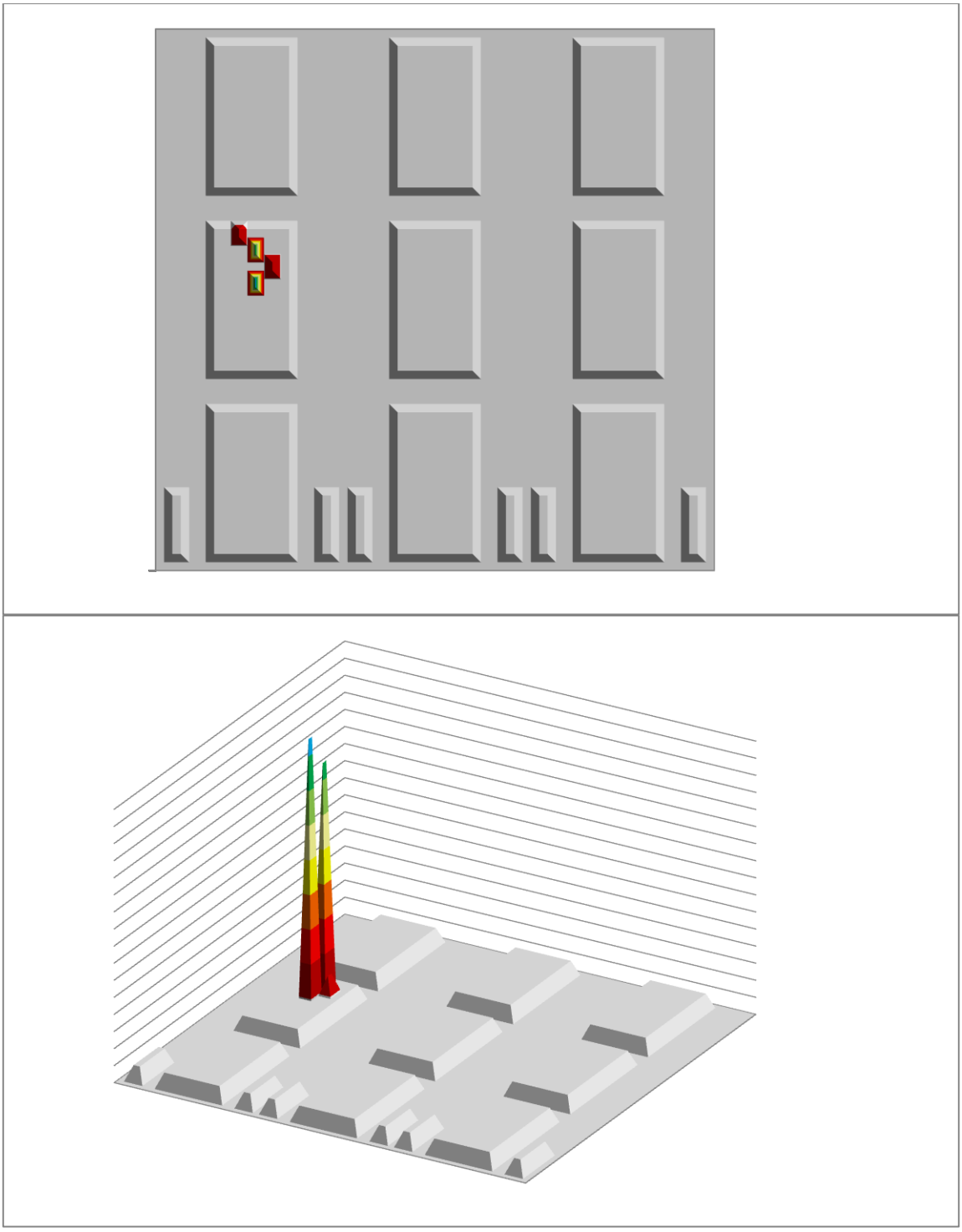

Fig. A.13. Gas tank fill level sensitivity analysis results for vehicle (1,2).

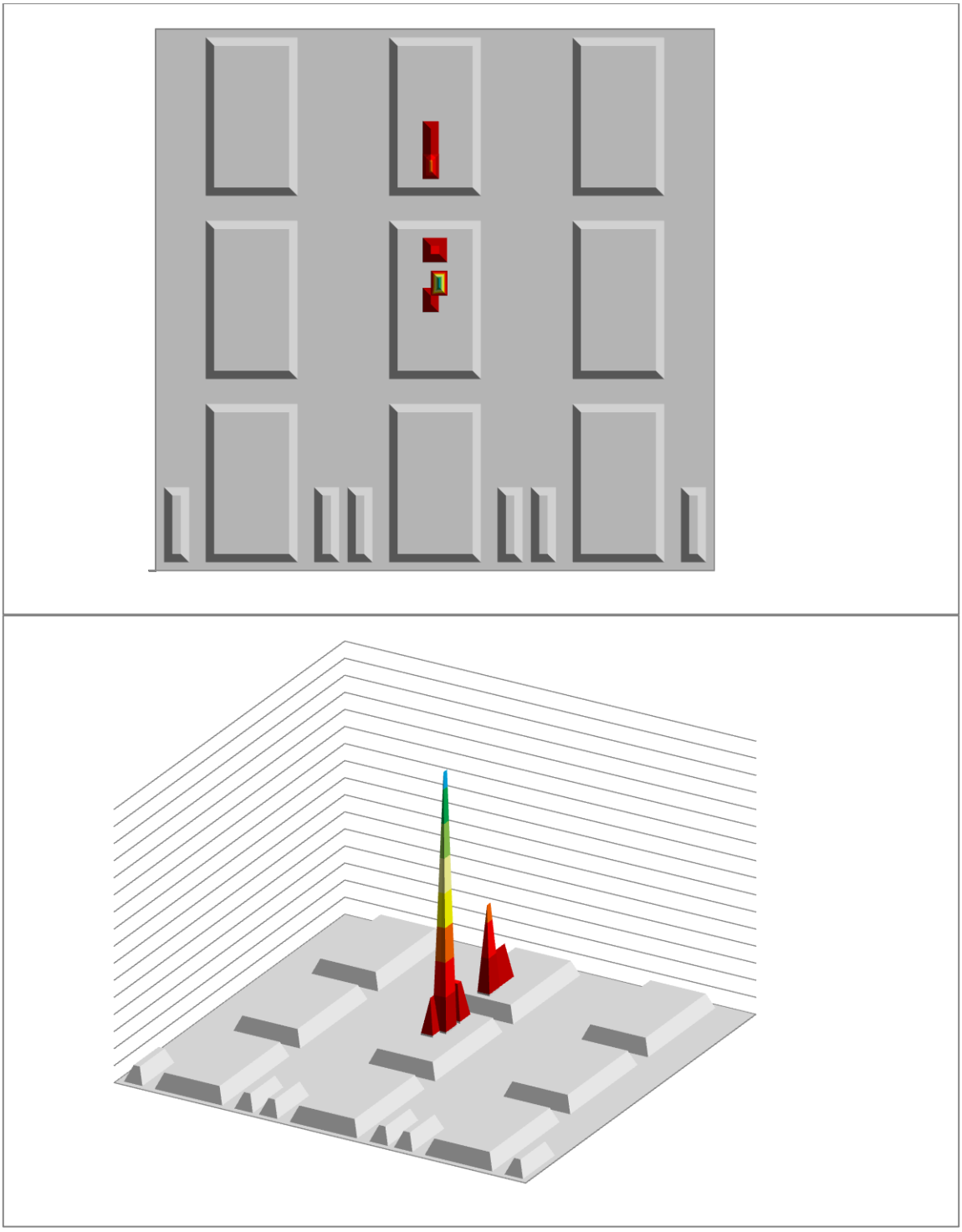

Fig. A.14. Gas tank fill level sensitivity analysis results for vehicle (2,2).

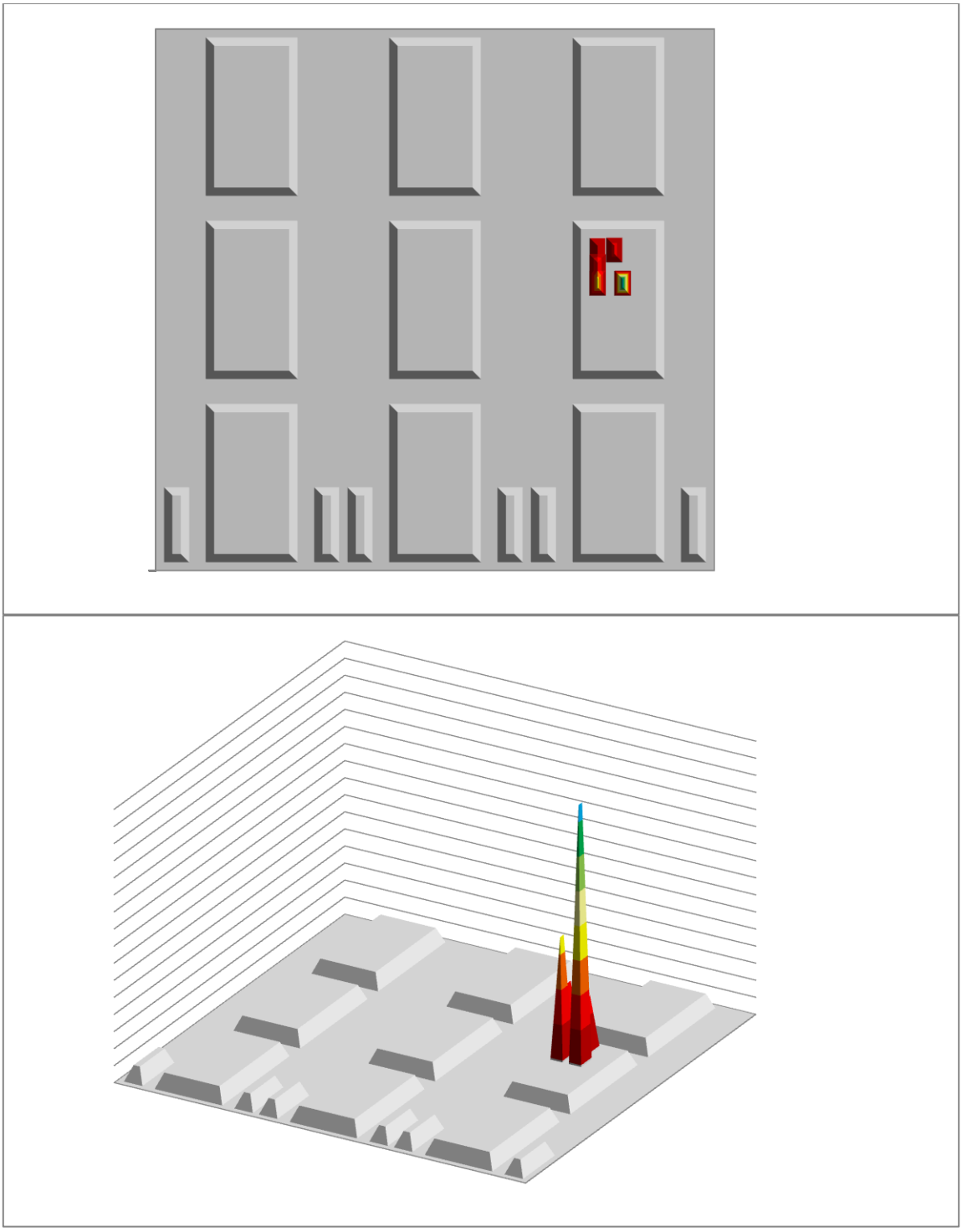

Fig. A.15. Gas tank fill level sensitivity analysis results for vehicle (3,2).

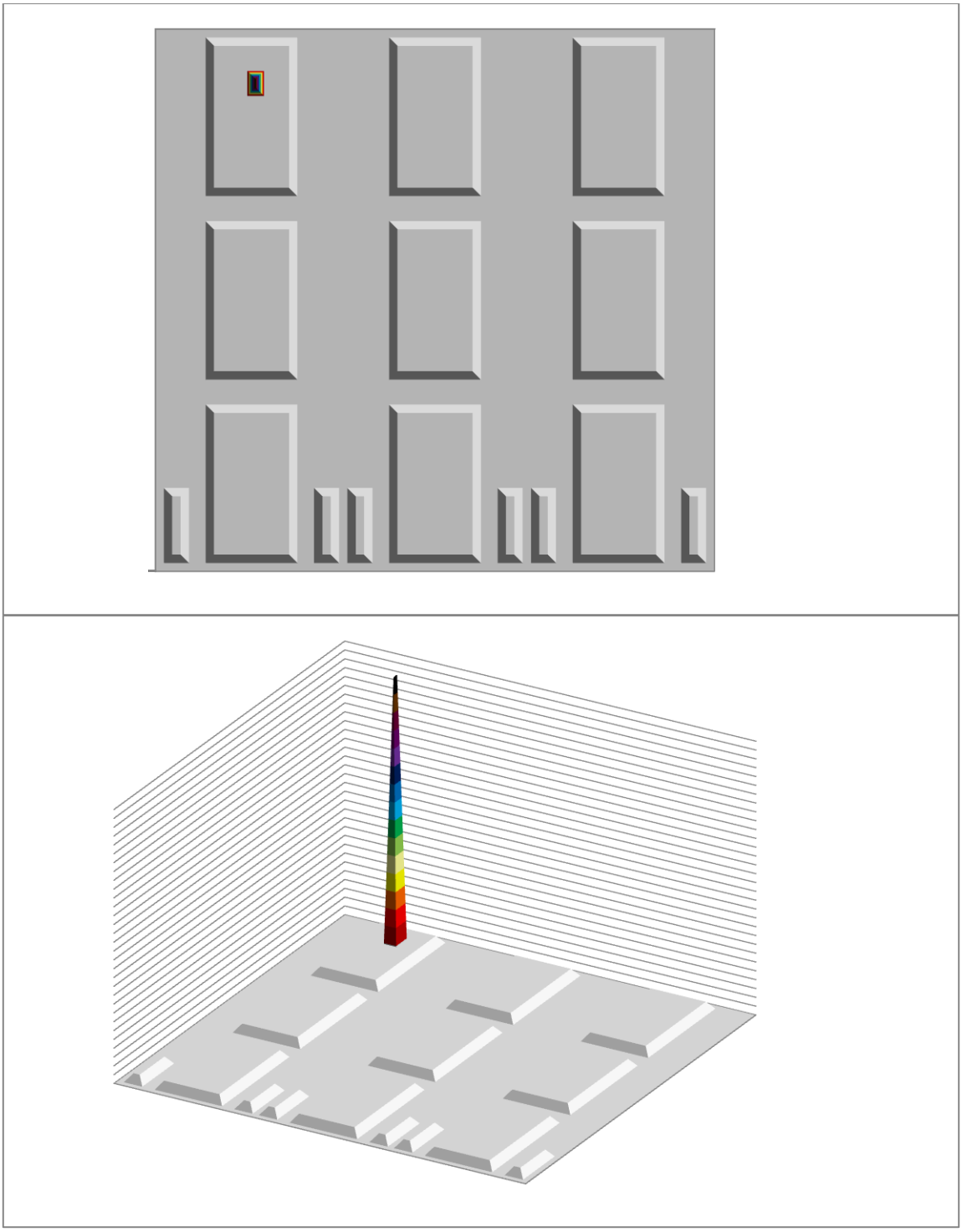

Fig. A.16. Gas tank fill level sensitivity analysis results for vehicle (1,3).

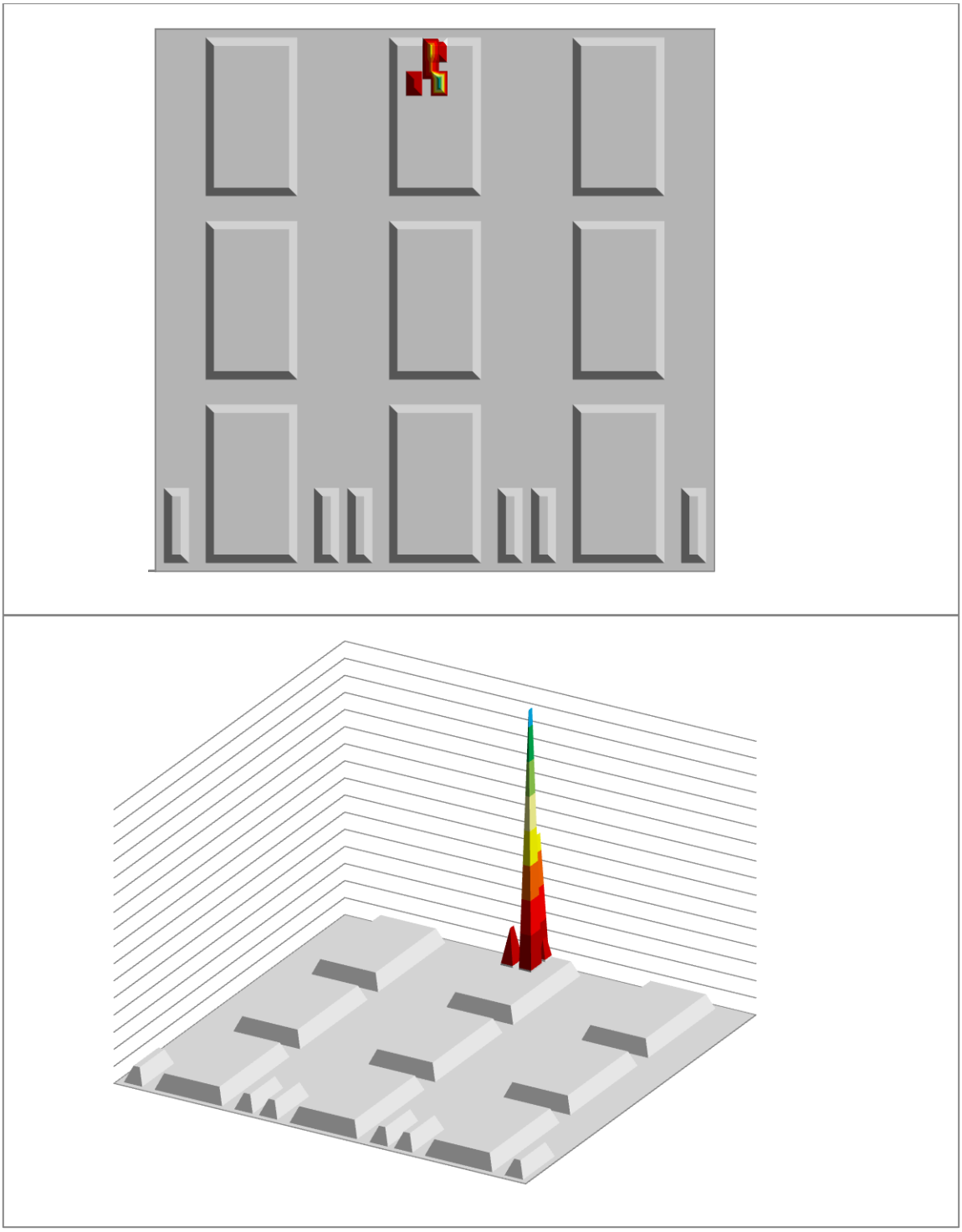

Fig. A.17. Gas tank fill level sensitivity analysis results for vehicle (2,3).

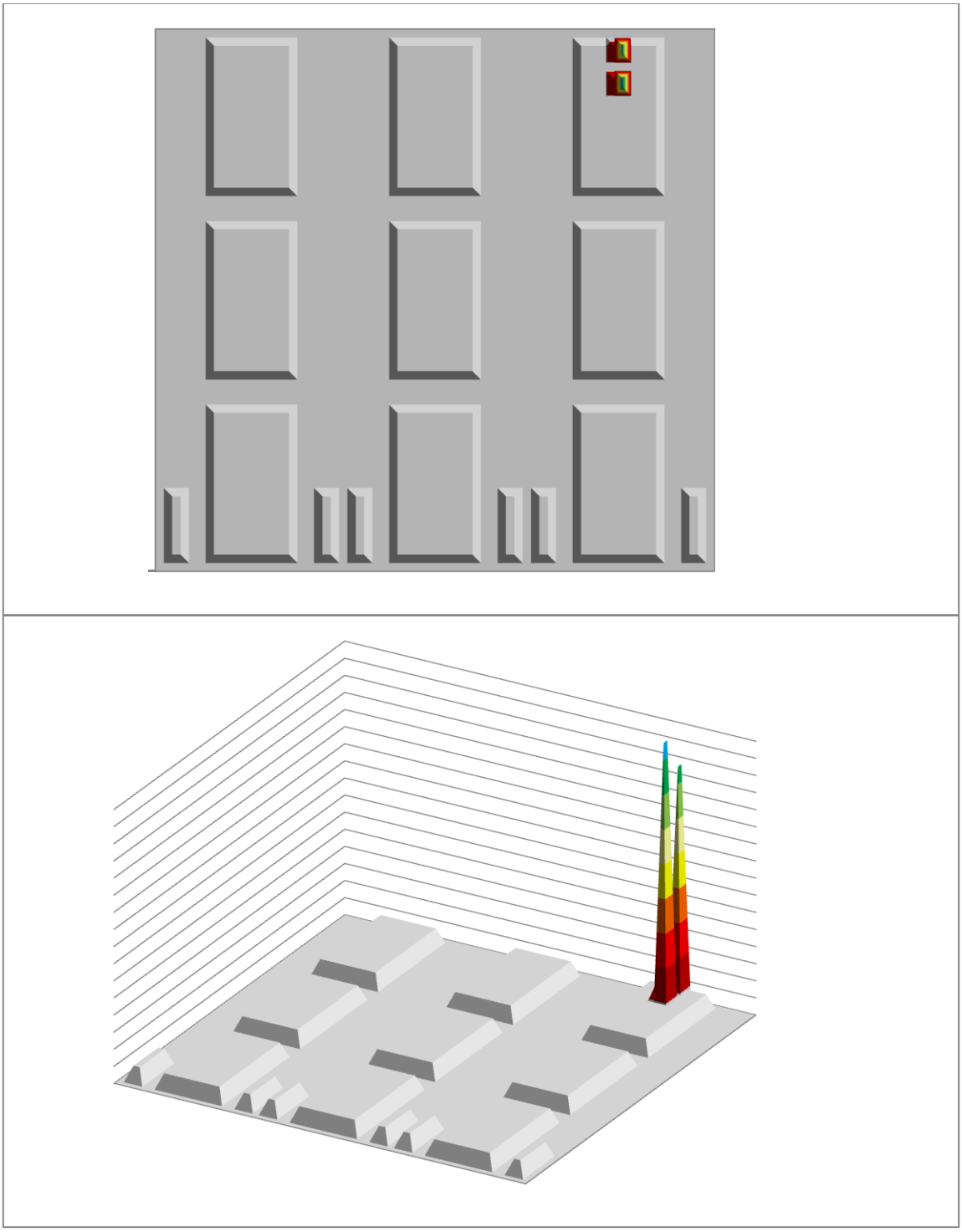

Fig. A.18. Gas tank fill level sensitivity analysis results for vehicle (3,3).

Physical Size Results

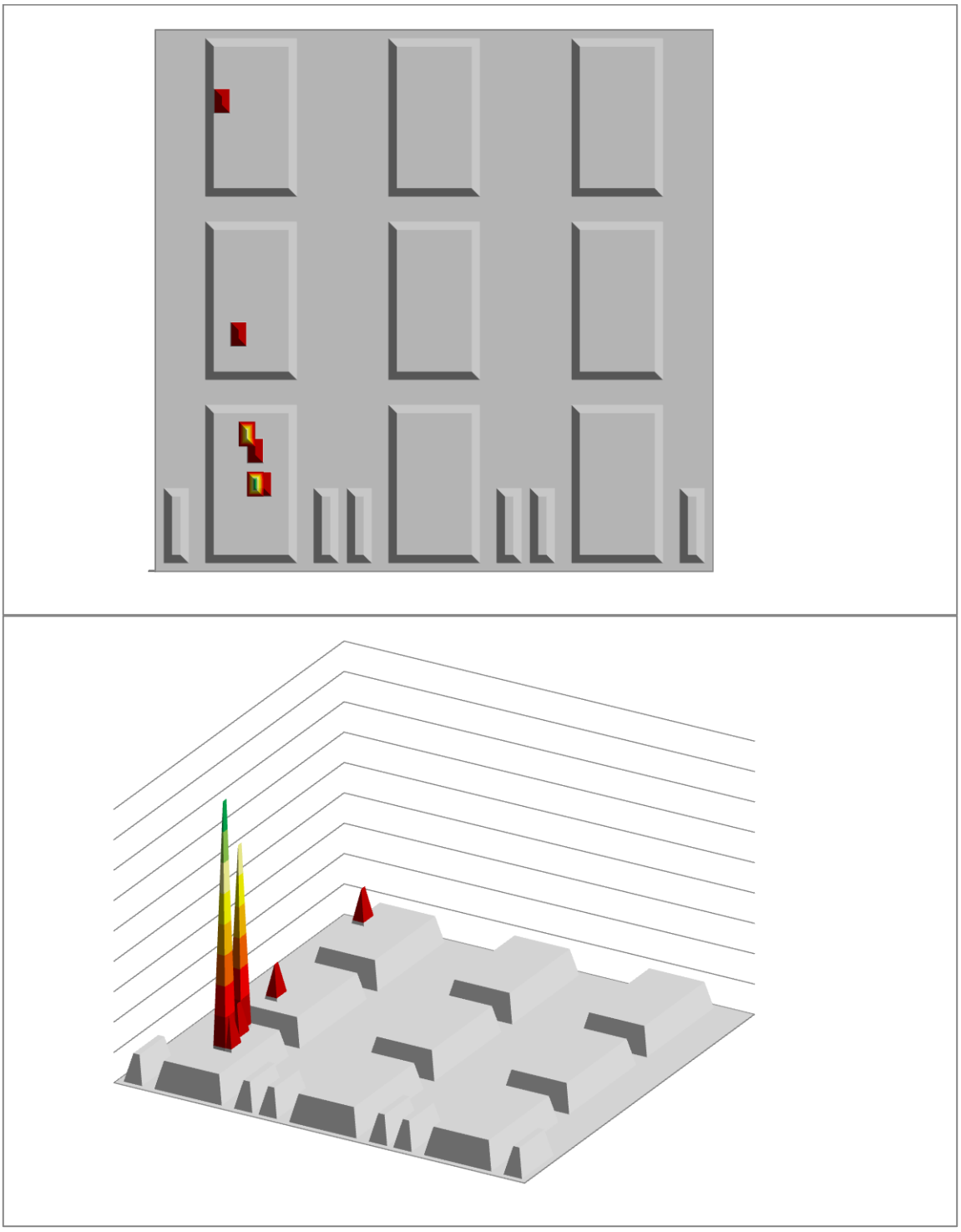

Fig. A.19. Physical size sensitivity analysis results for vehicle (1,1).

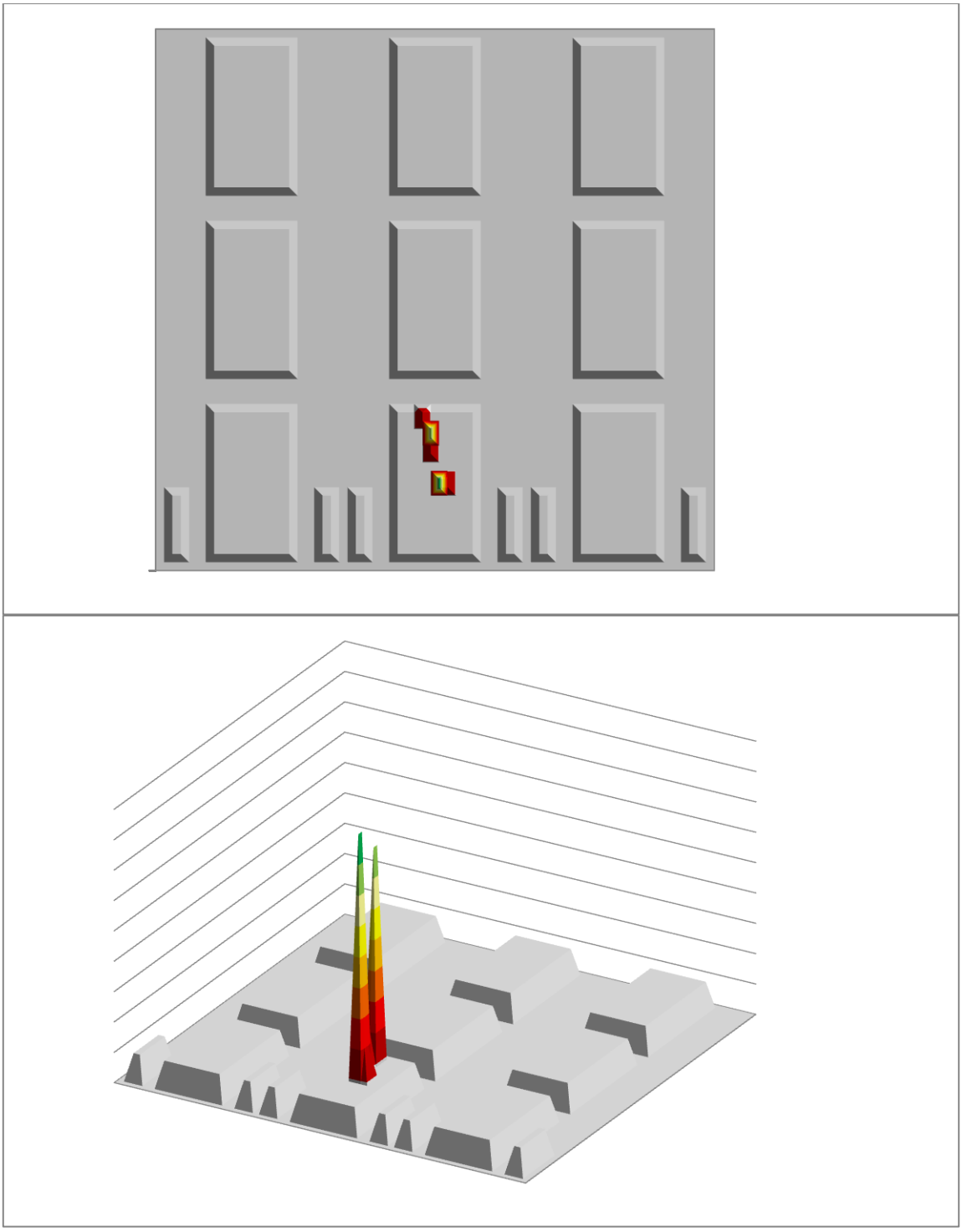

Fig. A.20. Physical size sensitivity analysis results for vehicle (2,1).

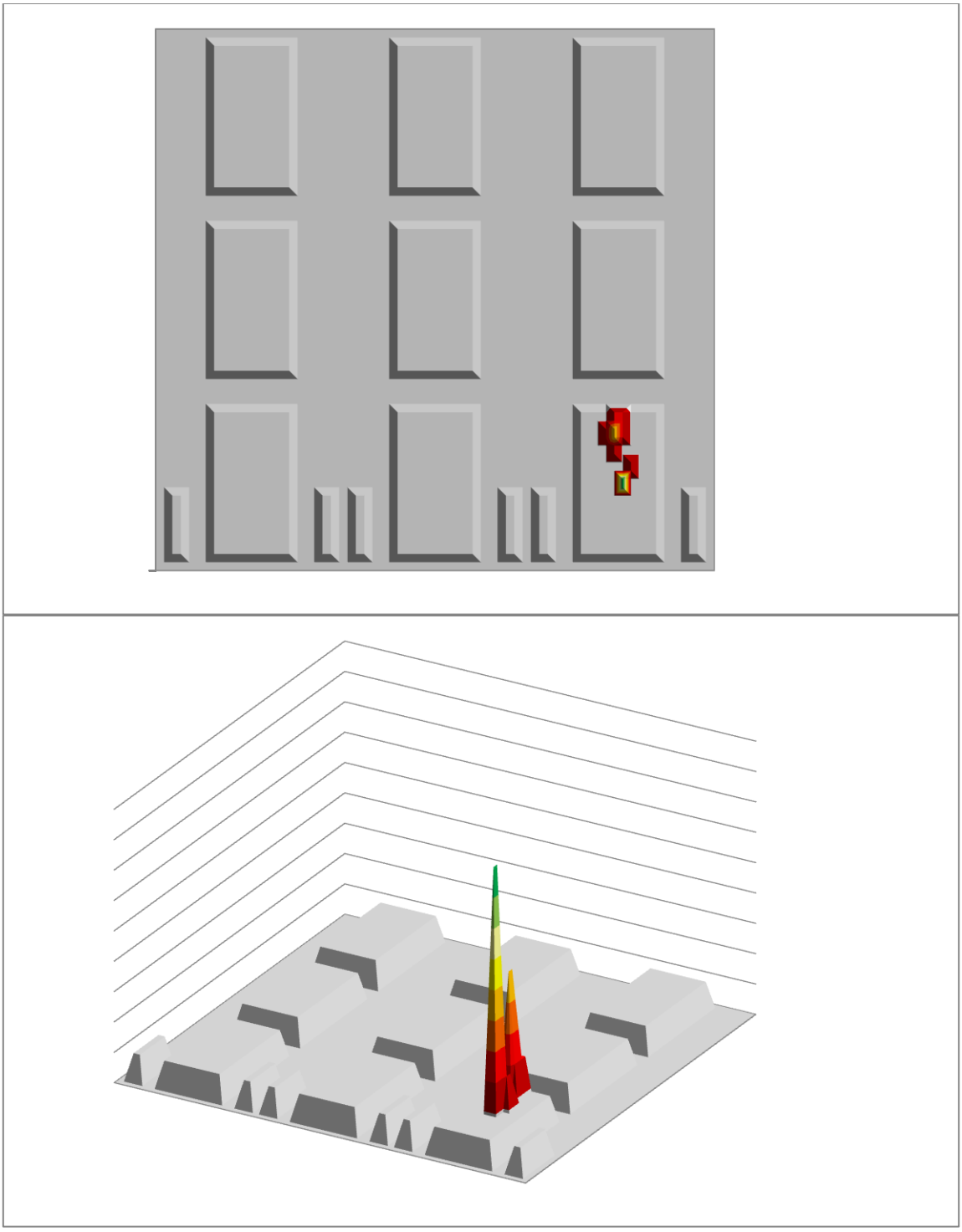

Fig. A.21. Physical size sensitivity analysis results for vehicle (3,1).

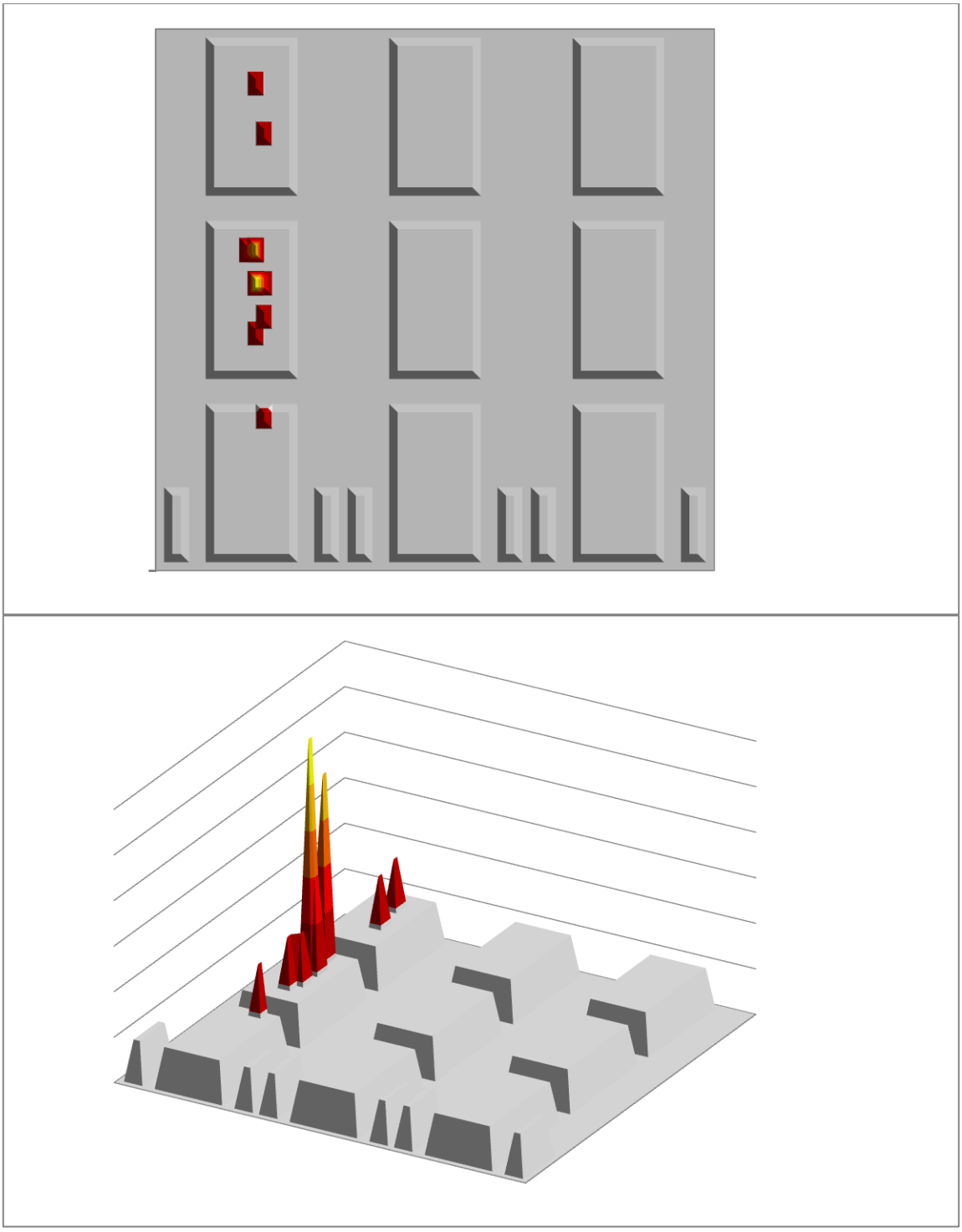

Fig. A.22. Physical size sensitivity analysis results for vehicle (1,2).

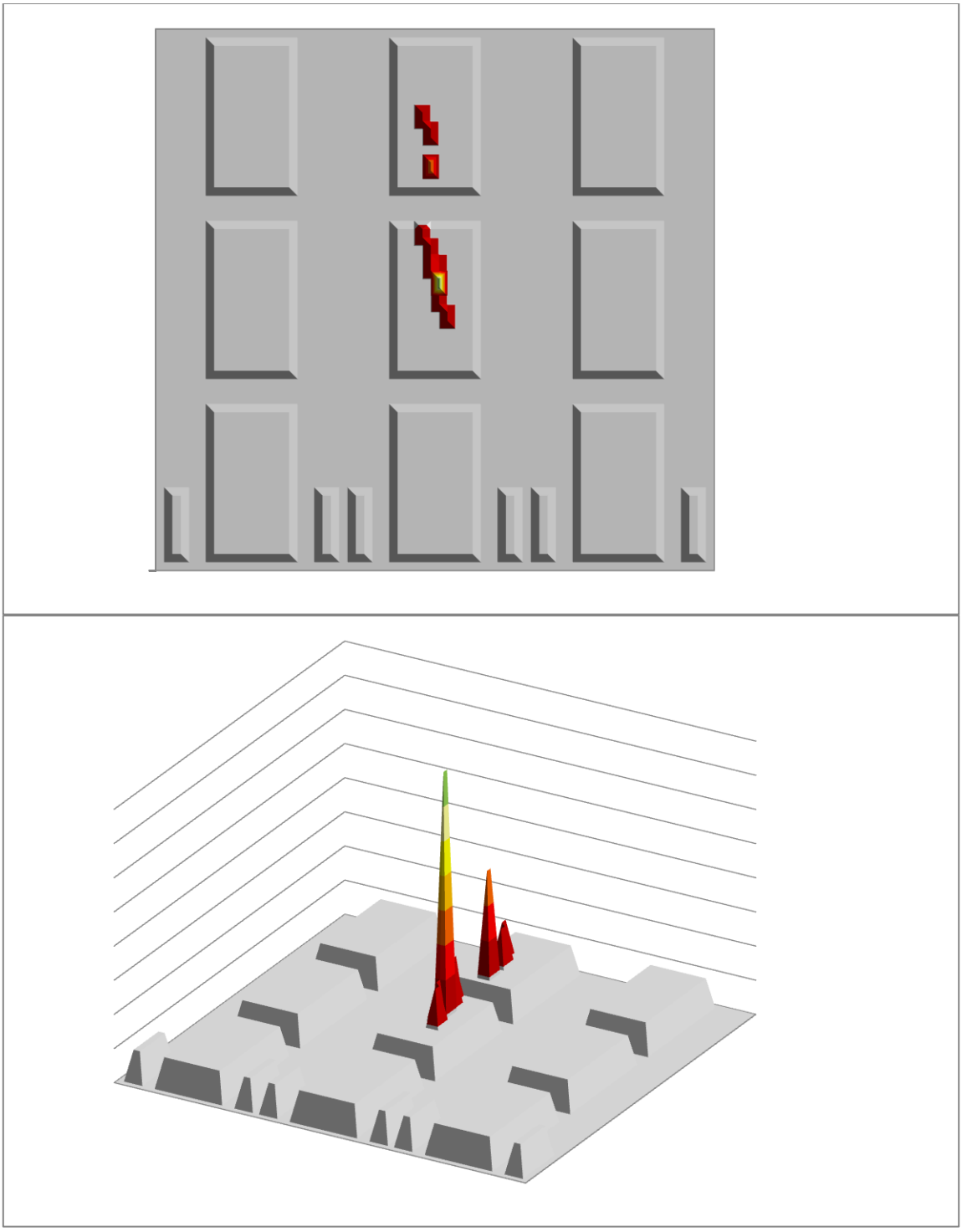

Fig. A.23. Physical size sensitivity analysis results for vehicle (2,2).

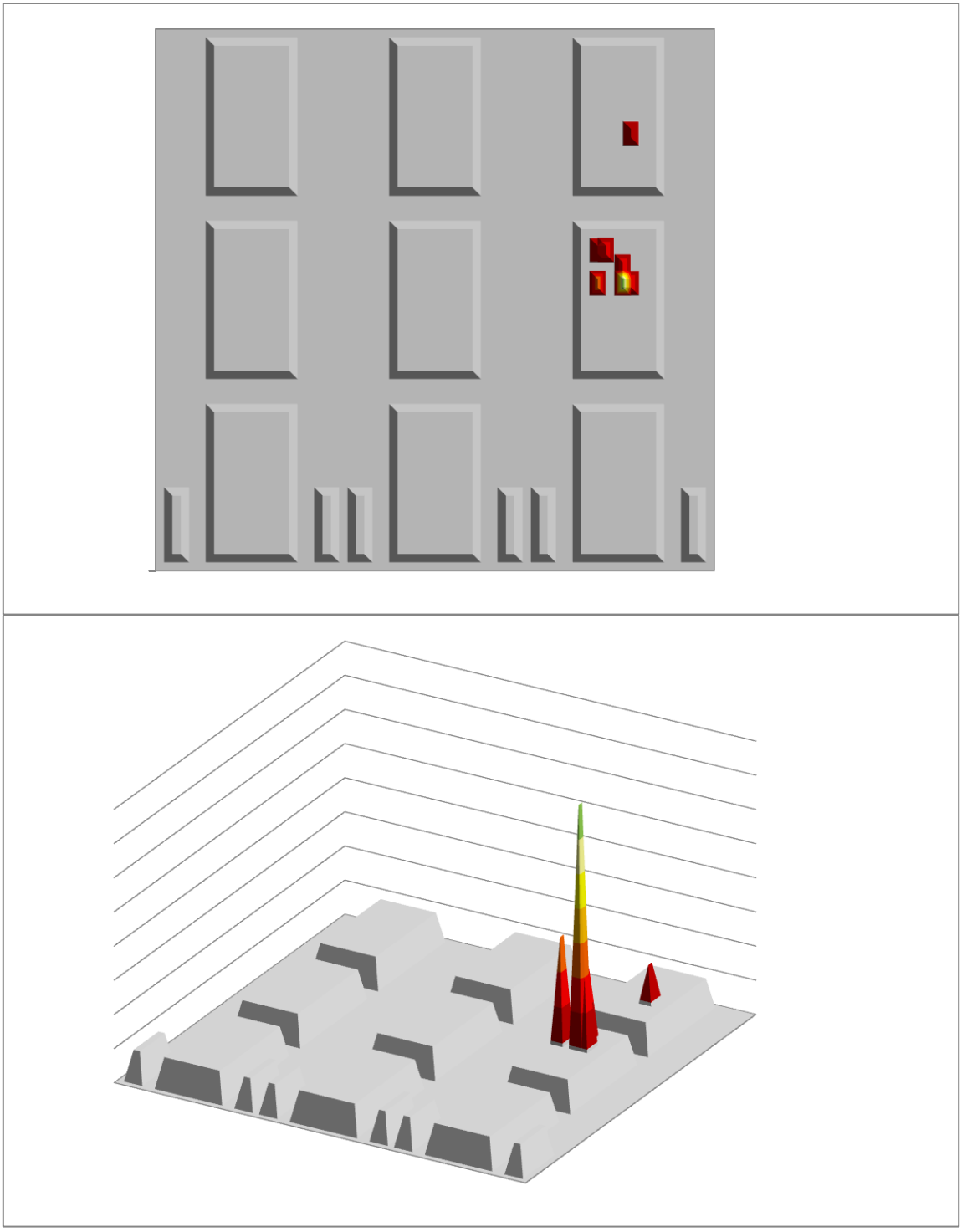

Fig. A.24. Physical size sensitivity analysis results for vehicle (3,2).

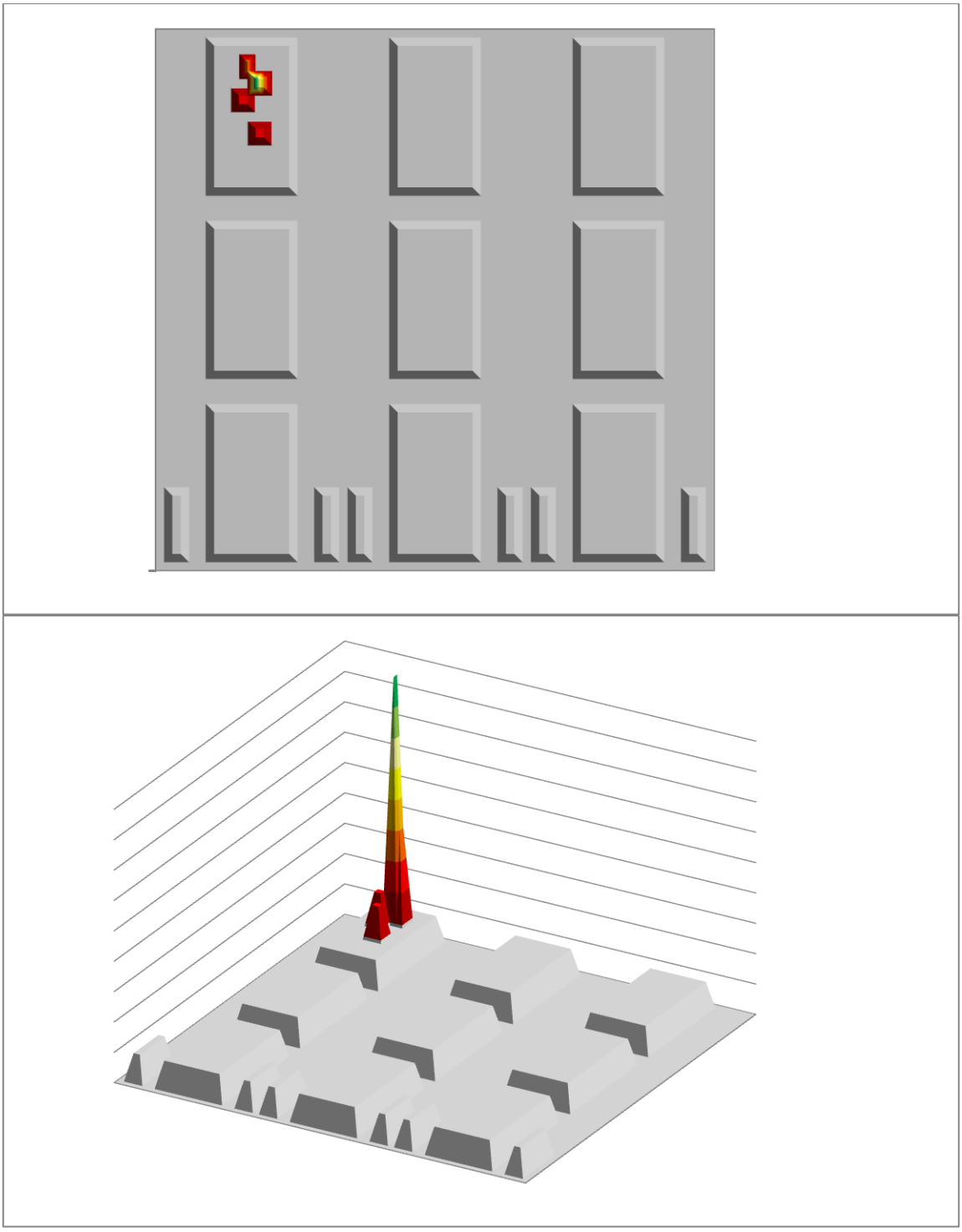

Fig. A.25. Physical size sensitivity analysis results for vehicle (1,3).

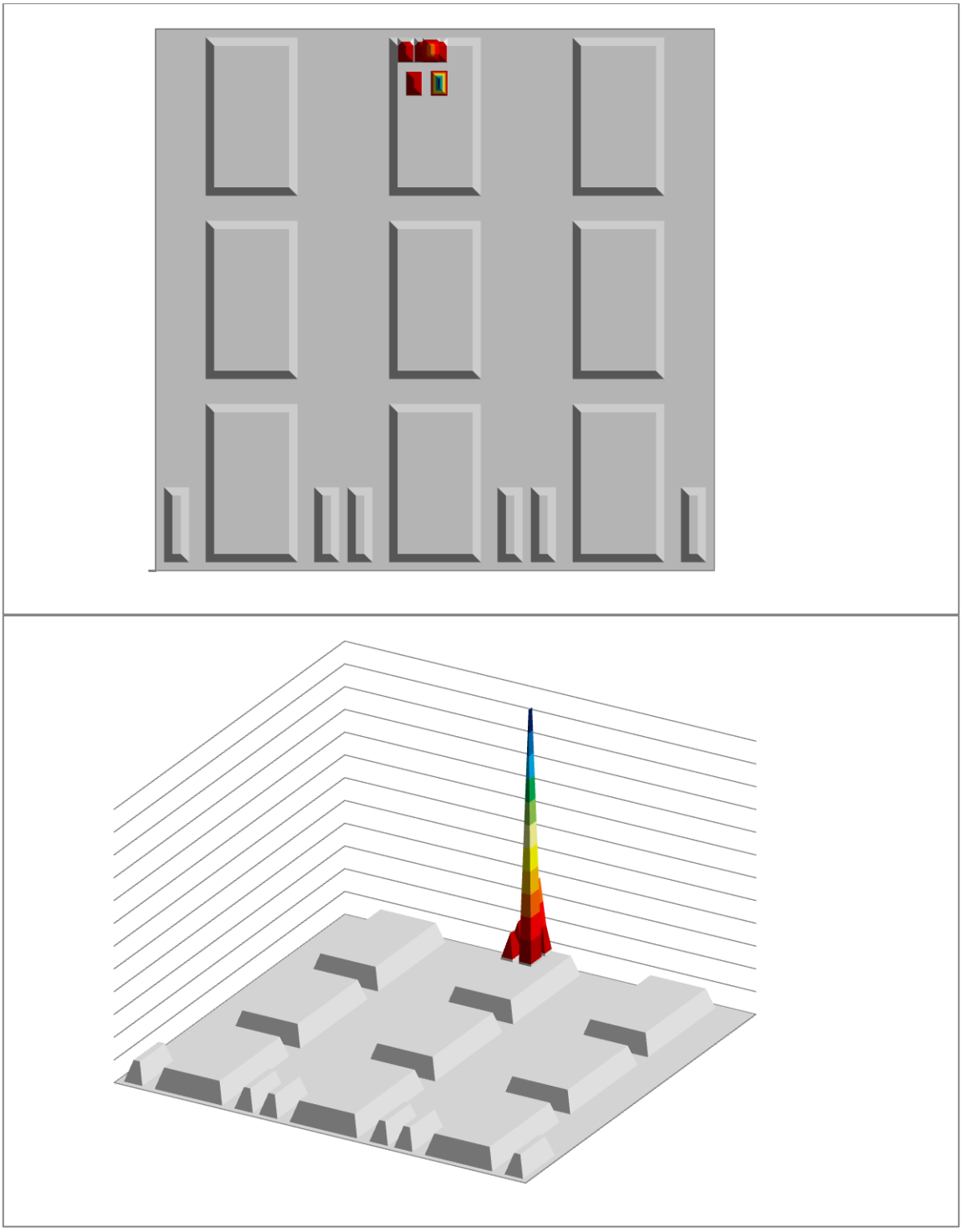

Fig. A.26. Physical size sensitivity analysis results for vehicle (2,3).

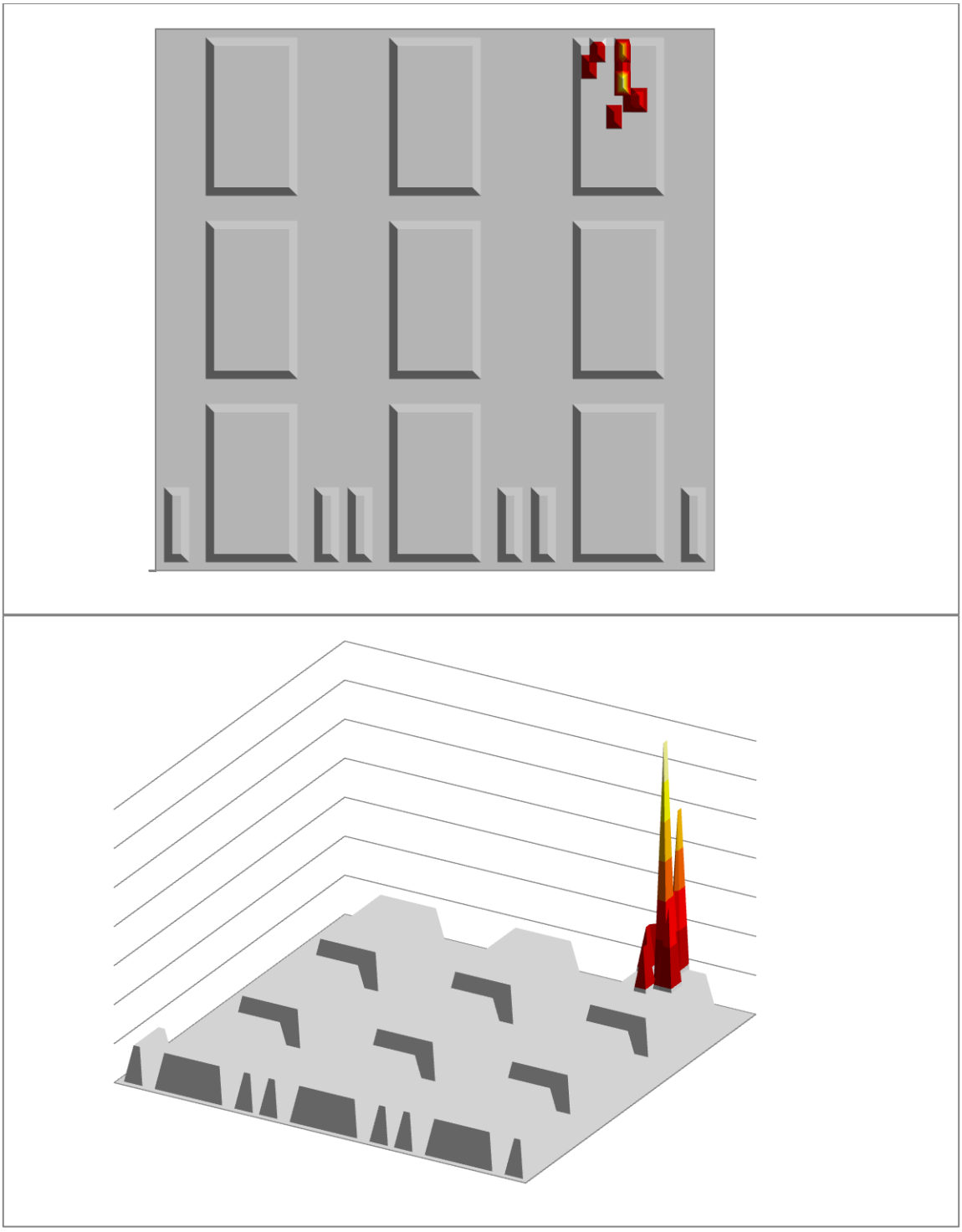

Fig. A.27. Physical size sensitivity analysis results for vehicle (3,3).

Detector Efficiency Results

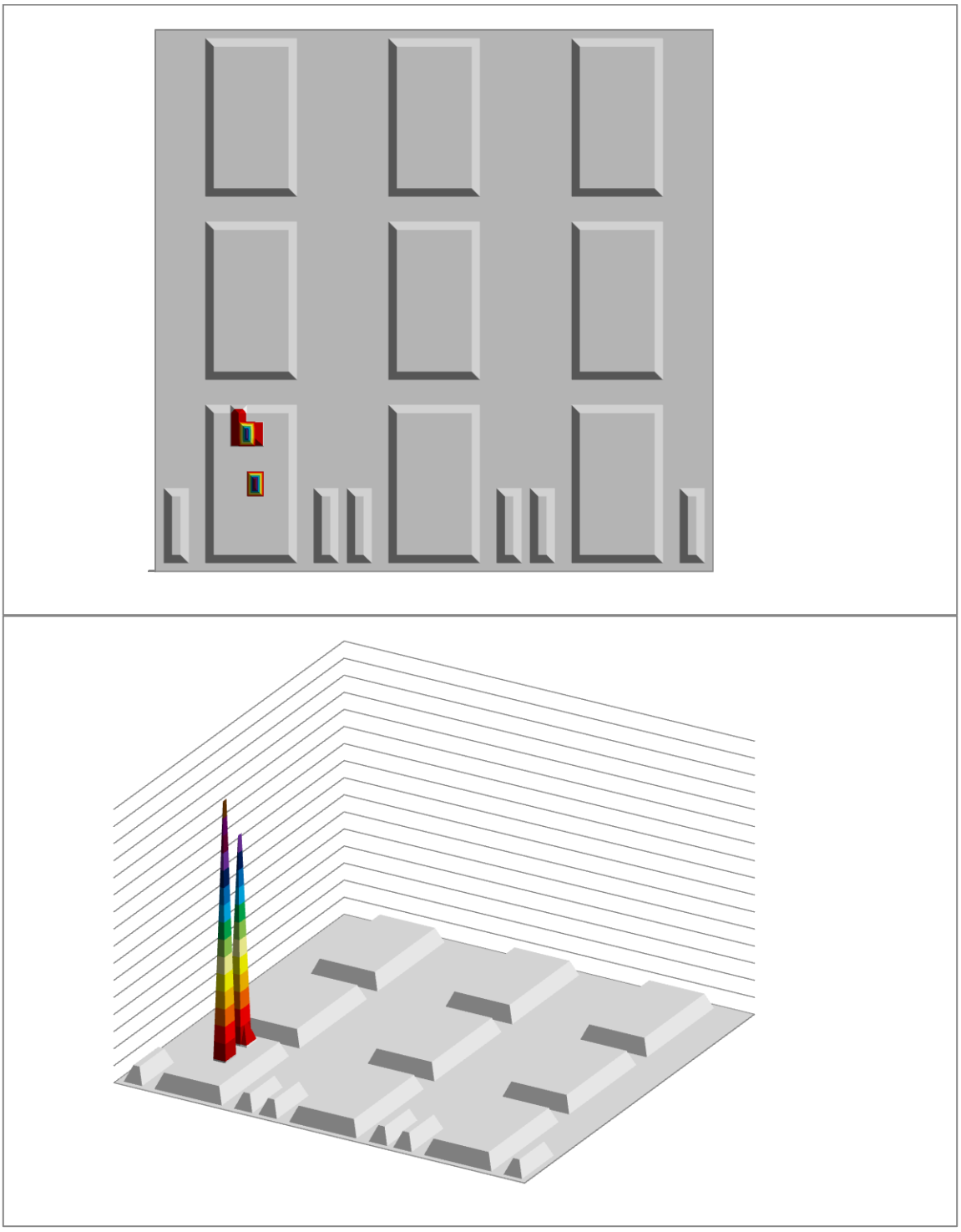

Fig. A.28. Detector efficiency sensitivity analysis results for vehicle (1,1).

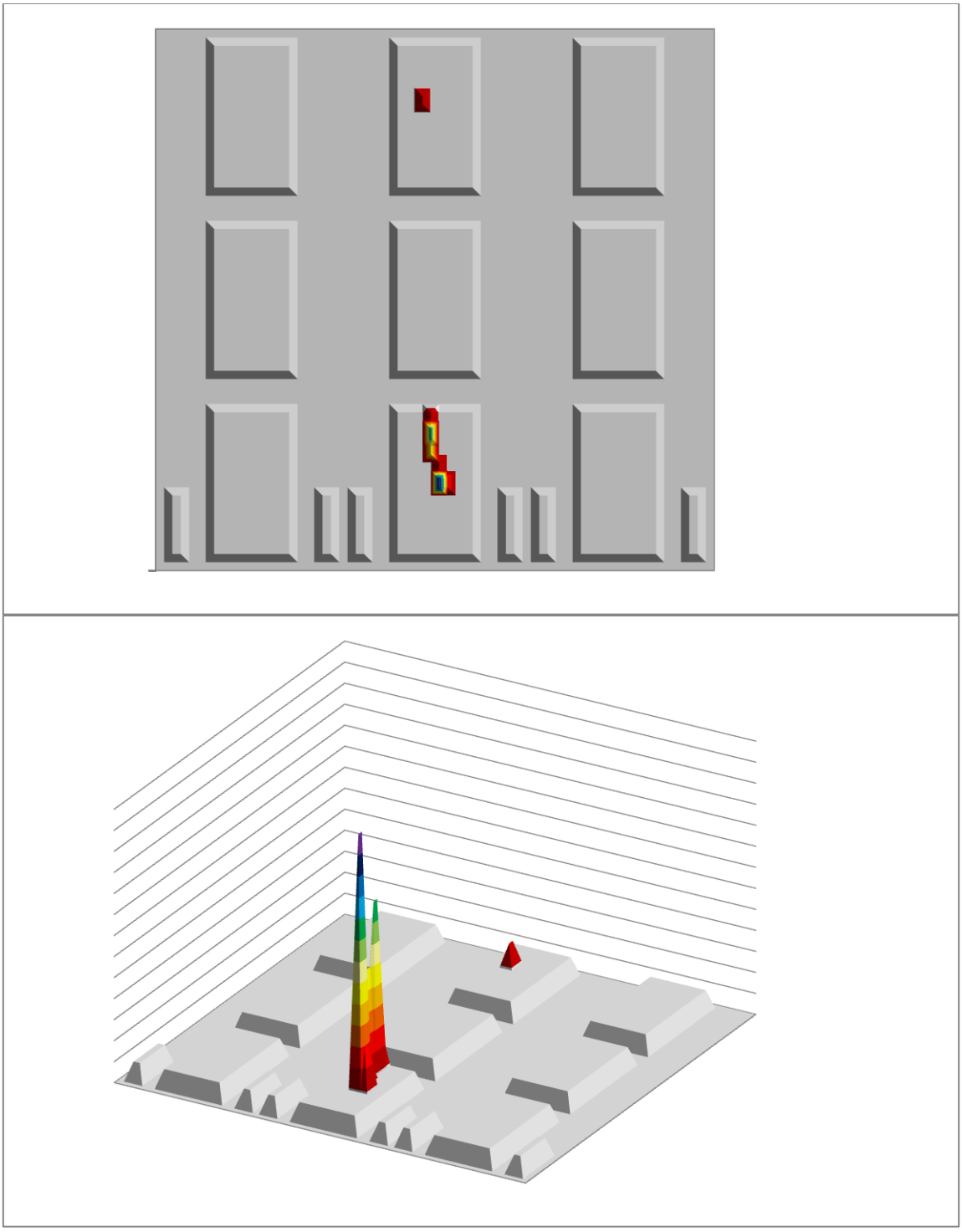

Fig. A.29. Detector efficiency sensitivity analysis results for vehicle (2,1).

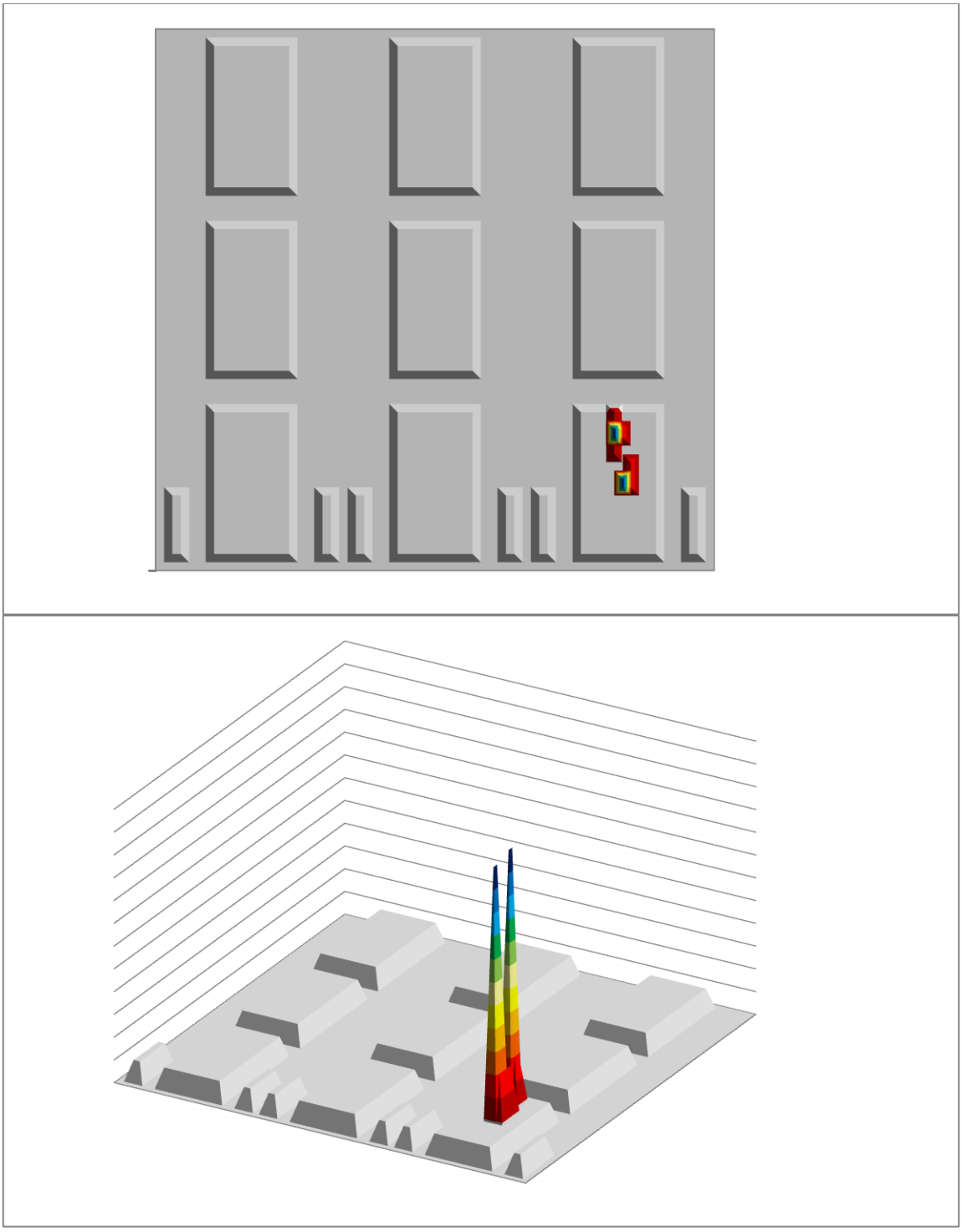

Fig. A.30. Detector efficiency sensitivity analysis results for vehicle (3,1).

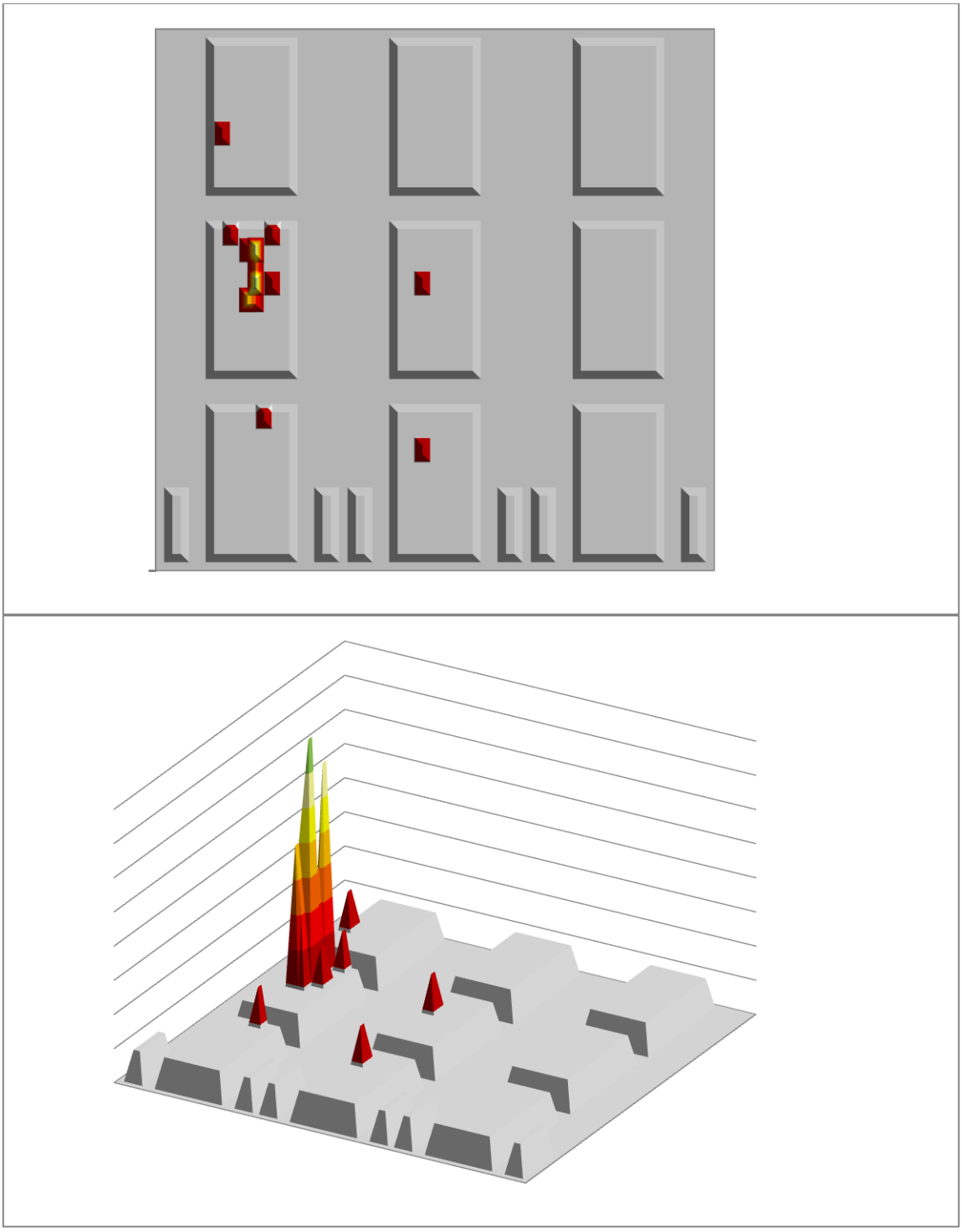

Fig. A.31. Detector efficiency sensitivity analysis results for vehicle (1,2).

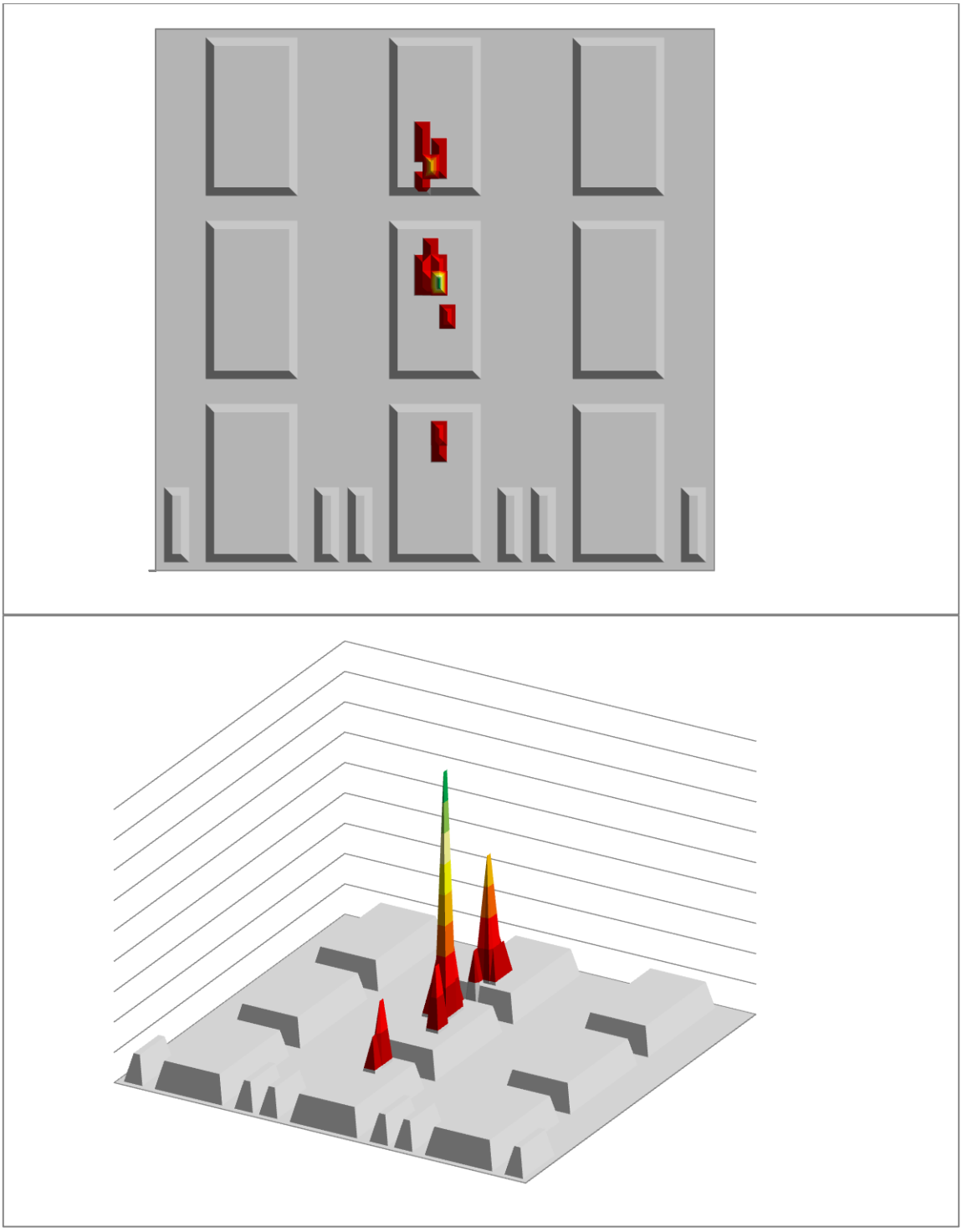

Fig. A.32. Detector efficiency sensitivity analysis results for vehicle (2,2).

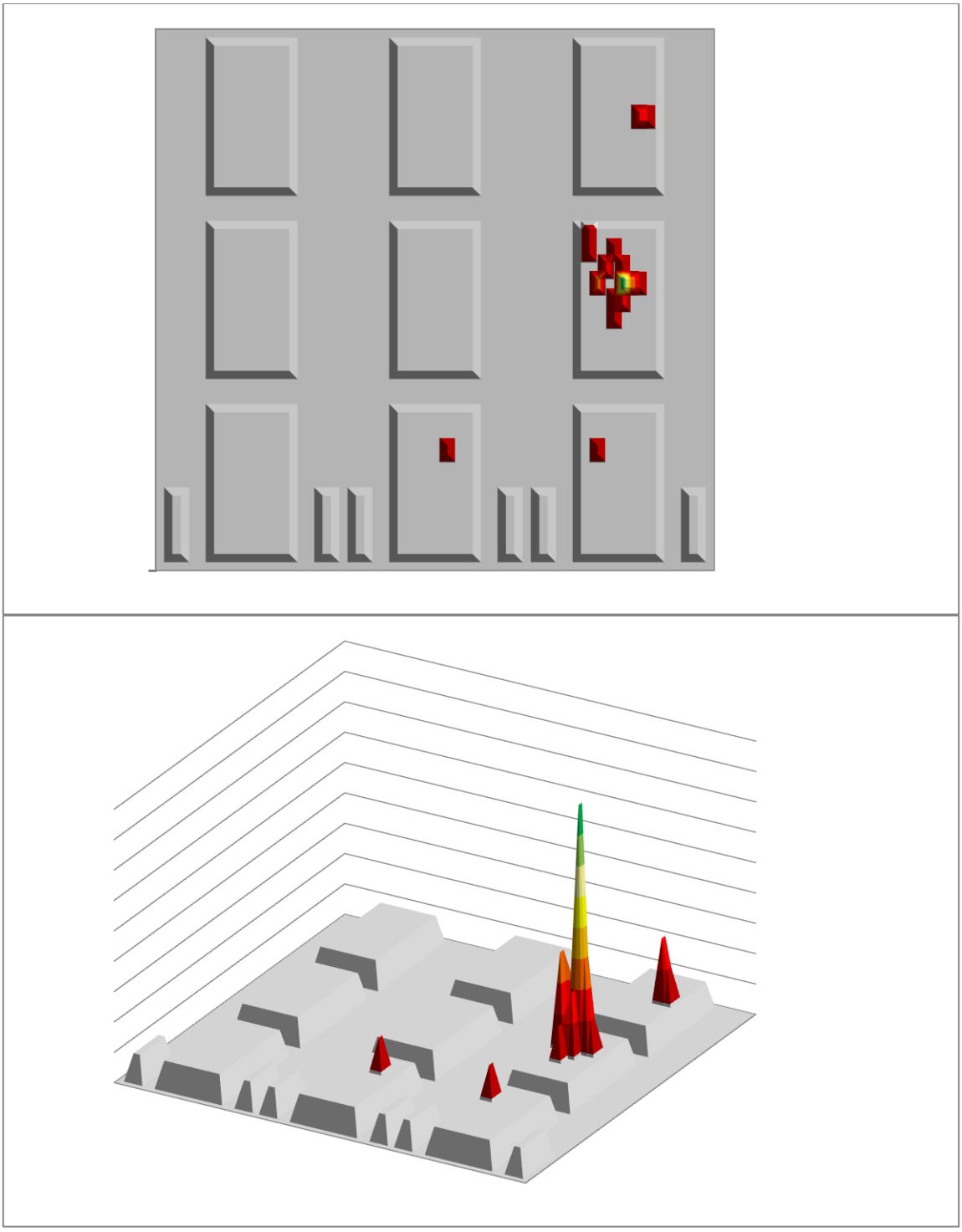

Fig. A.33. Detector efficiency sensitivity analysis results for vehicle (3,2).

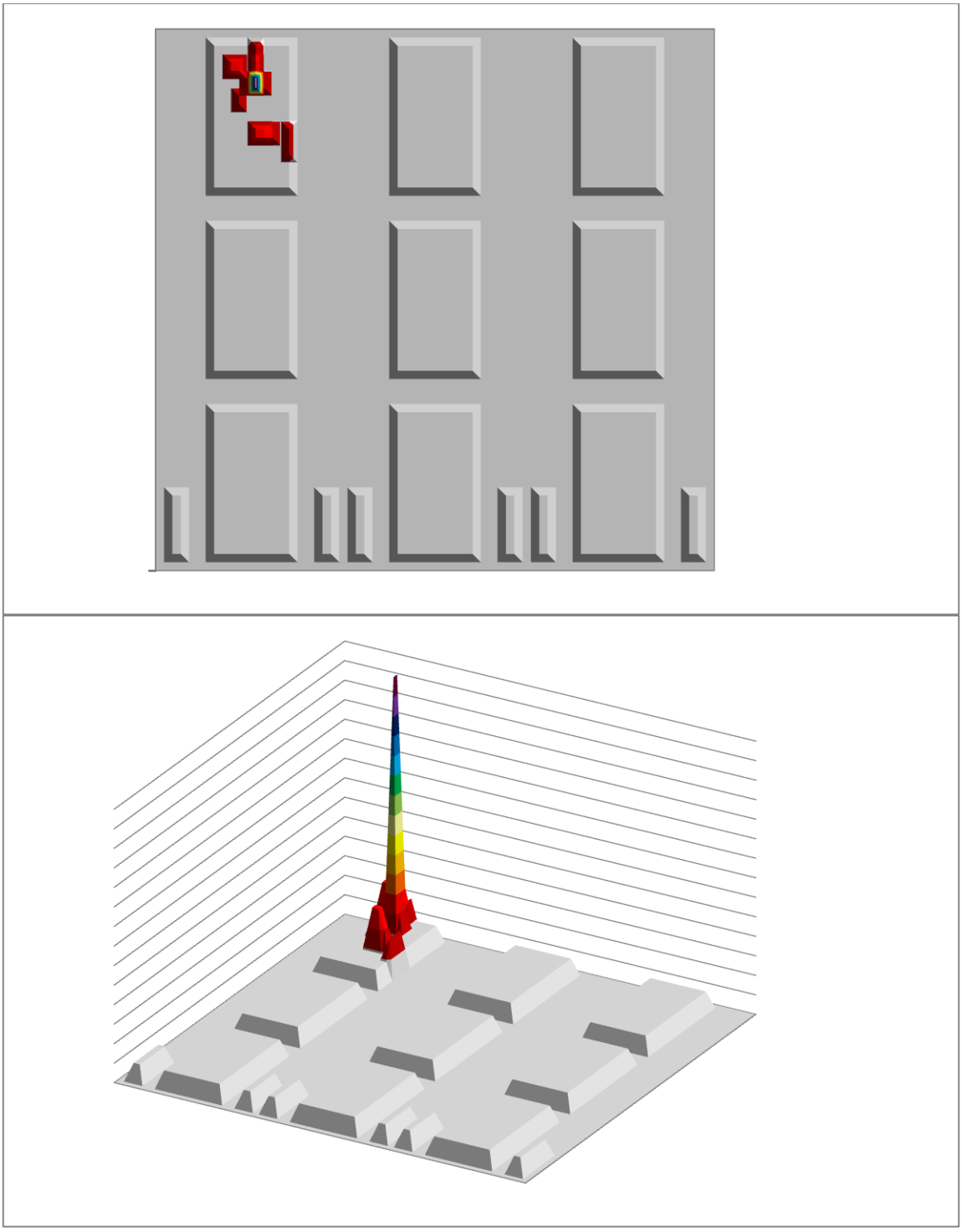

Fig. A.34. Detector efficiency sensitivity analysis results for vehicle (1,3).

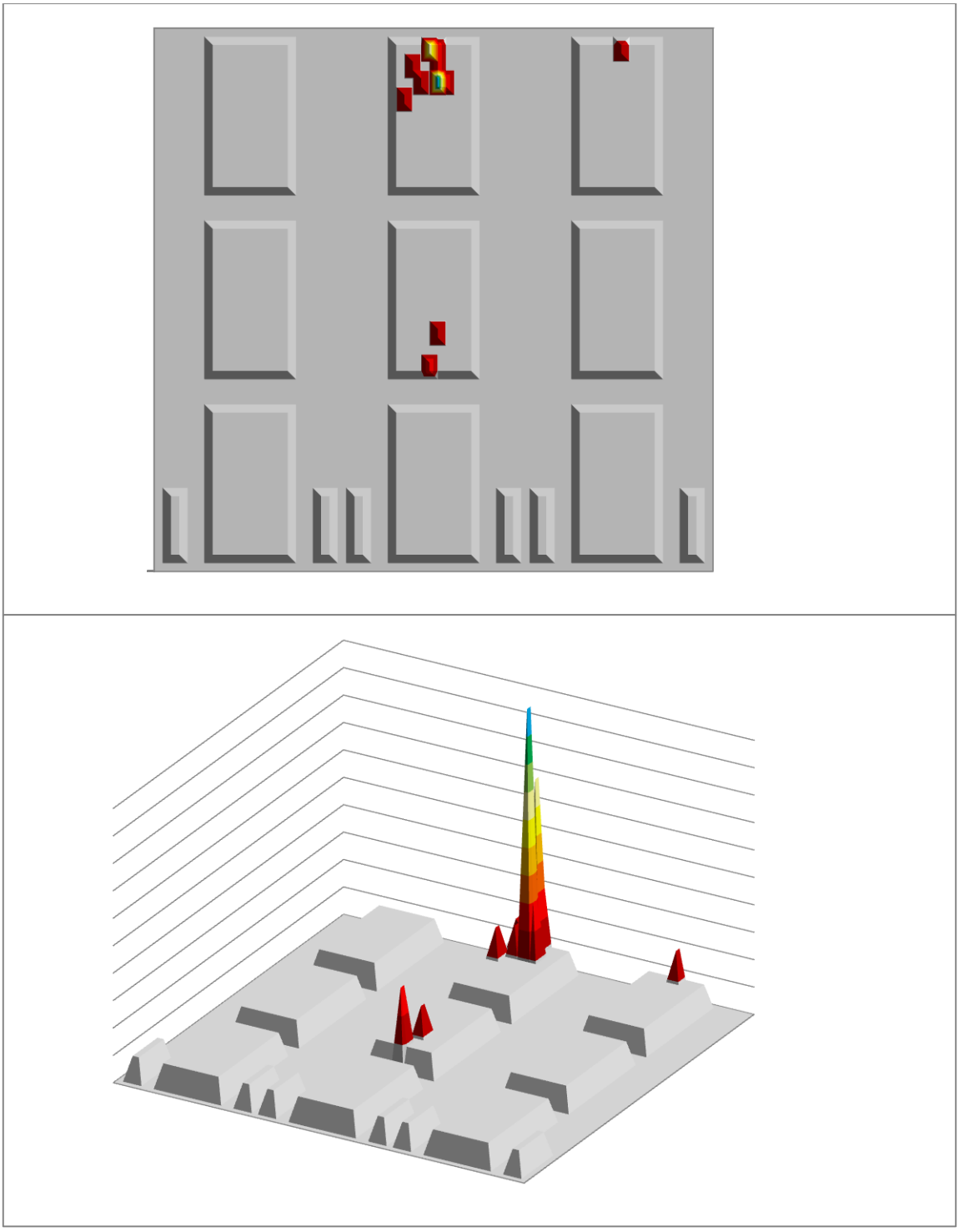

Fig. A.35. Detector efficiency sensitivity analysis results for vehicle (2,3).

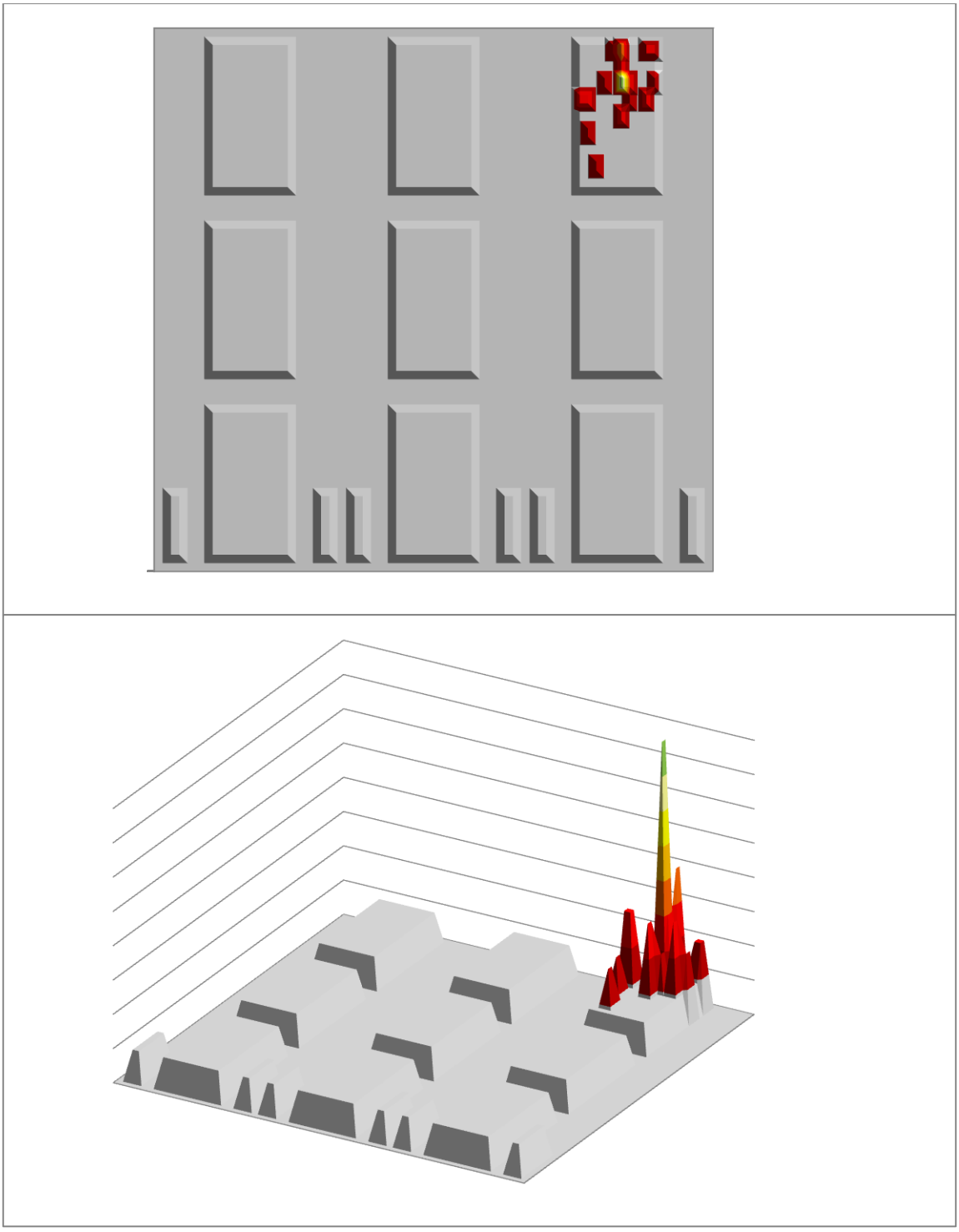

Fig. A.36. Detector efficiency sensitivity analysis results for vehicle (3,3).

APPENDIX B

SAMPLE PARTISN INPUT DECK

```
     1
  Distributed Source Test Case
/
/ block 1
/
  igeom=x-y-z ngroup=1 isn=8
  niso=1 mt=1 nzone=1
  im=15 it=15 jm=15 jt=15 km=15 kt=15
  T
/
/ block 2
/
  xmesh=0.0 1.2 2.4 3.6 4.8 6.0 7.2 8.4 9.6 10.8 12.0 13.2 14.4 15.6 16.8 18.0
  xints=1 1 1 1 1 1 1 1 1 1 1 1 1 1 1
  ymesh=0.0 1.2 2.4 3.6 4.8 6.0 7.2 8.4 9.6 10.8 12.0 13.2 14.4 15.6 16.8 18.0
  yints=1 1 1 1 1 1 1 1 1 1 1 1 1 1 1
  zmesh=0.0 1.2 2.4 3.6 4.8 6.0 7.2 8.4 9.6 10.8 12.0 13.2 14.4 15.6 16.8 18.0
  zints=1 1 1 1 1 1 1 1 1 1 1 1 1 1 1
  zones=15r1; 15r1; 15r1; 15r1; 15r1; 15r1; 15r1; 15r1;
              15r1; 15r1; 15r1; 15r1; 15r1; 15r1; 15r1;
        15r1; 15r1; 15r1; 15r1; 15r1; 15r1; 15r1; 15r1;
              15r1; 15r1; 15r1; 15r1; 15r1; 15r1; 15r1;
        15r1; 15r1; 15r1; 15r1; 15r1; 15r1; 15r1; 15r1;
              15r1; 15r1; 15r1; 15r1; 15r1; 15r1; 15r1;
        15r1; 15r1; 15r1; 15r1; 15r1; 15r1; 15r1; 15r1;
              15r1; 15r1; 15r1; 15r1; 15r1; 15r1; 15r1;
        15r1; 15r1; 15r1; 15r1; 15r1; 15r1; 15r1; 15r1;
              15r1; 15r1; 15r1; 15r1; 15r1; 15r1; 15r1;
        15r1; 15r1; 15r1; 15r1; 15r1; 15r1; 15r1; 15r1;
              15r1; 15r1; 15r1; 15r1; 15r1; 15r1; 15r1;
        15r1; 15r1; 15r1; 15r1; 15r1; 15r1; 15r1; 15r1;
              15r1; 15r1; 15r1; 15r1; 15r1; 15r1; 15r1;
        15r1; 15r1; 15r1; 15r1; 15r1; 15r1; 15r1; 15r1;
              15r1; 15r1; 15r1; 15r1; 15r1; 15r1; 15r1;
        15r1; 15r1; 15r1; 15r1; 15r1; 15r1; 15r1; 15r1;
              15r1; 15r1; 15r1; 15r1; 15r1; 15r1; 15r1;
        15r1; 15r1; 15r1; 15r1; 15r1; 15r1; 15r1; 15r1;
              15r1; 15r1; 15r1; 15r1; 15r1; 15r1; 15r1;
        15r1; 15r1; 15r1; 15r1; 15r1; 15r1; 15r1; 15r1;
              15r1; 15r1; 15r1; 15r1; 15r1; 15r1; 15r1;
        15r1; 15r1; 15r1; 15r1; 15r1; 15r1; 15r1; 15r1;
              15r1; 15r1; 15r1; 15r1; 15r1; 15r1; 15r1;
        15r1; 15r1; 15r1; 15r1; 15r1; 15r1; 15r1; 15r1;
              15r1; 15r1; 15r1; 15r1; 15r1; 15r1; 15r1;
        15r1; 15r1; 15r1; 15r1; 15r1; 15r1; 15r1; 15r1;
              15r1; 15r1; 15r1; 15r1; 15r1; 15r1; 15r1;
        15r1; 15r1; 15r1; 15r1; 15r1; 15r1; 15r1; 15r1;
              15r1; 15r1; 15r1; 15r1; 15r1; 15r1; 15r1;
  T
/
/ block 3
```

```
/
  lib=odninp
  maxord=0
  ihm=4 iht=3 ihs=4
  ifido=2
  T
  0.167 0.0 0.833 0.666 /
  T
  0.167 0.0 0.833 0.666 /
  T
/
/ block 4
/
  matls=isos
  assign=matls
  T
/
/ block 5
/
  ievt=0
  ibl=0 ibr=0 ibt=0 ibb=0 ibfrnt=0 ibback=0
  fluxp=1 kprint=8 xsectp=2 sourcp=3
  sourcx=15r1
  sourcy=15r1
  sourcz=15r1
  source=19.82
  T
/
/ block 6
/
  pted=1
  igrped=0
  T
```

APPENDIX C

SAMPLE MCNPX INPUT DECK

```
Base Case for Border Crossing
c
c @@@@@@@@@@@@@@@@@@@@@@@@@@@@@@@@@@@@@@@@@@@@@@@@@@@@@@@@@@@@@@@@@@@@@@@@@@@@@@@@@@@@@@@@@@
c
c Author: Karen Miller
c
c Date: 20 Aug 2009
c
c Description: Three lanes for vehicles - each containing a portal monitor - with three
c              vehicles in each lane.
c
c @@@@@@@@@@@@@@@@@@@@@@@@@@@@@@@@@@@@@@@@@@@@@@@@@@@@@@@@@@@@@@@@@@@@@@@@@@@@@@@@@@@@@@@@@@
c
c ----------------------------------------------------------------
c                              CELL CARDS
c ----------------------------------------------------------------
c
c ------------ LEFT PORTAL MONITOR 1 ------------
c
c *** Aluminum Instrument Case ***
c
c    mat    den     surfaces         importance
100   6    -2.7     1000 -1001       imp:n=1  $ aluminum case
c
c *** Helium-3 Tubes ***
c
c    mat    den     surfaces         importance
101   6    -2.7     -1002 1003       imp:n=1  $ aluminum tube 1
102   6    -2.7     -1004 1005       imp:n=1  $ aluminum tube 2
103   6    -2.7     -1006 1007       imp:n=1  $ aluminum tube 3
104   6    -2.7     -1008 1009       imp:n=1  $ aluminum tube 4
105   6    -2.7     -1010 1011       imp:n=1  $ aluminum tube 5
106   6    -2.7     -1012 1013       imp:n=1  $ aluminum tube 6
c
107   1  -5.00E-04  -1003            imp:n=1  $ he-3 fill tube 1
108   1  -5.00E-04  -1005            imp:n=1  $ he-3 fill tube 2
109   1  -5.00E-04  -1007            imp:n=1  $ he-3 fill tube 3
110   1  -5.00E-04  -1009            imp:n=1  $ he-3 fill tube 4
111   1  -5.00E-04  -1011            imp:n=1  $ he-3 fill tube 5
112   1  -5.00E-04  -1013            imp:n=1  $ he-3 fill tube 6
c
c *** Polyethylene Moderator ***
c
c    mat    den     surfaces               importance
113   2    -0.96    -1014 1002 1004 1006
                     1008 1010 1012        imp:n=1  $ he-3 tube bank
114   2    -0.96    -1015                  imp:n=1  $ back panel
115   2    -0.96    -1016                  imp:n=1  $ middle panel
116   2    -0.96    -1017                  imp:n=1  $ front panel
117   2    -0.96    -1018                  imp:n=1  $ left panel
118   2    -0.96    -1019                  imp:n=1  $ right panel
c
c *** Plastic Scintillator ***
c
c    mat    den     surfaces               importance
119   3   -1.032    -1020                  imp:n=1  $ left scintillator
120   3   -1.032    -1021                  imp:n=1  $ right scintillator
121   4   -7.92     -1022                  imp:n=1  $ SS304 spacer
c
c *** Air Gap ***
c
c    mat    den      surfaces              importance
122  10  -1.204E-03  -1023                 imp:n=1  $ top air gap
```

```
123  10  -1.204E-03  -1024                imp:n=1  $ bottom air gap
c
c *** SS304 Topper ***
c
c    mat    den      surfaces              importance
124   4    -7.92     -1025                 imp:n=1  $ SS304 topper
c
c ------------ RIGHT PORTAL MONITOR 1 ------------
c
c *** Aluminum Instrument Case ***
c
c    mat    den     surfaces         importance
200   6    -2.7     2000 -2001       imp:n=1  $ aluminum case
c
c *** Helium-3 Tubes ***
c
c    mat    den     surfaces         importance
201   6    -2.7     -2002 2003       imp:n=1  $ aluminum tube 1
202   6    -2.7     -2004 2005       imp:n=1  $ aluminum tube 2
203   6    -2.7     -2006 2007       imp:n=1  $ aluminum tube 3
204   6    -2.7     -2008 2009       imp:n=1  $ aluminum tube 4
205   6    -2.7     -2010 2011       imp:n=1  $ aluminum tube 5
206   6    -2.7     -2012 2013       imp:n=1  $ aluminum tube 6
c
207   1  -5.00E-04  -2003            imp:n=1  $ he-3 fill tube 1
208   1  -5.00E-04  -2005            imp:n=1  $ he-3 fill tube 2
209   1  -5.00E-04  -2007            imp:n=1  $ he-3 fill tube 3
210   1  -5.00E-04  -2009            imp:n=1  $ he-3 fill tube 4
211   1  -5.00E-04  -2011            imp:n=1  $ he-3 fill tube 5
212   1  -5.00E-04  -2013            imp:n=1  $ he-3 fill tube 6
c
c *** Polyethylene Moderator ***
c
c    mat    den     surfaces               importance
213   2    -0.96    -2014 2002 2004 2006
                     2008 2010 2012        imp:n=1  $ he-3 tube bank
214   2    -0.96    -2015                  imp:n=1  $ back panel
215   2    -0.96    -2016                  imp:n=1  $ middle panel
216   2    -0.96    -2017                  imp:n=1  $ front panel
217   2    -0.96    -2018                  imp:n=1  $ left panel
218   2    -0.96    -2019                  imp:n=1  $ right panel
c
c *** Plastic Scintillator ***
c
c    mat    den     surfaces               importance
219   3   -1.032    -2020                  imp:n=1  $ left scintillator
220   3   -1.032    -2021                  imp:n=1  $ right scintillator
221   4   -7.92     -2022                  imp:n=1  $ SS304 spacer
c
c *** Air Gap ***
c
c    mat    den      surfaces              importance
222  10  -1.204E-03  -2023                imp:n=1  $ top air gap
223  10  -1.204E-03  -2024                imp:n=1  $ bottom air gap
c
c *** SS304 Topper ***
c
c    mat    den      surfaces              importance
224   4    -7.92     -2025                 imp:n=1  $ SS304 topper
c
c ------------ LEFT PORTAL MONITOR 2 ------------
c
c *** Aluminum Instrument Case ***
c
c    mat    den     surfaces         importance
125   6    -2.7     1100 -1101       imp:n=1  $ aluminum case
c
c *** Helium-3 Tubes ***
c
c    mat    den     surfaces         importance
126   6    -2.7     -1102 1103       imp:n=1  $ aluminum tube 1
127   6    -2.7     -1104 1105       imp:n=1  $ aluminum tube 2
128   6    -2.7     -1106 1107       imp:n=1  $ aluminum tube 3
129   6    -2.7     -1108 1109       imp:n=1  $ aluminum tube 4
130   6    -2.7     -1110 1111       imp:n=1  $ aluminum tube 5
131   6    -2.7     -1112 1113       imp:n=1  $ aluminum tube 6
c
```

```
132   1  -5.00E-04  -1103           imp:n=1  $ he-3 fill tube 1
133   1  -5.00E-04  -1105           imp:n=1  $ he-3 fill tube 2
134   1  -5.00E-04  -1107           imp:n=1  $ he-3 fill tube 3
135   1  -5.00E-04  -1109           imp:n=1  $ he-3 fill tube 4
136   1  -5.00E-04  -1111           imp:n=1  $ he-3 fill tube 5
137   1  -5.00E-04  -1113           imp:n=1  $ he-3 fill tube 6
c
c *** Polyethylene Moderator ***
c
c    mat    den     surfaces              importance
138   2    -0.96    -1114 1102 1104 1106
                     1108 1110 1112       imp:n=1  $ he-3 tube bank
139   2    -0.96    -1115                 imp:n=1  $ back panel
140   2    -0.96    -1116                 imp:n=1  $ middle panel
141   2    -0.96    -1117                 imp:n=1  $ front panel
142   2    -0.96    -1118                 imp:n=1  $ left panel
143   2    -0.96    -1119                 imp:n=1  $ right panel
c
c *** Plastic Scintillator ***
c
c    mat    den     surfaces              importance
144   3   -1.032    -1120                 imp:n=1  $ left scintillator
145   3   -1.032    -1121                 imp:n=1  $ right scintillator
146   4   -7.92     -1122                 imp:n=1  $ SS304 spacer
c
c *** Air Gap ***
c
c    mat    den      surfaces              importance
147  10  -1.204E-03  -1123                imp:n=1  $ top air gap
148  10  -1.204E-03  -1124                imp:n=1  $ bottom air gap
c
c *** SS304 Topper ***
c
c    mat    den      surfaces              importance
149   4    -7.92     -1125                 imp:n=1  $ SS304 topper
c
c ------------ RIGHT PORTAL MONITOR 2 ------------
c
c *** Aluminum Instrument Case ***
c
c    mat    den     surfaces         importance
225   6    -2.7     2100 -2101       imp:n=1  $ aluminum case
c
c *** Helium-3 Tubes ***
c
c    mat    den     surfaces         importance
226   6    -2.7     -2102 2103       imp:n=1  $ aluminum tube 1
227   6    -2.7     -2104 2105       imp:n=1  $ aluminum tube 2
228   6    -2.7     -2106 2107       imp:n=1  $ aluminum tube 3
229   6    -2.7     -2108 2109       imp:n=1  $ aluminum tube 4
230   6    -2.7     -2110 2111       imp:n=1  $ aluminum tube 5
231   6    -2.7     -2112 2113       imp:n=1  $ aluminum tube 6
c
232   1  -5.00E-04  -2103           imp:n=1  $ he-3 fill tube 1
233   1  -5.00E-04  -2105           imp:n=1  $ he-3 fill tube 2
234   1  -5.00E-04  -2107           imp:n=1  $ he-3 fill tube 3
235   1  -5.00E-04  -2109           imp:n=1  $ he-3 fill tube 4
236   1  -5.00E-04  -2111           imp:n=1  $ he-3 fill tube 5
237   1  -5.00E-04  -2113           imp:n=1  $ he-3 fill tube 6
c
c *** Polyethylene Moderator ***
c
c    mat    den     surfaces              importance
238   2    -0.96    -2114 2102 2104 2106
                     2108 2110 2112       imp:n=1  $ he-3 tube bank
239   2    -0.96    -2115                 imp:n=1  $ back panel
240   2    -0.96    -2116                 imp:n=1  $ middle panel
241   2    -0.96    -2117                 imp:n=1  $ front panel
242   2    -0.96    -2118                 imp:n=1  $ left panel
243   2    -0.96    -2119                 imp:n=1  $ right panel
c
c *** Plastic Scintillator ***
c
c    mat    den     surfaces              importance
244   3   -1.032    -2120                 imp:n=1  $ left scintillator
245   3   -1.032    -2121                 imp:n=1  $ right scintillator
246   4   -7.92     -2122                 imp:n=1  $ SS304 spacer
```

```
c
c *** Air Gap ***
c
c    mat    den      surfaces              importance
247  10  -1.204E-03  -2123                 imp:n=1  $ top air gap
248  10  -1.204E-03  -2124                 imp:n=1  $ bottom air gap
c
c *** SS304 Topper ***
c
c    mat    den      surfaces              importance
249   4    -7.92     -2125                 imp:n=1  $ SS304 topper
c
c ------------ LEFT PORTAL MONITOR 3 ------------
c
c *** Aluminum Instrument Case ***
c
c    mat    den     surfaces         importance
150   6    -2.7     1200 -1201       imp:n=1  $ aluminum case
c
c *** Helium-3 Tubes ***
c
c    mat    den     surfaces         importance
151   6    -2.7     -1202 1203       imp:n=1  $ aluminum tube 1
152   6    -2.7     -1204 1205       imp:n=1  $ aluminum tube 2
153   6    -2.7     -1206 1207       imp:n=1  $ aluminum tube 3
154   6    -2.7     -1208 1209       imp:n=1  $ aluminum tube 4
155   6    -2.7     -1210 1211       imp:n=1  $ aluminum tube 5
156   6    -2.7     -1212 1213       imp:n=1  $ aluminum tube 6
c
157   1  -5.00E-04  -1203            imp:n=1  $ he-3 fill tube 1
158   1  -5.00E-04  -1205            imp:n=1  $ he-3 fill tube 2
159   1  -5.00E-04  -1207            imp:n=1  $ he-3 fill tube 3
160   1  -5.00E-04  -1209            imp:n=1  $ he-3 fill tube 4
161   1  -5.00E-04  -1211            imp:n=1  $ he-3 fill tube 5
162   1  -5.00E-04  -1213            imp:n=1  $ he-3 fill tube 6
c
c *** Polyethylene Moderator ***
c
c    mat    den     surfaces               importance
163   2    -0.96    -1214 1202 1204 1206
                     1208 1210 1212        imp:n=1  $ he-3 tube bank
164   2    -0.96    -1215                  imp:n=1  $ back panel
165   2    -0.96    -1216                  imp:n=1  $ middle panel
166   2    -0.96    -1217                  imp:n=1  $ front panel
167   2    -0.96    -1218                  imp:n=1  $ left panel
168   2    -0.96    -1219                  imp:n=1  $ right panel
c
c *** Plastic Scintillator ***
c
c    mat    den     surfaces               importance
169   3   -1.032    -1220                  imp:n=1  $ left scintillator
170   3   -1.032    -1221                  imp:n=1  $ right scintillator
171   4   -7.92     -1222                  imp:n=1  $ SS304 spacer
c
c *** Air Gap ***
c
c    mat    den      surfaces              importance
172  10  -1.204E-03  -1223                 imp:n=1  $ top air gap
173  10  -1.204E-03  -1224                 imp:n=1  $ bottom air gap
c
c *** SS304 Topper ***
c
c    mat    den      surfaces              importance
174   4    -7.92     -1225                 imp:n=1  $ SS304 topper
c
c ------------ RIGHT PORTAL MONITOR 3 ------------
c
c *** Aluminum Instrument Case ***
c
c    mat    den     surfaces         importance
250   6    -2.7     2200 -2201       imp:n=1  $ aluminum case
c
c *** Helium-3 Tubes ***
c
c    mat    den     surfaces         importance
251   6    -2.7     -2202 2203       imp:n=1  $ aluminum tube 1
252   6    -2.7     -2204 2205       imp:n=1  $ aluminum tube 2
```

```
253   6    -2.7     -2206 2207       imp:n=1  $ aluminum tube 3
254   6    -2.7     -2208 2209       imp:n=1  $ aluminum tube 4
255   6    -2.7     -2210 2211       imp:n=1  $ aluminum tube 5
256   6    -2.7     -2212 2213       imp:n=1  $ aluminum tube 6
c
257   1  -5.00E-04  -2203            imp:n=1  $ he-3 fill tube 1
258   1  -5.00E-04  -2205            imp:n=1  $ he-3 fill tube 2
259   1  -5.00E-04  -2207            imp:n=1  $ he-3 fill tube 3
260   1  -5.00E-04  -2209            imp:n=1  $ he-3 fill tube 4
261   1  -5.00E-04  -2211            imp:n=1  $ he-3 fill tube 5
262   1  -5.00E-04  -2213            imp:n=1  $ he-3 fill tube 6
c
c *** Polyethylene Moderator ***
c
c    mat    den     surfaces               importance
263   2    -0.96    -2214 2202 2204 2206
                     2208 2210 2212        imp:n=1  $ he-3 tube bank
264   2    -0.96    -2215                  imp:n=1  $ back panel
265   2    -0.96    -2216                  imp:n=1  $ middle panel
266   2    -0.96    -2217                  imp:n=1  $ front panel
267   2    -0.96    -2218                  imp:n=1  $ left panel
268   2    -0.96    -2219                  imp:n=1  $ right panel
c
c *** Plastic Scintillator ***
c
c    mat    den     surfaces               importance
269   3   -1.032    -2220                  imp:n=1  $ left scintillator
270   3   -1.032    -2221                  imp:n=1  $ right scintillator
271   4   -7.92     -2222                  imp:n=1  $ SS304 spacer
c
c *** Air Gap ***
c
c    mat    den      surfaces              importance
272  10  -1.204E-03  -2223                 imp:n=1  $ top air gap
273  10  -1.204E-03  -2224                 imp:n=1  $ bottom air gap
c
c *** SS304 Topper ***
c
c    mat    den      surfaces              importance
274   4    -7.92     -2225                  imp:n=1  $ SS304 topper
c
c ------------ VEHICLE (1,1) ------------
c
c *** Engine Block ***
c
c    mat    den     surfaces           importance
300   4    -1.98    -3000              imp:n=1  $ engine block, SS304 at 25% of full density
c
c *** Passenger Compartment ***
c
c    mat    den     surfaces           importance
301   5    -7.84    -3001 3002         imp:n=1  $ carbon steel frame
302  11    -0.01    -3002              imp:n=1  $ passenger compartment, polyurethane foam at 50% of
full density
c
c *** Trunk & Gas Tank ***
c
c    mat    den     surfaces           importance
303   5    -7.84    -3003 3004         imp:n=1  $ carbon steel frame
304   7    -0.70    -3004 -3005        imp:n=1  $ gasoline
305  10  -1.204E-03 -3004 3005         imp:n=1  $ air space in trunk
c
c *** Windows ***
c
c    mat    den     surfaces           importance
306   8    -2.52    -3006 3007         imp:n=1  $ glass windows
307  10  -1.204E-03 -3007              imp:n=1  $ air space
c
c *** Tires ***
c
c    mat    den     surfaces           importance
308  12    -1.50    -3008 3009 -3016   imp:n=1  $ rubber tire, right front
309  10  -1.204E-03 -3009 -3016        imp:n=1  $ air in tire, right front
c
310  12    -1.50    -3010 3011 -3016   imp:n=1  $ rubber tire, left front
311  10  -1.204E-03 -3011 -3016        imp:n=1  $ air in tire, left front
c
```

```
312  12    -1.50    -3012 3013 -3016   imp:n=1  $ rubber tire, right back
313  10  -1.204E-03 -3013 -3016        imp:n=1  $ air in tire, right back
c
314  12    -1.50    -3014 3015 -3016   imp:n=1  $ rubber tire, left back
315  10  -1.204E-03 -3015 -3016        imp:n=1  $ air in tire, left back
c
c ------------ VEHICLE (2,1) ------------
c
c *** Engine Block ***
c
c    mat    den     surfaces           importance
316   4    -1.98    -3100              imp:n=1  $ engine block, SS304 at 25% of full density
c
c *** Passenger Compartment ***
c
c    mat    den     surfaces           importance
317   5    -7.84    -3101 3102         imp:n=1  $ carbon steel frame
318  11    -0.01    -3102              imp:n=1  $ passenger compartment, polyurethane foam at 50% of
full density
c
c *** Trunk & Gas Tank ***
c
c    mat    den     surfaces           importance
319   5    -7.84    -3103 3104         imp:n=1  $ carbon steel frame
320   7    -0.70    -3104 -3105        imp:n=1  $ gasoline
321  10  -1.204E-03 -3104 3105         imp:n=1  $ air space in trunk
c
c *** Windows ***
c
c    mat    den     surfaces           importance
322   8    -2.52    -3106 3107         imp:n=1  $ glass windows
323  10  -1.204E-03 -3107              imp:n=1  $ air space
c
c *** Tires ***
c
c    mat    den     surfaces           importance
324  12    -1.50    -3108 3109 -3116   imp:n=1  $ rubber tire, right front
325  10  -1.204E-03 -3109 -3116        imp:n=1  $ air in tire, right front
c
326  12    -1.50    -3110 3111 -3116   imp:n=1  $ rubber tire, left front
327  10  -1.204E-03 -3111 -3116        imp:n=1  $ air in tire, left front
c
328  12    -1.50    -3112 3113 -3116   imp:n=1  $ rubber tire, right back
329  10  -1.204E-03 -3113 -3116        imp:n=1  $ air in tire, right back
c
330  12    -1.50    -3114 3115 -3116   imp:n=1  $ rubber tire, left back
331  10  -1.204E-03 -3115 -3116        imp:n=1  $ air in tire, left back
c
c ------------ VEHICLE (3,1) ------------
c
c *** Engine Block ***
c
c    mat    den     surfaces           importance
332   4    -1.98    -3200              imp:n=1  $ engine block, SS304 at 25% of full density
c
c *** Passenger Compartment ***
c
c    mat    den     surfaces           importance
333   5    -7.84    -3201 3202         imp:n=1  $ carbon steel frame
334  11    -0.01    -3202              imp:n=1  $ passenger compartment, polyurethane foam at 50% of
full density
c
c *** Trunk & Gas Tank ***
c
c    mat    den     surfaces           importance
335   5    -7.84    -3203 3204         imp:n=1  $ carbon steel frame
336   7    -0.70    -3204 -3205        imp:n=1  $ gasoline
337  10  -1.204E-03 -3204 3205         imp:n=1  $ air space in trunk
c
c *** Windows ***
c
c    mat    den     surfaces           importance
338   8    -2.52    -3206 3207         imp:n=1  $ glass windows
339  10  -1.204E-03 -3207              imp:n=1  $ air space
c
c *** Tires ***
c
```

```
c    mat    den     surfaces           importance
340  12    -1.50    -3208 3209 -3216   imp:n=1  $ rubber tire, right front
341  10  -1.204E-03 -3209 -3216        imp:n=1  $ air in tire, right front
c
342  12    -1.50    -3210 3211 -3216   imp:n=1  $ rubber tire, left front
343  10  -1.204E-03 -3211 -3216        imp:n=1  $ air in tire, left front
c
344  12    -1.50    -3212 3213 -3216   imp:n=1  $ rubber tire, right back
345  10  -1.204E-03 -3213 -3216        imp:n=1  $ air in tire, right back
c
346  12    -1.50    -3214 3215 -3216   imp:n=1  $ rubber tire, left back
347  10  -1.204E-03 -3215 -3216        imp:n=1  $ air in tire, left back
c
c ------------ VEHICLE (1,2) ------------
c
c *** Engine Block ***
c
c    mat    den     surfaces           importance
348   4    -1.98    -3300              imp:n=1  $ engine block, SS304 at 25% of full density
c
c *** Passenger Compartment ***
c
c    mat    den     surfaces           importance
349   5    -7.84    -3301 3302         imp:n=1  $ carbon steel frame
350  11    -0.01    -3302              imp:n=1  $ passenger compartment, polyurethane foam at 50% of
full density
c
c *** Trunk & Gas Tank ***
c
c    mat    den     surfaces           importance
351   5    -7.84    -3303 3304         imp:n=1  $ carbon steel frame
352   7    -0.70    -3304 -3305        imp:n=1  $ gasoline
353  10  -1.204E-03 -3304 3305         imp:n=1  $ air space in trunk
c
c *** Windows ***
c
c    mat    den     surfaces           importance
354   8    -2.52    -3306 3307         imp:n=1  $ glass windows
355  10  -1.204E-03 -3307              imp:n=1  $ air space
c
c *** Tires ***
c
c    mat    den     surfaces           importance
356  12    -1.50    -3308 3309 -3316   imp:n=1  $ rubber tire, right front
357  10  -1.204E-03 -3309 -3316        imp:n=1  $ air in tire, right front
c
358  12    -1.50    -3310 3311 -3316   imp:n=1  $ rubber tire, left front
359  10  -1.204E-03 -3311 -3316        imp:n=1  $ air in tire, left front
c
360  12    -1.50    -3312 3313 -3316   imp:n=1  $ rubber tire, right back
361  10  -1.204E-03 -3313 -3316        imp:n=1  $ air in tire, right back
c
362  12    -1.50    -3314 3315 -3316   imp:n=1  $ rubber tire, left back
363  10  -1.204E-03 -3315 -3316        imp:n=1  $ air in tire, left back
c
c ------------ VEHICLE (2,2) ------------
c
c *** Engine Block ***
c
c    mat    den     surfaces           importance
364   4    -1.98    -3400              imp:n=1  $ engine block, SS304 at 25% of full density
c
c *** Passenger Compartment ***
c
c    mat    den     surfaces           importance
365   5    -7.84    -3401 3402         imp:n=1  $ carbon steel frame
366  11    -0.01    -3402              imp:n=1  $ passenger compartment, polyurethane foam at 50% of
full density
c
c *** Trunk & Gas Tank ***
c
c    mat    den     surfaces           importance
367   5    -7.84    -3403 3404         imp:n=1  $ carbon steel frame
368   7    -0.70    -3404 -3405        imp:n=1  $ gasoline
369  10  -1.204E-03 -3404 3405         imp:n=1  $ air space in trunk
c
c *** Windows ***
```

```
c
c    mat    den     surfaces           importance
370   8    -2.52    -3406 3407         imp:n=1  $ glass windows
371  10  -1.204E-03 -3407              imp:n=1  $ air space
c
c *** Tires ***
c
c    mat    den     surfaces           importance
372  12    -1.50    -3408 3409 -3416   imp:n=1  $ rubber tire, right front
373  10  -1.204E-03 -3409 -3416        imp:n=1  $ air in tire, right front
c
374  12    -1.50    -3410 3411 -3416   imp:n=1  $ rubber tire, left front
375  10  -1.204E-03 -3411 -3416        imp:n=1  $ air in tire, left front
c
376  12    -1.50    -3412 3413 -3416   imp:n=1  $ rubber tire, right back
377  10  -1.204E-03 -3413 -3416        imp:n=1  $ air in tire, right back
c
378  12    -1.50    -3414 3415 -3416   imp:n=1  $ rubber tire, left back
379  10  -1.204E-03 -3415 -3416        imp:n=1  $ air in tire, left back
c
c ------------ VEHICLE (3,2) ------------
c
c *** Engine Block ***
c
c    mat    den     surfaces           importance
380   4    -1.98    -3500              imp:n=1  $ engine block, SS304 at 25% of full density
c
c *** Passenger Compartment ***
c
c    mat    den     surfaces           importance
381   5    -7.84    -3501 3502         imp:n=1  $ carbon steel frame
382  11    -0.01    -3502              imp:n=1  $ passenger compartment, polyurethane foam at 50% of
full density
c
c *** Trunk & Gas Tank ***
c
c    mat    den     surfaces           importance
383   5    -7.84    -3503 3504         imp:n=1  $ carbon steel frame
384   7    -0.70    -3504 -3505        imp:n=1  $ gasoline
385  10  -1.204E-03 -3504 3505         imp:n=1  $ air space in trunk
c
c *** Windows ***
c
c    mat    den     surfaces           importance
386   8    -2.52    -3506 3507         imp:n=1  $ glass windows
387  10  -1.204E-03 -3507              imp:n=1  $ air space
c
c *** Tires ***
c
c    mat    den     surfaces           importance
388  12    -1.50    -3508 3509 -3516   imp:n=1  $ rubber tire, right front
389  10  -1.204E-03 -3509 -3516        imp:n=1  $ air in tire, right front
c
390  12    -1.50    -3510 3511 -3516   imp:n=1  $ rubber tire, left front
391  10  -1.204E-03 -3511 -3516        imp:n=1  $ air in tire, left front
c
392  12    -1.50    -3512 3513 -3516   imp:n=1  $ rubber tire, right back
393  10  -1.204E-03 -3513 -3516        imp:n=1  $ air in tire, right back
c
394  12    -1.50    -3514 3515 -3516   imp:n=1  $ rubber tire, left back
395  10  -1.204E-03 -3515 -3516        imp:n=1  $ air in tire, left back
c
c ------------ VEHICLE (1,3) ------------
c
c *** Engine Block ***
c
c    mat    den     surfaces           importance
400   4    -1.98    -3600              imp:n=1  $ engine block, SS304 at 25% of full density
c
c *** Passenger Compartment ***
c
c    mat    den     surfaces           importance
401   5    -7.84    -3601 3602         imp:n=1  $ carbon steel frame
402  11    -0.01    -3602              imp:n=1  $ passenger compartment, polyurethane foam at 50% of
full density
c
c *** Trunk & Gas Tank ***
```

```
c
c    mat    den     surfaces           importance
403   5    -7.84    -3603 3604         imp:n=1  $ carbon steel frame
404   7    -0.70    -3604 -3605        imp:n=1  $ gasoline
405  10  -1.204E-03 -3604 3605         imp:n=1  $ air space in trunk
c
c *** Windows ***
c
c    mat    den     surfaces           importance
406   8    -2.52    -3606 3607         imp:n=1  $ glass windows
407  10  -1.204E-03 -3607              imp:n=1  $ air space
c
c *** Tires ***
c
c    mat    den     surfaces           importance
408  12    -1.50    -3608 3609 -3616   imp:n=1  $ rubber tire, right front
409  10  -1.204E-03 -3609 -3616        imp:n=1  $ air in tire, right front
c
410  12    -1.50    -3610 3611 -3616   imp:n=1  $ rubber tire, left front
411  10  -1.204E-03 -3611 -3616        imp:n=1  $ air in tire, left front
c
412  12    -1.50    -3612 3613 -3616   imp:n=1  $ rubber tire, right back
413  10  -1.204E-03 -3613 -3616        imp:n=1  $ air in tire, right back
c
414  12    -1.50    -3614 3615 -3616   imp:n=1  $ rubber tire, left back
415  10  -1.204E-03 -3615 -3616        imp:n=1  $ air in tire, left back
c
c ------------ VEHICLE (2,3) ------------
c
c *** Engine Block ***
c
c    mat    den     surfaces           importance
416   4    -1.98    -3700              imp:n=1  $ engine block, SS304 at 25% of full density
c
c *** Passenger Compartment ***
c
c    mat    den     surfaces           importance
417   5    -7.84    -3701 3702         imp:n=1  $ carbon steel frame
418  11    -0.01    -3702              imp:n=1  $ passenger compartment, polyurethane foam at 50% of
full density
c
c *** Trunk & Gas Tank ***
c
c    mat    den     surfaces           importance
419   5    -7.84    -3703 3704         imp:n=1  $ carbon steel frame
420   7    -0.70    -3704 -3705        imp:n=1  $ gasoline
421  10  -1.204E-03 -3704 3705         imp:n=1  $ air space in trunk
c
c *** Windows ***
c
c    mat    den     surfaces           importance
422   8    -2.52    -3706 3707         imp:n=1  $ glass windows
423  10  -1.204E-03 -3707              imp:n=1  $ air space
c
c *** Tires ***
c
c    mat    den     surfaces           importance
424  12    -1.50    -3708 3709 -3716   imp:n=1  $ rubber tire, right front
425  10  -1.204E-03 -3709 -3716        imp:n=1  $ air in tire, right front
c
426  12    -1.50    -3710 3711 -3716   imp:n=1  $ rubber tire, left front
427  10  -1.204E-03 -3711 -3716        imp:n=1  $ air in tire, left front
c
428  12    -1.50    -3712 3713 -3716   imp:n=1  $ rubber tire, right back
429  10  -1.204E-03 -3713 -3716        imp:n=1  $ air in tire, right back
c
430  12    -1.50    -3714 3715 -3716   imp:n=1  $ rubber tire, left back
431  10  -1.204E-03 -3715 -3716        imp:n=1  $ air in tire, left back
c
c ------------ VEHICLE (3,3) ------------
c
c *** Engine Block ***
c
c    mat    den     surfaces           importance
432   4    -1.98    -3800              imp:n=1  $ engine block, SS304 at 25% of full density
c
c *** Passenger Compartment ***
```

```
c
c    mat    den     surfaces           importance
433   5    -7.84    -3801 3802         imp:n=1  $ carbon steel frame
434  11    -0.01    -3802              imp:n=1  $ passenger compartment, polyurethane foam at 50% of
full density
c
c *** Trunk & Gas Tank ***
c
c    mat    den     surfaces           importance
435   5    -7.84    -3803 3804         imp:n=1  $ carbon steel frame
436   7    -0.70    -3804 -3805        imp:n=1  $ gasoline
437  10  -1.204E-03 -3804 3805         imp:n=1  $ air space in trunk
c
c *** Windows ***
c
c    mat    den     surfaces           importance
438   8    -2.52    -3806 3807         imp:n=1  $ glass windows
439  10  -1.204E-03 -3807              imp:n=1  $ air space
c
c *** Tires ***
c
c    mat    den     surfaces           importance
440  12    -1.50    -3808 3809 -3816   imp:n=1  $ rubber tire, right front
441  10  -1.204E-03 -3809 -3816        imp:n=1  $ air in tire, right front
c
442  12    -1.50    -3810 3811 -3816   imp:n=1  $ rubber tire, left front
443  10  -1.204E-03 -3811 -3816        imp:n=1  $ air in tire, left front
c
444  12    -1.50    -3812 3813 -3816   imp:n=1  $ rubber tire, right back
445  10  -1.204E-03 -3813 -3816        imp:n=1  $ air in tire, right back
c
446  12    -1.50    -3814 3815 -3816   imp:n=1  $ rubber tire, left back
447  10  -1.204E-03 -3815 -3816        imp:n=1  $ air in tire, left back
c
c ------------ UNIVERSE ------------
c
c *** Universe ***
c
c    mat    den      surfaces                              importance
900  10  -1.204E-03  -9999  9000 1001 2001 1101 2101
                      1201 2201 3000 3001 3003 3006 3008
                      3010 3012 3014 3100 3101 3103 3106
                      3108 3110 3112 3114 3200 3201 3203
                      3206 3208 3210 3212 3214 3300 3301
                      3303 3306 3308 3310 3312 3314 3400
                      3401 3403 3406 3408 3410 3412 3414
                      3500 3501 3503 3506 3508 3510 3512
                      3514 3600 3601 3603 3606 3608 3610
                      3612 3614 3700 3701 3703 3706 3708
                      3710 3712 3714 3800 3801 3803 3806
                      3808 3810 3812 3814                   imp:n=1  $ inside the universe, dry air
901   9    -2.35     -9999 -9000                           imp:n=1  $ concrete floor
902   0               9999                                  imp:n=0  $ the nothing

c ---------------------------------------------------------------
c                            SURFACE CARDS
c ---------------------------------------------------------------
c
c ------------ LEFT PORTAL MONITOR 1 ------------
c
c *** Aluminum Instrument Case ***
c
c          Vx   Vy   Vz   A1x   A1y  A1z  A2x  A2y    A2z  A3x  A3y   A3z
1000  box   0.1  0.1  0.1  30.0  0.0  0.0  0.0  126.0  0.0  0.0  0.0  168.0 $ inner box wall
1001  box   0.0  0.0  0.0  30.2  0.0  0.0  0.0  126.2  0.0  0.0  0.0  168.2 $ outer box wall
c
c *** Helium-3 Tubes ***
c
c          Vx   Vy     Vz   Hx   Hy   Hz     R
1002  rcc   9.1  25.6  70.0  0.0  0.0  92.0  3.3  $ outer tube 1 wall
1003  rcc   9.1  25.6  70.1  0.0  0.0  91.8  3.2  $ inner tube 1 wall
c
1004  rcc   9.1  38.6  70.0  0.0  0.0  92.0  3.3  $ outer tube 2 wall
1005  rcc   9.1  38.6  70.1  0.0  0.0  91.8  3.2  $ inner tube 2 wall
c
1006  rcc   9.1  51.6  70.0  0.0  0.0  92.0  3.3  $ outer tube 3 wall
1007  rcc   9.1  51.6  70.1  0.0  0.0  91.8  3.2  $ inner tube 3 wall
```

```
c
1008  rcc   9.1  74.6  70.0  0.0  0.0  92.0  3.3  $ outer tube 4 wall
1009  rcc   9.1  74.6  70.1  0.0  0.0  91.8  3.2  $ inner tube 4 wall
c
1010  rcc   9.1  87.6  70.0  0.0  0.0  92.0  3.3  $ outer tube 4 wall
1011  rcc   9.1  87.6  70.1  0.0  0.0  91.8  3.2  $ inner tube 4 wall
c
1012  rcc   9.1 100.6  70.0  0.0  0.0  92.0  3.3  $ outer tube 4 wall
1013  rcc   9.1 100.6  70.1  0.0  0.0  91.8  3.2  $ inner tube 4 wall
c
c *** Polyethylene Moderator ***
c
c           Vx   Vy     Vz   A1x   A1y  A1z  A2x  A2y   A2z  A3x  A3y   A3z
1014  box   2.6  19.1  70.0  13.0  0.0  0.0  0.0  88.0  0.0  0.0  0.0   92.0  $ he-3 tube bank
1015  box   0.1  19.1   0.1   2.5  0.0  0.0  0.0  88.0  0.0  0.0  0.0  161.9  $ back panel
1016  box  15.6  19.1  70.0   2.5  0.0  0.0  0.0  88.0  0.0  0.0  0.0   92.0  $ middle panel
1017  box  27.1  19.1   0.1   3.0  0.0  0.0  0.0  88.0  0.0  0.0  0.0  161.9  $ front panel
1018  box   0.1   0.1   0.1  30.0  0.0  0.0  0.0  19.0  0.0  0.0  0.0  161.9  $ left panel
1019  box   0.1 126.1   0.1  30.0  0.0  0.0  0.0 -19.0  0.0  0.0  0.0  161.9  $ right panel
c
c *** Plastic Scintillator ***
c
c           Vx   Vy     Vz   A1x  A1y  A1z  A2x  A2y   A2z  A3x  A3y  A3z
1020  box  18.1  19.1  70.0  4.0  0.0  0.0  0.0  39.0  0.0  0.0  0.0  92.0  $ left scintillator
1021  box  18.1 107.1  70.0  4.0  0.0  0.0  0.0 -39.0  0.0  0.0  0.0  92.0  $ right scintillator
1022  box  18.1  58.1  70.0  4.0  0.0  0.0  0.0  10.0  0.0  0.0  0.0  92.0  $ SS304 spacer
c
c *** Air Gap ***
c
c            Vx    Vy    Vz    A1x  A1y  A1z  A2x  A2y   A2z  A3x  A3y  A3z
1023  box   22.1  19.1  70.0   5.0  0.0  0.0  0.0  88.0  0.0  0.0  0.0  92.0  $ top air gap
1024  box    2.6  19.1   0.1  24.5  0.0  0.0  0.0  88.0  0.0  0.0  0.0  69.9  $ bottom air gap
c
c *** SS304 Topper ***
c
c            Vx   Vy    Vz    A1x   A1y  A1z  A2x   A2y   A2z  A3x  A3y  A3z
1025  box    0.1  0.1  162.0  30.0  0.0  0.0  0.0  126.0  0.0  0.0  0.0  6.1  $ SS304 topper
c
c ------------ RIGHT PORTAL MONITOR 1 ------------
c
c *** Aluminum Instrument Case ***
c
c           Vx    Vy   Vz   A1x   A1y  A1z  A2x  A2y    A2z  A3x  A3y   A3z
2000  box  279.9  0.1  0.1  30.0  0.0  0.0  0.0  126.0  0.0  0.0  0.0  168.0 $ inner box wall
2001  box  279.8  0.0  0.0  30.2  0.0  0.0  0.0  126.2  0.0  0.0  0.0  168.2 $ outer box wall
c
c *** Helium-3 Tubes ***
c
c           Vx    Vy     Vz   Hx   Hy   Hz     R
2002  rcc  300.9  25.6  70.0  0.0  0.0  92.0  3.3  $ outer tube 1 wall
2003  rcc  300.9  25.6  70.1  0.0  0.0  91.8  3.2  $ inner tube 1 wall
c
2004  rcc  300.9  38.6  70.0  0.0  0.0  92.0  3.3  $ outer tube 2 wall
2005  rcc  300.9  38.6  70.1  0.0  0.0  91.8  3.2  $ inner tube 2 wall
c
2006  rcc  300.9  51.6  70.0  0.0  0.0  92.0  3.3  $ outer tube 3 wall
2007  rcc  300.9  51.6  70.1  0.0  0.0  91.8  3.2  $ inner tube 3 wall
c
2008  rcc  300.9  74.6  70.0  0.0  0.0  92.0  3.3  $ outer tube 4 wall
2009  rcc  300.9  74.6  70.1  0.0  0.0  91.8  3.2  $ inner tube 4 wall
c
2010  rcc  300.9  87.6  70.0  0.0  0.0  92.0  3.3  $ outer tube 4 wall
2011  rcc  300.9  87.6  70.1  0.0  0.0  91.8  3.2  $ inner tube 4 wall
c
2012  rcc  300.9 100.6  70.0  0.0  0.0  92.0  3.3  $ outer tube 4 wall
2013  rcc  300.9 100.6  70.1  0.0  0.0  91.8  3.2  $ inner tube 4 wall
c
c *** Polyethylene Moderator ***
c
c           Vx     Vy    Vz   A1x   A1y  A1z  A2x  A2y   A2z  A3x  A3y   A3z
2014  box  294.4  19.1  70.0  13.0  0.0  0.0  0.0  88.0  0.0  0.0  0.0   92.0  $ he-3 tube bank
2015  box  307.4  19.1   0.1   2.5  0.0  0.0  0.0  88.0  0.0  0.0  0.0  161.9  $ back panel
2016  box  291.9  19.1  70.0   2.5  0.0  0.0  0.0  88.0  0.0  0.0  0.0   92.0  $ middle panel
2017  box  279.9  19.1   0.1   3.0  0.0  0.0  0.0  88.0  0.0  0.0  0.0  161.9  $ front panel
2018  box  279.9   0.1   0.1  30.0  0.0  0.0  0.0  19.0  0.0  0.0  0.0  161.9  $ left panel
2019  box  279.9 126.1   0.1  30.0  0.0  0.0  0.0 -19.0  0.0  0.0  0.0  161.9  $ right panel
c
```

```
c *** Plastic Scintillator ***
c
c           Vx    Vy     Vz   A1x  A1y  A1z  A2x  A2y   A2z  A3x  A3y  A3z
2020  box  287.9  19.1  70.0  4.0  0.0  0.0  0.0  39.0  0.0  0.0  0.0  92.0  $ left scintillator
2021  box  287.9 107.1  70.0  4.0  0.0  0.0  0.0 -39.0  0.0  0.0  0.0  92.0  $ right scintillator
2022  box  287.9  58.1  70.0  4.0  0.0  0.0  0.0  10.0  0.0  0.0  0.0  92.0  $ SS304 spacer
c
c *** Air Gap ***
c
c            Vx    Vy    Vz    A1x  A1y  A1z  A2x  A2y   A2z  A3x  A3y  A3z
2023  box  282.9  19.1  70.0   5.0  0.0  0.0  0.0  88.0  0.0  0.0  0.0  92.0  $ top air gap
2024  box  282.9  19.1   0.1  24.5  0.0  0.0  0.0  88.0  0.0  0.0  0.0  69.9  $ bottom air gap
c
c *** SS304 Topper ***
c
c            Vx   Vy    Vz    A1x   A1y  A1z  A2x   A2y   A2z  A3x  A3y  A3z
2025  box  279.9  0.1  162.0  30.0  0.0  0.0  0.0  126.0  0.0  0.0  0.0  6.1  $ SS304 topper
c
c ------------ LEFT PORTAL MONITOR 2 ------------
c
c *** Aluminum Instrument Case ***
c
c             Vx   Vy   Vz   A1x   A1y  A1z  A2x  A2y    A2z  A3x  A3y   A3z
1100  box   330.1  0.1  0.1  30.0  0.0  0.0  0.0  126.0  0.0  0.0  0.0  168.0 $ inner box wall
1101  box   330.0  0.0  0.0  30.2  0.0  0.0  0.0  126.2  0.0  0.0  0.0  168.2 $ outer box wall
c
c *** Helium-3 Tubes ***
c
c            Vx     Vy    Vz   Hx   Hy   Hz     R
1102  rcc   339.1  25.6  70.0  0.0  0.0  92.0  3.3  $ outer tube 1 wall
1103  rcc   339.1  25.6  70.1  0.0  0.0  91.8  3.2  $ inner tube 1 wall
c
1104  rcc   339.1  38.6  70.0  0.0  0.0  92.0  3.3  $ outer tube 2 wall
1105  rcc   339.1  38.6  70.1  0.0  0.0  91.8  3.2  $ inner tube 2 wall
c
1106  rcc   339.1  51.6  70.0  0.0  0.0  92.0  3.3  $ outer tube 3 wall
1107  rcc   339.1  51.6  70.1  0.0  0.0  91.8  3.2  $ inner tube 3 wall
c
1108  rcc   339.1  74.6  70.0  0.0  0.0  92.0  3.3  $ outer tube 4 wall
1109  rcc   339.1  74.6  70.1  0.0  0.0  91.8  3.2  $ inner tube 4 wall
c
1110  rcc   339.1  87.6  70.0  0.0  0.0  92.0  3.3  $ outer tube 4 wall
1111  rcc   339.1  87.6  70.1  0.0  0.0  91.8  3.2  $ inner tube 4 wall
c
1112  rcc   339.1 100.6  70.0  0.0  0.0  92.0  3.3  $ outer tube 4 wall
1113  rcc   339.1 100.6  70.1  0.0  0.0  91.8  3.2  $ inner tube 4 wall
c
c *** Polyethylene Moderator ***
c
c           Vx     Vy     Vz   A1x  A1y  A1z  A2x  A2y   A2z  A3x  A3y   A3z
1114  box  332.6  19.1  70.0  13.0  0.0  0.0  0.0  88.0  0.0  0.0  0.0   92.0  $ he-3 tube bank
1115  box  330.1  19.1   0.1   2.5  0.0  0.0  0.0  88.0  0.0  0.0  0.0  161.9  $ back panel
1116  box  345.6  19.1  70.0   2.5  0.0  0.0  0.0  88.0  0.0  0.0  0.0   92.0  $ middle panel
1117  box  357.1  19.1   0.1   3.0  0.0  0.0  0.0  88.0  0.0  0.0  0.0  161.9  $ front panel
1118  box  330.1   0.1   0.1  30.0  0.0  0.0  0.0  19.0  0.0  0.0  0.0  161.9  $ left panel
1119  box  330.1 126.1   0.1  30.0  0.0  0.0  0.0 -19.0  0.0  0.0  0.0  161.9  $ right panel
c
c *** Plastic Scintillator ***
c
c           Vx    Vy     Vz   A1x  A1y  A1z  A2x  A2y   A2z  A3x  A3y  A3z
1120  box  348.1  19.1  70.0  4.0  0.0  0.0  0.0  39.0  0.0  0.0  0.0  92.0  $ left scintillator
1121  box  348.1 107.1  70.0  4.0  0.0  0.0  0.0 -39.0  0.0  0.0  0.0  92.0  $ right scintillator
1122  box  348.1  58.1  70.0  4.0  0.0  0.0  0.0  10.0  0.0  0.0  0.0  92.0  $ SS304 spacer
c
c *** Air Gap ***
c
c            Vx     Vy    Vz    A1x  A1y  A1z  A2x  A2y   A2z  A3x  A3y  A3z
1123  box   352.1  19.1  70.0   5.0  0.0  0.0  0.0  88.0  0.0  0.0  0.0  92.0  $ top air gap
1124  box   332.6  19.1   0.1  24.5  0.0  0.0  0.0  88.0  0.0  0.0  0.0  69.9  $ bottom air gap
c
c *** SS304 Topper ***
c
c           Vx    Vy    Vz    A1x   A1y  A1z  A2x   A2y   A2z  A3x  A3y  A3z
1125  box  330.1  0.1  162.0  30.0  0.0  0.0  0.0  126.0  0.0  0.0  0.0  6.1  $ SS304 topper
c
c ------------ RIGHT PORTAL MONITOR 2 ------------
c
```

```
c *** Aluminum Instrument Case ***
c
c           Vx    Vy   Vz   A1x   A1y  A1z  A2x  A2y    A2z  A3x  A3y   A3z
2100  box  609.9  0.1  0.1  30.0  0.0  0.0  0.0  126.0  0.0  0.0  0.0  168.0 $ inner box wall
2101  box  609.8  0.0  0.0  30.2  0.0  0.0  0.0  126.2  0.0  0.0  0.0  168.2 $ outer box wall
c
c *** Helium-3 Tubes ***
c
c           Vx    Vy     Vz   Hx   Hy   Hz     R
2102  rcc  630.9  25.6  70.0  0.0  0.0  92.0  3.3  $ outer tube 1 wall
2103  rcc  630.9  25.6  70.1  0.0  0.0  91.8  3.2  $ inner tube 1 wall
c
2104  rcc  630.9  38.6  70.0  0.0  0.0  92.0  3.3  $ outer tube 2 wall
2105  rcc  630.9  38.6  70.1  0.0  0.0  91.8  3.2  $ inner tube 2 wall
c
2106  rcc  630.9  51.6  70.0  0.0  0.0  92.0  3.3  $ outer tube 3 wall
2107  rcc  630.9  51.6  70.1  0.0  0.0  91.8  3.2  $ inner tube 3 wall
c
2108  rcc  630.9  74.6  70.0  0.0  0.0  92.0  3.3  $ outer tube 4 wall
2109  rcc  630.9  74.6  70.1  0.0  0.0  91.8  3.2  $ inner tube 4 wall
c
2110  rcc  630.9  87.6  70.0  0.0  0.0  92.0  3.3  $ outer tube 4 wall
2111  rcc  630.9  87.6  70.1  0.0  0.0  91.8  3.2  $ inner tube 4 wall
c
2112  rcc  630.9 100.6  70.0  0.0  0.0  92.0  3.3  $ outer tube 4 wall
2113  rcc  630.9 100.6  70.1  0.0  0.0  91.8  3.2  $ inner tube 4 wall
c
c *** Polyethylene Moderator ***
c
c           Vx     Vy    Vz   A1x   A1y  A1z  A2x  A2y   A2z  A3x  A3y   A3z
2114  box  624.4  19.1  70.0  13.0  0.0  0.0  0.0  88.0  0.0  0.0  0.0   92.0  $ he-3 tube bank
2115  box  637.4  19.1   0.1   2.5  0.0  0.0  0.0  88.0  0.0  0.0  0.0  161.9  $ back panel
2116  box  621.9  19.1  70.0   2.5  0.0  0.0  0.0  88.0  0.0  0.0  0.0   92.0  $ middle panel
2117  box  609.9  19.1   0.1   3.0  0.0  0.0  0.0  88.0  0.0  0.0  0.0  161.9  $ front panel
2118  box  609.9   0.1   0.1  30.0  0.0  0.0  0.0  19.0  0.0  0.0  0.0  161.9  $ left panel
2119  box  609.9 126.1   0.1  30.0  0.0  0.0  0.0 -19.0  0.0  0.0  0.0  161.9  $ right panel
c
c *** Plastic Scintillator ***
c
c           Vx    Vy     Vz   A1x  A1y  A1z  A2x  A2y   A2z  A3x  A3y  A3z
2120  box  617.9  19.1  70.0  4.0  0.0  0.0  0.0  39.0  0.0  0.0  0.0  92.0  $ left scintillator
2121  box  617.9 107.1  70.0  4.0  0.0  0.0  0.0 -39.0  0.0  0.0  0.0  92.0  $ right scintillator
2122  box  617.9  58.1  70.0  4.0  0.0  0.0  0.0  10.0  0.0  0.0  0.0  92.0  $ SS304 spacer
c
c *** Air Gap ***
c
c           Vx    Vy    Vz    A1x  A1y  A1z  A2x  A2y   A2z  A3x  A3y  A3z
2123  box  612.9  19.1  70.0   5.0  0.0  0.0  0.0  88.0  0.0  0.0  0.0  92.0  $ top air gap
2124  box  612.9  19.1   0.1  24.5  0.0  0.0  0.0  88.0  0.0  0.0  0.0  69.9  $ bottom air gap
c
c *** SS304 Topper ***
c
c           Vx   Vy    Vz    A1x   A1y  A1z  A2x   A2y   A2z  A3x  A3y  A3z
2125  box  609.9  0.1  162.0  30.0  0.0  0.0  0.0  126.0  0.0  0.0  0.0  6.1  $ SS304 topper
c
c ------------ LEFT PORTAL MONITOR 3 ------------
c
c *** Aluminum Instrument Case ***
c
c             Vx   Vy   Vz   A1x   A1y  A1z  A2x  A2y    A2z  A3x  A3y   A3z
1200  box   660.1  0.1  0.1  30.0  0.0  0.0  0.0  126.0  0.0  0.0  0.0  168.0 $ inner box wall
1201  box   660.0  0.0  0.0  30.2  0.0  0.0  0.0  126.2  0.0  0.0  0.0  168.2 $ outer box wall
c
c *** Helium-3 Tubes ***
c
c            Vx     Vy    Vz   Hx   Hy   Hz     R
1202  rcc   669.1  25.6  70.0  0.0  0.0  92.0  3.3  $ outer tube 1 wall
1203  rcc   669.1  25.6  70.1  0.0  0.0  91.8  3.2  $ inner tube 1 wall
c
1204  rcc   669.1  38.6  70.0  0.0  0.0  92.0  3.3  $ outer tube 2 wall
1205  rcc   669.1  38.6  70.1  0.0  0.0  91.8  3.2  $ inner tube 2 wall
c
1206  rcc   669.1  51.6  70.0  0.0  0.0  92.0  3.3  $ outer tube 3 wall
1207  rcc   669.1  51.6  70.1  0.0  0.0  91.8  3.2  $ inner tube 3 wall
c
1208  rcc   669.1  74.6  70.0  0.0  0.0  92.0  3.3  $ outer tube 4 wall
1209  rcc   669.1  74.6  70.1  0.0  0.0  91.8  3.2  $ inner tube 4 wall
```

```
c
1210  rcc   669.1  87.6  70.0  0.0  0.0  92.0  3.3  $ outer tube 4 wall
1211  rcc   669.1  87.6  70.1  0.0  0.0  91.8  3.2  $ inner tube 4 wall
c
1212  rcc   669.1 100.6  70.0  0.0  0.0  92.0  3.3  $ outer tube 4 wall
1213  rcc   669.1 100.6  70.1  0.0  0.0  91.8  3.2  $ inner tube 4 wall
c
c *** Polyethylene Moderator ***
c
c           Vx     Vy     Vz   A1x  A1y  A1z  A2x  A2y   A2z  A3x  A3y   A3z
1214  box  662.6  19.1  70.0  13.0  0.0  0.0  0.0  88.0  0.0  0.0  0.0   92.0  $ he-3 tube bank
1215  box  660.1  19.1   0.1   2.5  0.0  0.0  0.0  88.0  0.0  0.0  0.0  161.9  $ back panel
1216  box  675.6  19.1  70.0   2.5  0.0  0.0  0.0  88.0  0.0  0.0  0.0   92.0  $ middle panel
1217  box  687.1  19.1   0.1   3.0  0.0  0.0  0.0  88.0  0.0  0.0  0.0  161.9  $ front panel
1218  box  660.1   0.1   0.1  30.0  0.0  0.0  0.0  19.0  0.0  0.0  0.0  161.9  $ left panel
1219  box  660.1 126.1   0.1  30.0  0.0  0.0  0.0 -19.0  0.0  0.0  0.0  161.9  $ right panel
c
c *** Plastic Scintillator ***
c
c           Vx    Vy     Vz   A1x  A1y  A1z  A2x  A2y   A2z  A3x  A3y  A3z
1220  box  678.1  19.1  70.0  4.0  0.0  0.0  0.0  39.0  0.0  0.0  0.0  92.0  $ left scintillator
1221  box  678.1 107.1  70.0  4.0  0.0  0.0  0.0 -39.0  0.0  0.0  0.0  92.0  $ right scintillator
1222  box  678.1  58.1  70.0  4.0  0.0  0.0  0.0  10.0  0.0  0.0  0.0  92.0  $ SS304 spacer
c
c *** Air Gap ***
c
c            Vx     Vy    Vz    A1x  A1y  A1z  A2x  A2y   A2z  A3x  A3y  A3z
1223  box   682.1  19.1  70.0   5.0  0.0  0.0  0.0  88.0  0.0  0.0  0.0  92.0  $ top air gap
1224  box   662.6  19.1   0.1  24.5  0.0  0.0  0.0  88.0  0.0  0.0  0.0  69.9  $ bottom air gap
c
c *** SS304 Topper ***
c
c           Vx    Vy    Vz    A1x   A1y  A1z  A2x   A2y   A2z  A3x  A3y  A3z
1225  box  660.1  0.1  162.0  30.0  0.0  0.0  0.0  126.0  0.0  0.0  0.0  6.1  $ SS304 topper
c
c ------------ RIGHT PORTAL MONITOR 3 ------------
c
c *** Aluminum Instrument Case ***
c
c           Vx    Vy   Vz   A1x   A1y  A1z  A2x  A2y    A2z  A3x  A3y   A3z
2200  box  939.9  0.1  0.1  30.0  0.0  0.0  0.0  126.0  0.0  0.0  0.0  168.0 $ inner box wall
2201  box  939.8  0.0  0.0  30.2  0.0  0.0  0.0  126.2  0.0  0.0  0.0  168.2 $ outer box wall
c
c *** Helium-3 Tubes ***
c
c           Vx    Vy     Vz   Hx   Hy   Hz     R
2202  rcc  960.9  25.6  70.0  0.0  0.0  92.0  3.3  $ outer tube 1 wall
2203  rcc  960.9  25.6  70.1  0.0  0.0  91.8  3.2  $ inner tube 1 wall
c
2204  rcc  960.9  38.6  70.0  0.0  0.0  92.0  3.3  $ outer tube 2 wall
2205  rcc  960.9  38.6  70.1  0.0  0.0  91.8  3.2  $ inner tube 2 wall
c
2206  rcc  960.9  51.6  70.0  0.0  0.0  92.0  3.3  $ outer tube 3 wall
2207  rcc  960.9  51.6  70.1  0.0  0.0  91.8  3.2  $ inner tube 3 wall
c
2208  rcc  960.9  74.6  70.0  0.0  0.0  92.0  3.3  $ outer tube 4 wall
2209  rcc  960.9  74.6  70.1  0.0  0.0  91.8  3.2  $ inner tube 4 wall
c
2210  rcc  960.9  87.6  70.0  0.0  0.0  92.0  3.3  $ outer tube 4 wall
2211  rcc  960.9  87.6  70.1  0.0  0.0  91.8  3.2  $ inner tube 4 wall
c
2212  rcc  960.9 100.6  70.0  0.0  0.0  92.0  3.3  $ outer tube 4 wall
2213  rcc  960.9 100.6  70.1  0.0  0.0  91.8  3.2  $ inner tube 4 wall
c
c *** Polyethylene Moderator ***
c
c           Vx     Vy    Vz   A1x   A1y  A1z  A2x  A2y   A2z  A3x  A3y   A3z
2214  box  954.4  19.1  70.0  13.0  0.0  0.0  0.0  88.0  0.0  0.0  0.0   92.0  $ he-3 tube bank
2215  box  967.4  19.1   0.1   2.5  0.0  0.0  0.0  88.0  0.0  0.0  0.0  161.9  $ back panel
2216  box  951.9  19.1  70.0   2.5  0.0  0.0  0.0  88.0  0.0  0.0  0.0   92.0  $ middle panel
2217  box  939.9  19.1   0.1   3.0  0.0  0.0  0.0  88.0  0.0  0.0  0.0  161.9  $ front panel
2218  box  939.9   0.1   0.1  30.0  0.0  0.0  0.0  19.0  0.0  0.0  0.0  161.9  $ left panel
2219  box  939.9 126.1   0.1  30.0  0.0  0.0  0.0 -19.0  0.0  0.0  0.0  161.9  $ right panel
c
c *** Plastic Scintillator ***
c
c           Vx    Vy     Vz   A1x  A1y  A1z  A2x  A2y   A2z  A3x  A3y  A3z
```

```
2220  box  947.9  19.1  70.0  4.0  0.0  0.0  0.0  39.0  0.0  0.0  0.0  92.0  $ left scintillator
2221  box  947.9 107.1  70.0  4.0  0.0  0.0  0.0 -39.0  0.0  0.0  0.0  92.0  $ right scintillator
2222  box  947.9  58.1  70.0  4.0  0.0  0.0  0.0  10.0  0.0  0.0  0.0  92.0  $ SS304 spacer
c
c *** Air Gap ***
c
c            Vx    Vy    Vz    A1x  A1y  A1z  A2x  A2y   A2z  A3x  A3y  A3z
2223  box  942.9  19.1  70.0   5.0  0.0  0.0  0.0  88.0  0.0  0.0  0.0  92.0  $ top air gap
2224  box  942.9  19.1   0.1  24.5  0.0  0.0  0.0  88.0  0.0  0.0  0.0  69.9  $ bottom air gap
c
c *** SS304 Topper ***
c
c            Vx   Vy    Vz    A1x   A1y  A1z  A2x   A2y   A2z  A3x  A3y  A3z
2225  box  939.9  0.1  162.0  30.0  0.0  0.0  0.0  126.0  0.0  0.0  0.0  6.1  $ SS304 topper
c
c ------------ VEHICLE (1,1) ------------
c
c *** Engine Block ***
c
c            Vx   Vy    Vz    A1x   A1y  A1z  A2x  A2y   A2z  A3x  A3y  A3z
3000  box   80.0  0.0  15.0  150.0  0.0  0.0  0.0  90.0  0.0  0.0  0.0  68.0  $ engine block
c
c *** Passenger Compartment ***
c
c           Vx    Vy    Vz    A1x   A1y  A1z  A2x  A2y   A2z  A3x  A3y  A3z
3001  box  80.0  90.0  15.0  150.0  0.0  0.0  0.0  90.0  0.0  0.0  0.0  68.0  $ outer frame wall
3002  box  83.0  93.0  18.0  144.0  0.0  0.0  0.0  84.0  0.0  0.0  0.0  62.0  $ inner frame wall
c
c *** Trunk & Gas Tank ***
c
c           Vx    Vy     Vz    A1x   A1y  A1z  A2x  A2y   A2z  A3x  A3y  A3z
3003  box  80.0  180.0  15.0  150.0  0.0  0.0  0.0  90.0  0.0  0.0  0.0  68.0  $ outer frame wall
3004  box  83.0  183.0  18.0  144.0  0.0  0.0  0.0  84.0  0.0  0.0  0.0  62.0  $ inner frame wall
c
3005  pz    23.0  $ gas fill level (19.0=3.2gal, 21.0=9.6gal, 23.0=16gal, 25.0=22.4gal)
c
c *** Windows ***
c
c           Vx    Vy    Vz    A1x   A1y  A1z  A2x  A2y   A2z  A3x  A3y  A3z
3006  box  80.0  90.0  83.0  150.0  0.0  0.0  0.0  90.0  0.0  0.0  0.0  68.0  $ outer window wall
3007  box  81.0  91.0  84.0  148.0  0.0  0.0  0.0  88.0  0.0  0.0  0.0  66.0  $ inner window wall
c
c *** Tires ***
c
c            Vx     Vy    Vz    Hx   Hy   Hz    R
3008  rcc   80.0   61.0  29.0  18.0  0.0  0.0  29.0  $ outer tire wall, right front
3009  rcc   81.0   61.0  29.0  16.0  0.0  0.0  28.0  $ inner tire wall, right front
c
3010  rcc  230.0   61.0  29.0 -18.0  0.0  0.0  29.0  $ outer tire wall, left front
3011  rcc  229.0   61.0  29.0 -16.0  0.0  0.0  28.0  $ inner tire wall, left front
c
3012  rcc   80.0  209.0  29.0  18.0  0.0  0.0  29.0  $ outer tire wall, right back
3013  rcc   81.0  209.0  29.0  16.0  0.0  0.0  28.0  $ inner tire wall, right back
c
3014  rcc  230.0  209.0  29.0 -18.0  0.0  0.0  29.0  $ outer tire wall, left back
3015  rcc  229.0  209.0  29.0 -16.0  0.0  0.0  28.0  $ inner tire wall, left back
c
3016  pz    15.0  $ bottom of vehicle
c
c ------------ VEHICLE (2,1) ------------
c
c *** Engine Block ***
c
c            Vx   Vy    Vz    A1x   A1y  A1z  A2x  A2y   A2z  A3x  A3y  A3z
3100  box  410.0  0.0  15.0  150.0  0.0  0.0  0.0  90.0  0.0  0.0  0.0  68.0  $ engine block
c
c *** Passenger Compartment ***
c
c            Vx    Vy    Vz    A1x   A1y  A1z  A2x  A2y   A2z  A3x  A3y  A3z
3101  box  410.0  90.0  15.0  150.0  0.0  0.0  0.0  90.0  0.0  0.0  0.0  68.0  $ outer frame wall
3102  box  413.0  93.0  18.0  144.0  0.0  0.0  0.0  84.0  0.0  0.0  0.0  62.0  $ inner frame wall
c
c *** Trunk & Gas Tank ***
c
c           Vx    Vy     Vz    A1x   A1y  A1z  A2x  A2y   A2z  A3x  A3y  A3z
3103  box  410.0  180.0  15.0  150.0  0.0  0.0  0.0  90.0  0.0  0.0  0.0  68.0  $ outer frame wall
3104  box  413.0  183.0  18.0  144.0  0.0  0.0  0.0  84.0  0.0  0.0  0.0  62.0  $ inner frame wall
```

```
c
3105  pz    23.0  $ gas fill level (19.0=3.2gal, 21.0=9.6gal, 23.0=16gal, 25.0=22.4gal)
c
c *** Windows ***
c
c           Vx    Vy    Vz    A1x   A1y  A1z  A2x  A2y   A2z  A3x  A3y  A3z
3106  box  410.0  90.0  83.0  150.0  0.0  0.0  0.0  90.0  0.0  0.0  0.0  68.0  $ outer window wall
3107  box  411.0  91.0  84.0  148.0  0.0  0.0  0.0  88.0  0.0  0.0  0.0  66.0  $ inner window wall
c
c *** Tires ***
c
c            Vx     Vy    Vz    Hx   Hy   Hz    R
3108  rcc  410.0   61.0  29.0  18.0  0.0  0.0  29.0  $ outer tire wall, right front
3109  rcc  411.0   61.0  29.0  16.0  0.0  0.0  28.0  $ inner tire wall, right front
c
3110  rcc  560.0   61.0  29.0 -18.0  0.0  0.0  29.0  $ outer tire wall, left front
3111  rcc  559.0   61.0  29.0 -16.0  0.0  0.0  28.0  $ inner tire wall, left front
c
3112  rcc  410.0  209.0  29.0  18.0  0.0  0.0  29.0  $ outer tire wall, right back
3113  rcc  411.0  209.0  29.0  16.0  0.0  0.0  28.0  $ inner tire wall, right back
c
3114  rcc  560.0  209.0  29.0 -18.0  0.0  0.0  29.0  $ outer tire wall, left back
3115  rcc  559.0  209.0  29.0 -16.0  0.0  0.0  28.0  $ inner tire wall, left back
c
3116  pz    15.0  $ bottom of vehicle
c
c ------------ VEHICLE (3,1) ------------
c
c *** Engine Block ***
c
c            Vx   Vy    Vz    A1x   A1y  A1z  A2x  A2y   A2z  A3x  A3y  A3z
3200  box  740.0  0.0  15.0  150.0  0.0  0.0  0.0  90.0  0.0  0.0  0.0  68.0  $ engine block
c
c *** Passenger Compartment ***
c
c            Vx    Vy    Vz    A1x   A1y  A1z  A2x  A2y   A2z  A3x  A3y  A3z
3201  box  740.0  90.0  15.0  150.0  0.0  0.0  0.0  90.0  0.0  0.0  0.0  68.0  $ outer frame wall
3202  box  743.0  93.0  18.0  144.0  0.0  0.0  0.0  84.0  0.0  0.0  0.0  62.0  $ inner frame wall
c
c *** Trunk & Gas Tank ***
c
c           Vx    Vy     Vz    A1x   A1y  A1z  A2x  A2y   A2z  A3x  A3y  A3z
3203  box  740.0  180.0  15.0  150.0  0.0  0.0  0.0  90.0  0.0  0.0  0.0  68.0  $ outer frame wall
3204  box  743.0  183.0  18.0  144.0  0.0  0.0  0.0  84.0  0.0  0.0  0.0  62.0  $ inner frame wall
c
3205  pz    23.0  $ gas fill level (19.0=3.2gal, 21.0=9.6gal, 23.0=16gal, 25.0=22.4gal)
c
c *** Windows ***
c
c           Vx    Vy    Vz    A1x   A1y  A1z  A2x  A2y   A2z  A3x  A3y  A3z
3206  box  740.0  90.0  83.0  150.0  0.0  0.0  0.0  90.0  0.0  0.0  0.0  68.0  $ outer window wall
3207  box  741.0  91.0  84.0  148.0  0.0  0.0  0.0  88.0  0.0  0.0  0.0  66.0  $ inner window wall
c
c *** Tires ***
c
c            Vx     Vy    Vz    Hx   Hy   Hz    R
3208  rcc  740.0   61.0  29.0  18.0  0.0  0.0  29.0  $ outer tire wall, right front
3209  rcc  741.0   61.0  29.0  16.0  0.0  0.0  28.0  $ inner tire wall, right front
c
3210  rcc  890.0   61.0  29.0 -18.0  0.0  0.0  29.0  $ outer tire wall, left front
3211  rcc  889.0   61.0  29.0 -16.0  0.0  0.0  28.0  $ inner tire wall, left front
c
3212  rcc  740.0  209.0  29.0  18.0  0.0  0.0  29.0  $ outer tire wall, right back
3213  rcc  741.0  209.0  29.0  16.0  0.0  0.0  28.0  $ inner tire wall, right back
c
3214  rcc  890.0  209.0  29.0 -18.0  0.0  0.0  29.0  $ outer tire wall, left back
3215  rcc  889.0  209.0  29.0 -16.0  0.0  0.0  28.0  $ inner tire wall, left back
c
3216  pz    15.0  $ bottom of vehicle
c
c ------------ VEHICLE (1,2) ------------
c
c *** Engine Block ***
c
c            Vx    Vy     Vz    A1x   A1y  A1z  A2x  A2y   A2z  A3x  A3y  A3z
3300  box   80.0  350.0  15.0  150.0  0.0  0.0  0.0  90.0  0.0  0.0  0.0  68.0  $ engine block
c
```

```
c *** Passenger Compartment ***
c
c           Vx    Vy     Vz    A1x   A1y  A1z  A2x  A2y   A2z  A3x  A3y  A3z
3301  box  80.0  440.0  15.0  150.0  0.0  0.0  0.0  90.0  0.0  0.0  0.0  68.0  $ outer frame wall
3302  box  83.0  443.0  18.0  144.0  0.0  0.0  0.0  84.0  0.0  0.0  0.0  62.0  $ inner frame wall
c
c *** Trunk & Gas Tank ***
c
c           Vx    Vy     Vz    A1x   A1y  A1z  A2x  A2y   A2z  A3x  A3y  A3z
3303  box  80.0  530.0  15.0  150.0  0.0  0.0  0.0  90.0  0.0  0.0  0.0  68.0  $ outer frame wall
3304  box  83.0  533.0  18.0  144.0  0.0  0.0  0.0  84.0  0.0  0.0  0.0  62.0  $ inner frame wall
c
3305  pz    23.0  $ gas fill level (19.0=3.2gal, 21.0=9.6gal, 23.0=16gal, 25.0=22.4gal)
c
c *** Windows ***
c
c           Vx    Vy     Vz    A1x   A1y  A1z  A2x  A2y   A2z  A3x  A3y  A3z
3306  box  80.0  440.0  83.0  150.0  0.0  0.0  0.0  90.0  0.0  0.0  0.0  68.0  $ outer window wall
3307  box  81.0  441.0  84.0  148.0  0.0  0.0  0.0  88.0  0.0  0.0  0.0  66.0  $ inner window wall
c
c *** Tires ***
c
c            Vx     Vy    Vz    Hx   Hy   Hz    R
3308  rcc   80.0  411.0  29.0  18.0  0.0  0.0  29.0  $ outer tire wall, right front
3309  rcc   81.0  411.0  29.0  16.0  0.0  0.0  28.0  $ inner tire wall, right front
c
3310  rcc  230.0  411.0  29.0 -18.0  0.0  0.0  29.0  $ outer tire wall, left front
3311  rcc  229.0  411.0  29.0 -16.0  0.0  0.0  28.0  $ inner tire wall, left front
c
3312  rcc   80.0  559.0  29.0  18.0  0.0  0.0  29.0  $ outer tire wall, right back
3313  rcc   81.0  559.0  29.0  16.0  0.0  0.0  28.0  $ inner tire wall, right back
c
3314  rcc  230.0  559.0  29.0 -18.0  0.0  0.0  29.0  $ outer tire wall, left back
3315  rcc  229.0  559.0  29.0 -16.0  0.0  0.0  28.0  $ inner tire wall, left back
c
3316  pz    15.0  $ bottom of vehicle
c
c ------------ VEHICLE (2,2) ------------
c
c *** Engine Block ***
c
c            Vx    Vy     Vz    A1x   A1y  A1z  A2x  A2y   A2z  A3x  A3y  A3z
3400  box  410.0  350.0  15.0  150.0  0.0  0.0  0.0  90.0  0.0  0.0  0.0  68.0  $ engine block
c
c *** Passenger Compartment ***
c
c            Vx    Vy     Vz    A1x   A1y  A1z  A2x  A2y   A2z  A3x  A3y  A3z
3401  box  410.0  440.0  15.0  150.0  0.0  0.0  0.0  90.0  0.0  0.0  0.0  68.0  $ outer frame wall
3402  box  413.0  443.0  18.0  144.0  0.0  0.0  0.0  84.0  0.0  0.0  0.0  62.0  $ inner frame wall
c
c *** Trunk & Gas Tank ***
c
c           Vx     Vy     Vz    A1x   A1y  A1z  A2x  A2y   A2z  A3x  A3y  A3z
3403  box  410.0  530.0  15.0  150.0  0.0  0.0  0.0  90.0  0.0  0.0  0.0  68.0  $ outer frame wall
3404  box  413.0  533.0  18.0  144.0  0.0  0.0  0.0  84.0  0.0  0.0  0.0  62.0  $ inner frame wall
c
3405  pz    23.0  $ gas fill level (19.0=3.2gal, 21.0=9.6gal, 23.0=16gal, 25.0=22.4gal)
c
c *** Windows ***
c
c           Vx     Vy     Vz    A1x   A1y  A1z  A2x  A2y   A2z  A3x  A3y  A3z
3406  box  410.0  440.0  83.0  150.0  0.0  0.0  0.0  90.0  0.0  0.0  0.0  68.0  $ outer window wall
3407  box  411.0  441.0  84.0  148.0  0.0  0.0  0.0  88.0  0.0  0.0  0.0  66.0  $ inner window wall
c
c *** Tires ***
c
c            Vx     Vy    Vz    Hx   Hy   Hz    R
3408  rcc  410.0  411.0  29.0  18.0  0.0  0.0  29.0  $ outer tire wall, right front
3409  rcc  411.0  411.0  29.0  16.0  0.0  0.0  28.0  $ inner tire wall, right front
c
3410  rcc  560.0  411.0  29.0 -18.0  0.0  0.0  29.0  $ outer tire wall, left front
3411  rcc  559.0  411.0  29.0 -16.0  0.0  0.0  28.0  $ inner tire wall, left front
c
3412  rcc  410.0  559.0  29.0  18.0  0.0  0.0  29.0  $ outer tire wall, right back
3413  rcc  411.0  559.0  29.0  16.0  0.0  0.0  28.0  $ inner tire wall, right back
c
3414  rcc  560.0  559.0  29.0 -18.0  0.0  0.0  29.0  $ outer tire wall, left back
```

```
3415  rcc  559.0  559.0  29.0 -16.0  0.0  0.0  28.0  $ inner tire wall, left back
c
3416  pz    15.0  $ bottom of vehicle
c
c ------------ VEHICLE (3,2) ------------
c
c *** Engine Block ***
c
c            Vx    Vy     Vz    A1x   A1y  A1z  A2x  A2y   A2z  A3x  A3y  A3z
3500  box  740.0  350.0  15.0  150.0  0.0  0.0  0.0  90.0  0.0  0.0  0.0  68.0  $ engine block
c
c *** Passenger Compartment ***
c
c            Vx    Vy     Vz    A1x   A1y  A1z  A2x  A2y   A2z  A3x  A3y  A3z
3501  box  740.0  440.0  15.0  150.0  0.0  0.0  0.0  90.0  0.0  0.0  0.0  68.0  $ outer frame wall
3502  box  743.0  443.0  18.0  144.0  0.0  0.0  0.0  84.0  0.0  0.0  0.0  62.0  $ inner frame wall
c
c *** Trunk & Gas Tank ***
c
c           Vx    Vy     Vz    A1x   A1y  A1z  A2x  A2y   A2z  A3x  A3y  A3z
3503  box  740.0  530.0  15.0  150.0  0.0  0.0  0.0  90.0  0.0  0.0  0.0  68.0  $ outer frame wall
3504  box  743.0  533.0  18.0  144.0  0.0  0.0  0.0  84.0  0.0  0.0  0.0  62.0  $ inner frame wall
c
3505  pz    23.0  $ gas fill level (19.0=3.2gal, 21.0=9.6gal, 23.0=16gal, 25.0=22.4gal)
c
c *** Windows ***
c
c           Vx     Vy     Vz    A1x   A1y  A1z  A2x  A2y   A2z  A3x  A3y  A3z
3506  box  740.0  440.0  83.0  150.0  0.0  0.0  0.0  90.0  0.0  0.0  0.0  68.0  $ outer window wall
3507  box  741.0  441.0  84.0  148.0  0.0  0.0  0.0  88.0  0.0  0.0  0.0  66.0  $ inner window wall
c
c *** Tires ***
c
c            Vx     Vy    Vz    Hx   Hy   Hz    R
3508  rcc  740.0  411.0  29.0  18.0  0.0  0.0  29.0  $ outer tire wall, right front
3509  rcc  741.0  411.0  29.0  16.0  0.0  0.0  28.0  $ inner tire wall, right front
c
3510  rcc  890.0  411.0  29.0 -18.0  0.0  0.0  29.0  $ outer tire wall, left front
3511  rcc  889.0  411.0  29.0 -16.0  0.0  0.0  28.0  $ inner tire wall, left front
c
3512  rcc  740.0  559.0  29.0  18.0  0.0  0.0  29.0  $ outer tire wall, right back
3513  rcc  741.0  559.0  29.0  16.0  0.0  0.0  28.0  $ inner tire wall, right back
c
3514  rcc  890.0  559.0  29.0 -18.0  0.0  0.0  29.0  $ outer tire wall, left back
3515  rcc  889.0  559.0  29.0 -16.0  0.0  0.0  28.0  $ inner tire wall, left back
c
3516  pz    15.0  $ bottom of vehicle
c
c ------------ VEHICLE (1,3) ------------
c
c *** Engine Block ***
c
c            Vx    Vy     Vz    A1x   A1y  A1z  A2x  A2y   A2z  A3x  A3y  A3z
3600  box   80.0  700.0  15.0  150.0  0.0  0.0  0.0  90.0  0.0  0.0  0.0  68.0  $ engine block
c
c *** Passenger Compartment ***
c
c           Vx    Vy     Vz    A1x   A1y  A1z  A2x  A2y   A2z  A3x  A3y  A3z
3601  box  80.0  790.0  15.0  150.0  0.0  0.0  0.0  90.0  0.0  0.0  0.0  68.0  $ outer frame wall
3602  box  83.0  793.0  18.0  144.0  0.0  0.0  0.0  84.0  0.0  0.0  0.0  62.0  $ inner frame wall
c
c *** Trunk & Gas Tank ***
c
c           Vx    Vy     Vz    A1x   A1y  A1z  A2x  A2y   A2z  A3x  A3y  A3z
3603  box  80.0  880.0  15.0  150.0  0.0  0.0  0.0  90.0  0.0  0.0  0.0  68.0  $ outer frame wall
3604  box  83.0  883.0  18.0  144.0  0.0  0.0  0.0  84.0  0.0  0.0  0.0  62.0  $ inner frame wall
c
3605  pz    23.0  $ gas fill level (19.0=3.2gal, 21.0=9.6gal, 23.0=16gal, 25.0=22.4gal)
c
c *** Windows ***
c
c           Vx    Vy     Vz    A1x   A1y  A1z  A2x  A2y   A2z  A3x  A3y  A3z
3606  box  80.0  790.0  83.0  150.0  0.0  0.0  0.0  90.0  0.0  0.0  0.0  68.0  $ outer window wall
3607  box  81.0  791.0  84.0  148.0  0.0  0.0  0.0  88.0  0.0  0.0  0.0  66.0  $ inner window wall
c
c *** Tires ***
c
```

```
c            Vx     Vy    Vz    Hx   Hy   Hz    R
3608  rcc   80.0  761.0  29.0  18.0  0.0  0.0  29.0  $ outer tire wall, right front
3609  rcc   81.0  761.0  29.0  16.0  0.0  0.0  28.0  $ inner tire wall, right front
c
3610  rcc  230.0  761.0  29.0 -18.0  0.0  0.0  29.0  $ outer tire wall, left front
3611  rcc  229.0  761.0  29.0 -16.0  0.0  0.0  28.0  $ inner tire wall, left front
c
3612  rcc   80.0  909.0  29.0  18.0  0.0  0.0  29.0  $ outer tire wall, right back
3613  rcc   81.0  909.0  29.0  16.0  0.0  0.0  28.0  $ inner tire wall, right back
c
3614  rcc  230.0  909.0  29.0 -18.0  0.0  0.0  29.0  $ outer tire wall, left back
3615  rcc  229.0  909.0  29.0 -16.0  0.0  0.0  28.0  $ inner tire wall, left back
c
3616  pz    15.0  $ bottom of vehicle
c
c ------------ VEHICLE (2,3) ------------
c
c *** Engine Block ***
c
c            Vx    Vy     Vz    A1x   A1y  A1z  A2x  A2y   A2z  A3x  A3y  A3z
3700  box  410.0  700.0  15.0  150.0  0.0  0.0  0.0  90.0  0.0  0.0  0.0  68.0  $ engine block
c
c *** Passenger Compartment ***
c
c            Vx    Vy     Vz    A1x   A1y  A1z  A2x  A2y   A2z  A3x  A3y  A3z
3701  box  410.0  790.0  15.0  150.0  0.0  0.0  0.0  90.0  0.0  0.0  0.0  68.0  $ outer frame wall
3702  box  413.0  793.0  18.0  144.0  0.0  0.0  0.0  84.0  0.0  0.0  0.0  62.0  $ inner frame wall
c
c *** Trunk & Gas Tank ***
c
c           Vx     Vy     Vz    A1x   A1y  A1z  A2x  A2y   A2z  A3x  A3y  A3z
3703  box  410.0  880.0  15.0  150.0  0.0  0.0  0.0  90.0  0.0  0.0  0.0  68.0  $ outer frame wall
3704  box  413.0  883.0  18.0  144.0  0.0  0.0  0.0  84.0  0.0  0.0  0.0  62.0  $ inner frame wall
c
3705  pz    23.0  $ gas fill level (19.0=3.2gal, 21.0=9.6gal, 23.0=16gal, 25.0=22.4gal)
c
c *** Windows ***
c
c           Vx     Vy     Vz    A1x   A1y  A1z  A2x  A2y   A2z  A3x  A3y  A3z
3706  box  410.0  790.0  83.0  150.0  0.0  0.0  0.0  90.0  0.0  0.0  0.0  68.0  $ outer window wall
3707  box  411.0  791.0  84.0  148.0  0.0  0.0  0.0  88.0  0.0  0.0  0.0  66.0  $ inner window wall
c
c *** Tires ***
c
c            Vx     Vy    Vz    Hx   Hy   Hz    R
3708  rcc  410.0  761.0  29.0  18.0  0.0  0.0  29.0  $ outer tire wall, right front
3709  rcc  411.0  761.0  29.0  16.0  0.0  0.0  28.0  $ inner tire wall, right front
c
3710  rcc  560.0  761.0  29.0 -18.0  0.0  0.0  29.0  $ outer tire wall, left front
3711  rcc  559.0  761.0  29.0 -16.0  0.0  0.0  28.0  $ inner tire wall, left front
c
3712  rcc  410.0  909.0  29.0  18.0  0.0  0.0  29.0  $ outer tire wall, right back
3713  rcc  411.0  909.0  29.0  16.0  0.0  0.0  28.0  $ inner tire wall, right back
c
3714  rcc  560.0  909.0  29.0 -18.0  0.0  0.0  29.0  $ outer tire wall, left back
3715  rcc  559.0  909.0  29.0 -16.0  0.0  0.0  28.0  $ inner tire wall, left back
c
3716  pz    15.0  $ bottom of vehicle
c
c ------------ VEHICLE (3,3) ------------
c
c *** Engine Block ***
c
c            Vx    Vy     Vz    A1x   A1y  A1z  A2x  A2y   A2z  A3x  A3y  A3z
3800  box  740.0  700.0  15.0  150.0  0.0  0.0  0.0  90.0  0.0  0.0  0.0  68.0  $ engine block
c
c *** Passenger Compartment ***
c
c            Vx    Vy     Vz    A1x   A1y  A1z  A2x  A2y   A2z  A3x  A3y  A3z
3801  box  740.0  790.0  15.0  150.0  0.0  0.0  0.0  90.0  0.0  0.0  0.0  68.0  $ outer frame wall
3802  box  743.0  793.0  18.0  144.0  0.0  0.0  0.0  84.0  0.0  0.0  0.0  62.0  $ inner frame wall
c
c *** Trunk & Gas Tank ***
c
c           Vx    Vy     Vz    A1x   A1y  A1z  A2x  A2y   A2z  A3x  A3y  A3z
3803  box  740.0  880.0  15.0  150.0  0.0  0.0  0.0  90.0  0.0  0.0  0.0  68.0  $ outer frame wall
3804  box  743.0  883.0  18.0  144.0  0.0  0.0  0.0  84.0  0.0  0.0  0.0  62.0  $ inner frame wall
```

```
c
3805  pz    23.0  $ gas fill level (19.0=3.2gal, 21.0=9.6gal, 23.0=16gal, 25.0=22.4gal)
c
c *** Windows ***
c
c           Vx     Vy     Vz    A1x   A1y  A1z  A2x  A2y   A2z  A3x  A3y  A3z
3806  box  740.0  790.0  83.0  150.0  0.0  0.0  0.0  90.0  0.0  0.0  0.0  68.0  $ outer window wall
3807  box  741.0  791.0  84.0  148.0  0.0  0.0  0.0  88.0  0.0  0.0  0.0  66.0  $ inner window wall
c
c *** Tires ***
c
c            Vx     Vy    Vz    Hx   Hy   Hz    R
3808  rcc  740.0  761.0  29.0  18.0  0.0  0.0  29.0  $ outer tire wall, right front
3809  rcc  741.0  761.0  29.0  16.0  0.0  0.0  28.0  $ inner tire wall, right front
c
3810  rcc  890.0  761.0  29.0 -18.0  0.0  0.0  29.0  $ outer tire wall, left front
3811  rcc  889.0  761.0  29.0 -16.0  0.0  0.0  28.0  $ inner tire wall, left front
c
3812  rcc  740.0  909.0  29.0  18.0  0.0  0.0  29.0  $ outer tire wall, right back
3813  rcc  741.0  909.0  29.0  16.0  0.0  0.0  28.0  $ inner tire wall, right back
c
3814  rcc  890.0  909.0  29.0 -18.0  0.0  0.0  29.0  $ outer tire wall, left back
3815  rcc  889.0  909.0  29.0 -16.0  0.0  0.0  28.0  $ inner tire wall, left back
c
3816  pz    15.0  $ bottom of vehicle
c
c ------------ UNIVERSE ------------
c
c *** Universe ***
c
9000   pz      0.0  $ floor
9999   s  485.0  485.0  0.0  800.0  $ universe sphere

c
c ---------------------------------------------------------------
c                           MATERIAL CARDS
c ---------------------------------------------------------------
c
c *** Material 1 -- Helium-3 (density @ 4 atm = -5.00E-04 g/cm3) ***
c
m1     2003.60c     1.00
c
c *** Material 2 -- Polyethylene (density = -0.96 g/cm3) ***
c
m2     1001.60c     0.666
       6000.60c     0.333
mt2    poly.60t
c
c *** Material 3 -- Plastic Scintillator (density = -1.032 g/cm3) ***
c
m3     1001.60c    -0.524
       6000.60c    -0.476
mt3    poly.60t
c
c *** Material 4 -- Stainless Steel SS304 (density = -7.92 g/cm3, 25% den = -1.98 g/cm3) ***
c
m4    26056.60c     0.05936
      24052.60c     0.01743
      28058.60c     0.00772
      25055.60c     0.00174
c
c *** Material 5 -- Carbon Steel (density = -7.84 g/cm3) ***
c
m5    25055.60c     0.70
       6000.60c     0.12
      15031.60c     0.08
      16000.60c     0.10
c
c *** Material 6 -- Aluminum (density = -2.7 g/cm3) ***
c
m6    13027.60c     1.00
c
c *** Material 7 -- Gasoline (density = -0.70 g/cm3) ***
c
m7     6000.60c     0.308
       1001.60c     0.692
c
```

```
c *** Material 8 -- Glass (density = -2.52 g/cm3) ***
c
m8    14000.60c    -0.090
      11023.60c    -0.253
       8016.60c    -0.601
      20000.60c    -0.056
c
c *** Material 9 -- Concrete (density = -2.35 g/cm3) ***
c
m9     1001.60c    -0.006
       8016.60c    -0.508
      11023.60c    -0.002
      13027.60c    -0.049
      14000.60c    -0.320
      19000.60c    -0.019
      20000.60c    -0.084
      26000.60c    -0.012
c
c *** Material 10 -- Dry Air (density = -1.204E-03 g/cm3) ***
c
m10    7014.60c     0.7845
       8016.60c     0.2155
c
c *** Material 11 -- Polyurethane Foam (density = -0.02 g/cm3, 50% den = -0.01 g/cm3) ***
c
m11    1001.60c     42.0
       6012.60c     25.0
       8016.60c      6.0
       7014.66c      2.0
mt11   poly.60t
c
c *** Material 12 -- Rubber (density = -1.50 g/cm3) ***
c
m12    1001.60c      8.0
       6012.60c      5.0
mt12   poly.60t
c
c ---------------------------------------------------------------
c                             SOURCE CARDS
c ---------------------------------------------------------------
c
mode  n
c
nps   500000000
c
c *** Source located in passenger compartment of vehicle (1,1) ***
c
sdef  pos=162.5 142.5 52.5  erg=0.0235E-06
c
c sp1   -3  1.025  2.926
c
c Note: Constants for Cf-252 spontaneous fission: a=1.025, b=2.926
c       Watt's Fission Spectrum: f(E) = C exp(-E/a) sinh(bE)^1/2
c
c ---------------------------------------------------------------
c                             TALLY CARDS
c ---------------------------------------------------------------
c
c *** Reaction rate in portal monitor: 1 left ***
c
f4:n  (107 108 109 110 111 112)        $ track length tally in He-3 tubes
c fm4  -1  1  103                        $ reaction rate per unit volume
sd4   1.0                              $ volume in He-3 set to 1.0
c                                        tally units [counts/sec-source particle]
c
c *** Reaction rate in portal monitor: 1 right ***
c
f14:n  (207 208 209 210 211 212)       $ track length tally in He-3 tubes
c fm14  -1  1  103                       $ reaction rate per unit volume
sd14   1.0                             $ volume in He-3 set to 1.0
c                                       tally units [counts/sec-source particle]
c
c *** Reaction rate in portal monitor: 2 left ***
c
f24:n  (132 133 134 135 136 137)       $ track length tally in He-3 tubes
c fm24  -1  1  103                       $ reaction rate per unit volume
sd24   1.0                             $ volume in He-3 set to 1.0
```

```
c                                      tally units [counts/sec-source particle]
c
c *** Reaction rate in portal monitor: 2 right ***
c
f34:n  (232 233 234 235 236 237)       $ track length tally in He-3 tubes
c fm34  -1  1  103                       $ reaction rate per unit volume
sd34   1.0                             $ volume in He-3 set to 1.0
c                                      tally units [counts/sec-source particle]
c
c *** Reaction rate in portal monitor: 3 left ***
c
f44:n  (157 158 159 160 161 162)       $ track length tally in He-3 tubes
c fm44  -1  1  103                       $ reaction rate per unit volume
sd44   1.0                             $ volume in He-3 set to 1.0
c                                      tally units [counts/sec-source particle]
c
c *** Reaction rate in portal monitor: 3 right ***
c
f54:n  (257 258 259 260 261 262)       $ track length tally in He-3 tubes
c fm54  -1  1  103                       $ reaction rate per unit volume
sd54   1.0                             $ volume in He-3 set to 1.0
c                                      tally units [counts/sec-source particle]
```

APPENDIX D

INVERSE CODE

```
!*******************************************************************************
!
! AUTHOR: KAREN MILLER
!
! LANGUAGE: FORTRAN 90
!
! DESCRIPTION: Solves a 3-dimensional inverse transport problem. The system
!              size and number of cells are defined by the user in the source code.
!              The code requires an input file named "input.txt", which contains
!              the cross section data. All of the scattering cross sections are
!              read first. They should be entered in x-y planes, starting at the
!              bottom z plane up to the top z plane as follows:
!
!
!       sigma-s(1,jmax,1)   ...     sigma-s(imax,jmax,1)       *** bottom z plane ***
!          ...              ...       ...
!       sigma-s(1,2,1)      ...     sigma-s(imax,2,1)
!       sigma-s(1,1,1)      ...     sigma-s(imax,1,1)
!
!
!       sigma-s(1,jmax,2)   ...     sigma-s(imax,jmax,2)       *** second z plane ***
!          ...              ...       ...
!       sigma-s(1,2,2)      ...     sigma-s(imax,2,2)
!       sigma-s(1,1,2)      ...     sigma-s(imax,1,2)
!
!              .             .         .
!              .             .         .                        *** top z plane ***
!
!    then do the same for the total cross section:
!
!       sigma-t(1,jmax,1)   ...     sigma-t(imax,jmax,1)       *** bottom z plane ***
!          ...              ...       ...
!       sigma-t(1,2,1)      ...     sigma-t(imax,2,1)
!       sigma-t(1,1,1)      ...     sigma-t(imax,1,1)
!
!
!*******************************************************************************

!*******************************************************************************
!*$$$$$$$$$$$$$$$$$$$$$$$$$$$$$$$$$$$$$$$$$$$$$$$$$$$$$$$$$$$$$$$$$$$$$$$$$$$*
!*$  ---------------------------------------------------------------------  $*
!*$                                                                         $*
!*$                          V A R I A B L E S                              $*
!*$                                                                         $*
!*$  ---------------------------------------------------------------------  $*
!*$$$$$$$$$$$$$$$$$$$$$$$$$$$$$$$$$$$$$$$$$$$$$$$$$$$$$$$$$$$$$$$$$$$$$$$$$$$*
!*******************************************************************************

module variables
implicit none

! parameters
integer, parameter :: maxiter = 1000                  ! max number of source iterations
integer, parameter :: inpfile1 = 15                   ! input file number
integer, parameter :: inpfile2 = 16                   ! input file number
integer, parameter :: outfile = 17                    ! output file number
integer, parameter :: outermax = 5                    ! max number of outer iterations
real, parameter :: phitol = 1.0e-4                    ! tolerance on scalar flux
real, parameter :: invtolsys = 0.5                    ! tolerance on minimization

! variables
integer :: i, j, k                                    ! x, y,and z cell positions
integer :: imax, jmax, kmax                           ! total number cells
real    :: dx, dy, dz                                 ! length of each cell
real    :: xlength, ylength, zlength                  ! system length in x, y, and z directions
integer :: i0, j0, k0                                 ! guess for source position
```

```
real, allocatable, dimension(:,:,:) :: S                ! source strength
real    :: S0                                           ! initial guess for source strength

integer :: th                                           ! angle variable
integer :: theta                                        ! total number of angles
real, allocatable, dimension(:) :: w                    ! quadrature weights
real, allocatable, dimension(:) :: mu, eta, xi          ! angle cosines for quadrature set
real :: c1, c2, c3                                      ! angle cosine values
real :: w1, w2                                          ! angle weight values

real, allocatable, dimension(:,:,:) :: sigt             ! total cross section
real, allocatable, dimension(:,:,:) :: sigs             ! scattering cross section
real :: sigair, sigfloor, sigpoly, sigdet               ! sigt of air/cement

integer, dimension(9) :: zonexstart, zonexend           ! zone parameters
integer, dimension(9) :: zoneystart, zoneyend           ! zone parameters
integer, dimension(9) :: xx, yy                         ! initial guess locations
integer, allocatable, dimension(:,:) :: ztest           ! test parameter for zones
integer :: zone

real :: resmin                                          ! minimum residual
integer :: xmin, ymin, zmin                             ! location of min residual

integer :: iter                                         ! source iteration index
integer :: istart, iend, iincr                          ! start/end/increment of i for sweep
integer :: jstart, jend, jincr                          ! start/end/increment of j for sweep
integer :: kstart, kend, kincr                          ! start/end/increment of k for sweep

real, allocatable, dimension(:,:,:,:) :: den            ! denominator of discrete transport equation
real, allocatable, dimension(:,:,:,:) :: tx, ty,tz      ! coefficients for transport equation

real, allocatable, dimension(:,:,:,:) :: psi            ! cell-centered angular flux
real, allocatable, dimension(:,:,:,:) :: psih           ! angular flux on horizontal faces
real, allocatable, dimension(:,:,:,:) :: psiv           ! angular flux on vertical faces
real, allocatable, dimension(:,:,:,:) :: psit           ! angular flux on top and bottom faces
real, allocatable, dimension(:,:,:,:) :: xinc           ! incident angular flux in x direction (on
vert. face)
real, allocatable, dimension(:,:,:,:) :: yinc           ! incident angular flux in y direction (on
horz. face)
real, allocatable, dimension(:,:,:,:) :: zinc           ! incident angular flux in y direction (on
top face)
real, allocatable, dimension(:,:,:)   :: phi            ! scalar flux
real, allocatable, dimension(:,:,:)   :: oldphi         ! scalar flux at previous iteration step&

integer :: n                                            ! detector index
integer :: nmax                                         ! number of detectors
integer, allocatable, dimension(:) :: idetstart, idetend ! detector span in i direction
integer, allocatable, dimension(:) :: jdetstart, jdetend ! detector span in j direction
integer, allocatable, dimension(:) :: kdetstart, kdetend ! detector span in k direction
real, allocatable, dimension(:) :: M, Mnorm, Mest       ! measurements and uncertainties
real :: Mmax                                            ! largest measurement
real :: invtolrand                                      ! tolerance on minimization
real :: invtol                                          ! tolerance on minimization

integer :: outer, inner                                 ! index for outer iterations
real :: residual                                        ! total residual of least squares
real, allocatable, dimension(:) :: res                  ! residual of least squares
integer :: rescheck                                     ! check residual - yes or no?

real :: gradx, grady, gradz                             ! gradient

integer :: allocstatus                                  ! test variable for allocating arrays
integer :: ierror                                       ! test variable for opening files&

end module

!*****************************************************************************
!*$$$$$$$$$$$$$$$$$$$$$$$$$$$$$$$$$$$$$$$$$$$$$$$$$$$$$$$$$$$$$$$$$$$$$$$$$$*
!*$  ---------------------------------------------------------------------  $*
!*$                                                                         $*
!*$                        M A I N   P R O G R A M                          $*
!*$                                                                         $*
!*$  ---------------------------------------------------------------------  $*
!*$$$$$$$$$$$$$$$$$$$$$$$$$$$$$$$$$$$$$$$$$$$$$$$$$$$$$$$$$$$$$$$$$$$$$$$$$$*
!*****************************************************************************
```

```
program inverse3d
use variables
implicit none

nmax = 6
allocate (M(nmax), stat=allocstatus)

open(unit=outfile,file='output_d1_11_neg.txt',status='unknown',action='write',iostat=ierror)

! vehicle 1,1

M(1) =   3.400E+02
M(2) =   5.016E+02
M(3) =   6.189E+01
M(4) =   4.873E+00
M(5) =   5.571E-01
M(6) =   1.037E-01

invtolrand = 0.5
invtol = invtolsys + invtolrand

! -----------------------------------------
! SYSTEM SETUP
! -----------------------------------------
call system_setup

! -----------------------------------------
! INITIAL GUESS
! -----------------------------------------
call initial_guess

! -----------------------------------------
! FORWARD SOLVER
! -----------------------------------------
call forward_source
call forward_solver
call convergence

! -----------------------------------------
! INVERSE SOLVER
! -----------------------------------------
inverse: do zone = 1, 9

  if (ztest(xx(zone),yy(zone))==1) then
    write(outfile,408) xmin, ymin, zmin
    408 format(/ "Inverse code did not converge." / "Best guess = (", &
               & i2, ",", i2, ",", i2, ")")
    stop
  end if

  i0 = xx(zone)
  j0 = yy(zone)
  k0 = 3

  minimize: do outer = 1, outermax

    call adjoint_source
    call forward_solver
    call gradient_x
    call line_search_x

    call adjoint_source
    call forward_solver
    call gradient_y
    call line_search_y

    call adjoint_source
    call forward_solver
    call gradient_z
    call line_search_z

    write(outfile,410) outer, i0, j0, k0
    410 format ("Iteration: ", i3, ", (", i3, ",", i3, ",", i3, ")")

  end do minimize

end do inverse
```

```
! ----------------------------------------
! WRITE OUTPUT
! ----------------------------------------
write(outfile,411) outer, i0, j0, k0
411 format (/ "Converged at iteration ", i3 // "SOURCE POSITION: (", &
            & i3, ",", i3, ",", i3, ")")

end program


!*******************************************************************************
!*$$$$$$$$$$$$$$$$$$$$$$$$$$$$$$$$$$$$$$$$$$$$$$$$$$$$$$$$$$$$$$$$$$$$$$$$$$$*
!*$  ------------------------------------------------------------------------  $*
!*$                                                                            $*
!*$                           S U B R O U T I N E S                            $*
!*$                                                                            $*
!*$  ------------------------------------------------------------------------  $*
!*$$$$$$$$$$$$$$$$$$$$$$$$$$$$$$$$$$$$$$$$$$$$$$$$$$$$$$$$$$$$$$$$$$$$$$$$$$$*
!*******************************************************************************

!-------------------------------------------------------------------------------
! +----------------------------------------------------------------------+ |
! |                                                                      | |
! |                                                                      | |
! |                              system setup                            | |
! |                                                                      | |
! |                                                                      | |
! +----------------------------------------------------------------------+ |
!-------------------------------------------------------------------------------

subroutine system_setup
use variables
implicit none

!@@@@@@@@@@@@@@@@@@@@@@@@@@@@@@@@@@@@@@@@@@@@@@@@@@@@@@@@@@@@@@@@@@@@@@@@@@@
!
! INPUT GEOMETRY AND DETECTOR INFORMATION
!
!@@@@@@@@@@@@@@@@@@@@@@@@@@@@@@@@@@@@@@@@@@@@@@@@@@@@@@@@@@@@@@@@@@@@@@@@@@@

! ----------------------------------------
! SYSTEM LENGTH IN X, Y, AND Z DIRECTIONS
! ----------------------------------------
xlength = 960.0
ylength = 930.0
zlength = 240.0
! ----------------------------------------
! NUMBER OF CELLS IN X, Y, AND Z DIRECTIONS
! ----------------------------------------
imax = 64
jmax = 31
kmax = 4
! ----------------------------------------
! CALCULATE MESH SIZE
! ----------------------------------------
dx = xlength / real(imax)
dy = ylength / real(jmax)
dz = zlength / real(kmax)
! ----------------------------------------
! NUMBER OF ANGLES IN 3D S(6) QUADRATURE SET
! ----------------------------------------
theta = 48
! ----------------------------------------
! TOTAL CROSS SECTIONS OF AIR, THE FLOOR,
! POLY, AND THE DETECTOR MATERIAL
! ----------------------------------------
sigair = 5.009E-04
sigfloor = 2.305E-01
sigpoly = 1.680E-01
sigdet = 1.931E+00
! ----------------------------------------
! GUESS A SOURCE STRENGTH
! ----------------------------------------
S0 = 15000.0

! ----------------------------------------
```

```
! NUMBER OF DETECTORS
! -----------------------------------------
nmax = 6

allocate (idetstart(nmax), stat=allocstatus)
allocate (jdetstart(nmax), stat=allocstatus)
allocate (kdetstart(nmax), stat=allocstatus)
allocate (idetend(nmax), stat=allocstatus)
allocate (jdetend(nmax), stat=allocstatus)
allocate (kdetend(nmax), stat=allocstatus)
allocate (ztest(imax,jmax), stat=allocstatus)

! -----------------------------------------
! INPUT DETECTOR POSITIONS
! -----------------------------------------
idetstart(1) = 1
idetend(1) = 2
jdetstart(1) = 1
jdetend(1) = 4
kdetstart(1) = 3
kdetend(1) = 4

idetstart(2) = 19
idetend(2) = 20
jdetstart(2) = 1
jdetend(2) = 4
kdetstart(2) = 3
kdetend(2) = 4

idetstart(3) = 23
idetend(3) = 24
jdetstart(3) = 1
jdetend(3) = 4
kdetstart(3) = 3
kdetend(3) = 4

idetstart(4) = 41
idetend(4) = 42
jdetstart(4) = 1
jdetend(4) = 4
kdetstart(4) = 3
kdetend(4) = 4

idetstart(5) = 45
idetend(5) = 46
jdetstart(5) = 1
jdetend(5) = 4
kdetstart(5) = 3
kdetend(5) = 4

idetstart(6) = 63
idetend(6) = 64
jdetstart(6) = 1
jdetend(6) = 4
kdetstart(6) = 3
kdetend(6) = 4

! -----------------------------------------
! INPUT ZONE START AND END POINTS
! -----------------------------------------
zonexstart(1) = 1
zonexend(1) = 21
zoneystart(1) = 1
zoneyend(1) = 10

zonexstart(2) = 22
zonexend(2) = 43
zoneystart(2) = 1
zoneyend(2) = 10

zonexstart(3) = 44
zonexend(3) = 64
zoneystart(3) = 1
zoneyend(3) = 10

zonexstart(4) = 1
zonexend(4) = 21
```

```
zoneystart(4) = 11
zoneyend(4) = 21

zonexstart(5) = 22
zonexend(5) = 43
zoneystart(5) = 11
zoneyend(5) = 21

zonexstart(6) = 44
zonexend(6) = 64
zoneystart(6) = 11
zoneyend(6) = 21

zonexstart(7) = 1
zonexend(7) = 21
zoneystart(7) = 22
zoneyend(7) = 31

zonexstart(8) = 22
zonexend(8) = 43
zoneystart(8) = 22
zoneyend(8) = 31

zonexstart(9) = 44
zonexend(9) = 64
zoneystart(9) = 22
zoneyend(9) = 31

!@@@@@@@@@@@@@@@@@@@@@@@@@@@@@@@@@@@@@@@@@@@@@@@@@@@@@@@@@@@@@@@@@@@@@@@@@@@
!
! ALLOCATE ARRAYS
!
!@@@@@@@@@@@@@@@@@@@@@@@@@@@@@@@@@@@@@@@@@@@@@@@@@@@@@@@@@@@@@@@@@@@@@@@@@@@

allocate (w(theta), stat=allocstatus)
allocate (mu(theta), stat=allocstatus)
allocate (eta(theta), stat=allocstatus)
allocate (xi(theta), stat=allocstatus)
allocate (den(imax,jmax,kmax,theta), stat=allocstatus)
allocate (psi(imax,jmax,kmax,theta), stat=allocstatus)
allocate (psih(imax,jmax+1,kmax,theta), stat=allocstatus)
allocate (psiv(imax+1,jmax,kmax,theta), stat=allocstatus)
allocate (psit(imax,jmax,kmax+1,theta), stat=allocstatus)
allocate (xinc(imax,jmax+1,kmax,theta), stat=allocstatus)
allocate (yinc(imax+1,jmax,kmax,theta), stat=allocstatus)
allocate (zinc(imax,jmax,kmax+1,theta), stat=allocstatus)
allocate (phi(imax,jmax,kmax), stat=allocstatus)
allocate (oldphi(imax,jmax,kmax), stat=allocstatus)
allocate (tx(imax,jmax,kmax,theta), stat=allocstatus)
allocate (ty(imax,jmax,kmax,theta), stat=allocstatus)
allocate (tz(imax,jmax,kmax,theta), stat=allocstatus)
allocate (sigt(imax,jmax,kmax), stat=allocstatus)
allocate (sigs(imax,jmax,kmax), stat=allocstatus)
allocate (S(imax,jmax,kmax), stat=allocstatus)
allocate (Mnorm(nmax), stat=allocstatus)
allocate (Mest(nmax), stat=allocstatus)
allocate (res(nmax), stat=allocstatus)

!@@@@@@@@@@@@@@@@@@@@@@@@@@@@@@@@@@@@@@@@@@@@@@@@@@@@@@@@@@@@@@@@@@@@@@@@@@@
!
! ECHO SYSTEM INFORMATION TO OUTPUT FILE
!
!@@@@@@@@@@@@@@@@@@@@@@@@@@@@@@@@@@@@@@@@@@@@@@@@@@@@@@@@@@@@@@@@@@@@@@@@@@@

! ------------------------------------------
! WRITE SYSTEM INFORMATION TO OUTPUT FILE
! ------------------------------------------
write(outfile,100)
100 format("3D SOURCE LOCATION CODE" // "------------- SYSTEM DATA -------------" /)
write(outfile,130) xlength,ylength,zlength,imax,jmax,kmax,dx,dy,dz
130 format("XLENGTH = ", f8.3 / &
         & "YLENGTH = ", f8.3 / &
                  & "ZLENGTH = ", f8.3 / &
              & "IMAX = ", i5  / &
                   & "JMAX = ", i5  / &
              & "KMAX = ", i5  / &
                   & "DX = ", f8.2 / &
```

```
                  & "DY = ", f8.2 / &
                  & "DZ = ", f8.2 /)
write(outfile,140)
140 format("------------- MEASUREMENTS -------------" /)

!@@@@@@@@@@@@@@@@@@@@@@@@@@@@@@@@@@@@@@@@@@@@@@@@@@@@@@@@@@@@@@@@@@@@@@@@@@@
!
! READ CROSS SECTIONS FROM INPUT FILE
!
!@@@@@@@@@@@@@@@@@@@@@@@@@@@@@@@@@@@@@@@@@@@@@@@@@@@@@@@@@@@@@@@@@@@@@@@@@@@

! ------------------------------------------
! OPEN INPUT FILE
! ------------------------------------------
open(unit=inpfile1,file='xs.txt',status='old',action='read',iostat=ierror)

! ------------------------------------------
! READ CROSS SECTIONS
! ------------------------------------------
do k = 1, kmax
  do j = jmax, 1, -1
    read(inpfile1,*) (sigs(i,j,k),i=1,imax)
  end do
end do

do k = 1, kmax
  do j = jmax, 1, -1
    read(inpfile1,*) (sigt(i,j,k),i=1,imax)
  end do
end do

!@@@@@@@@@@@@@@@@@@@@@@@@@@@@@@@@@@@@@@@@@@@@@@@@@@@@@@@@@@@@@@@@@@@@@@@@@@@
!
! SET QUADRATURES WEIGHTS AND COSINES
!
!@@@@@@@@@@@@@@@@@@@@@@@@@@@@@@@@@@@@@@@@@@@@@@@@@@@@@@@@@@@@@@@@@@@@@@@@@@@

! ------------------------------------------
! ANGLE COSINES FOR S(6)
! ------------------------------------------
c1 = 0.2666355
c2 = 0.6815076
c3 = 0.9261808
! ------------------------------------------
! WEIGHTS FOR S(6)
! ------------------------------------------
w1 = 0.1761263
w2 = 0.1572071
! ------------------------------------------
! SET COSINE FOR POLAR ANGLES (MU)
! ------------------------------------------
do th = 1, theta
  if ((th==3).or.(th==10).or.(th==14).or.(th==19).or.(th==21) &
    & .or.(th==24).or.(th==27).or.(th==34).or.(th==38).or.(th==43) &
    & .or.(th==45).or.(th==48)) then
      mu(th) = c1
  elseif ((th==4).or.(th==9).or.(th==15).or.(th==18).or.(th==22) &
    & .or.(th==23).or.(th==28).or.(th==33).or.(th==39).or.(th==42) &
    & .or.(th==46).or.(th==47)) then
      mu(th) = -c1
  elseif ((th==2).or.(th==11).or.(th==13).or.(th==20).or.(th==26) &
    & .or.(th==35).or.(th==37).or.(th==44)) then
      mu(th) = c2
  elseif ((th==5).or.(th==8).or.(th==16).or.(th==17).or.(th==29) &
    & .or.(th==32).or.(th==40).or.(th==41)) then
          mu(th) = -c2
  elseif ((th==1).or.(th==12).or.(th==25).or.(th==36)) then
      mu(th) = c3
  else
      mu(th) = -c3
  end if
! ------------------------------------------
! SET SINE FOR POLAR ANGLES (ETA)
! ------------------------------------------
  if ((th==1).or.(th==6).or.(th==13).or.(th==16).or.(th==21) &
    & .or.(th==22).or.(th==25).or.(th==30).or.(th==37).or.(th==40) &
        & .or.(th==45).or.(th==46)) then
```

```
          eta(th) = c1
  elseif ((th==7).or.(th==12).or.(th==17).or.(th==20).or.(th==23) &
    & .or.(th==24).or.(th==31).or.(th==36).or.(th==41).or.(th==44) &
        &  .or.(th==47).or.(th==48)) then
          eta(th) = -c1
  elseif ((th==2).or.(th==5).or.(th==14).or.(th==15).or.(th==26) &
    & .or.(th==29).or.(th==38).or.(th==39)) then
          eta(th) = c2
  elseif ((th==8).or.(th==11).or.(th==18).or.(th==19).or.(th==32) &
    & .or.(th==35).or.(th==42).or.(th==43)) then
          eta(th) = -c2
  elseif ((th==3).or.(th==4).or.(th==27).or.(th==28)) then
      eta(th) = c3
  else
      eta(th) = -c3
  end if
! ------------------------------------------
! SET COSINE FOR AZIMUTHAL ANGLES (XI)
! ------------------------------------------
  if (th < 13) then
    xi(th) = c1
  elseif ((th > 24) .and. (th < 37)) then
    xi(th) = -c1
  elseif ((th > 12) .and. (th < 21)) then
    xi(th) = c2
  elseif ((th > 36) .and. (th < 45)) then
    xi(th) = -c2
  elseif ((th > 20) .and. (th < 25)) then
    xi(th) = c3
  else
    xi(th) = -c3
  end if
end do
! ------------------------------------------
! SET S(6) QUADRATURE WEIGHTS
! ------------------------------------------
do th = 1, theta
  if ((th==2).or.(th==5).or.(th==8).or.(th==11).or.(th==26).or. &
    & (th==29).or.(th==32).or.(th==35)) then
      w(th) = w2
  elseif ((th > 12) .and. (th < 21)) then
      w(th) = w2
  elseif ((th > 36) .and. (th < 45)) then
      w(th) = w2
  else
      w(th) = w1
  end if
end do

!@@@@@@@@@@@@@@@@@@@@@@@@@@@@@@@@@@@@@@@@@@@@@@@@@@@@@@@@@@@@@@@@@@@@@@@@@@@
!
! CALCULATE COEFFICIENTS FOR THE TRANSPORT EQUATION
!
!@@@@@@@@@@@@@@@@@@@@@@@@@@@@@@@@@@@@@@@@@@@@@@@@@@@@@@@@@@@@@@@@@@@@@@@@@@@

do th = 1, theta
  do i = 1, imax
    do j = 1, jmax
      do k = 1, kmax
         tx(i,j,k,th) = abs(mu(th))/sigt(i,j,k)/dx
        ty(i,j,k,th) = abs(eta(th))/sigt(i,j,k)/dy
         tz(i,j,k,th) = abs(xi(th))/sigt(i,j,k)/dz
        den(i,j,k,th) = 1.0 / (1.0+tx(i,j,k,th)+ty(i,j,k,th) &
                       & +tz(i,j,k,th))
      end do
    end do
  end do
end do

!@@@@@@@@@@@@@@@@@@@@@@@@@@@@@@@@@@@@@@@@@@@@@@@@@@@@@@@@@@@@@@@@@@@@@@@@@@@
!
! INITIALIZE FORWARD SOLVER ARRAYS
!
!@@@@@@@@@@@@@@@@@@@@@@@@@@@@@@@@@@@@@@@@@@@@@@@@@@@@@@@@@@@@@@@@@@@@@@@@@@@

do i = 1, imax
  do j = 1, jmax
```

```
    do k = 1, kmax
      phi(i,j,k) = 0.0
      oldphi(i,j,k) = 0.0
    end do
  end do
end do

do th = 1, theta
  do i = 1, imax
    do j = 1, jmax
      do k = 1, kmax
        psi(i,j,k,th) = 0.0
      end do
    end do
  end do
end do

do th = 1, theta
  do i = 1, imax+1
    do j = 1, jmax
      do k = 1, kmax
        psiv(i,j,k,th) = 0.0
      end do
    end do
  end do
end do

do th = 1, theta
  do i = 1, imax
    do j = 1, jmax+1
      do k = 1, kmax
        psih(i,j,k,th) = 0.0
      end do
    end do
  end do
end do

do th = 1, theta
  do i = 1, imax
    do j = 1, jmax
      do k = 1, kmax+1
        psit(i,j,k,th) = 0.0
      end do
    end do
  end do
end do


!@@@@@@@@@@@@@@@@@@@@@@@@@@@@@@@@@@@@@@@@@@@@@@@@@@@@@@@@@@@@@@@@@@@@@@@@@@@
!
! NORMALIZE MEASUREMENTS
!
!@@@@@@@@@@@@@@@@@@@@@@@@@@@@@@@@@@@@@@@@@@@@@@@@@@@@@@@@@@@@@@@@@@@@@@@@@@@

! ------------------------------------------
! DETERMINE THE LARGEST MEASUREMENT
! ------------------------------------------
Mmax = M(1)
do n = 2, nmax
  if (M(n) > Mmax) then
    Mmax = M(n)
  end if
end do

! ------------------------------------------
! NORMALIZE MEASUREMENTS
! ------------------------------------------
do n = 1, nmax
  Mnorm(n) = M(n) / Mmax
end do

! ------------------------------------------
! WRITE MEASUREMENTS TO OUTPUT FILE
! ------------------------------------------
do n = 1, nmax
  write(outfile,400) n, Mnorm(n)
  400 format ("M (", i1, ") = ", es10.3)
```

```
end do
write(outfile,405) invtol
405 format ( / "RESIDUAL TOLERANCE = ", es10.3)
write(outfile,401)
401 format (/ "--------------- RESULTS ---------------" /)

end subroutine

!-------------------------------------------------------------------------------
! +-----------------------------------------------------------------------+ |
! |                                                                       | |
! |                                                                       | |
! |                              initial guess                            | |
! |                                                                       | |
! |                                                                       | |
! +-----------------------------------------------------------------------+ |
!-------------------------------------------------------------------------------

!@@@@@@@@@@@@@@@@@@@@@@@@@@@@@@@@@@@@@@@@@@@@@@@@@@@@@@@@@@@@@@@@@@@@@@@@@@@
!
! CALCULATE INITIAL GUESS FOR SOURCE POSITION
!
!@@@@@@@@@@@@@@@@@@@@@@@@@@@@@@@@@@@@@@@@@@@@@@@@@@@@@@@@@@@@@@@@@@@@@@@@@@@

subroutine initial_guess
use variables
implicit none

! -----------------------------------------
! LOCAL VARIABLES
! -----------------------------------------
integer :: igstart, igincr, igend    ! coarse mesh, x-direction
integer :: jgstart, jgincr, jgend    ! coarse mesh, y-direction
integer :: z, zz                     ! counting variable
real :: igmin                        ! minimum residual
real, dimension(9) :: igres          ! residual
real :: a1                           ! dummy variable
integer :: a2, a3, a4, a5, a6, a7    ! dummy variables

! -----------------------------------------
! ASSIGN POSITIONS TO CHECK
! -----------------------------------------
igstart = ceiling(real(imax)/6.0)
igincr = ceiling(real(imax)/3.0)
igend = igstart+igincr+igincr

jgstart = ceiling(real(jmax)/6.0)-1
jgincr = ceiling(real(jmax)/3.0)+1
jgend = jgstart+jgincr+jgincr

k0 = 3

! -----------------------------------------
! CALCULATE RESIDUAL IN EACH ZONE
! -----------------------------------------
rescheck = 0
z = 1
do j0 = jgstart, jgend, jgincr
  do i0 = igstart, igend, igincr
    call forward_source
    call forward_solver
    call convergence
    igres(z) = residual
    xx(z) = i0
    yy(z) = j0
    z = z+1
  end do
end do
rescheck = 1

! -----------------------------------------
! PUT RESIDUALS IN ASCENDING ORDER
! -----------------------------------------
do z = 2, 9
  a1 = igres(z)
  a2 = xx(z)
  a3 = yy(z)
```

```
  a4 = zonexstart(z)
  a5 = zonexend(z)
  a6 = zoneystart(z)
  a7 = zoneyend(z)

  do zz = z-1, 1, -1
    if (igres(zz) <= a1) then
      exit
    else
      igres(zz+1) = igres(zz)
      xx(zz+1) = xx(zz)
      yy(zz+1) = yy(zz)
      zonexstart(zz+1) = zonexstart(zz)
      zonexend(zz+1) = zonexend(zz)
      zoneystart(zz+1) = zoneystart(zz)
      zoneyend(zz+1) = zoneyend(zz)
    end if
  end do

  igres(zz+1) = a1
  xx(zz+1) = a2
  yy(zz+1) = a3
  zonexstart(zz+1) = a4
  zonexend(zz+1) = a5
  zoneystart(zz+1) = a6
  zoneyend(zz+1) = a7
end do

! ------------------------------------------
! DEFINE NO-GO ZONES WITH LARGE RESDIUALS
! ------------------------------------------
do i = 1, imax
  do j = 1, jmax
    ztest(i,j) = 0
  end do
end do

do z = 2, 9
  if (igres(z) > 5.0*igres(1)) then

  write(*,*) "skip zone: ", "(", xx(z), yy(z), ")"
  write(outfile,*) "skip zone: ", z, "(", xx(z), yy(z), ")"

    do i = zonexstart(z), zonexend(z)
      do j = zoneystart(z), zoneyend(z)
        ztest(i,j) = 1
      end do
    end do
  end if
end do

! ------------------------------------------
! SET INITAL GUESS WITH SMALLEST RESIDUAL
! ------------------------------------------
i0 = xx(1)
j0 = yy(1)

! ------------------------------------------
! INITIALIZE GLOBAL MINIMUM
! ------------------------------------------
resmin = igres(1)
xmin = i0
ymin = j0
zmin = k0

! ------------------------------------------
! WRITE INITIAL GUESS
! ------------------------------------------
write(outfile,403) i0, j0, k0
403 format (/ "INITIAL GUESS = (", i3, ",", i3, ",", i3, ")" /)

end subroutine


!-------------------------------------------------------------------------------
! +-----------------------------------------------------------------------+ |
! |                                                                       | |
```

```
! |                                                                              | |
! |                              forward solver                                  | |
! |                                                                              | |
! |                                                                              | |
! +------------------------------------------------------------------------------+ |
!--------------------------------------------------------------------------------

!@@@@@@@@@@@@@@@@@@@@@@@@@@@@@@@@@@@@@@@@@@@@@@@@@@@@@@@@@@@@@@@@@@@@@@@@@@@@@@@
!
! ASSIGN THE SOURCE STRENGTH ARRAY FOR THE FORWARD SOLVER
!
!@@@@@@@@@@@@@@@@@@@@@@@@@@@@@@@@@@@@@@@@@@@@@@@@@@@@@@@@@@@@@@@@@@@@@@@@@@@@@@@

subroutine forward_source
use variables
implicit none

do i = 1, imax
  do j = 1, jmax
    do k = 1, kmax
      if ((i==i0).and.(j==j0).and.(k==k0)) then
        S(i,j,k) = S0
      else
        S(i,j,k) = 0.0
      end if
    end do
  end do
end do

end subroutine

!@@@@@@@@@@@@@@@@@@@@@@@@@@@@@@@@@@@@@@@@@@@@@@@@@@@@@@@@@@@@@@@@@@@@@@@@@@@@@@@
!
! CALCULATE THE SCALAR FLUX USING SOURCE ITERATION
!
!@@@@@@@@@@@@@@@@@@@@@@@@@@@@@@@@@@@@@@@@@@@@@@@@@@@@@@@@@@@@@@@@@@@@@@@@@@@@@@@

subroutine forward_solver
use variables
implicit none

fwdsolver: do iter = 1, maxiter
! -----------------------------------------
! RESET PHI AND OLDPHI
! -----------------------------------------
  do i = 1, imax
    do j = 1, jmax
      do k = 1, kmax
        oldphi(i,j,k) = phi(i,j,k)
        phi(i,j,k) = 0.0
      end do
    end do
  end do
! -----------------------------------------
! SET TRANSPORT SWEEP DIRECTION, START,
! AND END POINTS
! -----------------------------------------
  do th = 1, theta
    if (mu(th) > 0.0) then
      istart = 1
      iend = imax
      iincr = 1
    else
      istart = imax
      iend = 1
      iincr = -1
    end if
    if (eta(th) > 0.0) then
      jstart = 1
      jend = jmax
      jincr = 1
    else
      jstart = jmax
      jend = 1
      jincr = -1
    end if
    if (xi(th) > 0.0) then
```

```
      kstart = 1
      kend = kmax
      kincr = 1
    else
      kstart = kmax
      kend = 1
      kincr = -1
    end if
! ------------------------------------------
! BEGIN TRANSPORT SWEEP
! ------------------------------------------
    do i = istart, iend, iincr
      do j = jstart, jend, jincr
        do k = kstart, kend, kincr
! ------------------------------------------
! CALCULATE THE INCIDENT ANGULAR FLUX
! ------------------------------------------
          xinc(i,j,k,th) = psiv(i-(iincr-1)/2,j,k,th)
          yinc(i,j,k,th) = psih(i,j-(jincr-1)/2,k,th)
          zinc(i,j,k,th) = psit(i,j,k-(kincr-1)/2,th)
! ------------------------------------------
! CALCULATE THE CELL-CENTERED ANGULAR FLUX
! ------------------------------------------
          psi(i,j,k,th) = (xinc(i,j,k,th)*tx(i,j,k,th) + &
            & yinc(i,j,k,th)*ty(i,j,k,th) + &
            & zinc(i,j,k,th)*tz(i,j,k,th) + &
            & (S(i,j,k)+sigs(i,j,k)*oldphi(i,j,k))/sigt(i,j,k)) &
            & * den(i,j,k,th)
! ------------------------------------------
! CALCULATE THE EXITING ANGULAR FLUX
! ------------------------------------------
          psiv(i+(iincr+1)/2,j,k,th) = psi(i,j,k,th)
          psih(i,j+(jincr+1)/2,k,th) = psi(i,j,k,th)
          psit(i,j,k+(kincr+1)/2,th) = psi(i,j,k,th)
! ------------------------------------------
! CALCULATE THE CELL-CENTERED SCALAR FLUX
! ------------------------------------------
          phi(i,j,k) = phi(i,j,k) + w(th)*psi(i,j,k,th)
        end do
      end do
    end do
  end do
! ------------------------------------------
! TEST FOR CONVERGENCE OF PHI
! ------------------------------------------
  do i = 1, imax
    do j = 1, jmax
      do k = 1, kmax
        if ( abs(phi(i,j,k)-oldphi(i,j,k)) > phitol*abs(phi(i,j,k)) ) then
          if (iter == maxiter) then
            write(outfile,*) "Transport solver did not converge!"
            stop
          end if
          cycle fwdsolver
        end if
      end do
    end do
  end do
! ------------------------------------------
! EXIT SOURCE ITERATION LOOP IF CONVERGED
! ------------------------------------------
  exit fwdsolver
end do fwdsolver

! ------------------------------------------
! NORMALIZE CALCULATED MEASUREMENTS
! ------------------------------------------
do n = 1, nmax
  Mest(n) = 0.0
end do

do n = 1, nmax
  do i = idetstart(n), idetend(n)
    do j = jdetstart(n), jdetend(n)
      do k = kdetstart(n), kdetend(n)
        Mest(n) = Mest(n) + phi(i,j,k)
      end do
```

```
    end do
  end do
end do

Mmax = Mest(1)
do n = 2, nmax
  if (Mest(n) > Mmax) then
    Mmax = Mest(n)
  end if
end do

do n = 1, nmax
  Mest(n) = Mest(n) / Mmax
end do

end subroutine

!@@@@@@@@@@@@@@@@@@@@@@@@@@@@@@@@@@@@@@@@@@@@@@@@@@@@@@@@@@@@@@@@@@@@@@@@@@@@@@@
!
! CHECK TO SEE IF MEASUREMENTS HAVE CONVERGED
!
!@@@@@@@@@@@@@@@@@@@@@@@@@@@@@@@@@@@@@@@@@@@@@@@@@@@@@@@@@@@@@@@@@@@@@@@@@@@@@@@
subroutine convergence
use variables
implicit none

! ------------------------------------------
! CALCULATE RESIDUAL
! ------------------------------------------
do n = 1, nmax
  res(n) = 0.0
end do

residual = 0.0
do n = 1, nmax
  if (Mnorm(n) > 0.0001) then
    res(n) = (Mest(n) - Mnorm(n)) / Mnorm(n)
    residual = residual + abs(res(n))
  end if
end do

! ------------------------------------------
! TEST FOR CONVERGENCE - SMALL RESIDUAL
! ------------------------------------------
if (rescheck == 1) then
  if (residual < invtol) then
    write(outfile,200) i0, j0, k0, residual, invtol
    200 format (/ "Converged. Source position: (", i3, ",", i3, ",", i3, ")" / &
               & "Residual: ", es10.3 / "Tolerance:", es10.3)
    stop
  end if
end if

end subroutine

!-------------------------------------------------------------------------------
! +-----------------------------------------------------------------------+ |
! |                                                                       | |
! |                                                                       | |
! |                              inverse solver                           | |
! |                                                                       | |
! |                                                                       | |
! +-----------------------------------------------------------------------+ |
!-------------------------------------------------------------------------------

!@@@@@@@@@@@@@@@@@@@@@@@@@@@@@@@@@@@@@@@@@@@@@@@@@@@@@@@@@@@@@@@@@@@@@@@@@@@@@@@
!
! ASSIGN THE SOURCE STRENGTH ARRAY FOR THE ADJOINT SOLVER
!
!@@@@@@@@@@@@@@@@@@@@@@@@@@@@@@@@@@@@@@@@@@@@@@@@@@@@@@@@@@@@@@@@@@@@@@@@@@@@@@@

subroutine adjoint_source
use variables
implicit none

do i = 1, imax
  do j = 1, jmax
```

```
    do k = 1, kmax
      if ((i==i0).and.(j==j0).and.(k==k0)) then
        S(i,j,k) = residual
      else
        S(i,j,k) = 0.0
      end if
    end do
  end do
end do

end subroutine

!@@@@@@@@@@@@@@@@@@@@@@@@@@@@@@@@@@@@@@@@@@@@@@@@@@@@@@@@@@@@@@@
!
! CALCULATE THE GRADIENT IN THE X-DIRECTION
!
!@@@@@@@@@@@@@@@@@@@@@@@@@@@@@@@@@@@@@@@@@@@@@@@@@@@@@@@@@@@@@@@

subroutine gradient_x
use variables
implicit none

if ((i0 /= 1).and.(i0 /= imax)) then
  gradx = - (phi(i0+1,j0,k0)-phi(i0-1,j0,k0)) / (2.0*dx)
elseif (i0 == imax) then
  gradx = - (phi(i0,j0,k0)-phi(i0-1,j0,k0)) / dx
elseif (i0 == 1) then
  gradx = - (phi(i0+1,j0,k0)-phi(i0,j0,k0)) / dx
end if

end subroutine

!@@@@@@@@@@@@@@@@@@@@@@@@@@@@@@@@@@@@@@@@@@@@@@@@@@@@@@@@@@@@@@@
!
! CALCULATE THE GRADIENT IN THE Y-DIRECTION
!
!@@@@@@@@@@@@@@@@@@@@@@@@@@@@@@@@@@@@@@@@@@@@@@@@@@@@@@@@@@@@@@@

subroutine gradient_y
use variables
implicit none

if ((j0 /= 1).and.(j0 /= jmax)) then
  grady = - (phi(i0,j0+1,k0)-phi(i0,j0-1,k0)) / (2.0*dy)
elseif (j0 == jmax) then
  grady = - (phi(i0,j0,k0)-phi(i0,j0-1,k0)) / dy
elseif (j0 == 1) then
  grady = - (phi(i0,j0+1,k0)-phi(i0,j0,k0)) / dy
end if

end subroutine

!@@@@@@@@@@@@@@@@@@@@@@@@@@@@@@@@@@@@@@@@@@@@@@@@@@@@@@@@@@@@@@@
!
! CALCULATE THE GRADIENT IN THE Z-DIRECTION
!
!@@@@@@@@@@@@@@@@@@@@@@@@@@@@@@@@@@@@@@@@@@@@@@@@@@@@@@@@@@@@@@@

subroutine gradient_z
use variables
implicit none

if ((k0 /= 1).and.(k0 /= kmax)) then
  gradz = - (phi(i0,j0,k0+1)-phi(i0,j0,k0-1)) / (2.0*dz)
elseif (k0 == kmax) then
  gradz = - (phi(i0,j0,k0)-phi(i0,j0,k0-1)) / dz
elseif (k0 == 1) then
  gradz = - (phi(i0,j0,k0+1)-phi(i0,j0,k0)) / dz
end if

end subroutine

!@@@@@@@@@@@@@@@@@@@@@@@@@@@@@@@@@@@@@@@@@@@@@@@@@@@@@@@@@@@@@@@
!
! LINE SEARCH ALONG THE DIRECTION OF THE X-GRADIENT
!
!@@@@@@@@@@@@@@@@@@@@@@@@@@@@@@@@@@@@@@@@@@@@@@@@@@@@@@@@@@@@@@@
```

```
subroutine line_search_x
use variables
implicit none

! -----------------------------------------
! LOCAL VARIABLES
! -----------------------------------------
integer :: xstart, xend, xincr               ! start/end point for line search
integer :: ipred                             ! position holder
integer :: ii                                ! dummy index
real :: imin                                 ! minimum residual value
real, allocatable, dimension(:) :: ires      ! residual dummy

! -----------------------------------------
! ALLOCATE ARRAY
! -----------------------------------------
allocate (ires(imax), stat=allocstatus)

! -----------------------------------------
! SET START AND END POINTS FOR LINE SEARCH
! -----------------------------------------
ipred = i0

if (gradx > 0.0) then
  xstart = i0+1
  xend = imax
  xincr = 1
elseif (gradx < 0.0) then
  xstart = i0-1
  xend = 1
  xincr = -1
elseif (gradx==0.0) then
  xstart = i0-1
  xend = i0+1
  xincr = 1
end if

! -----------------------------------------
! CACLULATE THE CURRENT POSITION'S RESIDUAL
! AND SET TO THE MINIMIMUM
! -----------------------------------------
ii = 1
ires(ii) = residual
imin = ires(ii)

! -----------------------------------------
! FIND MINIMUM RESIDUAL ALONG THE GRADIENT
! -----------------------------------------
do i0 = xstart, xend, xincr

! -----------------------------------------
! CALCULATE RESIDUAL IF NOT AIR SPACE
! -----------------------------------------
  if ((sigt(i0,j0,k0)==sigair).or.(sigt(i0,j0,k0)==sigfloor).or. &
    & (sigt(i0,j0,k0)==sigpoly).or.(sigt(i0,j0,k0)==sigdet).or. &
    & (ztest(i0,j0)==1)) then
    cycle
  else
    call forward_source
    call forward_solver
    call convergence
  end if

! -----------------------------------------
! COMPARE NEW RESIDUAL TO LOCAL MINIMUM
! -----------------------------------------
  ii = ii+1
  ires(ii) = residual
  if (ires(ii) < imin) then
    imin = ires(ii)
    ipred = i0
  end if
end do

i0 = ipred
```

```
! ------------------------------------------
! COMPARE NEW RESIDUAL TO GLOBAL MINIMUM
! ------------------------------------------
if (imin < resmin) then
  resmin = imin
  xmin = i0
  ymin = j0
  zmin = k0
end if

end subroutine

!@@@@@@@@@@@@@@@@@@@@@@@@@@@@@@@@@@@@@@@@@@@@@@@@@@@@@@@@@@@@@@@@@@@@@@@@@@@@@@@
!
! LINE SEARCH ALONG THE DIRECTION OF THE Y-GRADIENT
!
!@@@@@@@@@@@@@@@@@@@@@@@@@@@@@@@@@@@@@@@@@@@@@@@@@@@@@@@@@@@@@@@@@@@@@@@@@@@@@@@

subroutine line_search_y
use variables
implicit none

! ------------------------------------------
! LOCAL VARIABLES
! ------------------------------------------
integer :: ystart, yend, yincr               ! start/end point for line search
integer :: jpred                             ! position holder
integer :: jj                                ! dummy index
real :: jmin                                 ! minimum residual value
real, allocatable, dimension(:) :: jres      ! residual dummy

! ------------------------------------------
! ALLOCATE ARRAY
! ------------------------------------------
allocate (jres(jmax), stat=allocstatus)

! ------------------------------------------
! SET START AND END POINTS FOR LINE SEARCH
! ------------------------------------------
jpred = j0

if (grady > 0.0) then
  ystart = j0+1
  yend = jmax
  yincr = 1
elseif (grady < 0.0) then
  ystart = j0-1
  yend = 1
  yincr = -1
elseif (grady==0.0) then
  ystart = j0-1
  yend = j0+1
  yincr = 1
end if

! ------------------------------------------
! CACLULATE THE CURRENT POSITION'S RESIDUAL
! AND SET TO THE MINIMIMUM
! ------------------------------------------
jj = 1
jres(jj) = residual
jmin = jres(jj)

! ------------------------------------------
! FIND MINIMUM RESIDUAL ALONG THE GRADIENT
! ------------------------------------------
do j0 = ystart, yend, yincr

! ------------------------------------------
! CALCULATE RESIDUAL IF NOT AIR SPACE
! ------------------------------------------
  if ((sigt(i0,j0,k0)==sigair).or.(sigt(i0,j0,k0)==sigfloor).or. &
    & (sigt(i0,j0,k0)==sigpoly).or.(sigt(i0,j0,k0)==sigdet).or. &
    & (ztest(i0,j0)==1)) then
    cycle
  else
    call forward_source
```

```
    call forward_solver
    call convergence
  end if

! ------------------------------------------
! COMPARE NEW RESIDUAL TO LOCAL MINIMUM
! ------------------------------------------
  jj = jj+1
  jres(jj) = residual
  if (jres(jj) < jmin) then
    jmin = jres(jj)
    jpred = j0
  end if
end do

j0 = jpred

! ------------------------------------------
! COMPARE NEW RESIDUAL TO GLOBAL MINIMUM
! ------------------------------------------
if (jmin < resmin) then
  resmin = jmin
  xmin = i0
  ymin = j0
  zmin = k0
end if

end subroutine

!@@@@@@@@@@@@@@@@@@@@@@@@@@@@@@@@@@@@@@@@@@@@@@@@@@@@@@@@@@@@@@@@@@@@@@@@@@@
!
! LINE SEARCH ALONG THE DIRECTION OF THE Z-GRADIENT
!
!@@@@@@@@@@@@@@@@@@@@@@@@@@@@@@@@@@@@@@@@@@@@@@@@@@@@@@@@@@@@@@@@@@@@@@@@@@@

subroutine line_search_z
use variables
implicit none

! ------------------------------------------
! LOCAL VARIABLES
! ------------------------------------------
integer :: zstart, zend, zincr               ! start/end point for line search
integer :: kpred                             ! position holder
integer :: kk                                ! dummy index
real :: kmin                                 ! minimum residual value
real, allocatable, dimension(:) :: kres      ! residual dummy

! ------------------------------------------
! ALLOCATE ARRAY
! ------------------------------------------
allocate (kres(kmax), stat=allocstatus)

! ------------------------------------------
! SET START AND END POINTS FOR LINE SEARCH
! ------------------------------------------
kpred = k0

if (gradz > 0.0) then
  zstart = k0+1
  zend = kmax
  zincr = 1
elseif (gradz < 0.0) then
  zstart = k0-1
  zend = 1
  zincr = -1
elseif (gradz==0.0) then
  zstart = k0-1
  zend = k0+1
  zincr = 1
end if

! ------------------------------------------
! CACLULATE THE CURRENT POSITION'S RESIDUAL
! AND SET TO THE MINIMIMUM
! ------------------------------------------
kk = 1
```

```
kres(kk) = residual
kmin = kres(kk)

! -----------------------------------------
! FIND MINIMUM RESIDUAL ALONG THE GRADIENT
! -----------------------------------------
do k0 = zstart, zend, zincr

! -----------------------------------------
! CALCULATE RESIDUAL IF NOT AIR SPACE
! -----------------------------------------
  if ((sigt(i0,j0,k0)==sigair).or.(sigt(i0,j0,k0)==sigfloor).or. &
    & (sigt(i0,j0,k0)==sigpoly).or.(sigt(i0,j0,k0)==sigdet).or. &
    & (ztest(i0,j0)==1)) then
    cycle
  else
    call forward_source
    call forward_solver
    call convergence
  end if

! -----------------------------------------
! COMPARE NEW RESIDUAL TO LOCAL MINIMUM
! -----------------------------------------
  kk = kk+1
  kres(kk) = residual
  if (kres(kk) < kmin) then
    kmin = kres(kk)
    kpred = k0
  end if
end do

k0 = kpred

! -----------------------------------------
! COMPARE NEW RESIDUAL TO GLOBAL MINIMUM
! -----------------------------------------
if (kmin < resmin) then
  resmin = kmin
  xmin = i0
  ymin = j0
  zmin = k0
end if

end subroutine
```

VITA

Name: Karen Ann Miller

Address: Texas A&M University
3473 TAMU
College Station, TX 77843-3473

E-mail Address: karen_miller@tamu.edu

Education: B.S., Nuclear Engineering, Texas A&M University, 2004
Ph.D., Nuclear Engineering, Texas A&M University, 2010